



SAPIENZA
UNIVERSITÀ DI ROMA

Modeling Nuclear Dynamics in the Age of Multimessenger Astrophysics

Facoltà di Scienze Matematiche Fisiche e Naturali
Dottorato di Ricerca in Fisica (XXXV cycle)

Andrea Sabatucci
ID number 1609795

Advisor
Prof. Omar Benhar

Co-Advisor
Dr. Andrea Maselli

Academic Year 2021/2022

Modeling Nuclear Dynamics in the Age of Multimessenger Astrophysics
PhD thesis. Sapienza University of Rome

© 2023 Andrea Sabatucci. All rights reserved

This thesis has been typeset by L^AT_EX and the Sapthesis class.

Author's email: andrea.sabatucci@uniroma1.it

"Gutta cavat lapidem, non vi sed saepe cadendo".

Contents

Introduction	1
1 Neutron Stars	5
1.1 Internal composition	6
1.1.1 Outer crust	7
1.1.2 Inner crust	8
1.1.3 The core	9
1.2 Stellar structure equations	9
1.2.1 General Relativity	10
1.2.2 TOV equations	13
1.2.3 Boundary conditions	15
1.2.4 A necessary condition for the stability of a star	16
1.2.5 Early considerations about the EOS	17
1.3 Tidal deformability	18
1.3.1 Newtonian theory	19
1.3.2 Relativistic theory	21
1.4 The equation of state of cold nuclear matter	24
2 Nuclear Hamiltonian	29
2.1 Nucleon-nucleon interaction	30
2.1.1 Phenomenological potentials	32
2.2 Three-nucleon potential	37
2.3 Relativistic corrections	39
2.3.1 Boost corrections: classical description	42
2.3.2 Relativistic Hamiltonians	45
2.3.3 Relativistic corrections to meson exchange potential	48
2.4 Chiral potentials	51
3 Nuclear Matter Theory	55
3.1 Correlated Basis Function approach	56
3.1.1 Cluster expansion	56
3.2 Jastrow variational approach	58
3.2.1 Pair distribution function	62
3.2.2 Statistical correlations	63
3.2.3 Diagrammatic rules	64
3.2.4 Kinetic energy	67

3.2.5	Fermi Hypernetted Chain summation scheme	69
3.3	Extension to operatorial correlations	71
3.4	Monte Carlo methods	73
3.5	The equation of state of Akmal Pandharipande and Revenhall	76
3.5.1	Interplay between boost and NNN interaction	80
4	CBF Effective Interaction	83
4.1	Boost corrections	88
4.2	Analysis with a density dependent NN interaction	92
4.3	Calculation with a realistic NNN interaction	96
5	Constraining Three-nucleon Forces with Multimessenger Astronomy	105
5.1	Modeling nuclear dynamics beyond nuclear density	106
5.2	Methods and observations	109
5.2.1	Astrophysical datasets	111
5.2.2	Simulations for 2G and 3G detectors	112
5.3	Results	113
6	Summary and Outlook	119
	Appendix	125
A	Derivation of One-Pion Exchange Potential	125
B	AV6 Algebra	129
B.1	Projection operators	130
B.2	Pair exchange operator	130
C	Parametrization of the APR Energy Density	133
D	Energy Per Nucleon	135
D.1	Matrix elements	136
E	Boost Calculation Details	139
	Bibliography	141

Introduction

The description of nuclear matter at low temperature and high density, exceeding several times nuclear saturation density $\varrho_0 = 0.16 \text{ fm}^{-3}$, is still an open and challenging problem. If on one hand Quantum Chromo-Dynamics (QCD) is well established as the fundamental theory of strong interactions, on the other hand its non-perturbative nature at low energies together with the phenomenon of color confinement severely limits its applicability to describe the properties of cold and dense nuclear matter. Indeed the confinement of quarks and gluons inside hadrons hides the fundamental degrees of freedom in nuclear interactions, which have to be studied within effective models, in a similar way to what happens with atoms and molecules. Besides being in principle disadvantageous, QCD calculations of nuclear matter can still be attempted via lattice simulations. However, despite the great progress of recent years, lattice QCD is still limited by the occurrence of the sign problem when applied to study matter at zero temperature and finite chemical potential, see [1, 2]. Therefore, in order to consistently describe the properties of nuclear matter, we have to rely upon largely phenomenological models as much as possible constrained by empirical data.

In this respect astrophysical observations involving Neutron Stars (NSs) are of prominent importance in order to shed new light on the nature of nuclear interactions. NSs are extremely compact objects composed mainly by neutrons and a small fraction of protons, electrons and muons. Inside their core the density can exceed ϱ_0 by large factors, whereas temperature remains well below the typical Fermi temperature of nucleons $\sim 10^{12} \text{ K}$. Therefore NSs are unique laboratories to investigate the properties of dense and cold nuclear matter. They exhibit strong magnetic fields and during the cooling phase subsequent to their formation, also strong neutrino emissions. Moreover, because of their compactness, general relativity can not be neglected when studying their structure. Because of all these properties NSs represent exceptional environments in which all the fundamental interactions come into play.

The first detection of gravitational waves (GWs) emitted by a binary neutron star (BNS) system, performed by the LIGO/Virgo collaboration in the summer of 2017 [3, 4] opened the possibility of a new source of information, marking the beginning of the era of multimessenger astronomy.

Lying at the interface between electromagnetic (EM) observatories, GW interferometers, and Earth based laboratories, multimessenger astrophysics has the potential to shape a novel view of both structure and dynamics of dense nuclear matter. Mass-radius measurements of rotating pulsars are rapidly improving thanks to the information provided by the NASA satellite NICER [5–10], which has recently targeted the most massive NS known so far. Remarkably, NICER observations of PSR

J0030+0451 and PSR J0740+662—the inferred masses of which are $M = 1.34_{-0.15}^{+0.16}$ [7] ($M = 1.44_{-0.14}^{+0.15} M_{\odot}$ [8]) and $M = 2.072_{-0.066}^{+0.067} M_{\odot}$, respectively—yield comparable values of the stellar radius, pointing to a stiff nuclear matter equation of state (EOS). On the other hand, constraints inferred from binary NS mergers detected by the LIGO/Virgo Collaboration, and in particular from the landmark discovery of GW170817, [3, 4, 11], have already ruled out some of the stiffest EOSs, which predict large tidal deformabilities, hinting instead to a softer matter content [12–17]. In addition, astrophysical data are being complemented by the information coming from terrestrial experiments, such as heavy-ion collisions or the recent measurement of the neutron skin thickness of lead, performed at Jefferson Lab by the PREX-II Collaboration [18–25].

Posterior distributions inferred from space- and ground-based facilities have been widely exploited in a variety of multimessenger analyses, aimed at constraining models of the EOS or specific properties of neutron star matter. Examples of this approach include reconstruction of the EOS within both phenomenological and non-parametric frameworks, calculations based on microscopic models, and analyses focused on features such as the occurrence of phase transitions, or the behavior of the symmetry energy above nuclear density [26–55]; for recent reviews, see also Refs. [56–58] and references therein.

Among the several existing frameworks attempting to describe nuclear matter properties, non-relativistic Nuclear Many-Body Theory (NMBT) has proved to be extremely consistent and to have a remarkable predictive power. Within this framework, nuclear systems are pictured in terms of point-like nucleons, the dynamics of which is completely determined by the Hamiltonian

$$\mathcal{H} = \sum_i \frac{p_i^2}{2m} + \sum_{i<j} v_{ij} + \sum_{i<j<k} V_{ijk} ,$$

where m and p_i denote the mass and momentum of the i -th nucleon, respectively. Interactions between matter constituents are driven by the nucleon-nucleon (NN) potential v_{ij} —providing an accurate description of the two-nucleon system in both bound and scattering states—supplemented by the three-nucleon (NNN) potential V_{ijk} , whose inclusion is needed to implicitly take into account the occurrence of processes involving the internal structure of nucleons. As a consequence, the role of NNN interactions is expected to become more and more important with increasing density.

The ultimate goal of NMBT is to carry out a unified description for all nuclear phenomena, starting from a microscopic dynamics tuned to reproduce the observed properties of exactly solvable few-nucleon systems [59, 60].

Starting from the above equation, a number of different EOSs have been obtained using both different Hamiltonian models and different many-body techniques. Purely phenomenological Hamiltonians, fitted to the properties of two- and three-nucleon systems, have been shown to provide a very accurate account of the energies of the ground and low-lying excited states of nuclei with mass number $A \leq 12$, as well as of their radii [61]. In addition, they allow for reproducing the empirical value of the equilibrium density of isospin-symmetric matter (SNM) ρ_0 ; see, e.g., Ref. [62].

Over the past two decades, a great deal of attention has been given to a novel generation of nuclear Hamiltonians, derived using the formalism of Chiral Effective

Field Theory (χ EFT). Within χ EFT, the nuclear potentials are obtained from effective Lagrangians comprising pion and nucleon degrees of freedom, constrained by the chiral symmetry of strong interactions. The main advantage of this approach is the capability to determine two- and many-nucleon potentials in a fully consistent fashion. However, being based on a low momentum expansion its applicability is inherently limited to densities $\lesssim 2\rho_0$ [63, 64].

Among the phenomenological models, a state-of-the-art Hamiltonian comprises the Argonne v18 (AV18) NN potential plus the Urbana IX (UIX) NNN potential. Such an Hamiltonian in combination with a variational approach to the many-body problem was used to obtain the EOSs of Akmal Pandharipande and Revenhal (APR) [62, 65], widely used in astrophysical simulations involving NSs as well as supernova explosions. The AV18 potential is represented in coordinate space as a sum over 18 operators, necessary to fit the NN scattering phase shifts in all different channels. This potential provides an accurate description of the scattering data up to energies ~ 600 MeV in the laboratory frame. Note that this is the energy scale typical of nucleon-nucleon scattering in strongly degenerate matter at densities up to $\sim 4\rho_0$. Since the core of NSs as massive as $\sim 2M_\odot$ should be characterized by densities as large as $\sim 5\rho_0$, it appears that the AV18 potential is well suited to describe neutron star matter. Recently some accurate calculations of nuclear matter properties have shown that a simplified Hamiltonian comprising the Argonne v6' (AV6P) and the UIX interactions produces an EOS nearly identical to its AV18+UIX counterpart [66]. The AV6P potential is a re-projection of the full AV18 onto the first six operators. The algebraic properties of such a potential results in a dramatic simplification in the many-body calculations.

In Ref [67] the authors proposed to use the AV6P+UIX Hamiltonian to derive an effective interaction suited to be applied in perturbation theory. The ability of such a formalism to enable perturbative calculations with respect to the Fermi gas basis, allows to compute several nuclear matter properties well beyond the EOS of cold nuclear matter, such as nucleon effective mass, neutrino mean free-path and finite temperature properties.

Being largely determined by a fit over NN scattering data, NN potentials are defined in the reference frame in which the center-of-mass momentum of the interacting pair, \mathbf{P}_{ij} , vanishes. As a consequence, in order to consistently describe NN interactions in the locally inertial frame associated with a NS, v_{ij} must be boosted to a frame in which $\mathbf{P}_{ij} \neq 0$, introducing a correction $\delta v_{ij}(\mathbf{P}_{ij}, \mathbf{r}_{ij})$ [68, 69].

Detailed calculations of the energy of nuclear matter performed including δv_{ij} show that the contribution of relativistic effects is repulsive and is responsible for the $\sim 37\%$ of the repulsive contribution arising from NNN interactions [70, 71]. As a consequence, besides the additional term δv_{ij} , the Hamiltonian including relativistic corrections, \mathcal{H}_R , has to account also for a modified NNN potential, featuring a softer repulsive component. Recently the authors of Ref. [48] have pointed out how this modification of the NNN interaction has a strong impact on NS observables, underlining the necessity of further investigation about the interplay between relativistic corrections and NNN interactions.

In this Thesis we have investigated the possibility of employing a relativistic Hamiltonian \mathcal{H}_R for the calculation of an effective interaction along the line proposed in Ref. [67]. As an important part of this effort, we present a detailed analysis of

the effects of the boost on the radial shape of the effective interaction.

Because of the strong relation between boost corrections and irreducible NNN interactions, in the last part of this Thesis we present the results of an analysis aimed at inferring direct information on the NNN repulsion from multimessenger astrophysical observations [72–74]. Indeed, unlike the NN potential, phenomenological models of NNN interactions are only constrained by the physics at saturation density, but their contribution to the EOS becomes larger and larger as the density increases. Also in light of their connection with boost corrections, whose introduction yields another source of uncertainty on the NNN potentials, it is clear that any additional information about the behavior of such interaction at high density would represent a significant breakthrough. The Thesis is structured as follows. In Chapter 1 we summarize the main properties of neutron star structure and observables. In Chapter 2 we introduce the concept of nuclear Hamiltonian. The main features of phenomenological interaction potentials, as well as a comprehensive and pedagogical discussion of relativistic effects are presented. We give an introduction to the basic concepts of the many-body theory and methods, necessary to describe infinite nuclear matter, in Chapter 3. In the final section of that chapter we also review in depth the characterizing traits of the APR EOSs. In Chapter 4 we finally introduce the effective interaction formalism. A formal description of the introduction of boost corrections within this framework, as well as their impact on the shape of the radial functions of the effective interaction is presented. In Chapter 5 we report a detailed analysis about the sensitivity of NS observables to NNN interactions. Finally in Chapter 6 we summarize all the work and expose our conclusions and potential future developments.

Unless otherwise stated, and with the exception of Chapter 1, we employ a system of units with $\hbar = c = 1$. Moreover, within the whole Thesis we will refer with ϱ to the number density and with ρ to the matter density. Summation over repeated indices is usually understood.

Chapter 1

Neutron Stars

Neutron Stars (NSs) are extremely compact astrophysical objects, with typical observed masses around one or two solar masses and estimated radii of about ten kilometers. Therefore one can imagine something as massive as our Sun but concentrated in a spherical region whose circumference is comparable to the GRA, the major highway surrounding Rome. In such conditions matter is super-compressed forming the perfect environment for the occurrence of unprecedented physical phenomena. In this sense, the observation of NS phenomenology opens a window onto microscopic physics in a regime which is impossible to be achieved in laboratory experiments.

NSs are believed to be one of the possible outcomes of the evolution of very massive stars. During the central phase of a star's evolution, the pressure needed to balance the gravitational attraction is provided by the thermonuclear reactions that happen in its core. When the fuel is all burnt out there is nothing left to contrast the self-gravity of the object and the star collapses. As the contraction goes on the temperature increases until thermonuclear reactions burning heavier elements set in and a new equilibrium is reached. This thermonuclear evolution goes on until the formation of the heaviest element allowed by the star's initial mass. For progenitor masses $\sim 8M_{\odot}$ (with M_{\odot} labeling the mass of the Sun), according to current theories, the collapse proceeds until it is halted by the degeneracy pressure of the electrons. The outer layers of the stars are then expelled as solar wind giving birth to a white dwarf, usually composed of oxygen and carbon. If the progenitor mass is in the range $\sim 8 - 10 M_{\odot}$ oxygen-neon-magnesium stars can form, but they are quite rare. White dwarfs can exist in stable configurations only if their mass is smaller than the Chandrasekhar limit, $M_{CH} \sim 1.4 M_{\odot}$.

If the mass of the progenitor belongs to the range $\sim 8M_{\odot} < m < 20 - 30M_{\odot}$ the evolution follows a different path. Nuclear processes are able to burn elements heavier than carbon and oxygen, and exothermic nuclear reactions can proceed until the production of ^{56}Fe , which is the most stable element in nature¹.

The process producing the iron core starts with silicon burning and goes through

¹No element heavier than ^{56}Fe can be generated by nuclear fusion of lighter elements through exothermic reactions.

these stages:



In addition to the appearance of the ${}^{56}\text{Fe}$, the above process produces neutrinos that interact very little with the surrounding matter and thus go away from the star bringing out a relevant fraction of energy. Moreover, as the core density increases, the inverse β decay (electronic capture)



that contributes to the production of neutrinos and therefore subtracts energy from the star, becomes more and more efficient. Other than the production of neutrinos, electronic capture tends to increase the number of neutrons. Therefore heavier elements than ${}^{56}\text{Fe}$ may be produced through neutron capture, that is an endothermic process. Finally there is another endothermic reaction, known as photo-disintegration that may take place. It is ignited by high energy photons ($> 8\text{MeV}$) and occurs as



All these processes have the effect of decreasing the kinetic energy and thus the pressure inside the core, destabilizing the star. When the mass of the core exceeds the Chandrasekar limit it collapses within a fraction of second and the interior matter can reach densities $\rho \sim 10^{14}\text{g/cm}^3$ i.e. comparable with the central density of atomic nuclei $\rho_0 = 2.67 \cdot 10^{14}\text{g/cm}^3$. At this stage the core behaves as a giant nucleus, made mostly of neutrons, and reacts elastically to further compression producing a shock wave which ejects a significant fraction of matter in the outer layers of the star in a great explosion. This phenomenon is called supernova explosion: the luminosity of the star suddenly increases to values exceeding the luminosity of the Sun ($L_\odot = 3.832 \cdot 10^{33}\text{erg/s}$) by a factor $\sim 10^9$, and elements heavier than ${}^{56}\text{Fe}$ are created. The remnant of this explosion is a nebula, in the middle of which sits the remnant of the core: a neutron star.

Neutron stars are often observed as *pulsars*, i.e. radio sources whose emission exhibits a very sharp periodicity, blinking on and off at a constant frequency. This periodicity is due to the fact that pulsars are rapidly rotating objects with strong magnetic fields ($B \sim 10^{11} - 10^{13}\text{Gauss}$) which emit beams of radio waves from the magnetic poles, that are not aligned with the rotation axis. The beam is clearly visible only when it points in the direction of the detectors.

In the rest of this chapter we will give an overview of the current knowledge of the internal structure of neutron stars.

1.1 Internal composition

As already mentioned in the Introduction, the description of matter at supranuclear density ($\rho > \rho_0$), which is believed to compose the core of a neutron star, is still

an open problem and represents one of the main challenges of modern physics. Nevertheless, there is a quite general consensus regarding the behavior of matter at lower densities because of the information coming from the experimental data about neutron rich nuclei. Typically a neutron star is thought to be composed by a sequence of layers with different composition and density, as depicted in Figure 1.1. Proceeding from the exterior, we first encounter an outer crust, 0.3 km thick, an inner crust, $\sim 0.5 \text{ km}$ thick and a core that extends over 10 km .

The density of the neutron star core ranges between $\sim \rho_0$ ($= 2.67 \cdot 10^{14} \text{ g/cm}^3$) at the boundary with the inner crust to a central value that can be as large as $\rho \sim 4 \cdot 10^{15} \text{ g/cm}^3$. All models of EOS based on hadronic degrees of freedom predict that in the density range $\rho_0 < \rho < 2\rho_0$ neutron star matter consists mainly of neutrons together with a small fraction of protons, electrons and muons in β equilibrium and electrically neutral. This picture may change significantly at larger densities with the appearance of heavy strange baryons, such as the Σ^- produced by the weak reaction



that could be energetically favored when the sum of electron and neutron chemical potential equals the one of Σ^- . Finally since nucleons are composite objects of size $\sim 0.5 - 1.0 \text{ fm}$ i.e. of density $\sim 10^{15}$, one could expect that whenever matter reaches these conditions a transition to a new phase may take place. This could lead to a situation in which quarks are no longer confined into hadrons [75]. A recent study has pointed out how deconfined quark matter is very likely to be present in the innermost region of maximally massive neutron stars, with masses exceeding $\sim 2 M_\odot$ [34].

In the description of the neutron star interior we shall assume that the temperature is equal to zero and that matter is transparent to neutrinos. The first assumption is justified because the observed temperature of neutron stars are $T \leq 10^9 \text{ K}$, whereas the Fermi temperature of neutrons ($T_F = \epsilon_F/k_B$) at the typical densities of neutron stars reaches $\sim 3 \cdot 10^{11} - 10^{12} \text{ K} \gg 10^9 \text{ K}$. The second assumption follows from the fact that the mean free path of neutrinos in nuclear matter at temperature $T \leq 10^9 \text{ K}$ is much larger than the typical radius of a neutron star.

For an extensive treatment of the topics touched in this first chapter, the interested reader can look at Ref. [76] and references therein.

1.1.1 Outer crust

The outer crust corresponds to densities ranging from $\sim 10^7 \text{ g/cm}^3$ to $\rho_d = 4 \cdot 10^{11} \text{ g/cm}^3$. It is a solid layer composed by a lattice of heavy nuclei immersed in an electron gas. Proceeding towards the star interior the density increases, and the inverse β decay becomes more and more efficient, thanks to the increasing Fermi momentum of the electron gas that shifts the energy balance. As a result a large number of neutrons are produced in the density region $10^7 - 10^{11} \text{ g/cm}^3$ and new nuclear species appear through the sequence



This process is called *neutronization*. In this region the pressure is mainly due to the degenerate electron gas. When the density approaches the so called neutron

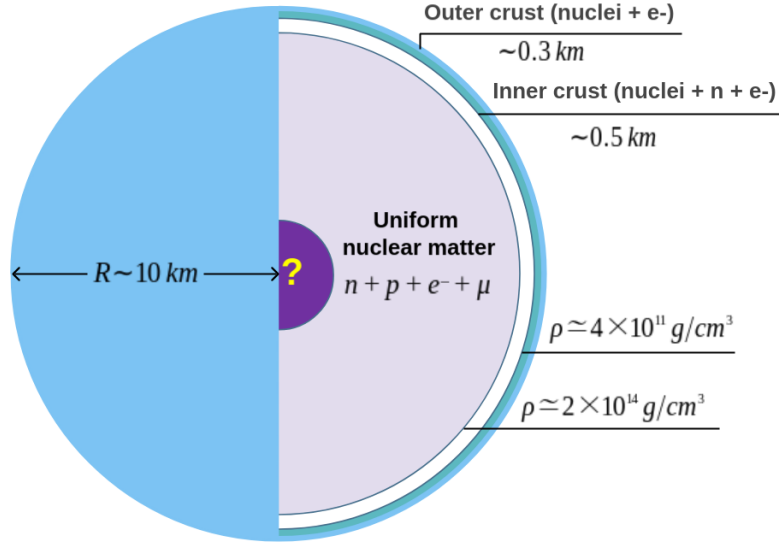


Figure 1.1. Schematic illustration of neutron star section.

drip density, ρ_d , all nuclear bound states available for neutrons are filled, therefore they can no longer live bound to nuclei and start to leak out. This effect is called *neutron drip*.

1.1.2 Inner crust

In this region density ranges between ρ_d and $\rho_0 = 2.67 \cdot 10^{14} \text{ g/cm}^3$. As already said, in this regime, since neutrons created by electron capture begins to drip out of the nuclei, the ground state corresponds to a mixture of two phases: matter consisting in neutron rich nuclei containing also the relevant fraction of protons, referred to as Proton Rich Matter (PRM), and a neutron gas (NG). In addition there is the electron gas to ensure charge neutrality. The fundamental state of matter in this region is affected by the density of the two phases ρ_{PRM} and ρ_{NG} , by the proton fraction in PRM and by the geometrical properties of the structures that are formed by the two phases which strongly depend on surface effects at the interface of different phases. Recent studies suggest that at densities $\rho_d < \rho < 0.35\rho_0$ the PRM is arranged in spheres, surrounded by a gas of electrons and neutrons. For higher densities the separation between spheres decreases up to the touching limit. In the region with $0.35\rho_0 < \rho < 0.5\rho_0$ the spheres merge forming bar-type structures, and when $0.5\rho_0 < \rho < 0.56\rho_0$ bars merge to form slab-type structures. With increasing density nuclear matter occupies most of the volume with the exception of tubes that later becomes bubbles of the neutron-electron gas. Because of the peculiar shape of these phases they take the name of *nuclear pasta* (*gnocchi*, *spaghetti*, *lasagna*) [77,78]. A schematic representation of these pasta phases can be seen in Fig. 1.2. Finally when the density approaches ρ_0 a new transition to uniform nuclear matter occurs and the two phases form an homogeneous fluid of protons, neutrons and electrons.

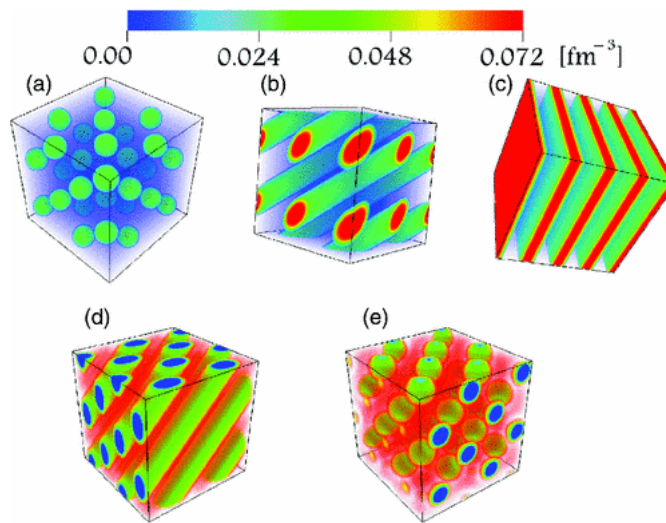


Figure 1.2. Schematic representation of nuclear pasta phases in the inner crust [78]

1.1.3 The core

The core matter is characterized by densities $\rho \gtrsim 10^{14} \text{ g/cm}^3$ and it can be thought as an homogeneous fluid of p , n , e^- in β equilibrium. At higher densities several processes may occur. For instance, as the density increases, electrons become more energetic and therefore their chemical potential, that is the energy needed to insert a new particle in the system at equilibrium, increases too. As the electrons chemical potential exceeds the rest mass of the muon, $m_\mu = 105.7 \text{ MeV}/c^2$, the neutron decay



becomes energetically favoured than the usual β decay, leading to the appearance of muons. At these densities the main contribution to the pressure must come from neutrons. However it cannot be associated with the Pauli exclusion principle only, because we cannot consider the neutrons as non-interacting particles. The treatment of the interacting problem is made very complex by the very nature of the strong interactions and the EOS of matter at supranuclear density depends on the particular model employed to describe nuclear dynamics. A detailed description of the behavior of matter in these conditions is reserved to the next chapters of this Thesis.

1.2 Stellar structure equations

Since neutron stars are astrophysical objects we need a way to link the description of their internal composition to macroscopic observables, such as mass and radius. Within the framework of Newtonian gravity we can derive the equations describing the stellar structure by imposing the hydrostatic equilibrium of a self gravitating perfect fluid. Unfortunately because of their high compactness we can't neglect the spacetime curvature when dealing with neutron stars (typical values of mass and radius give $GM/Rc^2 \sim 10^{-1}$) and General Relativity must be employed. In

the following section we will make a brief recap of General Relativity in order to introduce the basic concepts necessary to carry out the Tolman-Oppenheimer and Volkoff (TOV) equations, the general relativistic analogue of the stellar structure equations.

1.2.1 General Relativity

General Relativity is the spacetime theory of gravity proposed by Einstein in 1915. Within this framework spacetime becomes for the first time an active physical entity whose curvature is responsible for gravitational phenomena. This revolutionary theory is entirely based upon two principles:

- the Equivalence Principle, stating that in any given spacetime point it's always possible to choose a local inertial reference frame in which the physical laws are those described by special relativity i.e. in absence of gravity;
- the Principle of General Covariance stating that physical laws have to be the same in every coordinate system.

The Equivalence Principle establishes the connection between gravity and the spacetime curvature. Before Einstein published his work, Gauss identified a class of metric spaces in which the curvature could be locally ruled out. The concept of curvature is strongly related to how one can calculate the distance between two points, therefore stating that the curvature can be locally eliminated is equivalent to say that the distance between two points, which are sufficiently close to each others, can be evaluated using the euclidean formula

$$ds^2 = \sum_{i=1}^N dx_i^2, \quad (1.9)$$

where N is the dimension of the metric space. In a similar manner the Equivalence Principle states that is always possible to chose two events that are close enough such that the distance between them is given by

$$ds^2 = -dx_0^2 + \sum_{i=1}^3 dx_i^2. \quad (1.10)$$

Therefore the equivalence principle is basically the same principle that Gauss used for the definition of non-euclidean geometries. According to this principle we expect that the equations of gravity will look very similar to those of Riemannian geometry. The relevant quantity in such a framework becomes the metric tensor $g_{\mu\nu}$ that allows to compute the distance between two points according to

$$ds^2 = g_{\mu\nu}(x) dx^\mu dx^\nu. \quad (1.11)$$

The metric tensor depends on the spacetime point in which it is evaluated, and on the particular choice of coordinate system. In a locally inertial frame (LIF) we have that the metric tensor becomes the same of the flat spacetime i.e. $g_{\mu\nu} = \eta_{\mu\nu}$ with

$$\eta_{\mu\nu} = \begin{pmatrix} -1 & 0 & 0 & 0 \\ 0 & 1 & 0 & 0 \\ 0 & 0 & 1 & 0 \\ 0 & 0 & 0 & 1 \end{pmatrix}. \quad (1.12)$$

Being ξ^α a set of coordinates in a LIF and x^α a coordinate set in a generic reference frame then we have

$$ds^2 = \eta_{\mu\nu} d\xi^\mu d\xi^\nu = \eta_{\mu\nu} \frac{\partial \xi^\mu}{\partial x^\alpha} \frac{\partial \xi^\nu}{\partial x^\beta} dx^\alpha dx^\beta = g_{\alpha\beta} dx^\alpha dx^\beta. \quad (1.13)$$

From the last equation we can infer the transformation law of the metric tensor

$$\begin{aligned} x^\alpha &\rightarrow x^{\alpha'}(x^\mu) \\ g_{\alpha\beta} &\rightarrow g_{\alpha'\beta'} = \frac{\partial x^\mu}{\partial x^{\alpha'}} \frac{\partial x^\nu}{\partial x^{\beta'}} g_{\mu\nu} \equiv \Lambda_{\alpha'}^\mu \Lambda_{\beta'}^\nu g_{\mu\nu}. \end{aligned} \quad (1.14)$$

We define the inverse metric $g^{\mu\nu}$ as:

$$g^{\mu\alpha} g_{\alpha\nu} = \delta^\mu_\nu, \quad (1.15)$$

that allows for raising and lowering a tensor index through

$$A^\mu{}_\nu = g^{\mu\alpha} A_{\alpha\nu}. \quad (1.16)$$

We can also deduce the geodesic equation, i.e. the equation of motion of a particle under the effect of gravity when observed in a generic reference frame. If the ξ^α s are the coordinates in a LIF and τ is the proper time of the particle we have

$$\frac{d^2 \xi^\alpha}{d\tau^2} = 0. \quad (1.17)$$

Using the general coordinate transformation $\xi^\alpha = \xi^\alpha(x^\mu)$ and after making some composite derivatives we get

$$\frac{d^2 x^\alpha}{d\tau^2} + \Gamma_{\mu\nu}^\alpha \left[\frac{dx^\mu}{d\tau} \frac{dx^\nu}{d\tau} \right] = 0, \quad (1.18)$$

where the quantities

$$\Gamma_{\mu\nu}^\alpha = \frac{\partial x^\alpha}{\partial \xi^\lambda} \frac{\partial \xi^\lambda}{\partial x^\mu \partial x^\nu}, \quad (1.19)$$

are called *affine connections* or *Christoffel symbols* and satisfy

$$\Gamma_{\mu\nu}^\alpha = \frac{1}{2} g^{\alpha\lambda} (g_{\mu\lambda,\nu} + g_{\lambda\nu,\mu} - g_{\mu\nu,\lambda}). \quad (1.20)$$

We remark the fact that the affine connections aren't tensors since they don't obey the tensor transformation rules. The Christoffel symbols can be used to define a *covariant derivative* i.e. a derivative that transforms like a tensor under the change of coordinate frames. The covariant derivative of a vector V^μ is defined as

$$V^\mu{}_{;\alpha} = V^\mu{}_{,\alpha} + \Gamma_{\alpha\beta}^\mu V^\beta. \quad (1.21)$$

It can be shown that $V^\mu{}_{;\alpha}$ transforms as a tensor and that in a locally inertial frame the covariant derivative reduces to the usual derivative, which means $V^\mu{}_{;\alpha} = V^\mu{}_{,\alpha}$.

All these considerations can be made more formal by using the theory of the differentiable manifolds, but we won't go into the details.

We limit ourselves to report the Einstein equations that embody the dynamics of gravitation

$$G_{\mu\nu} = \frac{8\pi G}{c^4} T_{\mu\nu}. \quad (1.22)$$

In the above equation $T^{\mu\nu}$ is the energy-momentum tensor whose components are defined as follows. T_{00} is the energy density, T_{0i} is the energy which flows per unit time across a unit surface orthogonal to the axis x^i , and T_{ij} is the amount of the i -th component of momentum which flows per unit time across the unit surface orthogonal to the axis x^j . $G_{\mu\nu}$ is the so-called Einstein tensor and its related to the underlying spacetime geometry. It is defined as

$$G_{\mu\nu} = \left(R_{\mu\nu} - \frac{1}{2} g_{\mu\nu} R \right) \quad (1.23)$$

where $R_{\mu\nu}$ and R depend upon the metric tensor and its derivatives and are therefore directly related to the spacetime curvature. Equation (1.22) establishes a connection between the spacetime geometry and the amount of mass-energy that is present.

It is interesting to see how we can recover Newtonian gravity from the Einstein equations. Let us consider a non relativistic particle in a weak and stationary gravitational field. Since $v \ll c$ it follows

$$\frac{dx^i}{dt} \ll c \Rightarrow \frac{dx^i}{d\tau} \ll \frac{cdt}{d\tau} = \frac{dx^0}{d\tau}. \quad (1.24)$$

The geodesic equation (1.18) therefore becomes:

$$\frac{d^2 x^\mu}{d\tau^2} + \Gamma_{00}^\mu \left(\frac{dx^0}{d\tau} \right)^2 = 0. \quad (1.25)$$

If we use the assumption that the field is stationary, i.e. we can take a time-independent metric tensor, according to equation (1.20) we have

$$\Gamma_{00}^\mu = \frac{1}{2} g^{\mu\lambda} (g_{0\lambda,0} + g_{\lambda 0,0} - g_{00,\lambda}) = -\frac{1}{2} g^{\mu\lambda} g_{00,\lambda}. \quad (1.26)$$

Now we consider the case of a weak gravitational field, which means that we can chose a reference frame in which the metric is nearly flat

$$g_{\mu\nu} = \eta_{\mu\nu} + h_{\mu\nu}, \quad |h_{\mu\nu}| \ll 1. \quad (1.27)$$

Since we are going to keep only the leading order in $h_{\mu\nu}$ we can raise and lower its indices with the flat metric $\eta_{\mu\nu}$. Substituting Eq. (1.27) into (1.26) we have

$$\Gamma_{00}^\mu \sim -\frac{1}{2} \eta^{\mu\lambda} \frac{\partial h_{00}}{\partial x^\lambda} \quad (1.28)$$

that put into (1.25) yields

$$\frac{d^2 x^i}{d\tau^2} = \frac{1}{2} \frac{\partial h_{00}}{\partial x^i} \left(\frac{cdt}{d\tau} \right)^2. \quad (1.29)$$

If we rescale the time coordinate according to $cdt/d\tau = 1$ we find

$$\frac{d^2\mathbf{x}}{dt^2} = \frac{c^2}{2}\nabla h_{00}. \quad (1.30)$$

Since the equation of motion of a particle in a Newtonian gravitational field is given by

$$\frac{d^2\mathbf{x}}{dt^2} = \nabla\Phi, \quad (1.31)$$

if we take $\Phi = -GM/r$ and impose that h_{00} vanishes at infinity we finally have the correspondence we were looking for

$$h_{00} = -\frac{2\Phi}{c^2} \quad \text{and} \quad g_{00} = -\left(1 + \frac{2\Phi}{c^2}\right). \quad (1.32)$$

The Newtonian potential Φ satisfies the Poisson equation

$$\nabla^2\Phi = 4\pi G\rho, \quad (1.33)$$

where ρ is the matter density. Substituting (1.32) into Eq. (1.33) yields

$$\nabla^2 g_{00} = -\frac{8\pi G}{c^4}T_{00} \quad (1.34)$$

where we have used the identity

$$\frac{T_{00}}{c^2} = \rho, \quad (1.35)$$

which holds in the non-relativistic limit. Since Eq. (1.34) can also be obtained as the limit in the case of weak stationary field for the $(0,0)$ component of the Einstein equations, we can finally say that in the limit of weak field and little velocity General Relativity reduces to Newtonian gravity.

1.2.2 TOV equations

In order to carry out the general relativistic stellar structure equations we have to solve the Einstein equations in the presence of matter. Hereafter we shall use geometric units $G = c = 1$.

We can model a star as a stationary spherically symmetric perfect fluid in chemical, hydrostatic and thermodynamic equilibrium. A fluid is said to be perfect if both viscosity and heat flow are absent. The motion of the fluid is described by the vector field of the four-velocity u^α that will define a worldtube in the spacetime. Consider a small volume of fluid and a point P_0 in its center of mass. We put ourselves in a locally inertial reference frame with the origin in P_0 and such that P_0 is at rest. We name it a locally inertial comoving frame (LICF). We have to take into account a worldvolume small enough to be covered by the LICF, and large enough with respect to the scale of the microscopic dynamics of the system. The fluid element enclosed in this worldvolume can be described by the usual thermodynamic quantities.

In this LICF the stress-energy tensor of the fluid assumes the form

$$T^{\mu\nu} = \begin{pmatrix} \epsilon & 0 & 0 & 0 \\ 0 & P & 0 & 0 \\ 0 & 0 & P & 0 \\ 0 & 0 & 0 & P \end{pmatrix} \quad (1.36)$$

where ϵ is the energy density and P is the pressure. The components T^{0i} vanish because the fluid is at rest and there is no heat flux. The absence of viscosity put at zero the components T^{ij} with $i \neq j$. Since we are in a LICF we also have

$$g_{\mu\nu} = \eta_{\mu\nu} \quad \text{and} \quad u^\alpha = (1, 0, 0, 0), \quad (1.37)$$

Putting together Eqs. (1.36) and (1.37), $T^{\mu\nu}$ can be written as

$$T^{\mu\nu} = u^\mu u^\nu (\epsilon + P) + g^{\mu\nu} P. \quad (1.38)$$

This definition of $T^{\mu\nu}$ involves a tensorial equation and therefore it holds any reference frame.

The Einstein equations can be solved together with the additional condition coming from the energy and momentum conservation, i.e.

$$T^{\mu\nu}{}_{;\nu} = 0. \quad (1.39)$$

Since we are interested in the structure of a spherically symmetric, non rotating and stationary star, the most general metric according to these properties can be written as

$$ds^2 = g_{\mu\nu} dx^\mu dx^\nu = -e^{2\nu(r)} dt^2 + e^{2\lambda(r)} dr^2 + r^2 (d\theta^2 + \sin^2 \theta d\phi^2), \quad (1.40)$$

thus

$$g_{\mu\nu} = \begin{pmatrix} -e^{2\nu(r)} & 0 & 0 & 0 \\ 0 & e^{2\lambda(r)} & 0 & 0 \\ 0 & 0 & r^2 & 0 \\ 0 & 0 & 0 & r^2 \sin^2 \theta \end{pmatrix}. \quad (1.41)$$

With this metric and with the hypothesis that the fluid is at rest, the 4-velocity u^α is given by

$$-1 = u^\alpha u^\beta g_{\alpha\beta} = (u^0)^2 g_{00} \Rightarrow u^\alpha = (e^{-\nu(r)}, 0, 0, 0). \quad (1.42)$$

Since $R_{\mu\nu}$ and R are defined respectively as

$$R_{\mu\nu} = \left(\Gamma_{\mu\alpha,\nu}^\alpha - \Gamma_{\mu\nu,\alpha}^\alpha - \Gamma_{\mu\nu}^\alpha \Gamma_{\alpha\beta}^\beta + \Gamma_{\mu\beta}^\alpha \Gamma_{\nu\alpha}^\beta \right) \quad (1.43)$$

and

$$R = g^{\mu\nu} R_{\mu\nu}, \quad (1.44)$$

we can finally write the non vanishing components of the Einstein equations as

$$\begin{aligned} a) \quad G_{00} &= 8\pi T_{00} \Rightarrow \frac{1}{r^2} e^{2\nu} \frac{d}{dr} \left[r (1 - e^{-2\lambda}) \right] = 8\pi \epsilon e^{2\nu} \\ b) \quad G_{rr} &= 8\pi T_{rr} \Rightarrow -\frac{1}{r^2} e^{2\lambda} (1 - e^{-2\lambda}) + \frac{2}{r} \nu_{,r} = 8\pi P e^{2\lambda} \\ c) \quad G_{\theta\theta} &= 8\pi T_{\theta\theta} \Rightarrow r^2 e^{-2\lambda} \left[\nu_{,rr} + \nu_{,r}^2 + \frac{\nu_{,r}}{r} - \nu_{,r} \lambda_{,r} - \frac{\lambda_{,r}}{r} \right] = 8\pi r^2 P. \end{aligned} \quad (1.45)$$

From equation (1.39) it follows

$$\nu_{,r} = -\frac{P_{,r}}{\epsilon + P}, \quad (1.46)$$

that combined with (1.45) leads to the final set of equations

$$\left\{ \begin{array}{l} \frac{dM(r)}{dr} = 4\pi r^2 \epsilon(r) \\ \frac{dP}{dr} = -\frac{[\epsilon(r) + P(r)] [M(r) + 4\pi r^3 P(r)]}{r [r - 2M(r)]} \end{array} \right. \quad (1.47)$$

where $M(r)$ is defined as

$$M(r) = \frac{1}{2} r \left(1 - e^{-2\lambda(r)} \right). \quad (1.48)$$

The set of equations (1.47) was derived independently by Tolman [79] and Oppenheimer and Volkoff [80] in 1939 and for this reason they are called the TOV equations. The second equation of (1.47) can be cast into the form

$$\frac{dP}{dr} = -\epsilon(r) \frac{GM(r)}{r^2} \left[1 + \frac{P(r)}{\epsilon(r)} \right] \left[1 + \frac{4\pi r^3 P(r)}{M(r)} \right] \left[1 - \frac{2GM(r)}{r} \right]^{-1}, \quad (1.49)$$

where we have restored the gravitational constant G . This form makes explicit the physical origin of the different contributions. The first term is the same that is present in its Newtonian counterpart, with the mass density replaced by the energy density. The second and third terms represent relativistic corrections that vanish when $P/\epsilon \ll 1$ i.e. when the constituents of matter are non-relativistic particles. Finally the last term accounts for spacetime curvature, indeed it vanishes when $GM/r \ll 1$. Therefore it is clear that in the non-relativistic limit the TOV equations reduce to the usual Newtonian equations. Finally we remark the fact that these equations cannot be solved without the knowledge of the equation of state (EOS) describing the behavior matter in the star interior, that in our case assumes the form of a $P(\epsilon)$ relation.

1.2.3 Boundary conditions

In order to solve the set of equations (1.47), for any given EOS $P(\epsilon)$, we have to specify two boundary conditions: $M(r_0)$ and $P(r_0)$. We can always chose as a boundary condition $M(r=0) = 0$. This choice can be justified as follows. Take a tiny sphere of radius x and circumference $2\pi x$. The proper radius will be

$$\int_0^x e^{\lambda} dr \simeq e^{\lambda} x. \quad (1.50)$$

Therefore the ratio between the circumference and the proper radius will be $2\pi e^{-\lambda}$. But we know that the spacetime is locally flat, and since a flat space-time implies that such a ratio should be 2π , we will have that as $r \rightarrow 0$ then $e^{\lambda} \rightarrow 1$. Because of the relation

$$e^{2\lambda} = \frac{1}{1 - \frac{2M(r)}{r}}, \quad (1.51)$$

it follows that $M(r)$ has to go to zero faster than r . The quantity

$$M(R) = 4\pi \int_0^R r^2 \epsilon(r) dr, \quad (1.52)$$

can be interpreted as the total mass-energy inside the radius R .

For any assigned EOS now we have a one-parameter family of solutions, identified by the value of the energy density at $r = 0$, i.e. $\epsilon(r = 0) = \epsilon_0$. Outside the star, instead, $P = 0$ and $\epsilon = 0$, and the Einstein equations reduce to those in vacuum, whose unique solution is given by the Schwarzschild metric.

1.2.4 A necessary condition for the stability of a star

The solution of the TOV equations, with the appropriate boundary conditions, describe the equilibrium configuration of a star. In principle this equilibrium could be stable or unstable. We are now interested in discussing whenever one of these two possible scenarios may occur. Suppose to have solved the TOV equations for any value of the central energy density ϵ_0 , i.e. to have found the function $M(\epsilon_0)$ that relates the total gravitational mass of the star to its central energy density.

A typical $M(\epsilon_0)$ curve is illustrated in Fig. 1.3.

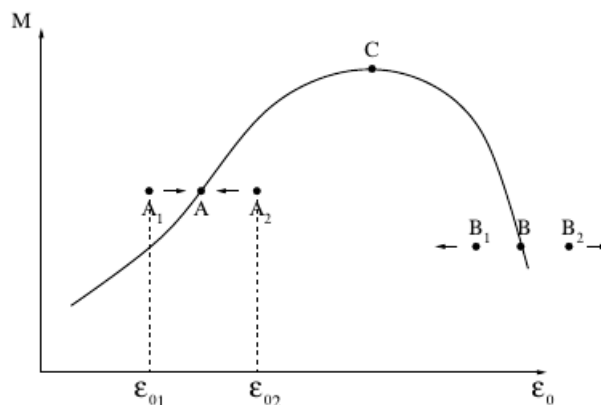


Figure 1.3. The mass of a star as function of the central energy density [81]

Now consider an equilibrium configuration such as the one labelled as A in the figure. Let's consider a small perturbation of the central density, we can have two possible outcomes. If the density decreases to a value ϵ_{01} , the star will have a mass that is above the value required for hydrostatic equilibrium (A_1 in the picture), therefore the gravitational attraction generates a further contraction and the density increases until the equilibrium is reached. Conversely if the density increases to a value ϵ_{02} , the star will be in a configuration (A_2) in which its mass is too low in order for gravity to balance the internal pressure. This generates an expansion that lowers the density and brings the star again in an equilibrium configuration. After these considerations we can conclude that the equilibrium in A is stable.

Conversely, a similar discussion can be done about the point B in the picture, which lays on the right branch of the curve $M(\epsilon_0)$ with respect to its maximum.

From Fig. 1.3 we infer that a displacement to a configuration B_1 leads to a gravity weaker than the internal pressure and an uncontrolled expansion causes the density to become lower and lower. Alternatively the displacement to a configuration B_2 provides the star to collapse under its own gravity. Therefore the equilibrium in B is unstable. In light of the previous discussion we can conclude that a necessary condition for the stability of a star is provided by the requirement

$$\frac{dM}{d\epsilon_0} > 0. \quad (1.53)$$

The previous condition represents only a necessary requirement for the stability, but not a sufficient one. In order to conclude if a given configuration is effectively stable it is necessary to analyze the oscillation behavior of the star. A comprehensive description of the theory of radial oscillation is beyond the scope of this Thesis, we limit ourselves to a qualitative but somehow instructive explanation. According to the theory of radial perturbation each star has an infinite number of proper oscillation modes ω_n , with $n = 0, 1, 2, \dots$. During the star oscillation each fluid element is moved from its equilibrium position by a radial displacement $\xi(r, t)$. In the n -th mode this radial displacement takes the form

$$\xi(r, t) = u_n(r)e^{i\omega_n t}. \quad (1.54)$$

where $u_n(r)$ is the oscillation amplitude and ω_n is the frequency. The oscillation frequency of different modes are ordered according to

$$\omega_0^2 < \omega_1^2 < \omega_2^2 < \dots, \quad (1.55)$$

and ω_0 is referred to as the fundamental mode. Since ω_n^2 could be either positive or negative, it turns out that if $\omega_n^2 > 0$ we have that Eq. (1.54) actually describes an oscillation around the equilibrium configuration. On the other hand if $\omega_n^2 < 0$ we have that the radial displacement can grow exponentially making the mode unstable. Since the modes are ordered according to Eq. (1.55) it is clear that if the fundamental mode is stable every other mode will also be.

1.2.5 Early considerations about the EOS

The equation of state is a relation between the thermodynamic quantities of a given system, reflecting the microscopic behavior of its constituents. In the case of neutron stars, as we said in the previous section, we are looking for an EOS of the form

$$P = P(\epsilon), \quad (1.56)$$

which is called a *barotropic* equation of state. However the thermodynamic quantities characterizing a fluid, such as the one present inside a neutron star, could be more than just the pressure and the energy density. In the most general case we should have the pressure P , the energy density ϵ , the temperature T and the number of particles N . Therefore a generic EOS should be in principle of the form $f(P, \epsilon, T, N) = 0$. Anyway a barotropic EOS turns out to be perfectly suited for the description of NS matter. First of all we can rule out the temperature dependence by noting that

the typical observed NS temperatures, which are of the order of $T \sim 10^9 K$, are much smaller than the Fermi temperature of nucleons at the typical NS densities, $T_F \sim 10^{11-12} K$. Thanks to these considerations we can safely put $T = 0$. Concerning the dependence on the number of particles N , we can exploit an accidental symmetry of the Universe, the conservation of the baryon number. If we assume that the star does not contain antimatter and that the number of mesons is negligible, the baryon number coincides with the number of baryons in the system. Since baryons are much heavier than electrons, muons and neutrinos, the star rest mass can be considered as due to baryons only. Thanks to the baryon number conservation law we can fix N and rule out its dependence from the EOS.

At first one could be tempted to model NS matter with a degenerate neutron gas in the same way as what is done with electrons in white dwarfs. There was a pioneering study, carried out in 1939 by Oppenheimer and Volkoff [80], where they studied this possibility. This work has shown that stars made up by non-interacting neutrons should have a mass not larger than $\sim 0.8M_\odot$. This is in contrast with several observations of neutron stars with masses much bigger than this theoretical limit, pointing out that neutron star equilibrium requires an additional pressure other than the degeneracy one. The origin of this pressure has to be ascribed to hadronic interactions. Unfortunately the need to include dynamical effects in the EOS collides with the complexity of the fundamental theory of strong interactions. As a consequence all available descriptions of the EOS of neutron star matter are obtained within phenomenological or effective theoretical models as much as possible constrained by empirical data.

1.3 Tidal deformability

On August 17, 2017 Advanced LIGO and Advanced Virgo made the first observation of the gravitational-wave (GW) signal emitted by a binary neutron-star merger. This discovery opened the door to a new frontier in the search for EOS probes in astrophysical observation. It was shown in several works that the GW signals coming from a binary neutron star merger can be affected by measurable EOS dependent effects, such as rotational and tidal deformations. These effects contribute to distinguishing the signal provided by two neutron stars from that of two black holes which have no internal structure. Some features and techniques concerning how these effects can be seen in the gravitational waveforms, with particular attention to the high spin deformation effects, are reviewed in [82].

In this work we take in consideration only tidal effects whose relevance is quantified by a parameter known as the *tidal Love number*.

The idea is as follows. The orbital motion of a binary neutron star system produces GWs that carry out energy and angular momentum from the system. This causes the decreasing of the orbital radius, and conversely the increasing in the frequency. At early times the two objects have a large orbital separation and low orbital frequency. In this phase the bodies behave as point particles and the evolution of the frequency is primarily determined by the chirp mass \mathcal{M} , defined as

$$\mathcal{M} = \frac{(m_1 m_2)^{3/5}}{(m_1 + m_2)^{-1/5}}, \quad (1.57)$$

where m_1 and m_2 are the two component masses. As the orbit shrinks, relativistic effects related for example to spin-orbit and spin-spin couplings become increasingly relevant.

The details about the internal structure of the two objects become important as the orbit separation approaches the size of the bodies. For neutron stars, the tidal field of one of them induces a mass-quadrupole moment on the companion, which in turn generates the same effect on the other one, accelerating the coalescence. This effect is quantified by the ratio of the induced quadrupole moment to the external tidal field, that is proportional to the tidal deformability

$$\Lambda = \frac{2}{3} k_2 \left(\frac{c^2 R}{Gm} \right)^5, \quad (1.58)$$

where R and m are respectively the radius and the mass of the star, whereas k_2 is the second tidal Love number. For any given stellar mass m , R and k_2 are uniquely determined by the EOS of neutron-star matter. Tidal effects are predicted to become relevant near frequencies $f_{GW} \simeq 600 \text{ Hz}$, being potentially observable even if, at these frequencies, the stars are close to merge and the sensitivity of the instruments has begun to decrease. Experimentally the properties of the GW sources are inferred by matching the data with predicted waveforms.

We will not go into details about how tidal deformations affect the waveform of the measured GW signals. We are much interested in the definition and calculation of the tidal Love number and its relation to the underlying microscopic dynamics.

1.3.1 Newtonian theory

A tide is a deformation effect induced on a body because of the variation of the gravitational force acting on it. If we consider a quadrupolar tidal field its effect on a given body is characterized by the quantity \mathcal{E}_{ij} , known as tidal momentum and defined as

$$\mathcal{E}_{ij} = - \left. \frac{\partial^2 \Phi_{\text{ext}}}{\partial x_i \partial x_j} \right|_{\mathbf{x}=\mathbf{x}_c} \quad (1.59)$$

where i and j range from 1 to 3, Φ_{ext} is the Newtonian external potential and \mathbf{x}_c labels the position of the center of mass of the body.

Let's consider a non rotating spherical object A, under the gravitational field of a point-like source B, at distance a from the center of mass of A. We are interested in the force acting on a point P, with mass m_P , on the surface of A. We can therefore write the equation of motion of P in a generic reference frame as

$$m_P \mathbf{a}_P = -g_A m_P \cdot \hat{\mathbf{u}}_P + \mathbf{F}_{AB} = -g_A m_P \cdot \hat{\mathbf{u}}_P - m_P \nabla \Phi(\mathbf{r}_P). \quad (1.60)$$

In the above equation g_A is the surface gravity acceleration of A, \mathbf{r}_P is the position of P, $\Phi(\mathbf{r}_P)$ is the gravitational potential of B in the point \mathbf{r}_P and $\hat{\mathbf{u}}_P$ is given by

$$\hat{\mathbf{u}}_P = \frac{\mathbf{r}_P - \mathbf{r}_c}{|\mathbf{r}_P - \mathbf{r}_c|} \quad (1.61)$$

with \mathbf{r}_c being the position of the center of mass of A. We can now expand the gradient of $\Phi(\mathbf{x})$ around $\mathbf{x} = \mathbf{r}_c$ and keeping only the first two terms we find

$$\frac{\partial \Phi}{\partial x_i} \approx \left. \frac{\partial \Phi}{\partial x_i} \right|_{r_c} + \left. \frac{\partial^2 \Phi}{\partial x_j \partial x_i} \right|_{r_c} (\mathbf{x} - \mathbf{r}_c)_j = \left. \frac{\partial \Phi}{\partial x_i} \right|_{r_c} - \mathcal{E}_{ji} (\mathbf{x} - \mathbf{r}_c)_j. \quad (1.62)$$

If we now put ourselves in the center-of-mass frame of A and neglect the effect of rotations (both around the symmetry axis of the body and around the center of mass of the system A+B) we find that the tidal force acting on P—that is the force not ascribed to the own gravity of A—is given by

$$F_i^{\text{tidal}} = m_P x_j \mathcal{E}_{ji} = -m_P \frac{\partial \Phi^{\text{tidal}}}{\partial x_i} \quad (1.63)$$

where we labeled as x_i the position in the center-of-mass frame and we defined a tidal potential, whose minus gradient gives rise to the tidal force F^{tidal} , as

$$\Phi^{\text{tidal}} = \frac{1}{2} x_i x_j \mathcal{E}_{ij}. \quad (1.64)$$

The *tidal moment* \mathcal{E}_{ij} is a symmetric tensor, and since the gravitational potential satisfies the Laplace equation in vacuum it is also traceless. We call it a symmetric traceless (STL) tensor. Since we have a quadrupolar external tidal potential we expect that the body will develop a quadrupolar deformation, i.e. it will acquire a mass quadrupole moment Q_{ij} . The quadrupole moment is given by

$$Q_{ij} = \int d^3x \rho(\mathbf{x}) \left(x_i x_j - \frac{1}{3} r^2 \delta_{ij} \right), \quad (1.65)$$

where ρ is the mass density, x_i is the i -th coordinate with respect to a reference frame set in the center of mass of the body, and $r^2 = (\delta_{ij} x_i x_j)$. We also remark that Q_{ij} is another STL tensor.

In the case of a weak tidal field we will have a linear relation between Q_{ij} and \mathcal{E}_{ij} i.e.

$$Q_{ij} = -\lambda \mathcal{E}_{ij}, \quad (1.66)$$

and by dimensional considerations follows that

$$\lambda = \frac{2}{3} k_2 R^5 G^{-1}, \quad (1.67)$$

where R is the star radius, the factor $2/3$ is a convention and the adimensional constant k_2 is the second tidal Love number that quantifies the quadrupolar tidal deformation.

Using these expressions we can write the potential outside the body as a sum between the body and the external potentials, yielding

$$\Phi_{\text{tot}} = -\frac{M}{r} - \frac{3}{r^5} Q_{ij} x_i x_j + \frac{1}{2} \mathcal{E}_{ij} x_i x_j. \quad (1.68)$$

In this last equation the total potential was truncated to the leading, quadrupole order in a Taylor expansion of both the external and the body potential. The first

two terms account for the potential generated by the deformed object, indeed we can see a monopole and a quadrupole term, whereas the third contribution accounts for the external tidal potential. Substituting (1.66) and (1.67) into (1.68) we finally find

$$\Phi_{\text{tot}} = -\frac{M}{r} + \left[\frac{2k_2}{G} \left(\frac{R}{r} \right)^5 + \frac{1}{2} \right] \mathcal{E}_{ij} x_i x_j. \quad (1.69)$$

1.3.2 Relativistic theory

In the previous section we derived the expression of the total gravitational potential generated by a body under a quadrupolar tidal field, expressed by Eq. (1.68). Since we are interested in neutron star physics we have to transpose the previous discussion in the framework of general relativity. To this purpose we recall that in the weak field limit holds the identity

$$\Phi = -\frac{(1 + g_{00})}{2}, \quad (1.70)$$

which can be used to define the quantities Q_{ij} and \mathcal{E}_{ij} in general relativity. Indeed by combining (1.68) and (1.70) we find

$$-\frac{(1 + g_{00})}{2} = -\frac{M}{r} - \frac{3}{r^5} Q_{ij} x_i x_j + O\left(\frac{1}{r^3}\right) + \frac{1}{2} \mathcal{E}_{ij} x_i x_j + O(r^3) \quad (1.71)$$

where Q_{ij} and \mathcal{E}_{ij} are given respectively by (1.65) and (1.59). Nevertheless we are interested in fully relativistic stars. In the strong field case the equations (1.65) and (1.59) are no longer valid, but the expansion (1.71) still holds in the asymptotically flat region in the star local rest frame and can still be used to define the momenta Q_{ij} and \mathcal{E}_{ij} . In the following we follow the approach of [12, 83] in order to carry out the relativistic expression of the tidal Love number k_2 .

First of all we notice that since Q_{ij} and \mathcal{E}_{ij} are STL tensors, we can decompose them into

$$Q_{ij} = \sum_{m=-2}^2 \mathcal{E}_m \mathcal{Y}_{ij}^{2m}, \quad (1.72)$$

$$\mathcal{E}_{ij} = \sum_{m=-2}^2 Q_m \mathcal{Y}_{ij}^{2m}, \quad (1.73)$$

where \mathcal{Y}_{ij}^{2m} are defined as the symmetric traceless tensors satisfying

$$Y_{2m}(\theta, \phi) = \mathcal{Y}_{ij}^{2m} n_i n_j \quad (1.74)$$

with \mathbf{n} being the unit vector of a generic point in the three-dimensional space $\mathbf{n} = (\sin \theta \cos \phi, \sin \theta \sin \phi, \cos \theta)$. Equation (1.66) can therefore be written as:

$$Q_m = -\lambda \mathcal{E}_m \quad (1.75)$$

and without any loss of generality we can assume that only one \mathcal{E}_m is nonvanishing. This is sufficient to compute λ .

In order to find the expression for k_2 we start by examining the behaviour of the equilibrium configuration under linearized quadrupolar perturbations [12, 84]. The full metric of the spacetime is given by

$$g_{\alpha\beta} = g_{\alpha\beta}^{(0)} + h_{\alpha\beta}, \quad (1.76)$$

with $|h_{\alpha\beta}| \ll 1$ being a metric perturbation, and $g_{\alpha\beta}^{(0)}$ is the metric of a stationary and spherically symmetric spacetime given by (1.41). The angular dependence of $h_{\alpha\beta}$ is decomposed into spherical harmonics and we take into consideration only $l = 2$, static and even-parity perturbations in the Regge-Wheeler gauge. Under these hypothesis $h_{\alpha\beta}$ can be written as

$$h_{\alpha\beta} = Y_{2m}(\theta, \phi) \begin{pmatrix} -e^{2\nu(r)} H_0(r) & 0 & 0 & 0 \\ 0 & e^{2\lambda(r)} H_2(r) & 0 & 0 \\ 0 & 0 & r^2 K(r) & 0 \\ 0 & 0 & 0 & r^2 \sin^2 \theta K(r) \end{pmatrix}. \quad (1.77)$$

We want to solve the linearized Einstein equations

$$\delta G^\mu_\nu = 8\pi \delta T^\mu_\nu. \quad (1.78)$$

The variation of the stress-energy tensor can be written as

$$\delta T^\mu_\nu = \text{diag}(-\delta\epsilon, \delta P, \delta P, \delta P), \quad (1.79)$$

and since $P = P(\epsilon)$ we have

$$\delta\epsilon = \left(\frac{dP}{d\epsilon} \right)^{-1} \delta P. \quad (1.80)$$

By using equations (1.76) and (1.77) one can compute the components of δG^μ_ν and finally solve Eq. (1.78). After some calculations one finds that all the radial functions in the metric perturbation $h_{\alpha\beta}$ can be related to a unique function $H(r) \equiv H_0(r)$ which satisfies the following differential equation

$$\begin{aligned} H'' + H' \left\{ \frac{2}{r} + e^{2\lambda} \left[\frac{2M(r)}{r^2} + 4\pi r(P - \epsilon) \right] \right\} + \\ + H \left[-\frac{6e^{2\lambda}}{r^2} + 4\pi e^{2\lambda} \left(5\epsilon + 9P + \frac{\epsilon + P}{dP/d\epsilon} \right) - (2\nu')^2 \right] = 0 \end{aligned} \quad (1.81)$$

where we refer to d/dr with the prime index. We can find the boundary conditions for the previous differential equation requiring regularity of H at $r = 0$. Solving for H near $r = 0$ yields

$$H(r) = a_0 r^2 \left\{ 1 - \frac{2\pi}{7} \left[5\epsilon(0) + 9P(0) + \frac{\epsilon(0) + P(0)}{(dP/d\epsilon)(0)} \right] r^2 + O(r^3) \right\} \quad (1.82)$$

where a_0 is a constant that can be eliminated using continuity of H and its derivative across $r = R$. We remind that our purpose is to define the quantities Q_{ij} and \mathcal{E}_{ij} through the asymptotic expansion of Eq. (1.71). Therefore we want to find the

expression of $H(r)$ outside the star. In this region the metric of the unperturbed spacetime is given by the Schwarzschild solution and the components of the stress-energy tensor are all zero. In this region Eq. (1.81) becomes

$$H'' + \left(\frac{2}{r} - \lambda'\right) H' - \left(\frac{6e^{2\lambda}}{r^2} + (2\lambda')^2\right) H = 0. \quad (1.83)$$

In the Schwarzschild solution λ and ν satisfy

$$e^{2\nu} = 1 - \frac{2M}{r} \quad (1.84)$$

and

$$e^{2\lambda} = \frac{1}{1 - \frac{2M}{r}}. \quad (1.85)$$

With the change of variable $x = (r/M - 1)$, Eq. (1.83) can be cast into the form of a Legendre equation with $l = m = 2$

$$(x^2 - 1) H'' + 2xH' - 6 \left(6 + \frac{4}{x^2 - 1}\right) H = 0. \quad (1.86)$$

The general solution of the above equation is written in terms of the associated Legendre functions $Q_2^2(x)$ and $P_2^2(x)$ as

$$H = c_1 Q_2^2(x) + c_2 P_2^2(x), \quad (1.87)$$

where c_1 and c_2 are two coefficients to be determined. After substituting the explicit form of the associated Legendre functions into Eq. (1.87), and performing an asymptotic expansion for large r , we obtain

$$H(r) = \frac{8}{5} \left(\frac{M}{r}\right)^3 c_1 + O\left(\left(\frac{M}{r}\right)^4\right) + 3 \left(\frac{r}{M}\right)^2 c_2 + O\left(\frac{r}{M}\right), \quad (1.88)$$

where the coefficients c_1 and c_2 can now be determined by matching Eq. (1.88) with the asymptotic expansion (1.71). Using also (1.75) we find that the coefficients c_1 and c_2 are given by

$$c_1 = \frac{15}{8} \frac{1}{M^3} \lambda \mathcal{E}, \quad c_2 = \frac{1}{3} M^2 \mathcal{E}. \quad (1.89)$$

Finally one can find λ in terms of H and its derivative at the star's surface from the explicit form of Eq. (1.87). By using Eq. (1.67), the expression for the second tidal Love number k_2 can be carried out

$$\begin{aligned} k_2 = & \frac{8C^5}{5} (1 - 2C)^2 [2 + 2C(y - 1) - y] \\ & \times \left\{ 2C [6 - 3y + 3C(5y - 8)] + 4C^3 [13 - 11y + C(3y - 2) + 2C^2(1 + y)] + \right. \\ & \left. + 3(1 - 2C)^2 [2 - y + 2C(y - 1)] \log(1 - 2C) \right\}^{-1}, \end{aligned} \quad (1.90)$$

where the quantities C and y are defined as

$$C = \frac{M}{R}, \quad y = \frac{RH'(R)}{H(R)}. \quad (1.91)$$

This result tells us that the ingredients we need in order to evaluate the tidal Love number k_2 are the star compactness and the quantity y which can be computed by integrating Eq. (1.81) in the region $0 < r < R$. We notice that (1.81) depends only on quantities that can be determined by solving the unperturbed problem. Therefore in order to numerically evaluate y and C we only need to integrate the TOV equations together with Eq. (1.81).

1.4 The equation of state of cold nuclear matter

We have already said that the equation of state of a given system is a non-trivial relation linking the thermodynamic quantities. The most iconic example of EOS is the perfect gas law

$$P = k_B \varrho T \quad (1.92)$$

which account for a good description of very dilute systems. A more general expression can be achieved by considering the previous equation as the leading order of a Taylor expansion in powers of the number density ϱ

$$P = k_B \varrho T \left[1 + \varrho B(T) + \varrho^2 C(T) + \dots \right], \quad (1.93)$$

which is known as virial expansion. We have just mentioned that in the particular case of neutron stars we are looking for an EOS of the form

$$P = P(\epsilon), \quad (1.94)$$

with ϵ being the energy density of the system. Such a relation can be carried out by knowing the expression $\epsilon = \epsilon(\varrho)$ and then applying the thermodynamic definition of pressure

$$P = - \left. \frac{\partial E}{\partial V} \right|_{N,T} = \epsilon(\varrho) - \varrho \frac{\partial \epsilon}{\partial \varrho}. \quad (1.95)$$

In principle if we have a microscopic description of core matter, which gives us this $\epsilon(\varrho)$ relation, we will be able to compute the NS properties predicted by such a model, and compare such predictions with astrophysical observations. Actually the picture is slightly more complicated. The description we have carried out before refers to a single component fluid, or at least to a system where the chemical composition is always the same. Nevertheless, the NS core is believed to be composed of a uniform fluid of neutrons, protons, electrons and muons. The chemical composition, i.e. the relative fraction of all these particle species is determined by the conditions of β -equilibrium², charge neutrality and baryon number conservation. Such requirements will produce a chemical composition which changes with density. The chemical composition of β -stable matter can be obtained by minimizing the energy density ϵ with respect to the densities of all the particle species contributing to the β -equilibrium, with the additional constraints of charge neutrality and baryon number conservation. In other words we have to minimize the quantity

$$F(\varrho, \varrho_n, \varrho_p, \varrho_e, \varrho_\mu) = \epsilon(\varrho, \varrho_n, \varrho_p, \varrho_e, \varrho_\mu) - \lambda_B(\varrho - \varrho_n - \varrho_p) - \lambda_Q(\varrho_p - \varrho_e - \varrho_\mu), \quad (1.96)$$

² β -equilibrium is referred to the balance between the two processes of neutron decay, $n \rightarrow p + e^- (\mu^-) + \bar{\nu}_e (\bar{\nu}_\mu)$ and electronic (muonic) capture $e^- (\mu^-) + p \rightarrow n + \nu_e (\nu_\mu)$.

where ϱ_α , with $\alpha = n, p, e, \mu$, labels respectively the density of neutrons, protons, electrons and muons, whereas λ_B and λ_Q are two Lagrange multipliers. By solving the equations

$$\frac{\partial F}{\partial \varrho_\alpha} = 0, \quad \frac{\partial F}{\partial \lambda_B} = \frac{\partial F}{\partial \lambda_Q} = 0, \quad (1.97)$$

we find the conditions

$$\varrho = \varrho_p + \varrho_n, \quad \varrho_p = \varrho_e + \varrho_\mu, \quad (1.98)$$

and

$$\mu_n = \mu_p + \mu_e, \quad \mu_\mu = \mu_e, \quad (1.99)$$

where μ_α is referred to the chemical potential of the particle α , defined through

$$\mu_\alpha = \left. \frac{\partial \epsilon}{\partial \varrho_\alpha} \right|_{\varrho, \varrho_\beta \neq \varrho_\alpha}. \quad (1.100)$$

Since the interaction energy contribution, coming from the lepton sector can be neglected with respect to nuclear interactions, the energy density of such a system is usually written as

$$\epsilon = \epsilon_B(\varrho, x_p) + \epsilon_l(\varrho_e, \varrho_\mu), \quad (1.101)$$

where the term ϵ_l represents the energy density coming from a degenerate lepton gas, whereas the term ϵ_B accounts for all the nuclear interactions, and its expression should be in principle carried out from a consistent theoretical framework describing nuclear matter. We notice that in Eq. (1.101) we have introduced the proton fraction x_p , through which the neutron and proton density are expressed as

$$\varrho_p = x_p \varrho, \quad \varrho_n = (1 - x_p) \varrho. \quad (1.102)$$

We also stress that in the above discussion we have always neglected neutrinos. This approximation is justified by theoretical calculations of neutrino mean free path inside the neutron star core, which have shown how neutron star matter becomes transparent to neutrinos as soon as the temperature drops below $T \sim 10^{10} K$.

The quantity $\epsilon_B(\varrho, x_p)$ is the main object of theoretical calculations aimed at carrying out an accurate description of nuclear matter properties. Very different frameworks, as well as a broad set of EOSs have been developed so far. In Fig. 1.4 we can see the mass-radius diagram (a) and the tidal deformabilities (b) predicted by some of these models. We can see how different models account for different NS observables. In this respect the occurrence of more and more accurate measurements of NS properties is expected to have the potential, in the upcoming future, to strongly improve our knowledge about the behavior of ultra-dense and cold nuclear matter.

As a final remark we underline that all the EOSs considered in Fig. 1.4, as well as the discussion we have undergone so far, take into consideration only nucleonic EOSs, i.e. EOSs that are derived by assuming matter to be composed by only nucleons and leptons. When the density increases very much, however, it is also possible the appearance of other degrees of freedom, such as the production of strange baryons as the result of weak processes. In recent years also the possibility of a phase transition to deconfined quark matter, leading to the so-called hybrid stars was seriously explored [50, 87–89]. Besides, representing a very intriguing possibility,

almost every model developed so far results in a sizable softening of the EOS. Such a soft matter content is little compatible with the recent mass-radius measurements performed by the NICER collaboration, suggesting that ~ 1.4 and $\sim 2 M_{\odot}$ NSs have essentially comparable radii.

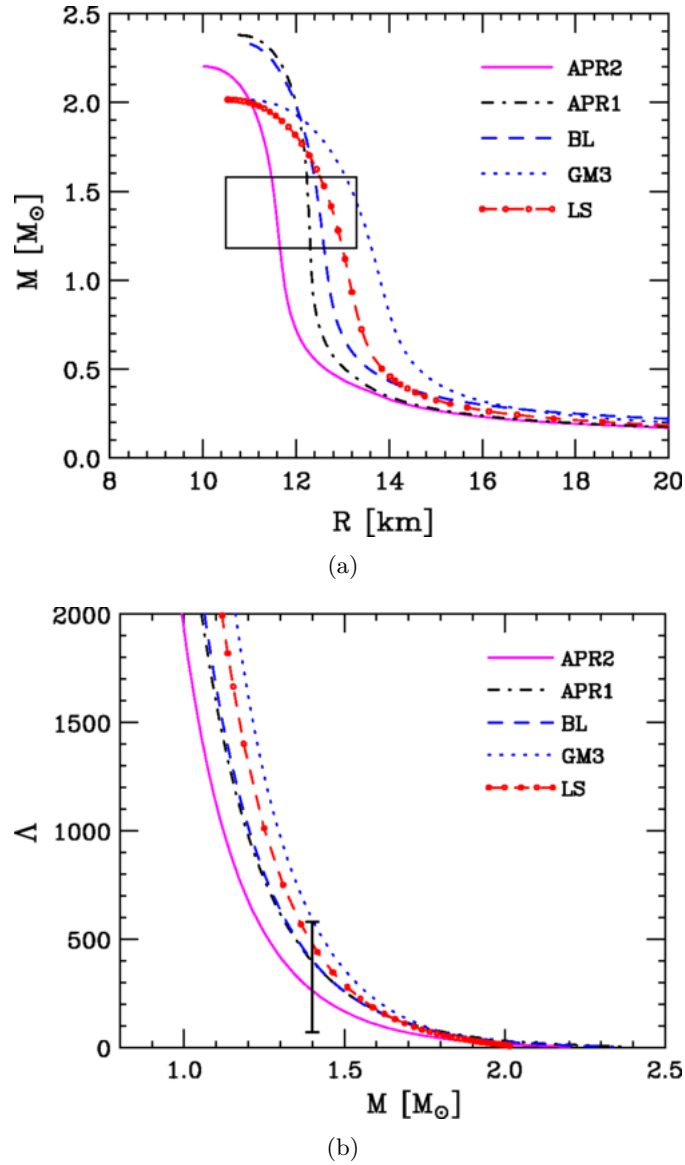


Figure 1.4. Mass-radius diagram (a) and tidal deformability as function of the NS mass (b) predicted by different EOSs models. The APR1, APR2 and BL EOSs are derived within non-relativistic nuclear many-body theory [62, 67]. The GM3 EOS is derived within the framework of the relativistic mean field [85]. Finally the LS model is a phenomenological model derived starting from the liquid drop model and imposing constraints from nuclear phenomenology [86]. Constraints coming from the GW observation of the GW170817 event are also shown. The picture is taken from Ref. [48].

Chapter 2

Nuclear Hamiltonian

The existence of atomic nuclei, as well as a lot of other nuclear phenomena, are a manifestation of the fundamental force known as strong interaction. Although the fundamental theory of strong interactions is today well established as the Quantum Chromo-Dynamics (QCD), a direct application of such a formalism to nuclear physics involves insurmountable difficulties, other than being conceptually unnecessary. Indeed because of the confinement of quarks and gluons inside hadrons, the relevant degrees of freedom described by QCD are always hidden in nuclear interactions. Nuclear phenomena are therefore more efficiently described in terms of residual forces between hadrons, similar to the van der Waals interactions occurring between molecules. In addition, because of the particular behavior of the strong coupling constant, a direct application of QCD is only possible through non-perturbative approaches involving lattice calculations. Such techniques other than being limited by current computational resources, are also affected by the occurrence of the so called sign-problem, which limits its applicability only to a limited region of the QCD phase diagram. However, it is worth to mention that, besides its non-perturbative nature at the typical NS densities, some studies have recently shown how QCD perturbative calculations, performed in the regime of asymptotic freedom, can still be used to infer indirect information on the nuclear matter EOS [90,91]. In light of these considerations the study of nuclear systems has to rely upon phenomenological and effective approaches as much as possible constrained by the large set of experimental data. In this chapter, and in the rest of this Thesis, we will explore an approach where nucleons are the relevant degrees of freedom. In this framework —known as Nuclear Many Body Theory (NMBT) —nucleons are treated as non-relativistic point-like particles whose dynamics is described by the Hamiltonian

$$\mathcal{H} = \sum_i \frac{\mathbf{p}_i^2}{2m} + \sum_{i<j} v_{ij} + \sum_{i<j<k} V_{ijk}, \quad (2.1)$$

where \mathbf{p}_i labels the momentum of the i -th nucleon, m is the average nucleon mass $\sim 939 \text{ MeV}/c^2$ and finally v_{ij} and V_{ijk} represent respectively nucleon-nucleon (NN) and three-nucleon (NNN) interaction potentials.

Since this formalism is based upon two crucial assumptions, it is important to comment a little about them. A comprehensive discussion about the non-relativistic approximation is postponed to the section concerning relativistic corrections. Here

we are going to focus on the principal experimental evidences allowing the treatment of nucleons as point particles, even if they have an internal structure. First of all the measured proton charge radius, inferred from elastic scattering of electrons on hydrogen, suggests that at typical nuclear densities the wave functions of two nucleons exhibit a negligible overlap [92]. This feature is observed up to inter-particle distances of $\sim 1.0 fm$ where the overlap becomes significant and the point-like approximation could be no longer justified. Moreover, as also stated in the discussion of Ref. [63], the observation of the y -scaling in electron scattering off a broad set of different targets shows that the beam particles can couple to nucleons carrying momenta up to $\sim 700 MeV$, strongly suggesting that even in presence of a significant overlap between nucleons their internal quark structure is largely unaffected.

2.1 Nucleon-nucleon interaction

Phenomenological potentials are derived by imposing a very general analytical and operatorial structure, as much as possible inspired by theoretical considerations. They involve a set of free parameters, which are fitted in order to reproduce a large body of observations regarding two-nucleon systems, both in bound and scattering states.

Some important features of a realistic NN interaction can be deduced by very general considerations coming from empirical observations about atomic nuclei.

- The observation that the central density of atomic nuclei tends to a constant value $\rho_0 = 0.16 fm^{-3}$, independently on the mass number A , suggests that nuclei are almost incompressible i.e. that nucleons cannot be put arbitrarily close to each others. A comparison between the charge-density distributions of nuclei with different A is reported in Fig. 2.1. This general feature of atomic nuclei is known as the *saturation* of nuclear density. Strictly speaking, this is a clear manifestation that NN interactions should exhibit a strong repulsive core at short distances. Therefore the interaction potential $v(\mathbf{r})$ shall obey

$$v(\mathbf{r}) > 0, \quad |\mathbf{r}| < r_c, \quad (2.2)$$

with r_c being the radius of the repulsive core.

- The evidence that the nuclear binding energy per nucleon is roughly the same for all nuclei with mass number $A \geq 20$ can be ascribed to a finite interaction range r_0 . Indeed, the fact that after a certain size the nucleus binding energy doesn't change anymore by adding further nucleons, implies that the interaction doesn't affect the constituents that are too far apart, yielding

$$v(\mathbf{r}) = 0, \quad |\mathbf{r}| > r_0. \quad (2.3)$$

- The strong similarities that can be found in the spectra of the so called *mirror nuclei*¹ are a strong evidence that protons and neutrons have similar nuclear interactions, i.e. that nuclear forces are charge symmetric.

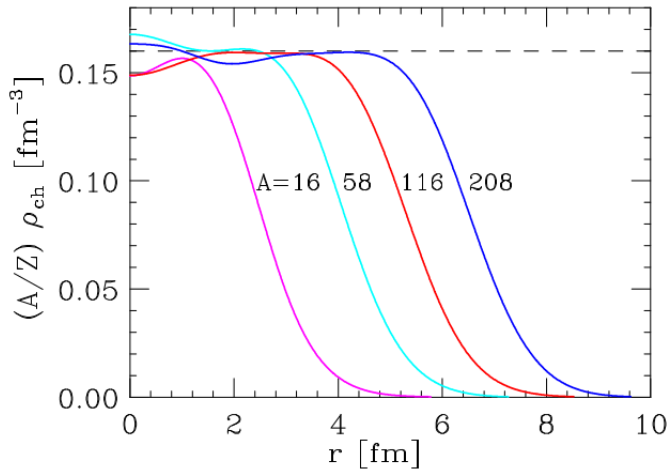


Figure 2.1. Radial dependence of the charge-density in atomic nuclei with different mass number A , inferred from elastic electron-nucleus scattering experiments [93].

Charge invariance of nuclear forces is a manifestation of a more general symmetry of nature known as *isospin symmetry*. The observation that protons and neutrons have nearly the same mass is a natural insight about the existence of an underlying approximate symmetry, which we know to be explicitly broken by the mass difference between *up* and *down* quarks. By assuming protons and neutrons as the fundamental degrees of freedom, the dynamics of free nucleons would be described by a Lagrangian density of the form

$$\mathcal{L} = \bar{\psi}^N (i\gamma^\mu \partial_\mu - m) \psi^N, \quad (2.4)$$

where the index i runs over the type of nucleon and m is the average nucleon mass. We can identify the quantity ψ^N as a two-component object

$$\psi^N = \begin{pmatrix} \psi_p \\ \psi_n \end{pmatrix}, \quad (2.5)$$

with ψ_p and ψ_n labeling proton and neutron spinors respectively.

The Lagrangian of Eq. (2.4) is clearly invariant under the global $SU(2)$ transformation group

$$\psi_i^N \rightarrow \psi_i'^N = U_{ij} \psi_j^N \quad (2.6)$$

with

$$U_{ij} = e^{ig^a \tau_{ij}^a}, \quad (2.7)$$

where the g^a are three continuous parameters ($a = 1, 2, 3$) and the τ^a are the generators of the group, that in the case of $SU(2)$ can be identified with the three Pauli matrices ($\sigma^1, \sigma^2, \sigma^3$) acting on the isospin space. The Pauli matrices are 2×2 hermitian matrices satisfying the commutation relations

$$[\sigma^a, \sigma^b] = 2i\epsilon^{abc} \sigma^c. \quad (2.8)$$

¹Mirror nuclei are nuclei with the same mass number A but with Z differing by one unit.

These considerations show that a nucleon can be described by a doublet in a spin-like space, named isospin space. Proton and neutron therefore represent the two isospin projections, that for convention are chosen as the eigenstates corresponding to the eigenvalues $+1/2$ and $-1/2$ of the $\tau^3/2$ operator respectively. Using the classical composition rules the two nucleon states can be organized in the total isospin basis $|T, T_3\rangle$, as follows

$$\begin{aligned} |1, 1\rangle &= |p, p\rangle \\ |1, 0\rangle &= \frac{1}{\sqrt{2}} (|p, n\rangle + |n, p\rangle) \\ |1, -1\rangle &= |n, n\rangle \\ |0, 0\rangle &= \frac{1}{\sqrt{2}} (|p, n\rangle - |n, p\rangle). \end{aligned} \quad (2.9)$$

We can observe that proton-proton and neutron-neutron pairs always have total isospin $T = 1$, whereas a proton-neutron pair may have either $T = 0$ or $T = 1$. Isospin invariance implies that the interaction between two nucleons depends on their total isospin T but not on T_3 , because T_3 doesn't commute with a generic $SU(2)$ isospin transformation. Therefore two protons, as well as a couple of neutrons, will interact in the same way as a proton and a neutron in the $T = 1$ isospin-state (provided that they are coupled to the same spin channel).

Other important details of the NN interaction are provided by the study of the two-nucleon systems. In nature it is observed only one NN bound state: the nucleus of deuterium, or deuteron (2H), composed by a proton and a neutron with total spin and isospin $S = 1$ and $T = 0$ respectively. This is a clear manifestation that nuclear forces possess a strong spin-isospin dependence. Another important information is that the deuteron exhibits a non-vanishing electric quadrupole moment, implying that its charge distribution is not spherically symmetric. This reflects a noncentral behavior of the NN interaction.

2.1.1 Phenomenological potentials

A first theoretical description of the interactions between two nucleons was attempted by Yukawa in 1935 [94]. He made the hypothesis that such a force was mediated by a particle corresponding to an energy quantum of the nuclear field (on the same line of the well understood theory of electromagnetic interactions). The observation that nuclear interactions have a finite range $r_0 \sim 1 - 2 fm$, leads Yukawa to estimate the mass m of the mediator to be

$$m \sim \frac{1}{r_0} \sim 100 - 200 MeV. \quad (2.10)$$

The idea of Yukawa was successfully implemented identifying the exchanged particle with the π -meson (*pion*) whose mass is $m_\pi \sim 139.6 MeV$. Experiments show that the pion is a spin zero pseudoscalar particle that comes in three charge states denoted π^+ , π^- , and π^0 . Let's see how to build a Lagrangian that embodies the Yukawa's idea, accounting in addition for the observation that nuclear interactions conserve parity. Our starting point is the free Lagrangian of Eq. (2.4) supplemented with an interaction term fulfilling all the symmetry properties of the system. The most simple case is the interaction with a scalar boson Π yielding

$$\mathcal{L} = \bar{\psi}^N (i\gamma^\mu \partial_\mu - m)\psi^N + \mathcal{L}_\Pi + g\bar{\psi}^N \Pi \psi^N, \quad (2.11)$$

where we have also included the term \mathcal{L}_Π containing the Π kinetic terms and all its self interactions.

We know that the total Lagrangian must be $SU(2)$ invariant. This requirement leads the field Π to fulfill the following transformation rule

$$\Pi \rightarrow \Pi' = U\Pi U^\dagger. \quad (2.12)$$

The above relation implies the field Π to be an object of the adjoint representation of $SU(2)$. We can therefore write

$$\Pi = \pi^a \tau^a \quad (2.13)$$

where τ^a are the $SU(2)$ generators in the fundamental representation. Since a runs from 1 to 3 we have found that the field mediating the interaction must be a triplet of isospin with components π^a . Since the pion turns out to be a pseudoscalar particle ² the interaction becomes

$$\mathcal{L}_I = ig\pi^a \tau_{ij}^a \bar{\psi}_i^N \gamma^5 \psi_j^N, \quad (2.14)$$

where the γ^5 matrix is added in order to still conserve parity.

Armed with this Lagrangian we can now study the nucleon-nucleon scattering at the leading order in perturbation theory. The one-pion-exchange (OPE) process is described by the Feynman diagram in Fig. 2.2.

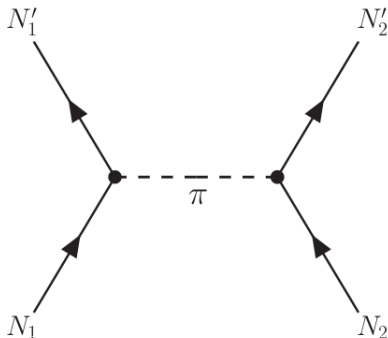


Figure 2.2. Feynman diagram describing the one pion exchange process between two nucleons. Time goes from bottom to top.

We have an initial state $|i\rangle = |p_1, s_1; p_2, s_2\rangle$, made by two nucleons with momentum p_1, p_2 and spin polarization s_1, s_2 respectively, which goes into a final state $|f\rangle = |p_{1'}, s_{1'}; p_{2'}, s_{2'}\rangle$. Actually we have to assign to each nucleon a further quantum number which labels if it is a proton or a neutron, i.e. its isospin projection.

From Eq. (2.14) follows that we can take as the interaction vertex the quantity $ig\gamma^5\tau_{ij}^a$. We can now evaluate the invariant amplitude of this process using the standard Feynman diagram techniques, obtaining

$$i\mathcal{M} = -g^2 \bar{u}(p_{2'}, s_{2'}) \gamma^5 u(p_2, s_2) \frac{1}{k^2 - m_\pi^2} \bar{u}(p_{1'}, s_{1'}) \gamma^5 u(p_1, s_1) \langle \tau_1^a \rangle \langle \tau_2^a \rangle, \quad (2.15)$$

²Observing the process $\pi^- + d \rightarrow n + n$ it was established that the intrinsic parity of the pion is negative.

where

$$\langle \tau_1^a \rangle = \eta_1^\dagger \tau^a \eta_1; \quad \langle \tau_2^a \rangle = \eta_2^\dagger \tau^a \eta_2 \quad (2.16)$$

with η_i being the two component Pauli spinor defining the isospin state of the i -th nucleon.

The invariant amplitude of Eq. (2.15) in the non-relativistic limit allows to define a NN interaction potential that can be written in coordinate space as

$$\begin{aligned} v_\pi(\mathbf{r}) &= \frac{g^2}{4m^2} (\boldsymbol{\tau}_1 \cdot \boldsymbol{\tau}_2) (\boldsymbol{\sigma}_1 \cdot \boldsymbol{\nabla}) (\boldsymbol{\sigma}_2 \cdot \boldsymbol{\nabla}) \frac{e^{-m_\pi r}}{r} = \\ &= \frac{g^2}{(4\pi)^2} \frac{m_\pi^3}{4m^2} \frac{1}{3} (\boldsymbol{\tau}_1 \cdot \boldsymbol{\tau}_2) \left\{ \left[(\boldsymbol{\sigma}_1 \cdot \boldsymbol{\sigma}_2) + S_{12} \left(1 + \frac{3}{x} + \frac{3}{x^2} \right) \right] \frac{e^{-x}}{x} \right. \\ &\quad \left. - \frac{4\pi}{m_\pi^3} (\boldsymbol{\sigma}_1 \cdot \boldsymbol{\sigma}_2) \delta^{(3)}(\mathbf{r}) \right\}, \end{aligned} \quad (2.17)$$

where $x = m_\pi r$, $\boldsymbol{\tau}_i$ are the isospin generators acting on the i -th particle and

$$S_{12} = \frac{3}{r^2} (\boldsymbol{\sigma}_1 \cdot \mathbf{r}) (\boldsymbol{\sigma}_2 \cdot \mathbf{r}) - (\boldsymbol{\sigma}_1 \cdot \boldsymbol{\sigma}_2), \quad (2.18)$$

accounts for the non-central part of the interaction.

For $g^2/4\pi = 14$, the above potential provides an accurate description of the long range part ($r > 1.5 fm$) of the NN interaction, as shown by the very good agreement with NN scattering data in states of high angular momentum. In these states, because of the strong centrifugal barrier, the probability of finding the two nucleons at small relative distance is negligible. At intermediate and short range other more complicated processes, such as the exchange of two pions or heavier mesons can occur. Moreover when the relative distance becomes very small, $\sim 0.5 fm$, nucleons, are expected to overlap and the dynamics of their internal degrees of freedom becomes relevant. In this regime the interaction should be in principle dictated by QCD.

Because of all these effects a good description of the full NN interaction requires the definition of a phenomenological potential, whose general form can be written as

$$v = \tilde{v}_\pi + v_R, \quad (2.19)$$

where \tilde{v}_π is the potential given by Eq. (2.17) stripped of the δ -function contribution and v_R describes the interactions at medium and short range. If we look at the general expression of Eq. (2.17), we notice that the \tilde{v}_π contribution can be written in the general form

$$v_{ij} = \sum_p v^p(r_{ij}) O_{ij}^p \quad (2.20)$$

where the quantities O^p are a set of six operators defined as

$$O_{ij}^p = 1, (\boldsymbol{\tau}_i \cdot \boldsymbol{\tau}_j), (\boldsymbol{\sigma}_i \cdot \boldsymbol{\sigma}_j), (\boldsymbol{\sigma}_i \cdot \boldsymbol{\sigma}_j)(\boldsymbol{\tau}_i \cdot \boldsymbol{\tau}_j), S_{ij}, S_{ij}(\boldsymbol{\tau}_i \cdot \boldsymbol{\tau}_j), \quad (2.21)$$

where the indices i and j are referred to the general i -th and j -th nucleons.

This operator structure can be derived also by more general considerations. If we keep in mind what we said in the previous section, we know that a generic NN interaction should have a strong spin-isospin dependence, it should be invariant

under the $SU(2)$ isospin transformations and it should exhibit a non-central behavior. We can therefore write the NN potential in the general form

$$v = \sum_{S,T} [v_{TS}(r) + \delta_{S1}v_{tT}(r)S_{12}] P_S \Pi_T. \quad (2.22)$$

In the above equation S and T run over the possible total spin and isospin of the interacting pair, r is the distance between the two particles, S_{12} is given by (2.18) and P_S and Π_T are two projection operators. The operator P_S is the projector onto the subspace identified by total spin S , with $S = 0, 1$, and take the form

$$P_0 = \frac{1}{4}(1 - \boldsymbol{\sigma}_1 \cdot \boldsymbol{\sigma}_2), \quad P_1 = \frac{1}{4}(3 + \boldsymbol{\sigma}_1 \cdot \boldsymbol{\sigma}_2). \quad (2.23)$$

It is easy to show that these operators satisfy

$$P_0 + P_1 = 1, \quad P_S|S'\rangle = \delta_{SS'}|S'\rangle, \quad P_S P_{S'} = \delta_{S'S} P_S. \quad (2.24)$$

The projector Π_T is defined in the same way but in the isospin space i.e. by substituting σ^a with τ^a . It is easy to show that by combining Eq. (2.22) and Eq. (2.23) we can write the NN potential in the form appearing in Eq. (2.20).

After all these considerations a general form of the phenomenological potential of Eq. (2.19) can be written as

$$v_{ij} = \sum_p [\tilde{v}_\pi^p(r_{ij}) + v_I^p(r_{ij}) + v_S^p(r_{ij})] O_{ij}^p, \quad (2.25)$$

with v_I and v_S labeling the intermediate and short range interaction components respectively. In more sophisticated potentials the set of operators is expanded from the six ones of Eq. (2.21) and can reach even eighteen components, as in the case of the Argonne v_{18} (AV18) potential [95]. Operators with $p = 7, \dots, 14$ account for spin-orbit interactions and other non-static terms, whereas the $p = 15, \dots, 18$ account for small charge symmetry violations. The shapes of the radial functions is determined by means of a parametrization inspired by theoretical considerations about meson exchange potentials. For example the intermediate range components are usually assumed to come mainly from two-pion-exchange processes [96]. Finally the parameters involved in their definition are determined by fitting the large body of existing data coming from two-nucleon systems. We shall just mention that the forty parameters involved in the definition of the AV18 potential, are determined by an accurate fit of the proton-proton (pp) and neutron-proton (np) scattering phase shifts up to the pion production threshold, low-energy neutron-neutron (nn) scattering parameters and deuteron binding energy.

The first six operators $O_{ij}^{p \leq 6}$, other than providing the dominant contribution in nuclear matter among all the eighteen components, benefit from another crucial property. They are a closed set under the usual composition rule and form an algebra. Indeed we have that

$$O_{ij}^p O_{ij}^q = \sum_l K^{pql} O_{ij}^l. \quad (2.26)$$

These considerations have motivated the development of an interaction potential labeled as Argonne v'_6 (AV6P) in which the full AV18 is projected onto the first six

operators only [97]. This potential reproduces remarkably well the NN scattering phase shifts in the 1S_0 channel ($l = 0$, $S = 0$ and $T = 1$), as well as the deuteron binding energy with an accuracy of 1%.

In Fig. 2.3 is illustrated a comparison between the radial dependence of the components $v^p(r_{ij})$, with $p = 1, 3, 5$, for the AV18 and AV6P potentials. We can see that in the basis represented by the first six operators of Eq. (2.21), the two potentials appear to be quite different. This is just to further remark that the AV6P is not just a simple truncation of the AV18 potential. Anyway, we can see in Fig. 2.4 that the two potentials are exactly the same in the 1S_0 channel, which is related to the components written in the six-operator basis through

$$v_{S=0,T=1} = v^1 + v^2 + 3(v^3 + v^4). \quad (2.27)$$

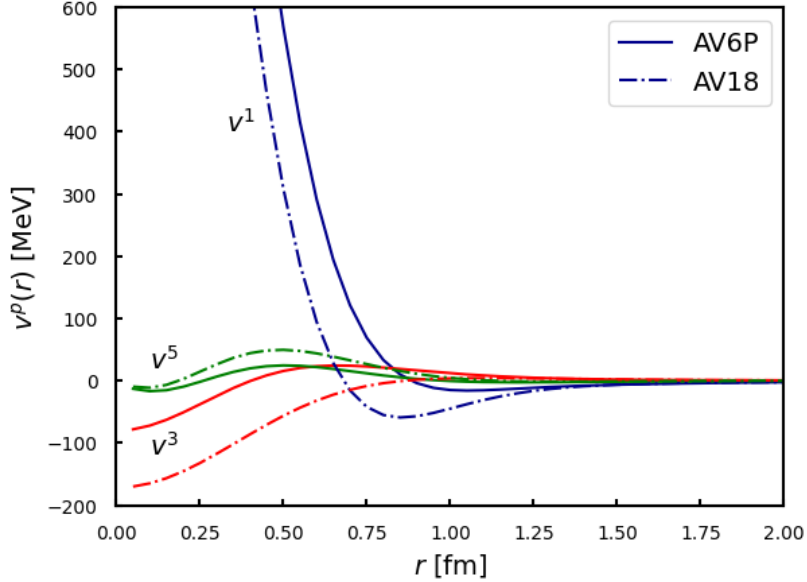


Figure 2.3. Comparison between the radial dependence of the potentials AV6P (solid lines) and AV18 (dot-dashed lines). The different contributions coming from the first (blue), third (red) and fifth (green) component are shown for both potentials.

Figure 2.4 clearly shows the specific features of nuclear forces. We can see that the interaction is attractive at inter-particle distances between one and two femtometers, typical in atomic nuclei. Then with increasing distance the potential rapidly goes to zero, in accordance with the observation of a finite interaction range. Finally a very strong repulsion can be observed when the interacting particles become closer than ~ 1 fm. This feature of the NN interaction is crucial because it prevents a perturbative treatment of the nuclear Hamiltonian and motivated the development of more and more sophisticated approaches in order to achieve a satisfactory description of nuclear systems, by solving the nuclear many-body problem.

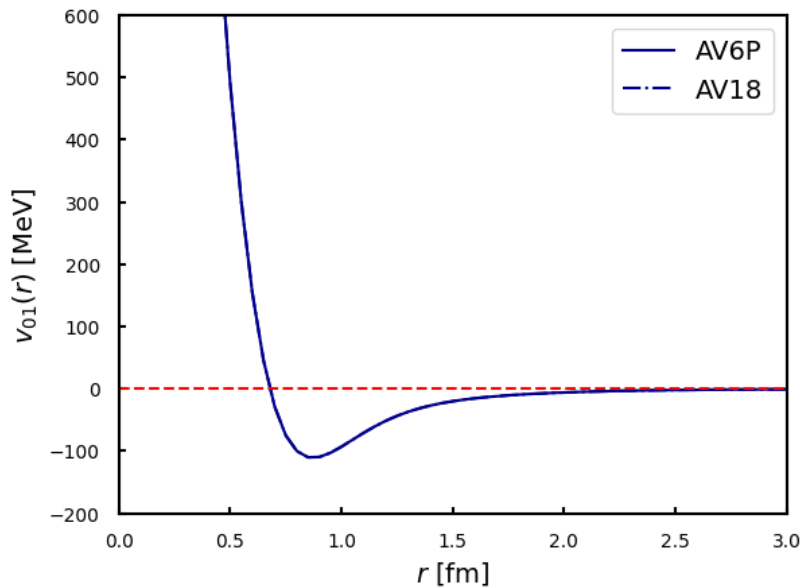


Figure 2.4. Radial dependence of the NN potentials AV6P and AV18 in the state characterized by relative angular momentum $l = 0$, and total spin and isospin respectively $S = 0$ and $T = 1$. We can see how the two potentials perfectly overlap in this channel.

2.2 Three-nucleon potential

The introduction of NNN interactions in the nuclear Hamiltonian turns out to be necessary in order to correctly reproduce the properties of three nucleon systems, such as ${}^3\text{H}$ and ${}^3\text{He}$, which are missed by only considering NN potentials. Since we are used to dealing with point-like particles the meaning of three-body interactions may appear a little obscure. Actually NNN potentials are just a way to introduce the effects related to the internal structure of nucleons in our point-particle formalism. By considering the example represented by the Feynman diagram in Fig. 2.5 their nature will be evident. This diagram describes a two-pion-exchange process between three nucleons, with the excitation of a Δ -resonance (with $M_\Delta \approx 1232 \text{ MeV}$) as an intermediate state. Because of the presence of the Δ -resonance, this Feynman diagram cannot be reduced to a combination of two OPE processes and must be included in the Hamiltonian as a NNN contribution $V_{ijk}^{2\pi}$.

In their pioneering work J. Fujita and H. Miyazawa [98] argued that the dominant three-body force among nucleons should just come from processes described by the Feynman diagram of Fig. 2.5. Therefore commonly used phenomenological NNN potentials, such as the UIX model [97], are written as

$$V_{ijk} = V_{ijk}^{2\pi} + V_{ijk}^R, \quad (2.28)$$

where $V_{ijk}^{2\pi}$ is the Fujita Miyazawa two-pion-exchange potential, which provides an attractive interaction, and the V_{ijk}^R is a purely phenomenological repulsive term.

The explicit expression of these two contributions is given by

$$V_{ijk}^{2\pi} = A_{2\pi} \sum_{\text{cycl}} \left\{ \{X_{ij}, X_{jk}\} \{\boldsymbol{\tau}_i \cdot \boldsymbol{\tau}_j, \boldsymbol{\tau}_j \cdot \boldsymbol{\tau}_k\} + \frac{1}{4} [X_{ij}, X_{jk}] [\boldsymbol{\tau}_i \cdot \boldsymbol{\tau}_j, \boldsymbol{\tau}_j \cdot \boldsymbol{\tau}_k] \right\} \quad (2.29)$$

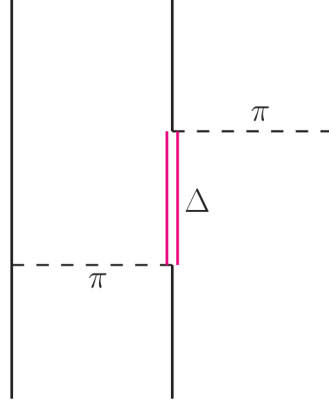


Figure 2.5. Feynman diagram representing the two-pion-exchange process described by the Fujita-Miyazawa interaction potential.

and

$$V_{ijk}^R = U_0 \sum_{\text{cycl}} T^2(m_\pi r_{ij}) T^2(m_\pi r_{jk}), \quad (2.30)$$

where the sums are extended to all cyclical permutations of the particle indices i , j and k . In the above equations the operators X_{ij} are defined as

$$X_{ij} = Y(m_\pi r_{ij}) \boldsymbol{\sigma}_i \cdot \boldsymbol{\sigma}_j + T(m_\pi r_{ij}) S_{ij}, \quad (2.31)$$

where the radial functions $Y(x)$ and $T(x)$ have the form

$$Y(x) = \frac{e^{-x}}{x} \xi(x), \quad (2.32)$$

$$T(x) = \left(1 + \frac{3}{x} + \frac{3}{x^2} \right) Y(x), \quad (2.33)$$

with $\xi(x)$ being a short range cutoff that can be written as $\xi(r) = 1 - e^{-cr^2}$, while the parameter c is usually fixed at ~ 2.0 fm.

The coupling constants $A_{2\pi}$ and U_0 , entering the definition of $V_{ijk}^{2\pi}$ and V_{ijk}^R respectively, are two free parameters that are adjusted in order to correctly reproduce the binding energy of ${}^3\text{H}$ and ${}^4\text{He}$, together with the correct value of the equilibrium density of isospin-symmetric nuclear matter (SNM) $\rho_0 = 0.16 \text{ fm}^{-3}$.

It is worth to mention that the ground state expectation value of the NNN interaction $\langle V_{ijk} \rangle$ is usually much smaller than the corresponding one coming from NN potential $\langle v_{ij} \rangle$. For instance in ${}^3\text{H}$ and ${}^4\text{He}$ it turns out to be $\langle V_{ijk} \rangle / \langle v_{ij} \rangle \sim 3\%$. However, because of the large cancellations between the kinetic and the two-nucleon potential energy, the contribution coming from $\langle V_{ijk} \rangle$ is not negligible, indeed it accounts for $\sim 15\%$ of the total ground state energy in ${}^3\text{H}$ and ${}^4\text{He}$ [70, 99]. Since the ratio between NN and NNN potentials appears to be very small, by extending this argument to three- and four-body interactions we can assume the contribution coming from more-than-three-body forces to be negligible³. This conclusion is

³This is certainly true at nuclear densities, but to which extent this argument can be extended to the typical neutron star densities is not completely clear.

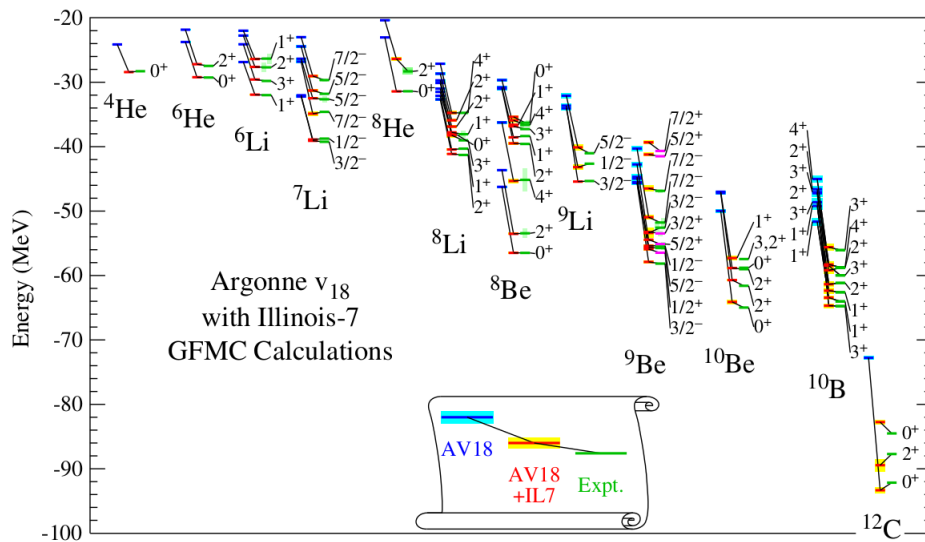


Figure 2.6. Comparison between the energies of the ground end excited states computed by Carlson *et al* and the experimental data. The calculation was performed with and without three-body forces. In both cases the NN potential is the AV18 model whereas for the NNN potential it employed the advanced model referred to as IL7. The picture is taken from [99]

supported by the very good predictive power of Hamiltonians comprising up to three-body potentials, when used to compute the properties of atomic nuclei with more than three nucleons. The results of the exact calculations of ground and low-lying excited states, performed by Carlson *et al* [99], for atomic nuclei with $A \leq 12$ is reported in Fig. 2.6. We can see that the introduction of a NNN potential improves by a large extent the agreement with the experimental data.

2.3 Relativistic corrections

The treatment of nucleons as non-relativistic particles has proved to allow for a satisfactory description of both atomic nuclei and of a great variety of nuclear matter properties. Anyway, the reliability of the description of nucleons as non-relativistic objects, when dealing with matter at the high densities typical of the neutron star core, may be questionable. Indeed all the equations of states derived within the framework of non-relativistic theories predict a speed of sound that becomes superluminal when the density increases too much. Moreover, additional care is required by noting that with increasing density, also the validity of the point-like approximation may start to blunder. Therefore one should also be aware of which assumption breaks down first.

A rough estimate of the relevance of relativistic effects in nuclear matter can be carried out by comparing the Fermi momentum of nucleons with their rest mass at different densities. We know that an infinite system of particles benefits from translation invariance which makes the momentum a good quantum number in

order to classify its energy states. Because of the fermionic nature of nucleons the Pauli exclusion principle forbids two particles to occupy the same quantum level. Therefore in the ground state we can imagine fermions to occupy higher and higher momentum states, uniformly distributed in a sphere whose radius is referred to as the Fermi momentum k_F . If we enclose the system in a cubic volume the average distance between two subsequent states will be $2\pi/L$ where L is the side of the box. Therefore we can define a unit volume in the momentum space as $(2\pi)^3/V$, with $V = L^3$, as the average k -space volume surrounding each state. The number of states N_s can be carried out as the ratio between the volume of the sphere and the unit volume, yielding

$$N_s = \frac{V}{6\pi^2} k_F^3. \quad (2.34)$$

The number of states is closely related to the number of particles N through the degeneracy of the momentum states ν , and together with the previous equation allows to define a relation between the density of particles ρ and the Fermi momentum of the system

$$\rho = \frac{N}{V} = \frac{1}{6\pi^2} \nu k_F^3. \quad (2.35)$$

At this point we can compute the values of the ratio k_F^2/m^2 at different densities as

$$\frac{k_F^2}{m^2} = \left(\frac{6\pi^2 \rho}{\nu m^3} \right)^{\frac{2}{3}}. \quad (2.36)$$

The previous equation provides $k_F^2/m^2 \sim 0.1 - 0.3$ for densities ranging between once and four times the nuclear saturation density ρ_0 , suggesting that some kind of relativistic corrections may contribute as a small fraction of the average single particle energy. Conversely we have that the condition $k_F/m \sim 1$ is achieved by considering densities as large as $\rho \sim 40\rho_0$, very well above the typical values expected inside a neutron star.

A somewhat similar discussion can be addressed also to atomic nuclei. Instead of using arguments based on the Fermi momentum we can invoke the indetermination principle in order to estimate the average momentum of bounded nucleons. It turns out that for $\Delta x \sim 1.6$ fm, which is the average measured nucleon-nucleon distance in nuclei like oxygen and carbon, we have $\langle p^2 \rangle/m^2 \sim 0.05$. According to what argued by Carlson *et al* in Ref. [70] this is an indication that relativistic corrections could be comparable to the contribution coming from three-body forces and should be taken into account.

The problem of considering relativistic corrections in nuclear matter is a highly non-trivial task and can be approached in different manners. The first thing one could think is to develop an effective field theory in which the relevant degrees of freedom are nucleons. This kind of theory will be relativistic by construction, being based on the formalism of quantum field theory. A model of nucleons interacting by means of scalar and vector mesons was first proposed by Walecka [100]. Unfortunately this kind of theory can be solved only in the mean field approximation, i.e. by replacing the meson fields in the equation of motion with their ground state expectation values. This approximation is not fully justified at the typical densities of neutron

star matter and turns out to produce an oversimplified dynamics which is unable to capture the strong correlations between nucleons.

Here we are going to discuss an alternative approach, formalized by Krajcik and Foldy [68, 101], referred to as Relativistic Hamiltonians. This formalism attempts to obtain a covariant description of a system with a fixed number of particles within the framework of non-relativistic quantum mechanics. This description is achieved by imposing the commutation relations of the Poincarè group on the Hilbert space of the system, whose generators are defined through an expansion in $1/c$, with c being the speed of light. Foldy and Krajcik have shown that there exists a way to define the generators of the Poincarè group up to every order in $1/c$.

Before going on it is important to clarify what is intended by "covariant description" in the context of a system with a fixed number of particles. To this purpose we want to resume some points highlighted in the brilliant discussion performed by Leslie L. Foldy in one of his works [101]. We want to introduce the concept of relativity in the description of a quantum system of particles, whose interactions are expressed in terms of a potential depending on their dynamical variables, rather than being mediated by a field. In this context it is known that we can't invoke the classical concepts of relativity as related to Lorentz transformations between the spacetime coordinates of a given particle, in a given position and at a given time instant. Anyway we can just notice that the necessity to connect the concept of relativity to the symmetry of an underlying spacetime continuum is only an additional requirement that is needed by classical theory but that is unnecessary in a quantum description. In other words we are not interested in finding a theory perfectly describing every aspect of nature, for which the description of the spacetime, as well as the possibility of creating and destroying particles will be mandatory, but we just want to carry out a relativistic covariant description of a quantum system. In this sense by directly citing Foldy our viewpoint should be that *"if we wish to examine the basic implications or demands of relativistic covariance stripped of all extraneous ideas and free of all preconceptions, we stand on more secure ground in retreating to the position that the Lorentz group expresses the relationship between physical phenomena viewed by different observers"*. Strictly speaking relativistic covariance is just meant as the equivalence between different observers describing the same physical phenomena. Such an equivalence will be established by means of the Lorentz transformation group.

Let us suppose to have two different observers A and B . A given abstract state of the system, referred to as Ψ , will be described by the observer A with a state vector $|\psi\rangle_A$, in its 'private' Hilbert space \mathcal{H}_A . In the same way the observer B will describe the system with a vector $|\psi\rangle_B$ belonging to the Hilbert space \mathcal{H}_B . Since the vectors $|\psi\rangle_A$ and $|\psi\rangle_B$ describe the same abstract state Ψ , we can establish a one-to-one correspondence between the Hilbert spaces of the two observers. In order for the physics to be the same as described by different observers, the transition probabilities to a given state Φ should be the same in every private Hilbert space. Therefore we should have the identity

$$|{}_A\langle\phi|\psi\rangle_A|^2 = |{}_B\langle\phi|\psi\rangle_B|^2 \quad (2.37)$$

for every couple of state vectors and equivalent observers. The equality of the transition probabilities implies that the one-to-one correspondence between the

Hilbert spaces of different observers should be an isomorphism. Since all the observers are isomorphic between each other we can define a unique 'public' space Ω , which all the other spaces are isomorphic to. This means that two states $|\psi\rangle_A$ and $|\psi\rangle_B$, describing the same abstract state, but belonging to different Hilbert spaces, will be represented by two different state vectors in the public Hilbert space Ω . In this sense the isomorphism between different spaces becomes an automorphism in the public space Ω . Let us take the two observers A and B to be connected by the Lorentz transformation Λ . If we label $|\psi_A\rangle$ and $|\psi_B\rangle$ the state vectors respectively representing $|\psi\rangle_A$ and $|\psi\rangle_B$, in the public space Ω , we will have that the isomorphism between A and B , will be represented by a linear operator $U(\Lambda)$, such that

$$|\psi_B\rangle = U(\Lambda)|\psi_A\rangle. \quad (2.38)$$

The equality of the transition probabilities, together with the previous definition leads to

$$|\langle\phi_B|\psi_B\rangle|^2 = |\langle\phi_A|U^\dagger(\Lambda)U(\Lambda)|\psi_A\rangle|^2 = |\langle\phi_A|\psi_A\rangle|^2, \quad (2.39)$$

which implies that the operator $U(\Lambda)$ should be unitary. Since the previous discussion can be applied to any couple of equivalent observers, we can take a third observer C which is related to A by the transformation Λ_{AC} . We can also define the Lorentz transformation Λ_{BC} connecting B and C , and rename the transformation Λ between A and B as Λ_{AB} . At this point we have

$$|\psi_C\rangle = U(\Lambda_{BC})|\psi_B\rangle = U(\Lambda_{BC})U(\Lambda_{AB})|\psi_A\rangle = U(\Lambda_{AC})|\psi_A\rangle, \quad (2.40)$$

yielding to

$$U(\Lambda_{AC}) = U(\Lambda_{BC})U(\Lambda_{AB}). \quad (2.41)$$

Since the Lorentz transformations form a group under the composition rule

$$\Lambda_{AC} = \Lambda_{BC} \circ \Lambda_{AB}, \quad (2.42)$$

the set of linear operators $U(\Lambda)$ defines a representation of the Lorentz group on the public Hilbert space Ω . In conclusion we can define a relativistic system as a quantum mechanical system, whose state vectors form a representation space for the Lorentz group.

2.3.1 Boost corrections: classical description

In this section a very pedagogical and intuitive discussion of a given type of relativistic correction, referred to as boost corrections, is presented. Boost corrections are additional interaction terms arising when we observe a two-particle system in a reference frame different from its center of mass. Strictly speaking we have to be careful when we use a non-relativistic potential in order to describe the relativistic system. Indeed because the Lorentz transformation between different reference frames involves also the Hamiltonian of the system, we have no guarantee that an interaction potential defined within a non-relativistic framework, in a specific reference frame, will not be affected by that Lorentz transformation. Let us consider a two-particle system with the Hamiltonian

$$\mathcal{H} = \frac{\mathbf{p}_1^2}{2m_1} + \frac{\mathbf{p}_2^2}{2m_2} + v(\mathbf{r}) \quad (2.43)$$

where $\mathbf{r} = \mathbf{r}_2 - \mathbf{r}_1$. At this point we can define the center-of-mass variables

$$\begin{aligned}\mathbf{P} &= \mathbf{p}_1 + \mathbf{p}_2 \\ \mathbf{q} &= \frac{1}{2}(\mathbf{p}_2 - \mathbf{p}_1),\end{aligned}\tag{2.44}$$

with which the Hamiltonian can be written as

$$\mathcal{H} = \frac{\mathbf{P}^2}{2M} + \frac{\mathbf{q}^2}{2\mu} + v(\mathbf{r}),\tag{2.45}$$

with $M = m_1 + m_2$ and $\mu = m_1 m_2 / (m_1 + m_2)$. This expression for the Hamiltonian holds in every reference frame within non-relativistic mechanics. If we make a Galileian transformation to another inertial frame we will have

$$\begin{aligned}\mathbf{r} &\rightarrow \mathbf{r}' = \mathbf{r} \\ \mathbf{q} &\rightarrow \mathbf{q}' = \mathbf{q} \\ \mathbf{P} &\rightarrow \mathbf{P}' = \mathbf{P} + M\mathbf{V}_T,\end{aligned}\tag{2.46}$$

where \mathbf{V}_T is the relative velocity between the two reference frames. It is straightforward to see that under this transformation the part of the Hamiltonian describing the relative motion remains unchanged.

Let us move to a relativistic picture and consider two particles, with the same mass m , interacting through a potential $v(\mathbf{r})$ in their center of mass frame. In this frame, where $\mathbf{P} = 0$, we can label the Hamiltonian as $H(\mathbf{q}, \mathbf{r})$. We are interested in carrying out the Hamiltonian in a generic reference frame, $H'(\mathbf{P}', \mathbf{q}', \mathbf{r}')$. In order to avoid unnecessary complications we can also take the two particles to be at rest with respect to their center of mass and consider a boost to a frame where $\mathbf{p}'_1 = \mathbf{p}'_2 = \mathbf{P}'/2$. This implies $\mathbf{q} = \mathbf{q}' = 0$. Under all these assumptions the Hamiltonian in the center of mass takes the form

$$H(\mathbf{r}) = M + v(\mathbf{r}).\tag{2.47}$$

We can define the 4-vector P such that

$$P^\nu = (H, \mathbf{0}).\tag{2.48}$$

If we now perform a boost transformation defined by the velocity $\mathbf{v} = \beta\hat{\mathbf{u}}$ between the two frames, we have that the 4-vector P will transform according to

$$P \rightarrow P' = (H', \mathbf{P}')\tag{2.49}$$

with

$$\begin{aligned}H' &= \gamma H, \\ \mathbf{P}' &= \beta\gamma H\hat{\mathbf{u}},\end{aligned}\tag{2.50}$$

where γ is defined in the usual way as $\gamma = (1 - \beta^2)^{-\frac{1}{2}}$.

Since P is a 4-vector its magnitude should be a Lorentz scalar, yielding

$$H^2 = H'^2 - \mathbf{P}'^2,\tag{2.51}$$

which implies

$$H' = \sqrt{H^2 + \mathbf{P}'^2} = H \sqrt{1 + \frac{\mathbf{P}'^2}{H^2}} \approx H \left(1 + \frac{\mathbf{P}'^2}{2H^2} - \frac{\mathbf{P}'^4}{8H^4} \right). \quad (2.52)$$

In the last step of the previous equation we have expanded in powers of \mathbf{P}'^2/H^2 . We are assuming that all the momenta are very much smaller than the rest mass of the particles m . Since the leading term in the Hamiltonian H is $M = 2m$ this justifies the expansion. If we now assume that the potential energy $v(\mathbf{r})$ is of the same order of the non-relativistic kinetic energy $\mathbf{p}^2/2m$, we can treat it as an $O(1/m)$ term. With this additional condition, by inserting the explicit expression of H into the previous equation and keeping only terms up to order $1/m^3$, we have

$$H' = H + \frac{\mathbf{P}'^2}{2M} - \frac{\mathbf{P}'^2}{2M^2}v(\mathbf{r}) - \frac{\mathbf{P}'^4}{8M^3} + O\left(\frac{1}{m^4}\right). \quad (2.53)$$

In the previous equation we can identify the second and fourth terms in the right hand side as those coming from the kinetic contribution of the center of mass motion, whereas the third term is a relativistic correction to the interaction potential that depends on the total momentum of the interacting particles. We have still to express the Hamiltonian H' in terms of the distance \mathbf{r}' in the boosted frame. Indeed we notice that the interaction potential appearing in the previous equation is still written in terms of the relative distance in the center of mass frame \mathbf{r} , which is related to that in the boosted frame through Lorentz contraction. Therefore if we define the component of the vector \mathbf{r} along the direction of the boost as $r_u \equiv \mathbf{r} \cdot \hat{\mathbf{u}}$, we have

$$r_u = \gamma r'_u. \quad (2.54)$$

Since

$$\gamma = \frac{H'}{H} = 1 + \frac{\mathbf{P}'^2}{2M^2} + O\left(\frac{1}{m^3}\right), \quad (2.55)$$

we have that

$$\mathbf{r} \approx \mathbf{r}' + \frac{\mathbf{P}'^2}{2M^2}(\hat{\mathbf{u}} \cdot \mathbf{r}')\hat{\mathbf{u}} = \mathbf{r}' + \frac{1}{2M^2}(\mathbf{P}' \cdot \mathbf{r}')\mathbf{P}' \quad (2.56)$$

Substituting into the expression for the potential we have

$$v(\mathbf{r}) = v(\mathbf{r}') + \frac{1}{2M^2}(\mathbf{P}' \cdot \mathbf{r}')\mathbf{P}' \cdot \nabla v(\mathbf{r}') + O\left(\frac{1}{m^4}\right). \quad (2.57)$$

Putting all the pieces together we finally have the expression for the Hamiltonian in the boosted frame up to order $1/m^3$

$$H(\mathbf{P}, \mathbf{r}) = 2m + \frac{\mathbf{P}^2}{4m} - \frac{\mathbf{P}^4}{64m^3} + v(\mathbf{r}) - \frac{\mathbf{P}^2}{8m^2}v(\mathbf{r}) + \frac{1}{8m^2}\mathbf{P} \cdot \mathbf{r}\mathbf{P} \cdot \nabla v(\mathbf{r}), \quad (2.58)$$

where the prime indices have been suppressed in order to lighten the notation.

An additional contribution to the boost correction can be also provided by Thomas precession, a purely relativistic effect which is related to the non-commutativity of two non-collinear Lorentz boosts. The fact that the commutation relations between different boosts doesn't form a sub-algebra of the Lorentz group turns into the fact

that the rest frame of a particle following a curved trajectory rotates. This rotation will cause the precession of the spin of the particle. From classical mechanics we know that the time derivatives of a vector in two reference frames which rotate with respect to each other are related by

$$\frac{d\mathbf{S}}{dt} = \left(\frac{d\mathbf{S}}{dt}\right)' + \boldsymbol{\omega}_T \times \mathbf{S} \quad (2.59)$$

where the angular velocity of the rotating frame was shown by Thomas to be

$$\boldsymbol{\omega}_T = -\nabla v(\mathbf{r}) \times \frac{\mathbf{P}}{4m^2} \quad (2.60)$$

up to order $1/m^2$. The Thomas precession potential for the first particle is given by

$$\delta v_{TP}^1 = \mathbf{s}_1 \cdot \boldsymbol{\omega}_T = \frac{1}{8m^2} \boldsymbol{\sigma}_1 \cdot \mathbf{P} \times \nabla v(\mathbf{r}). \quad (2.61)$$

In the moving frame the two interacting particles have the same velocity but opposite accelerations. Therefore the total Thomas potential of the couple will be

$$\delta v_{TP}(\mathbf{P}, \mathbf{r}) = \frac{1}{8m^2} (\boldsymbol{\sigma}_1 - \boldsymbol{\sigma}_2) \cdot \mathbf{P} \times \nabla v(\mathbf{r}). \quad (2.62)$$

In summary, what emerges from this first discussion is that for a given interaction potential $v(\mathbf{r})$ defined in the rest frame of two interacting particles, its generalization to a generic reference frame involves the appearance of contributions depending on the total momentum $\mathbf{P} = \mathbf{p}_1 + \mathbf{p}_2$ of the interacting pair. Such terms can be collected together into the correction $\delta v(\mathbf{P}, \mathbf{r})$.

2.3.2 Relativistic Hamiltonians

Relativistic Hamiltonians are defined as the sum of relativistic one-body kinetic energies, two- and many-body interactions, and their boost corrections. The explicit form can be written as

$$\mathcal{H}_R = \sum_i \sqrt{m_i^2 + p_i^2} + \sum_{i<j} [\tilde{v}_{ij} + \delta v_{ij}(\mathbf{P}_{ij})] + \sum_{i<j<k} [\tilde{V}_{ijk} + \delta V_{ijk}(\mathbf{P}_{ijk})] \quad (2.63)$$

where \tilde{v}_{ij} and \tilde{V}_{ijk} label two- and three-body potentials in the rest frame of the interacting particles. In such frames we have that

$$\mathbf{P}_{ij} = \mathbf{p}_i + \mathbf{p}_j = 0 \quad (2.64)$$

and

$$\mathbf{P}_{ijk} = \mathbf{p}_i + \mathbf{p}_j + \mathbf{p}_k = 0. \quad (2.65)$$

respectively. The terms δv_{ij} and δV_{ijk} are the aforementioned boost corrections and are related to the motion of the center of mass of the interacting particles. These corrections will therefore vanish in the particle center of mass frame yielding

$$\begin{aligned} \delta v_{ij}(\mathbf{P}_{ij} = 0) &= 0, \\ \delta V_{ijk}(\mathbf{P}_{ijk} = 0) &= 0. \end{aligned} \quad (2.66)$$

We have already seen how the meaning of the two-body boost correction can be understood in terms of classical considerations. In this section we are going to review their formal derivation obtained by just imposing the symmetry of the system under the Poincarè group. In their pioneering works Krajcik and Foldy have derived such corrections through an expansion in powers of v/c or alternatively P/m , showing that they are defined to all orders in such an expansion. In the present discussion we are going to review only the calculation up to the leading order P^2/m^2 , following the approach of Ref. [69].

We're not going to discuss the three-body boost correction δV_{ijk} because there exist some arguments, based on exact calculation of light nuclei, according to which this kind of correction should be much smaller than its two-body counterpart, and could safely be neglected. A very heuristic argument confirming this point could be that, since δv_{ij} is found to account for a very small fraction of the two-nucleon potential energy, consequently the correction δV_{ijk} should account for a small part of the three-body one. Additionally, since the ratio between three- and two- nucleon interaction energies in light nuclei is tiny, the contribution of three-body boost corrections should be negligible with respect to its two-body counterpart at nuclear densities.

The potential \tilde{v}_{ij} is determined by the details of the interaction between particles and should in principle embody some relativistic effects. In practical uses it is usually obtained by fitting a given model upon the NN scattering data in their center of mass rest frame and the relativistic effects are therefore buried into this fitting procedure.

In order to carry out the expression for the boost correction we are going to impose relativistic covariance on a system of two interacting particles. As already discussed before, our requirement of relativistic covariance means that our system should be symmetric under the Poincarè group. According to the Wigner theorem we can build up a unitary representation of the group by imposing the commutation relation of the Poincarè algebra between the group generators

$$\begin{aligned} [P^i, P^j] &= [H, P^i] = [J^i, H] = 0, \\ [K^i, H] &= iP^i, \quad [J^i, J^j] = i\epsilon_{ijk}J^k, \\ [K^i, P^j] &= i\delta_{ij}H, \quad [J^i, K^j] = i\epsilon_{ijk}K^k, \\ [J^i, P^j] &= i\epsilon_{ijk}P^k, \quad [K^i, K^j] = -i\epsilon_{ijk}J^k. \end{aligned} \tag{2.67}$$

Let us consider two interacting particles with mass m and spin \mathbf{s} . We can define the generators of translations and rotations in the usual way as

$$\mathbf{P} = \mathbf{p}_1 + \mathbf{p}_2, \tag{2.68}$$

$$\mathbf{J} = \mathbf{r}_1 \times \mathbf{p}_1 + \mathbf{r}_2 \times \mathbf{p}_2 + \mathbf{s}_1 + \mathbf{s}_2, \tag{2.69}$$

which satisfy their commutation relations by construction. Then we can define

$$H = H_0 + H_I \tag{2.70}$$

where H_0 labels the Hamiltonian of two free particles, and H_I contains all the interaction terms. In order for the commutation relations to be satisfied we must impose

$$[P^i, H_I] = [J^i, H_I] = 0, \tag{2.71}$$

therefore the interaction should be translationally and rotationally invariant. As we introduce an interaction term in the Hamiltonian we have to modify also the boost generator according to

$$\mathbf{K} = \mathbf{K}_0 + \mathbf{K}_I \quad (2.72)$$

with

$$[J^i, K_I^j] = i\epsilon_{ijk}K_I^k, \quad (2.73)$$

which tells us that \mathbf{K}_I is actually a vector. Moreover we have that \mathbf{K}_I has to satisfy

$$[K_0^i, K_I^j] + [K_I^i, K_0^j] + [K_I^i, K_I^j] = 0 \quad (2.74)$$

$$[K_I^i, P^j] = iH_I\delta_{ij} \quad (2.75)$$

$$[K_I^i, H_0] = [H_I, K_0^i] + [H_I, K_I^i]. \quad (2.76)$$

At this point, since we are interested into relativistic corrections, we can expand H and \mathbf{K} in powers of $1/m^2$ and keep only the first terms. The expansions of H_0 and \mathbf{K}_0 yield

$$H_0 = 2m + \frac{1}{2m} (p_1^2 + p_2^2) + O\left(\frac{1}{m^3}\right), \quad (2.77)$$

and

$$\begin{aligned} \mathbf{K}_0 &= t\mathbf{P} + 2m\mathbf{R} \\ &+ \frac{1}{2m} \left[\frac{1}{2} (\mathbf{r}_1 p_1^2 + p_1^2 \mathbf{r}_1 + \mathbf{r}_2 p_2^2 + p_2^2 \mathbf{r}_2) - \mathbf{s}_1 \times \mathbf{p}_1 - \mathbf{s}_2 \times \mathbf{p}_2 \right] + O\left(\frac{1}{m^3}\right). \end{aligned} \quad (2.78)$$

We can expand H_I according to

$$H_I = v + \delta v + \dots \quad (2.79)$$

where we can assume that v is of order $1/m$ since in systems like nuclei the interaction energy is about the same order as the non-relativistic kinetic energy. The correction δv is of order $1/m^3$ and the ellipsis represents terms of order $1/m^4$ or higher. Finally we also assume that the non-relativistic potential v is independent of \mathbf{P} . At this point we can impose the commutation relations (2.75) and (2.76) and keeping only the leading terms we find

$$\mathbf{K}_I = v\mathbf{R} + O\left(\frac{1}{m^3}\right) \quad (2.80)$$

and

$$\begin{aligned} 2m[\mathbf{R}, \delta v] &= \frac{1}{2m} \left[(p_1^2 + p_2^2), v\mathbf{R} \right] \\ &+ \frac{1}{4m} \left[(\mathbf{r}_1 p_1^2 + p_1^2 \mathbf{r}_1 + \mathbf{r}_2 p_2^2 + p_2^2 \mathbf{r}_2) - \boldsymbol{\sigma}_1 \times \mathbf{p}_1 - \boldsymbol{\sigma}_2 \times \mathbf{p}_2 \right]. \end{aligned} \quad (2.81)$$

Evaluating the commutators one obtains the basic equation for δv

$$\begin{aligned} [\mathbf{R}, \delta v] &= -\frac{i}{4m^2} v\mathbf{P} - \frac{1}{4m^2} [\mathbf{r}\mathbf{P} \cdot \mathbf{p}, v] + \frac{1}{16m^2} [(\boldsymbol{\sigma}_1 + \boldsymbol{\sigma}_2) \times \mathbf{P}, v] \\ &+ \frac{1}{8m^2} [(\boldsymbol{\sigma}_1 - \boldsymbol{\sigma}_2) \times \mathbf{p}, v], \end{aligned} \quad (2.82)$$

where \mathbf{p} is the relative momentum. This equation can not determine δv uniquely, since we can always write

$$\delta v = \delta v' + \delta v(\mathbf{P}) \quad (2.83)$$

where $\delta v'$ commutes with \mathbf{R} . In this respect we can therefore define

$$\tilde{v} = v + \delta v' + \text{higher order terms independent of } \mathbf{P}. \quad (2.84)$$

The quantity \tilde{v} collects all the interaction terms that are independent of \mathbf{P} i.e. it represents the interaction in the center of mass frame embodying also relativistic corrections. Conversely $\delta v(\mathbf{P})$ represents the relativistic corrections related to the motion of the center of mass of the interacting pair, and it can be derived by Eq. (2.82) whose simplest solution can be written as

$$\delta v(\mathbf{P}) = -\frac{P^2}{8m^2}\tilde{v} + \frac{1}{8m^2}[\mathbf{P} \cdot \mathbf{rP} \cdot \nabla, \tilde{v}] + \frac{1}{8m^2}[(\boldsymbol{\sigma}_1 - \boldsymbol{\sigma}_2) \times \mathbf{P} \cdot \nabla, \tilde{v}]. \quad (2.85)$$

It is sufficient to use \tilde{v} up to order $1/m$ to have $\delta v(\mathbf{P})$ up to order $1/m^3$. If the potential is an independent function of the spin of the two particles, we find a simplified version of the previous equation

$$\delta v(\mathbf{P}) = -\frac{P^2}{8m^2}v(\mathbf{r}) + \frac{1}{8m^2}\mathbf{P} \cdot \mathbf{rP} \cdot \nabla v(\mathbf{r}) + \frac{1}{8m^2}(\boldsymbol{\sigma}_1 - \boldsymbol{\sigma}_2) \cdot \mathbf{P} \times \nabla v(\mathbf{r}). \quad (2.86)$$

We can immediately recognize how the previous equation coincides with the expression carried out in the previous section by only classical considerations. A further simplification comes by neglecting the last term coming from Thomas precession. Indeed it was shown from calculations of the binding energy of ${}^3\text{H}$ and ${}^4\text{He}$ that such a contribution is smaller than the other two. Moreover the appearance of additional terms, arising from the fact that the interaction potential could in principle depend on the spin and relative momentum of the interacting particles, were proved to be even smaller [102].

2.3.3 Relativistic corrections to meson exchange potential

A very instructive example in order to further understand the different contributions of relativistic corrections, is provided by studying relativistic effects in meson exchange potentials. Meson exchange potentials are derived from the non-relativistic limit of an interaction Hamiltonian defined in the QFT framework. In this sense we can consider relativistic corrections by taking into account higher order terms in the non-relativistic expansion. Let us consider two fermions interacting through a scalar boson field ϕ with mass μ_ϕ , as described by the interaction Hamiltonian

$$\mathcal{H}_I = G_S \phi \bar{\psi} \psi. \quad (2.87)$$

The invariant amplitude for a scattering process between two nucleons at leading order, represented by the Feynman diagram of Fig. 2.7, can be written as

$$i\mathcal{M} = G_S^2 \bar{u}_1(\mathbf{p}'_1) u_1(\mathbf{p}_1) \frac{-1}{q^2 - \mu_\phi^2 + i\epsilon} \bar{u}_2(\mathbf{p}'_2) u_2(\mathbf{p}_2), \quad (2.88)$$

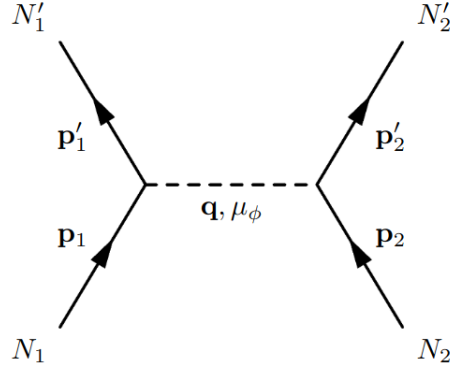


Figure 2.7. Feynman diagram of one boson exchange process.

Where we have defined a 4-vector $q^\mu = (\omega, \mathbf{q})$, with

$$\begin{aligned}\omega &= E_1' - E_1 = E_2 - E_2', \\ \mathbf{q} &= \mathbf{p}_1' - \mathbf{p}_1 = \mathbf{p}_2 - \mathbf{p}_2'.\end{aligned}\quad (2.89)$$

It is also useful to define the relative momenta \mathbf{p} and \mathbf{p}' according to

$$\begin{aligned}\mathbf{p} &= \frac{1}{2}(\mathbf{p}_1 - \mathbf{p}_2), \\ \mathbf{p}' &= \frac{1}{2}(\mathbf{p}_1' - \mathbf{p}_2') = \mathbf{p} + \mathbf{q}.\end{aligned}\quad (2.90)$$

Using the same arguments as in Appendix A we can relate the interaction potential to the invariant amplitude \mathcal{M} by means of

$$-i\mathcal{M} = \langle v(\mathbf{p}, \mathbf{q}, \mathbf{P}) \rangle + O\left(\frac{1}{m^4}\right), \quad (2.91)$$

providing we adjust the spinor normalization according to

$$u_i(\mathbf{p}_i) \rightarrow \sqrt{\frac{m}{E_i}} u_i(\mathbf{p}_i), \quad (2.92)$$

with

$$u_i(\mathbf{p}_i) = \sqrt{\frac{E_i + m}{2m}} \begin{pmatrix} \chi_i \\ \frac{\boldsymbol{\sigma} \cdot \mathbf{p}_i}{E_i + m} \chi_i \end{pmatrix}. \quad (2.93)$$

At this point we can expand the different contributions to the invariant amplitude in powers of $1/m$.

Since the leading term in ω is of order $1/m^2$, the propagator can be expressed as

$$\frac{1}{\omega^2 - \mathbf{q}^2 - \mu_\phi^2} = \frac{-1}{\mathbf{q}^2 + \mu_\phi^2} \left(1 - \frac{\omega^2}{\mathbf{q}^2 + \mu_\phi^2}\right)^{-1} \approx \frac{-1}{\mathbf{q}^2 + \mu_\phi^2} \left(1 + \frac{\omega^2}{\mathbf{q}^2 + \mu_\phi^2}\right). \quad (2.94)$$

Moreover, the terms $\bar{u}u$ gives a contribution of the kind

$$\bar{u}u = 1 + O\left(\frac{1}{m^2}\right), \quad (2.95)$$

therefore we can define the non-relativistic potential, which is the leading order term in the expansion of $-i\mathcal{M}$, as

$$v_0(\mathbf{q}) = -\frac{G_S^2}{\mathbf{q}^2 + \mu_\phi^2}. \quad (2.96)$$

By assuming $v_0(\mathbf{q})$ to be of order $1/m$, we find that it is sufficient to write down the expansion for the spinors only up to order $1/m^2$ in order to carry out the expression of the potential $v(\mathbf{p}, \mathbf{q}, \mathbf{P})$ up to order $1/m^3$.

Spinors normalized according to Eq. (2.92) give rise to

$$u_i(\mathbf{p}_i) = \left(1 - \frac{\mathbf{p}_i^2}{8m^2}\right) \begin{pmatrix} \chi_i \\ \frac{\boldsymbol{\sigma}_i \cdot \mathbf{p}_i}{2m} \chi_i \end{pmatrix} + O\left(\frac{1}{m^3}\right), \quad (2.97)$$

whereas the final expression for the propagator yields

$$G_S^2 \frac{-1}{\omega^2 - \mathbf{q}^2 - \mu_\phi^2} = v_0(\mathbf{q}) \left[1 + \frac{(\mathbf{P} \cdot \mathbf{q})^2}{4m^2(\mathbf{q}^2 + \mu_\phi^2)}\right] + O\left(\frac{1}{m^4}\right), \quad (2.98)$$

where we have substituted the explicit expression of ω

$$\omega = \frac{(\mathbf{P} \cdot \mathbf{q})^2}{4m^2} + O\left(\frac{1}{m^3}\right). \quad (2.99)$$

Since $\chi_i^\dagger \chi_i = 1$, we have that

$$\bar{u}_i(\mathbf{p}'_i) u_i(\mathbf{p}_i) = \left(1 - \frac{\mathbf{p}'_i{}^2}{8m^2} - \frac{\mathbf{p}_i^2}{8m^2}\right) \left(1 - \frac{\boldsymbol{\sigma}_i \cdot \mathbf{p}'_i \boldsymbol{\sigma}_i \cdot \mathbf{p}_i}{4m^2}\right). \quad (2.100)$$

By using the commutation relations of the Pauli matrices and after some algebraic manipulations we obtain that the spinor sector contributes to the invariant amplitude as

$$\begin{aligned} \bar{u}_1(\mathbf{p}'_1) u_1(\mathbf{p}_1) \bar{u}_2(\mathbf{p}'_2) u_2(\mathbf{p}_2) &= 1 - \frac{(\mathbf{p} + \mathbf{p}')^2}{4m^2} - \frac{i(\boldsymbol{\sigma}_1 + \boldsymbol{\sigma}_2) \cdot \mathbf{q} \times \mathbf{p}}{4m^2} \\ &\quad - \frac{\mathbf{P}^2}{4m^2} - \frac{i(\boldsymbol{\sigma}_1 - \boldsymbol{\sigma}_2) \cdot \mathbf{P} \times \mathbf{q}}{8m^2} + O\left(\frac{1}{m^3}\right). \end{aligned} \quad (2.101)$$

Putting all the pieces together we can finally write the interaction potential up to order $1/m^3$ as

$$v(\mathbf{p}, \mathbf{q}, \mathbf{P}) = \tilde{v}(\mathbf{p}, \mathbf{q}) + \delta v(\mathbf{q}, \mathbf{P}), \quad (2.102)$$

with

$$\tilde{v}(\mathbf{p}, \mathbf{q}) = v_0(\mathbf{q}) - \left[\frac{(\mathbf{p} + \mathbf{p}')^2}{4m^2} + \frac{i(\boldsymbol{\sigma}_1 + \boldsymbol{\sigma}_2) \cdot \mathbf{q} \times \mathbf{p}}{4m^2} \right] v_0(\mathbf{q}), \quad (2.103)$$

and

$$\delta v(\mathbf{q}, \mathbf{P}) = \left[-\frac{\mathbf{P}^2}{4m^2} + \frac{(\mathbf{P} \cdot \mathbf{q})^2}{4m^2(\mathbf{q}^2 + \mu_\phi^2)} - \frac{i(\boldsymbol{\sigma}_1 - \boldsymbol{\sigma}_2) \cdot \mathbf{P} \times \mathbf{q}}{8m^2} \right] v_0(\mathbf{q}). \quad (2.104)$$

In Eq. (2.102) we have grouped together the terms depending on the total momentum \mathbf{P} in order to underline the different nature of relativistic corrections. In accordance with what discussed in the previous section, the first term $\tilde{v}(\mathbf{p}, \mathbf{q})$, accounts for the interaction potential in the center-of-mass frame, and it is written as the non-relativistic potential v_0 plus some corrections that are independent of \mathbf{P} . These corrections should in principle depend on the nature of the interaction and could not be inferred by general considerations. Conversely the term $\delta v(\mathbf{q}, \mathbf{P})$ represents the widely discussed boost corrections and embodies all the effects related to motion of the full two-particle system. Indeed it could have been inferred by simply applying Eq. (2.86), which is related to Eq. (2.104) through a Fourier transform. Relativistic corrections to NN potential in its center-of-mass frame had been studied by Forest et al in Ref. [71]. In this work the authors had shown how the introduction of such effects result to be negligible with respect to the contribution coming from boost corrections.

2.4 Chiral potentials

A valuable alternative to phenomenological Hamiltonians is provided by a class of potentials derived within the framework of Chiral Effective Field Theory (χ EFT). This approach was originally developed by Weinberg in 1990s [103], who proposed to derive nuclear interactions from an effective field theory where the relevant degrees of freedom are low momentum nucleons and pions, whose interactions are constrained by the chiral symmetry of strong interactions. Chiral symmetry is an approximated symmetry of nature, both explicitly and spontaneously broken. It accounts for the symmetry of massless quarks under the $SU(2)_L \otimes SU(2)_R$ symmetry group.

The basic idea of χ EFT is to build up the most general Lagrangian, where the chosen degrees of freedom are pions and massless nucleons, symmetric under the group $SU(2)_L \otimes SU(2)_R$, and compatible with all the other basic symmetries, such as Lorentz invariance, parity conservation and baryon and lepton number conservation. The mass of the nucleons appears as a result of the spontaneous symmetry breaking and the pions can be identified with the Goldstone bosons of the model. Within this theory the interaction between nucleons occurs only by pion exchanges, accounting for long- and intermediate-range processes. All the heavier degrees of freedom are integrated out in contact terms, in a similar way to what happens in the Fermi theory of weak interactions with respect to the W and Z bosons. These contact interactions are responsible for the short range behavior of nuclear interactions, and their strength depends on unknown low-energy constants (LECs), to be determined by fitting nuclear data. Being an effective theory the Lagrangian potentially contains an infinite number of terms and must be truncated using a given power-counting scheme. Within the approach proposed by Weinberg, an expansion in powers of a typical momentum scale p , over a breakdown energy scale Λ_b is performed. The chiral Lagrangian can be therefore written as

$$\mathcal{L} = \mathcal{L}^{(0)} + \left(\frac{p}{\Lambda_b}\right)^2 \mathcal{L}^{(2)} + \left(\frac{p}{\Lambda_b}\right)^3 \mathcal{L}^{(3)} + \dots \quad (2.105)$$

The breakdown scale can be identified with the typical energy scale where the occurrence of heavier degrees of freedom can no longer be accounted by contact

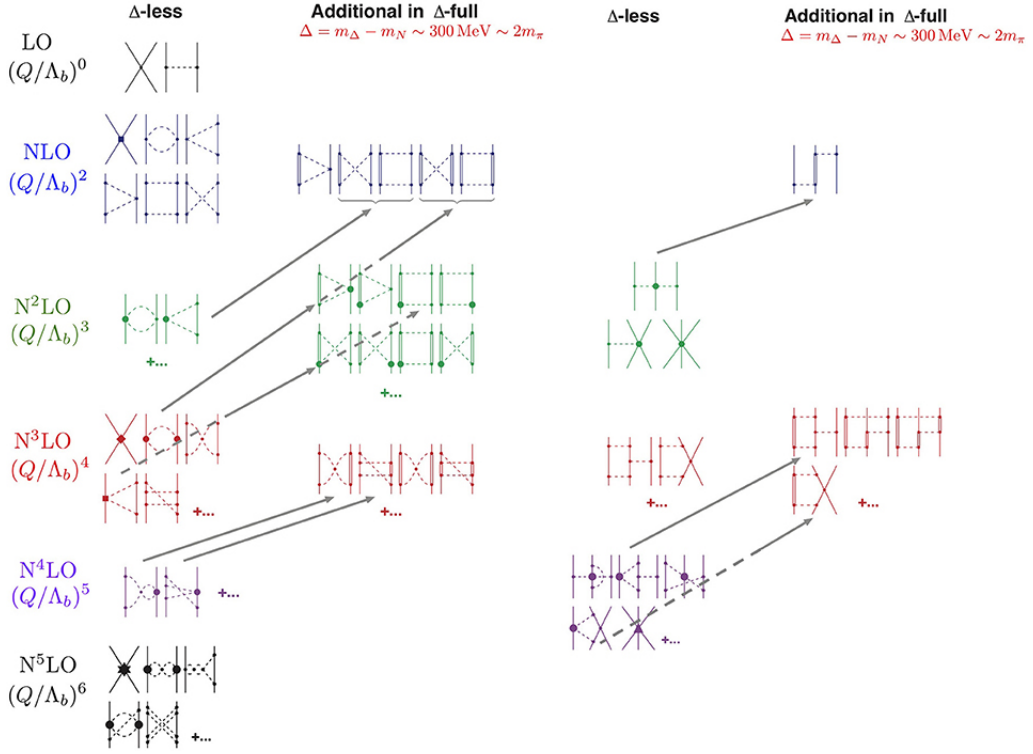


Figure 2.8. Chiral contributions to NN and NNN interactions based on Weinberg power counting scheme. The figure is taken from Ref [104].

interactions, and they should be explicitly considered within the theory. For this reason this Λ_b is usually set ~ 1 GeV, a typical scale where the exchange of heavier mesons, such as the ρ could play a significant role in nuclear interactions.

First derived chiral interactions were expressed in momentum space, and included only nucleons and pions. State-of-the-art models have been extended to include also Δ degrees of freedom, and a consistent procedure has been developed in order to obtain coordinate space representations, needed for the employment in Quantum Monte Carlo (QMC) calculations. See Ref [104] and references therein for an extensive review on this topic. In Fig. 2.8, taken from Ref [104], we can see how the Feynman diagrams, contributing to different orders in the chiral Lagrangian, are organized according to the Weinberg power counting scheme, both in the Δ and Δ -less theories.

Chiral potentials have proved to be extremely accurate in reproducing the binding energies and charge radii of nuclei with mass number $A \leq 16$, as well as the saturation properties of SNM. Moreover, in recent years they have also benefited from a great attention in the context of neutron star structure [105, 106].

The main and remarkable advantage of χ EFT lies in the capability of the formalism to carry out two- and many-nucleon interaction potentials in a fully consistent fashion. Moreover it also allows for improving the potential by adding higher order terms and to estimate the theoretical uncertainty. However, being based on a low momentum expansion its applicability is inherently limited when it comes to describe high density nuclear matter. Indeed recent analysis either

based on nuclear systematics, such as the analysis of NN scattering phase shifts and deuteron momentum distribution [63], or by astrophysical constraints [64], suggest that their applicability is limited up to $\rho \sim 2\rho_0$. However, because of the possibility to estimate the theoretical uncertainty χ EFT has proved to be very powerful in further constraint the EOS of nuclear matter at supranuclear. In several works, calculations of low density properties (up to $2\rho_0$) performed within χ EFT, with their uncertainty, have been used in combination with astrophysical data to constraint the free space of the nuclear matter EOS at the density relevant for NS physics. In particular it was shown how this kind of inference benefits with the addition of χ EFT calculations to the employed dataset [43–45, 91].

Chapter 3

Nuclear Matter Theory

In the previous chapter we discussed realistic expressions for the nuclear Hamiltonian. We introduced different ways to carry out an interaction potential suited to describe nucleon-nucleon scattering and few nucleon systems. The main goal of the theory of nuclear matter is the development of a complete framework able to carry out predictions of systems with an arbitrary number of constituents, starting from such a nuclear Hamiltonian. This means practically to solve the many-body Schrödinger equation

$$\mathcal{H}|\Psi_n\rangle = E_n|\Psi_n\rangle, \quad (3.1)$$

which involves severe difficulties even for the determination of the ground state energy E_0 . In order to circumvent the difficulties arising from the non-perturbative behavior of the nuclear potential, we have to rely upon approximated techniques. The first proposed approach, originally developed by K. Brueckner in the 1950s, is based on the replacement of the bare nucleon-nucleon potential with a well-behaved effective interaction, describing NN scattering in the nuclear medium and suitable to carry out calculations in perturbation theory [59, 107].

A different approach relies on exploiting the variational principle associated with the Schrödinger equation. It is known that the ground state of any quantum mechanical system is a lower bound for the energy expectation value over any other quantum state. Indeed every quantum state $|\psi\rangle$ can always be expressed as a linear combination of energy eigenstates

$$|\psi\rangle = \sum_n \langle E_n|\psi\rangle |E_n\rangle, \quad (3.2)$$

yielding

$$\frac{\langle\psi|H|\psi\rangle}{\langle\psi|\psi\rangle} = \frac{\sum_n E_n |\langle E_n|\psi\rangle|^2}{\sum_n |\langle E_n|\psi\rangle|^2} \geq \frac{E_0 \sum_n |\langle E_n|\psi\rangle|^2}{\sum_n |\langle E_n|\psi\rangle|^2} = E_0 \quad (3.3)$$

Therefore we can define a trial ground state $|\Psi_T\rangle$ such that

$$E_V = \frac{\langle\Psi_T|\mathcal{H}|\Psi_T\rangle}{\langle\Psi_T|\Psi_T\rangle} \geq \langle\Psi_0|\mathcal{H}|\Psi_0\rangle, \quad (3.4)$$

and performing a functional minimization of the variational energy E_V we can ideally find a good approximation for the ground state $|\Psi_0\rangle$. In the following sections we will see how to build up a reliable variational state by means of the Correlated Basis Function (CBF) approach.

3.1 Correlated Basis Function approach

In order to find a good choice for the trial ground state $|\Psi_T\rangle$ we can define a correlation operator \mathcal{F} such that

$$|\Psi_T\rangle = \mathcal{F}|\Phi_0\rangle, \quad (3.5)$$

with $|\Phi_0\rangle$ labeling the ground state of a nucleon Fermi gas. Realistic correlation operators are build up as a symmetric product of pair correlation operators

$$\mathcal{F} = \mathcal{S} \prod_{i<j} F_{ij}, \quad (3.6)$$

where F_{ij} is usually defined resembling the operatorial structure of the NN potential

$$F_{ij} = \sum_p f^p(r_{ij}) O_{ij}^p. \quad (3.7)$$

The symmetrization operator \mathcal{S} is necessary in order to obtain a trial ground state that is anti-symmetric under the exchange of different particles. Indeed, since in general we have that $[O_{ij}, O_{jk}] \neq 0$, the product of more operators acting on different pairs could be not symmetric under particle exchanges. At this point we can in principle determine the radial pair correlations $f^p(r)$, thanks to the variational principle

$$\frac{\delta E_V}{\delta f^p} = 0. \quad (3.8)$$

Nevertheless the computation of the expectation value of the many-body Hamiltonian on the correlated state $|\Psi_T\rangle$, as well as its normalization, involves $3A$ -dimensional integrations that are practically impossible already at the level of nuclei like carbon and oxygen. In order to overcome the difficulties associated with the large number of degrees of freedom we need to rely on some approximations. The short range nature of the nuclear interaction makes possible the so-called cluster expansion of the expectation values. Roughly speaking, since the correlation operator accounts for interaction effects, it is reasonable to think that when we move a subset of particles very far away from the others, the two 'clusters' will be uncorrelated among themselves. Mathematically this means that if we move m nucleons, labeled by $i_1 \dots i_m$, very far away from the remaining $A - m$, the correlation operator $\mathcal{F}(1 \dots A)$ factorizes according to

$$\mathcal{F}(1 \dots A) = \mathcal{F}_m(i_1 \dots i_m) \mathcal{F}_{A-m}(i_m \dots i_A). \quad (3.9)$$

The above property is referred to as the *cluster decomposition* property. Without loss of generality we can therefore impose $F_1 \equiv 1$ and $F_2(i, j) \equiv F_{ij}$ with

$$\lim_{r_{ij} \rightarrow \infty} F_{ij} = 1. \quad (3.10)$$

3.1.1 Cluster expansion

The cluster expansion of the matrix elements over a correlated state can be seen as reminiscent of the cluster expansion of the partition function of a classical fluid.

Following the treatment of J. Clark in Ref [108] we can define a partition function $G(\beta)$ as

$$G(\beta) = \log I(\beta) \quad (3.11)$$

with

$$I(\beta) = \langle \Psi | e^{\beta(\mathcal{H}-T_F)} | \Psi \rangle. \quad (3.12)$$

These definition allow us to write the energy of the system in the state $|\Psi\rangle$ as

$$E = T_F + \left. \frac{\partial}{\partial \beta} G(\beta) \right|_{\beta=0}. \quad (3.13)$$

We have defined $I(\beta)$ as a normalization integral of the full system of A particles. However, by invoking the cluster decomposition property we can also define the normalization integral for any sub sistem on an arbitrary number of $n < A$ particles. We can therefore write

$$\begin{aligned} I_i(\beta) &= \langle i | F_1^\dagger(1) e^{\beta(t_1 - \epsilon_1^F)} F_1(1) | i \rangle \\ I_{ij}(\beta) &= \langle ij | F_2^\dagger(12) e^{\beta(t_1 + t_2 + v_{12} - \epsilon_1^F - \epsilon_2^F)} F_2(12) | ij \rangle_a \\ &\vdots \\ I_{1\dots A}(\beta) &= \langle \Phi | \mathcal{F}^\dagger e^{\beta(\mathcal{H}-T_F)} \mathcal{F} | \Phi \rangle, \end{aligned} \quad (3.14)$$

where we have labeled with t_i the kinetic energy operator of the particle i , whereas ϵ_i^F labels the kinetic energy of the particle i in the Fermi gas approximation. We can see that, in the approximation of weak interaction and weak correlations, we can approximate $I_{ij} \approx I_i I_j$. Since we are not interested in this scenario, we need to correct the product of the one particle integrals with a term that depends on the pair correlation effects. This correction can be implemented in two ways, either by an additive term

$$I_{ij} = I_i I_j + X_{ij}, \quad (3.15)$$

or with a multiplicative factor

$$I_{ij} = I_i I_j Y_{ij}. \quad (3.16)$$

The second prescription exhibits a very powerful property. Since we know that $F_1 = 1$, it is straightforward that $I_i = 1$ and $I_{ij} = Y_{ij}$. With these definition the three-particle normalization integral I_{ijk} can be written as

$$I_{ijk}(\beta) = Y_{ij} Y_{jk} Y_{ik} Y_{ijk}. \quad (3.17)$$

Therefore for the A -particle term we can write

$$I(\beta) = \prod_{i < j} Y_{ij} \prod_{i < j < k} Y_{ijk} \cdots Y_{1\dots A}. \quad (3.18)$$

Thanks to the previous equation we obtain the following expression for the partition function $G(\beta)$

$$G(\beta) = \log I(\beta) = \sum_{i < j} \log Y_{ij} + \sum_{i < j < k} \log Y_{ijk} + \cdots + \log Y_{1\dots A} \quad (3.19)$$

By combining the previous equation with Eq. (3.13) we can write the energy of an A -body system as a sum of terms involving an increasing number of connected particles

$$E = T_F + (\Delta E)_2 + (\Delta E)_3 + \cdots + (\Delta E)_A. \quad (3.20)$$

This is the very nature of cluster expansion, i.e. the possibility of expanding an observable of an N -body system into a sum of terms describing the behavior of subsystems (clusters) involving an increasing number of correlated bodies.

3.2 Jastrow variational approach

The main features of cluster expansion are better understood within the Jastrow variational approach, which correspond to a simpler choice of the correlation operator. Let us take a correlated state of the form

$$|\Psi\rangle = F|\Phi_0\rangle \equiv \prod_{i<j} f(r_{ij})|\Phi_0\rangle. \quad (3.21)$$

In the previous equation $|\Phi_0\rangle$ is the ground state of a nucleon Fermi gas, that can be expressed as a Slater determinant of all the single particle states $\phi_{n_i}(x_i)$ according to

$$|\Phi_0\rangle = \frac{1}{\sqrt{A!}} \det \begin{vmatrix} \phi_{n_1}(x_1) & \phi_{n_1}(x_2) & \cdots & \phi_{n_1}(x_A) \\ \phi_{n_2}(x_1) & \phi_{n_2}(x_2) & \cdots & \phi_{n_2}(x_A) \\ \vdots & \vdots & \ddots & \vdots \\ \phi_{n_A}(x_1) & \phi_{n_A}(x_2) & \cdots & \phi_{n_A}(x_A) \end{vmatrix}, \quad (3.22)$$

where the index n_i labels the set of all quantum numbers of a single particle state, whereas x_i collects all the degrees of freedom of such a quantum wavefunction, both continuous and discrete. If we enclose the system in a finite volume V we can write

$$\phi_{n_a}(x_i) = \frac{1}{\sqrt{V}} e^{-i\mathbf{k}_a \cdot \mathbf{r}_i} \chi^a \eta^a \quad (3.23)$$

with χ^a and η^a being respectively the spinor and isospinor of the particle i in the a -th orbital. Within the variable x_i are collected the variable \mathbf{r}_i together with the discrete indices of the two spinors. In the following we will employ the symbolic writings

$$\int dx_i \equiv \text{Tr}_i \int d\mathbf{r}_i, \quad (3.24)$$

where Tr_i indicates the trace over the spin and isospin indices associated with the i -th particle. With these definitions we can see what happens to the normalization of the variational state

$$\langle \Psi | \Psi \rangle = \langle \Phi_0 | \prod_{i<j} f^2(r_{ij}) | \Phi_0 \rangle. \quad (3.25)$$

By defining the quantity

$$h(r_{ij}) = f^2(r_{ij}) - 1 \quad (3.26)$$

we have

$$\begin{aligned}\langle\Psi|\Psi\rangle &= \langle\Phi_0|\prod_{i<j}[1+h(r_{ij})]|\Phi_0\rangle \\ &= \langle\Phi_0|\Phi_0\rangle + \sum_{i<j}\langle\Phi_0|X^{(2)}(\mathbf{r}_i,\mathbf{r}_j)|\Phi_0\rangle + \sum_{i<j<k}\langle\Phi_0|X^{(3)}(\mathbf{r}_i,\mathbf{r}_j,\mathbf{r}_k)|\Phi_0\rangle + \dots\end{aligned}\quad (3.27)$$

From the previous expression it is clear that the normalization of the correlated state can be expressed as a sum of terms involving an increasing number of correlated particles. Because of the symmetry properties of the ground state Φ_0 the previous expression can be written as

$$\langle\Psi|\Psi\rangle = 1 + \binom{A}{2}\langle\Phi_0|X^{(2)}(\mathbf{r}_1,\mathbf{r}_2)|\Phi_0\rangle + \binom{A}{3}\langle\Phi_0|X^{(3)}(\mathbf{r}_1,\mathbf{r}_2,\mathbf{r}_3)|\Phi_0\rangle + \dots \quad (3.28)$$

with

$$X^{(2)}(\mathbf{r}_1,\mathbf{r}_2) = h(r_{12}) \quad (3.29)$$

and

$$\begin{aligned}X^{(3)}(\mathbf{r}_1,\mathbf{r}_2,\mathbf{r}_3) &= h(r_{12})h(r_{13}) + h(r_{12})h(r_{23}) + h(r_{23})h(r_{13}) \\ &\quad + h(r_{12})h(r_{13})h(r_{23}).\end{aligned}\quad (3.30)$$

We can define a diagrammatic representation which helps to visualize the expansion of Eq. (3.28)

$$\begin{aligned}\langle\Psi|\Psi\rangle &= 1 + \bullet\text{---}\bullet \\ &\quad + \begin{array}{c} \bullet \\ \diagup \quad \diagdown \\ \bullet\text{---}\bullet \end{array} + \begin{array}{c} \bullet \\ \diagdown \quad \diagup \\ \bullet\text{---}\bullet \end{array} + \begin{array}{c} \bullet \\ \diagup \quad \diagdown \\ \bullet\text{---}\bullet \end{array} + \begin{array}{c} \bullet \\ \diagdown \quad \diagup \\ \bullet\text{---}\bullet \end{array} + \dots\end{aligned}\quad (3.31)$$

From the previous equations we have seen that it's possible to express any amplitude between the correlated state $|\Psi\rangle$ as a sum of terms involving an increasing number of correlated particles, named clusters. Moreover we have mentioned that in principle we could derive a diagrammatic representation for each term of such an expansion. Indeed it is possible to carry out some general rules, through which we can write down the contribution of different cluster terms starting by their pictorial representation. In the following we are going to demonstrate these rules.

Let's consider the expectation value of an Hamiltonian H

$$H = \sum_i \frac{\mathbf{p}_i^2}{2m} + \sum_{i<j} v(\mathbf{r}_{ij}) \quad (3.32)$$

over the correlated state $|\Psi\rangle$. Since the Hamiltonian can be written as a kinetic part T plus a potential part V , we will discuss these two contributions separately. Let's start with the potential contribution. We can write it as

$$\langle V \rangle = \frac{\langle\Phi_0|F^\dagger V F|\Phi_0\rangle}{\langle\Phi_0|F^\dagger F|\Phi_0\rangle} = \frac{\mathcal{N}}{\mathcal{D}}. \quad (3.33)$$

We are going to separately discuss the contribution of the numerator \mathcal{N} and the denominator \mathcal{D} .

$$\mathcal{N} = \langle \Phi_0 | F^\dagger V F | \Phi_0 \rangle = \sum_{i < j} \langle \Phi_0 | F^\dagger v(\mathbf{r}_{ij}) F | \Phi_0 \rangle = \frac{A(A-1)}{2} \langle \Phi_0 | F^\dagger v(\mathbf{r}_{12}) F | \Phi_0 \rangle. \quad (3.34)$$

By explicitly writing the internal product we have

$$\mathcal{N} = \frac{A(A-1)}{2} \int d\mathbf{r}_1 d\mathbf{r}_2 v(\mathbf{r}_{12}) \text{Tr}_1 \text{Tr}_2 \int dx_3 \cdots dx_A F^2 | \Phi_0 \rangle^2. \quad (3.35)$$

The quantity F^2 can be written as

$$F^2 = \prod_{i < j} f^2(r_{ij}) = f^2(r_{12}) \prod_{i < j \neq 1, 2} 1 + h(r_{ij}), \quad (3.36)$$

which allows to move the contribution coming from $f^2(r_{12})$ out of the integral over $x_3 \dots x_A$. We notice that F^2 can be now expressed as

$$F^2 = f^2(r_{12}) \left[1 + \sum_{i \neq 1, 2} X^{(3)}(\mathbf{r}_1, \mathbf{r}_2; \mathbf{r}_i) + \sum_{i < j \neq 1, 2} X^{(4)}(\mathbf{r}_1, \mathbf{r}_2; \mathbf{r}_i, \mathbf{r}_j) + \cdots \right]. \quad (3.37)$$

We define as active particles the ones appearing in the interaction potential, i.e. those labeled by the indices 1 and 2 in the previous equations. The other $A - 2$ particles will be referred to as background particles. With this notation the term $X^{(n)}(\mathbf{r}_1, \mathbf{r}_2; \mathbf{r}_{i_1}, \dots, \mathbf{r}_{i_{n-2}})$, with $3 \leq n \leq A$ involves all the contributions arising by the correlations between either the active particles and the remaining $n - 2$ background particles, or among the background particles alone. By substituting this expression for the F^2 operator and exploiting the symmetry properties of the Fermi gas ground state function, we can write

$$\begin{aligned} \mathcal{N} = & \frac{1}{2} \int d\mathbf{r}_1 d\mathbf{r}_2 v(\mathbf{r}_{12}) f^2(r_{12}) \text{Tr}_1 \text{Tr}_2 \left[A(A-1) \int dx_3 \cdots dx_A | \Phi_0 \rangle^2 \right. \\ & \left. + \sum_{n=3}^A \binom{A}{n-2} \int dx_3 \cdots dx_n X^{(n)}(\mathbf{r}_1, \mathbf{r}_2; \mathbf{r}_3, \dots, \mathbf{r}_n) \int dx_{n+1} \cdots dx_A | \Phi_0 \rangle^2 \right]. \end{aligned} \quad (3.38)$$

We can define the n -body distribution function associated with a nucleon Fermi gas as

$$g_n^{FG}(\mathbf{r}_1 \dots \mathbf{r}_n) \equiv \frac{A!}{(A-n)!} \varrho^{-n} \text{Tr}_1 \cdots \text{Tr}_n \int dx_{n+1} \cdots dx_A | \Phi_0 \rangle^2. \quad (3.39)$$

With the above definition, our expression for the numerator of the potential energy contribution can be written as

$$\begin{aligned} \mathcal{N} = & \frac{1}{2} \int d\mathbf{r}_1 d\mathbf{r}_2 v(\mathbf{r}_{12}) f^2(r_{12}) \left[\varrho^2 g_2^{FG}(\mathbf{r}_1, \mathbf{r}_2) \right. \\ & \left. + \sum_{n=3}^A \frac{\varrho^n}{(n-2)!} \int d\mathbf{r}_3 \cdots d\mathbf{r}_n X^{(n)}(\mathbf{r}_1, \mathbf{r}_2; \mathbf{r}_3, \dots, \mathbf{r}_n) g_n^{FG}(\mathbf{r}_1, \dots, \mathbf{r}_n) \right]. \end{aligned} \quad (3.40)$$

In the previous equation we can recognize the cluster decomposition of the numerator. Indeed we have written its contribution as a sum of terms involving an increasing number n of correlated particles. Moreover we can see that the general n -th term of this expansion involves two different contributions, coming from the $X^{(n)}$ and the g_n^{FG} factor respectively. This underlines the different nature of the correlations involved in a system of fermions. In fact while $X^{(n)}$ accounts for dynamical correlations through the cluster expansion of the correlation operator F^2 , the g_n^{FG} is responsible for statistical correlations arising from the Pauli exclusion principle. This kind of correlations are present also in a non-interactive Fermi gas.

In order to carry out the diagrammatic rules we have to look in the eyes the Fermi distribution function g_n^{FG} . But before doing this we are going to qualitatively introduce an important feature of diagrammatic expansions. This property is the cancellation of disconnected diagrams between the denominator and the numerator. Following a similar procedure as what we did for \mathcal{N} , we can write the denominator as

$$\mathcal{D} = 1 + \sum_{n=2}^A \frac{\rho^n}{n!} \int d\mathbf{r}_1 \cdots d\mathbf{r}_n X^{(n)}(\mathbf{r}_1, \dots, \mathbf{r}_n) g_n^{FG}(\mathbf{r}_1, \dots, \mathbf{r}_n), \quad (3.41)$$

with $X^{(2)}$ and $X^{(3)}$ defined as in Eqs. (3.29) and (3.30). For the purpose of this qualitative discussion let's consider $g_n^{FG} = 1$. We can define a pictorial representation for \mathcal{N} and \mathcal{D} as

$$\mathcal{N} = \text{---} + \text{---} + \text{---} + \text{---} + \dots \quad (3.42)$$

and

$$\mathcal{D} = 1 + \text{---} + \text{---} + \dots \quad (3.43)$$

In the previous diagrams we have indicated with empty circles the active particles and with full circles the background particles. The dashed lines are referred to elementary pair correlations $h(r_{ij})$ and the bold line stands for the operator $v(r_{12})f^2(r_{12})$, connecting the active particles. We underline that for pedagogical reasons we have not included all the three and four body terms, but just some representative examples. We can see that the numerator can be factorized as

$$\mathcal{N} = \left(\text{---} + \text{---} + \text{---} + \dots \right) \left(1 + \text{---} + \dots \right) \quad (3.44)$$

explicitly showing that the second factor can be simplified with the denominator, leading to an expression involving only connected diagrams

$$\frac{\mathcal{N}}{\mathcal{D}} = \text{---} + \text{---} + \text{---} + \dots \quad (3.45)$$

3.2.1 Pair distribution function

The expansion we have carried out for the expectation value of the potential energy, is completely independent of the radial shape of the particular NN potential. Indeed we could have derived it in terms of the pair distribution function

$$p^{(2)}(\mathbf{r}_1, \mathbf{r}_2) = A(A-1) \frac{\text{Tr}_1 \text{Tr}_2 \int dx_3 \cdots dx_A |\Psi(x_1 \dots x_A)|^2}{\int dx_1 \cdots dx_A |\Psi(x_1 \dots x_A)|^2}, \quad (3.46)$$

which expresses the probability to find two particles in the position \mathbf{r}_1 and \mathbf{r}_2 . It's easy to see that we can write the expectation value of the operator $V = \sum_{i<j} v(r_{ij})$ as

$$\langle V \rangle = \frac{1}{2} \int d\mathbf{r}_1 d\mathbf{r}_2 v(r_{12}) p^{(2)}(\mathbf{r}_1, \mathbf{r}_2). \quad (3.47)$$

By looking at the expressions we have previously derived for \mathcal{N} and \mathcal{D} , and comparing them with Eq. (3.47), we can write

$$\begin{aligned} \mathcal{N}_p &= \varrho^2 f^2(r_{12}) \left[g_2^{FG}(\mathbf{r}_1, \mathbf{r}_2) \right. \\ &\quad \left. + \sum_{n=3}^A \frac{\varrho^{n-2}}{(n-2)!} \int d\mathbf{r}_3 \cdots d\mathbf{r}_n X^{(n)}(\mathbf{r}_1, \mathbf{r}_2; \mathbf{r}_3, \dots, \mathbf{r}_n) g_n^{FG}(\mathbf{r}_1, \dots, \mathbf{r}_n) \right]. \end{aligned} \quad (3.48)$$

and

$$\mathcal{D}_p = 1 + \sum_{n=2}^A \frac{\varrho^n}{n!} \int d\mathbf{r}_1 \cdots d\mathbf{r}_n X^{(n)}(\mathbf{r}_1, \dots, \mathbf{r}_n) g_n^{FG}(\mathbf{r}_1, \dots, \mathbf{r}_n), \quad (3.49)$$

where we have labeled as \mathcal{N}_p and \mathcal{D}_p respectively the numerator and the denominator appearing in the definition of $p^{(2)}(\mathbf{r}_1, \mathbf{r}_2)$ (obviously $\mathcal{D} \equiv \mathcal{D}_p$).

In a translationally invariant system the pair distribution function will depend only on the relative distance between the two particles, therefore we can define a quantity $g_2(r)$ with $r = |\mathbf{r}_1 - \mathbf{r}_2|$ such that

$$p^{(2)}(\mathbf{r}_1, \mathbf{r}_2) = \varrho^2 g_2(r). \quad (3.50)$$

The distribution $g_2(r)$ satisfies the following normalization condition

$$\varrho \int d\mathbf{r} [g_2(r) - 1] = -1. \quad (3.51)$$

The previous identity can be easily obtained by means of the definition of the one particle distribution function

$$p^{(1)}(\mathbf{r}_1) = \frac{1}{A-1} \int d\mathbf{r}_2 p^{(2)}(\mathbf{r}_1, \mathbf{r}_2), \quad (3.52)$$

and its normalization

$$\frac{1}{A} \int d\mathbf{r}_1 p^{(1)}(\mathbf{r}_1) = 1. \quad (3.53)$$

3.2.2 Statistical correlations

In order to derive the set of diagrammatic rules governing our expansion we still need to analyze the quantity $g_n^{FG}(\mathbf{r}_1, \dots, \mathbf{r}_n)$. First of all we are going to recall one property of the Slater determinant, according to which we can always express a function Φ_0 defined as in Eq. (3.22) in the form

$$\Phi_0(x_1 \dots x_A) = \sqrt{\frac{(A-k+1)!}{A!}} \sum_{n_1 < \dots < n_k = 1}^A (-1)^{n_1 + \dots + n_k + 1} \mathcal{A}[\phi_{n_1}(x_1) \dots \phi_{n_k}(x_k)] \times \Phi_0^{m \neq n_1 \dots n_k}(x_{k+1} \dots x_A). \quad (3.54)$$

In the previous equation the operator \mathcal{A} implements the antisymmetrization over the single particle states ϕ_{n_i} , whereas the quantity $\Phi_0^{m \neq n_1 \dots n_k}$ stands for a Slater determinant of $A-k$ single particle states, where we have excluded the orbitals $\{n_1, \dots, n_k\}$ from the set $n_i = \{1, \dots, A\}$. Thanks to this property, together with the orthogonality of the single particle wave functions, we can write

$$g_n^{FG}(\mathbf{r}_1, \dots, \mathbf{r}_n) = \varrho^{-n} \sum_{n_1, \dots, n_n} \text{Tr}_1 \dots \text{Tr}_n \phi_{n_1}^*(x_1) \dots \phi_{n_n}^*(x_n) \mathcal{A}[\phi_{n_1}(x_1) \dots \phi_{n_n}(x_n)]. \quad (3.55)$$

By tracing over the spinorial indices and summing over all the spin and isospin quantum states we can write

$$g_n^{FG}(\mathbf{r}_1, \dots, \mathbf{r}_n) = \frac{\nu^n}{\varrho^n} V^{-n} \sum_{\mathbf{k}_1, \dots, \mathbf{k}_n < |\mathbf{k}_F|} e^{i\mathbf{k}_1 \cdot \mathbf{r}_1} \dots e^{i\mathbf{k}_n \cdot \mathbf{r}_n} \mathcal{A} \left[e^{-i\mathbf{k}_1 \cdot \mathbf{r}_1} \dots e^{-i\mathbf{k}_n \cdot \mathbf{r}_n} \right]. \quad (3.56)$$

The antisymmetrization operator can be written as a series of terms involving an increasing number of combinations of pair-exchange operators \hat{P}_{ij} , as

$$\mathcal{A} = 1 - \sum_{i < j} \hat{P}_{ij} + \sum_{i < j < k} \hat{P}_{ij} \hat{P}_{jk} + \hat{P}_{ik} \hat{P}_{jk} + \dots \quad (3.57)$$

We recall that the exchange operator is defined as

$$\hat{P}_{ij} |k_i\rangle |k_j\rangle = |k_j\rangle |k_i\rangle. \quad (3.58)$$

In the wave function representation, the pair exchange operator acting over two momentum eigenstates with degeneracy ν , can be written as

$$\hat{P}_{ij} = \frac{1}{\nu} e^{i(\mathbf{k}_i - \mathbf{k}_j) \cdot \mathbf{r}_{ij}}. \quad (3.59)$$

Finally we can define the Slater function $l(k_F r_{ij})$ according to

$$l(k_F r_{ij}) = \frac{\nu}{\varrho} \sum_{\mathbf{k} < |\mathbf{k}_K|} \frac{1}{V} e^{i\mathbf{k} \cdot (\mathbf{r}_i - \mathbf{r}_j)}, \quad (3.60)$$

with

$$l(x) = 3 \left(\frac{\sin x - x \cos x}{x^3} \right). \quad (3.61)$$

The identity in Eq. (3.60) can be easily demonstrated by means of the substitution

$$\frac{1}{V} \sum_{\mathbf{k} < |\mathbf{k}_F|} \rightarrow \frac{1}{(2\pi)^3} \int_{\mathbf{k} < |\mathbf{k}_F|} d\mathbf{k}. \quad (3.62)$$

With all these definition it's easy to believe that the contribution of the Fermi distribution function to the n -body cluster term will involve a sum of an increasing number of Slater functions

$$g_n^F = 1 - \frac{1}{\nu} \sum_{i < j}^n l^2(k_F r_{ij}) + \sum_{i < j < k}^n \frac{2}{\nu^2} l(k_F r_{ij}) l(k_F r_{jk}) l(k_F r_{ik}) + \dots \quad (3.63)$$

By applying the former properties we can easily carry out the expression for the Fermi distribution function at two- and three-body cluster level as

$$g_2^{FG}(r_{12}) = 1 - \frac{1}{\nu} l^2(k_F r_{12}), \quad (3.64)$$

and

$$g_3^{FG}(r_{12}, r_{13}, r_{23}) = 1 - \frac{1}{\nu} l^2(k_F r_{12}) - \frac{1}{\nu} l^2(k_F r_{13}) - \frac{1}{\nu} l^2(k_F r_{23}) + \frac{2}{\nu^2} l(k_F r_{12}) l(k_F r_{23}) l(k_F r_{13}). \quad (3.65)$$

We can define a diagrammatic representation also for these statistical correlations

$$\begin{array}{c} \bullet \\ \curvearrowright \\ \bullet \end{array} \begin{array}{c} \bullet \\ \curvearrowleft \\ \bullet \end{array} = -\frac{1}{\nu} l^2(k_F r_{12}) \quad (3.66)$$

$$\begin{array}{c} \bullet \\ \curvearrowright \\ \bullet \\ \curvearrowright \\ \bullet \end{array} \begin{array}{c} \bullet \\ \curvearrowleft \\ \bullet \\ \curvearrowleft \\ \bullet \end{array} = \frac{2}{\nu^2} l(k_F r_{12}) l(k_F r_{23}) l(k_F r_{13}). \quad (3.67)$$

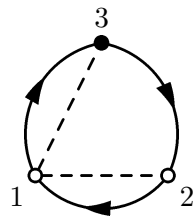
3.2.3 Diagrammatic rules

By putting together all the things we have introduced so far, we can finally write down a series of diagrammatic rules that can be used to express each contribution in the cluster expansion of the numerator and denominator of the pair distribution function.

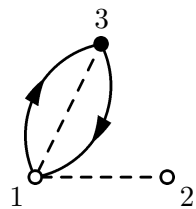
- Each diagram contains as much vertices as the order n of the cluster term. These vertices can be connected by both dynamical and statistical correlations. In the numerator expansion, open circles labels the active particles, whereas filled circles are associated to the background ones. To each background particle i is associated an integral over the coordinate \mathbf{r}_i contributing as a factor ϱ .

- A dashed line between vertices i and j represents dynamical correlations $h(r_{ij})$. Dynamical correlations cannot be superimposed.
- Solid oriented lines are associated with statistical correlations, and contribute as a factor $l(k_F r_{ij})/\nu$. Statistical lines appear only in closed loops and such loops cannot have a common vertex.
- Statistical loops between two particles contribute as a factor $l^2(k_F r_{ij})/\nu$, whereas loops involving more than two particles are multiplied by a factor -2ν .
- Vertices associated with background particles must be reached by at least one dynamical correlation line.

In the following we can see two examples of diagrams contributing to \mathcal{N}_p



$$\begin{aligned}
 &= h(r_{12}) \left[-\frac{l(k_F r_{12})}{\nu} \right] (-2\nu) \\
 &\times \varrho \int d\mathbf{r}_3 h(r_{13}) \left[-\frac{l(k_F r_{13})}{\nu} \right] \left[-\frac{l(k_F r_{23})}{\nu} \right] \quad (3.68)
 \end{aligned}$$



$$= \varrho h(r_{12}) \int d\mathbf{r}_3 h(r_{13}) \left[-\frac{l^2(k_F r_{13})}{\nu} \right]. \quad (3.69)$$

For comparison in Fig 3.1 we can see two forbidden diagrams. Fig 3.1 (a) is not allowed because there are two loops sharing a common vertex, whereas in diagram (b) we have a background particle that is not reached by any dashed line.

As a final remark let's discuss what happens to the combinatorial coefficients multiplying each cluster term, respectively $1/(n-2)!$ for the numerator and $1/n!$ for the denominator. These factors account for diagrams that are topologically equal, but differing only by permutations of the $n-2$ background particles. In Fig. 3.2 we can see two diagrams of this kind. We can account for this degeneracy by taking only one of them without any prefactor. On the other hand a prefactor is needed when considering diagrams that are invariant under the exchange of background particle indices. This is the case of the diagram in Eq. (3.70) where we have put a prefactor s^{-1} with $s=2$ accounting for the symmetry under the exchange $3 \rightleftharpoons 4$

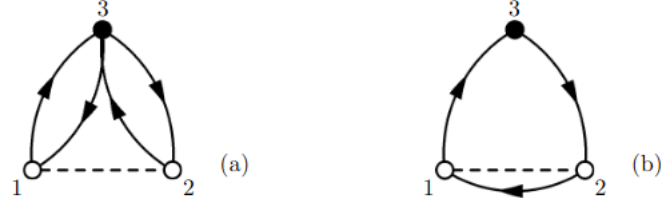


Figure 3.1. Two diagrams that are forbidden and therefore do not contribute to the diagrammatic expansion.

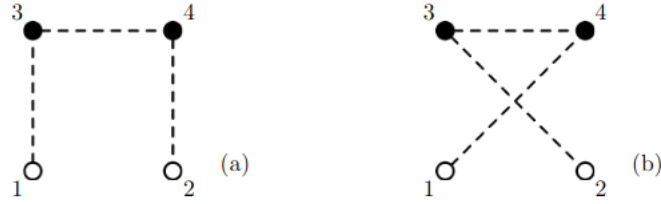


Figure 3.2. Two cluster diagrams with the same topology yielding identical cluster contributions

$$= \frac{1}{2} \varrho^2 \int d\mathbf{r}_3 d\mathbf{r}_4 h(r_{13}) h(r_{14}) h(r_{23}) h(r_{24}) h(r_{34}). \quad (3.70)$$

Diagrams in which from each vertex we can reach any others by following a series of correlation lines, are said to be linked, Fig. 3.3 (a). Otherwise they are called unlinked diagrams, Fig. 3.3 (b). Finally diagrams in which the integrals over background particles can be factorized are said to be reducible. Now we can formally demonstrate that all unlinked diagrams are simplified out between the numerator and denominator in the cluster expansion. Indeed we can always write the numerator \mathcal{N}_p as a sum of diagrams expressed as the product between linked and unlinked sub-diagrams

$$\mathcal{N}_p = \sum_{n < m} \mathcal{L}_n \times \mathcal{U}_{m-n}, \quad (3.71)$$

where we have labeled with \mathcal{L}_n the sum over all linked diagrams involving n particles, and with \mathcal{U}_{m-n} the sum over all the unlinked ones involving $n - m$ particles. The set of unlinked diagrams is defined in such a way that $\mathcal{U}_{m-n} = 0$ for $m < n$, yielding

$$\sum_{n < m} \mathcal{L}_n \mathcal{U}_{m-n} = \sum_{m=2}^A \sum_{n=2}^m \mathcal{L}_n \mathcal{U}_{m-n} = \sum_{n=2}^A \mathcal{L}_n \sum_{m=n}^A \mathcal{U}_{m-n} = \sum_{n=2}^A \mathcal{L}_n \sum_{m=0}^{A-n} \mathcal{U}_{m-n}. \quad (3.72)$$

At this point we can notice that the denominator can be expressed as

$$\mathcal{D}_p = \sum_{m=0}^A \mathcal{U}_m, \quad (3.73)$$

therefore in the limit $A \rightarrow \infty$ we have

$$\frac{\mathcal{N}_p}{\mathcal{D}_p} = \frac{\sum_{n=2}^{\infty} \mathcal{L}_n \sum_{m=0}^{\infty} \mathcal{U}_m}{\sum_{m=0}^{\infty} \mathcal{U}_m} = \sum_{n=2}^{\infty} \mathcal{L}_n. \quad (3.74)$$

The above demonstration, that holds in general for a system of an infinite number of constituents, is still valid in the case of a system with a finite number of fermions. Indeed thanks to a property of the Fermi gas distribution function, according to which

$$g_n^{FG} = 0 \text{ for } n > A, \quad (3.75)$$

we can extend the summations from A to ∞ without necessarily taking into account an infinite number of constituents. Because of this cancellation property we can finally write the general expression for the pair distribution function

$$g_2(r_{12}) = f^2(r_{12}) \left[g_2^{FG}(r_{12}) + \sum_{n>2} X_L^{(n)}(\mathbf{r}_1, \mathbf{r}_2) \right], \quad (3.76)$$

where the term $X_L^{(n)}$ indicates the sum of all linked cluster diagrams involving n particles. The cancellation of the unlinked diagrams is a general feature of diagrammatic expansions, and continues to hold even in the case of spin and isospin dependent correlations.

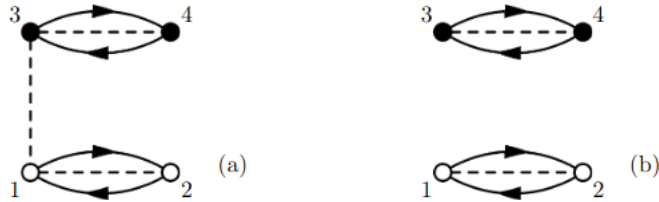


Figure 3.3. Here we can see an example of linked (a) and unlinked (b) cluster diagrams.

3.2.4 Kinetic energy

The expectation value of the kinetic energy on the correlated ground state yields a contribution

$$\begin{aligned} \langle T \rangle &= \frac{\langle \Phi_0 | F^\dagger T F | \Phi_0 \rangle}{\langle \Phi_0 | F^2 | \Phi_0 \rangle} \\ &= \frac{1}{\mathcal{N}(\Psi)} \left(-\frac{1}{2m} \right) \sum_i \int dx_1 \cdots dx_A \Phi_0^*(x_1 \dots x_A) F^\dagger \nabla_i^2 F \Phi_0(x_1 \dots x_A), \end{aligned} \quad (3.77)$$

where we have indicated as $\mathcal{N}(\Psi_T)$ the normalization of the variational state. Because of the symmetry of the trial ground state we have that

$$\sum_{i=1}^A \langle \Psi | \nabla_i^2 | \Psi \rangle = A \langle \Psi | \nabla_1^2 | \Psi \rangle. \quad (3.78)$$

Since we have that

$$\nabla_i^2 (F \Phi_0) = 2 \nabla_i F \cdot \nabla_i \Phi_0 + (\nabla_i^2 F) \Phi_0 + F \nabla_i^2 \Phi_0. \quad (3.79)$$

the kinetic energy contribution can be easily rewritten as

$$\langle T \rangle \equiv T_{PB} = T_F - \frac{1}{2m} \frac{1}{\mathcal{N}(\Psi)} \sum_i \int dx_1 \cdots dx_A \Phi_0^* F^\dagger \left(\nabla_i^2 F + 2 \nabla_i F \cdot \nabla_i \right) \Phi_0, \quad (3.80)$$

where we have used the identity

$$-\frac{1}{2m} \sum_i \langle \Phi_0 | F^2 \nabla_i^2 | \Phi_0 \rangle = \mathcal{N}(\Psi) T_F. \quad (3.81)$$

The subscript *PB* in Eq. (3.80) stands for Pandharipande-Bethe from Ref. [109]. Indeed there exist other ways to express the kinetic energy contribution, which are related to the PB representation throughout an integration by parts. These expressions are in principle equivalent, but they will produce different contributions at a finite order in the cluster expansion. The Clark-Whethaus (CW) [110] representation can be carried out integrating by parts the contribution coming from $\nabla_i^2 F \Phi_0 + \nabla_i F \cdot \nabla_i \Phi_0$ and exploiting the identity

$$\sum_i \left[(\nabla_i \Phi_0^*) \cdot F^\dagger (\nabla_i F) \Phi_0 - \Phi_0^* (\nabla_i F^\dagger) F \cdot \nabla_i \Phi_0 \right] = 0, \quad (3.82)$$

yielding

$$T_{CW} = T_F + \frac{1}{2m} \frac{1}{\mathcal{N}(\Psi)} \sum_i \int dx_1 \cdots dx_A \Phi_0^* (\nabla_i F^\dagger) \cdot (\nabla_i F) \Phi_0. \quad (3.83)$$

Finally we report also the Jackson-Feenberg (JF) expression whose derivation does not involve any additional difficulty

$$T_{JF} = -\frac{1}{4m} \frac{1}{\mathcal{N}(\Psi)} \sum_i \int dx_1 \cdots dx_A \left[\Phi_0^* F^\dagger (\nabla_i^2 F \Phi_0) - 2 (\nabla_i \Phi_0^* F^\dagger) \cdot (\nabla_i F \Phi_0) + (\nabla_i^2 \Phi_0^* F^\dagger) F \Phi_0 \right]. \quad (3.84)$$

In the Jastrow case, where the correlation operator is given by

$$F = \prod_{i < j} f(r_{ij}) \quad (3.85)$$

we have that

$$\nabla_i F = \sum_{j \neq i} \frac{\nabla_i f(r_{ij})}{f(r_{ij})} F. \quad (3.86)$$

In the CW expression of the kinetic energy we have

$$\begin{aligned} \nabla_i F \cdot \nabla_i F &= F^2 \sum_{k \neq i} \frac{\nabla_i f(r_{ik})}{f(r_{ik})} \cdot \sum_{j \neq i} \frac{\nabla_i f(r_{ij})}{f(r_{ij})} \\ &= F^2 \left[\sum_{j \neq i} \frac{\nabla_i f(r_{ij}) \cdot \nabla_i f(r_{ij})}{f^2(r_{ij})} + 2 \sum_{j < k \neq i} \frac{\nabla_i f(r_{ij}) \cdot \nabla_i f(r_{ik})}{f(r_{ij})f(r_{ik})} \right]. \end{aligned} \quad (3.87)$$

Summing over i and exploiting $\sum_{i,j \neq i} = 2 \sum_{i < j}$ we have

$$\frac{1}{2m} \sum_i \nabla_i F \cdot \nabla_i F = F^2 \sum_{i < j} T_{ij}^{(2)} + F^2 \sum_{i < j < k} T_{ijk}^{(3)} \quad (3.88)$$

with

$$T_{ij}^{(2)} = \frac{1}{m} \left[\frac{\nabla_i f(r_{ij}) \cdot \nabla_i f(r_{ij})}{f^2(r_{ij})} \right] \quad (3.89)$$

and

$$T_{ijk}^{(3)} = \frac{2}{m} \left[\frac{\nabla_i f(r_{ij}) \cdot \nabla_i f(r_{ik})}{f(r_{ij})f(r_{ik})} \right]. \quad (3.90)$$

Equation (3.88) shows that the kinetic energy contribution can be expressed as the sum of a two- and a three-body operators, $T_{ij}^{(2)}$ and $T_{ijk}^{(3)}$ respectively, whose cluster expansion can be obtained by applying the diagrammatic rules we have discussed in the previous section. Indeed, collecting together the two-body operators in the Hamiltonian, we can define an effective interaction as

$$w(r) = \frac{1}{m} \left[\frac{\nabla f(r)}{f(r)} \right]^2 + v(r). \quad (3.91)$$

The expectation value of $w(r)$ over the correlated ground state can be written in term of the pair distribution function $g_2(r)$ according to Eqs. (3.47),(3.50) as

$$\frac{1}{A} \sum_{i < j} \langle w_{ij} \rangle = \frac{\rho}{2} \int d\mathbf{r} w(r) g_2(r), \quad (3.92)$$

with $w_{ij} \equiv w(r_{ij})$. On the other hand, evaluating the expectation value of the operator $T_{ijk}^{(3)}$ requires the introduction of a three-body distribution function, whose definition does not involve any conceptual difficulty beyond the discussion of the previous section.

3.2.5 Fermi Hypernetted Chain summation scheme

The Jastrow variational approach, used in combination with central spin-isospin independent potentials, has been applied to obtain low order approximation of the nuclear matter ground state. Unfortunately the uncostrained minimization of the variational energy turns out to be unbounded from below when computed at any finite order in the cluster expansion. In order to circumvent this problem, some constrained minimization procedures have been attempted, for example by imposing

the additional requirement for the pair distribution function $g_2(r)$ to fulfill the normalization condition imposed by Eq. (3.51). This approach, while assuring a fast convergence of the cluster expansion has no guarantee to provide an accurate upper bound to the ground state energy. From the benchmark calculations performed by comparing finite order variational approaches and BHF results for different models of nucleon-nucleon potentials [111, 112], it was clear that an accurate description of the nuclear matter properties would have required the inclusion of many-body cluster contributions.

In order to improve finite order calculations a series of techniques have been developed, enabling the infinite summation of successive many-body clusters through integral equations. Indeed it is well known that an integral equation accounts for the summation of an infinite series of terms with the same topological structure. For example we can consider the two point green function in a generic field theory, $G(x, y)$, satisfying

$$G(x, y) = G_0(x, y) + \int dx' dy' G_0(x, x') \Sigma(x', y') G(y', y) \quad (3.93)$$

By consecutive iterations of the previous equation we get

$$G(x, y) = G_0(x, y) + \int dx' dy' G_0(x, x') \Sigma(x', y') G_0(y', y) + \dots \quad (3.94)$$

By defining the following diagrammatic rules

$$G_0(x, y) = \text{x} \text{---} \text{wavy line} \text{---} \text{y} \quad (3.95)$$

$$G(x, y) = \text{x} \text{---} \text{shaded circle} \text{---} \text{y} \quad (3.96)$$

$$\int dx dy \Sigma(x, y) = \text{x} \text{---} \text{circle} \text{---} \text{y} \quad (3.97)$$

$$(3.98)$$

We can write a pictorial expression of Eq. (3.94) as

$$\text{x} \text{---} \text{shaded circle} \text{---} \text{y} = \text{x} \text{---} \text{wavy line} \text{---} \text{y} + \text{x} \text{---} \text{circle} \text{---} \text{y} + \text{x} \text{---} \text{circle} \text{---} \text{circle} \text{---} \text{y} + \dots \quad (3.99)$$

In a similar manner there exist some techniques allowing to sum together different cluster diagrams with a similar topology. The first such analysis was performed at

the end of the 1950s regarding the pair distribution function of classical liquids [113]. The starting point is the identification of elementary structures that can be used to construct more complex diagrams by successive series and parallel connections. The contributions of the resulting diagrams can be summed up to all orders by means of an integral equation, referred to as Hyper-Netted-Chain (HNC) equation. The HNC summation method was later extended to quantum Bose and Fermi liquids. In the case of Fermi systems described using spin and isospin independent Jastrow correlation functions, the result is a system of coupled integral equations, dubbed Fermi Hyper-Netted Chain, or FHNC, equations [114]. A detailed description of such techniques is beyond the purpose of this Thesis. For the interested reader an extensive review on this subject can be found in Ref. [93]. The FHNC equations are solved numerically by iterations. For dense systems like liquid helium or nuclear matter, however, achieving convergence is difficult, and often requires the use of an algorithm to smooth out oscillations occurring in the iterative process.

3.3 Extension to operatorial correlations

In order to obtain more accurate results, state-of-the-art calculations of nuclear matter properties require the introduction of more complicated forms of the correlation operator, which has to resemble the operatorial structure of the nucleon-nucleon interaction. This consideration leads to the definition of a pair correlator F_{ij} as in Eq. (3.7). When extending the formalism of cluster expansion to spin-isospin dependent operators we face a set of difficulties related to the non-commutative nature of two subsequent pair correlations, and a direct extension of the FHNC equations is usually not possible. In order to overcome this problem an approximated technique referred to as Single Operator Chain (FHNC/SOC) summation scheme, was developed by Pandharipande and Wiringa [115]. Within this approach it is derived a set of coupled integral equations allowing to sum over the hypernetted chains of central links (FHNC) and single chains of operator links.

In order to extend the cluster expansion formalism of the Jastrow approach, we can introduce a set of pair distribution functions $g_2^p(r)$ defined as

$$g_2^p(\mathbf{r}_{12}) = \frac{A(A-1)}{\varrho^2} \frac{\text{Tr}_1 \text{Tr}_2 \int dx_3 \cdots dx_A \Phi_0^*(X) \mathcal{F}^\dagger O_{12}^p \mathcal{F} \Phi_0(X)}{\int dx_1 \cdots dx_A \Phi_0^*(X) \mathcal{F}^\dagger \mathcal{F} \Phi_0(X)} = \frac{\mathcal{N}^p}{\mathcal{D}}, \quad (3.100)$$

where we have introduced the compact notation $X \equiv x_1, \dots, x_A$. With this definition we can write the expectation value of any operator $V \equiv \sum_{i<j} v_{ij}$ with $v_{ij} \equiv \sum_p v^p(r_{ij}) O_{ij}^p$ as

$$\langle V \rangle = A \frac{\varrho}{2} \int d\mathbf{r} v^p(r) g_2^p(\mathbf{r}). \quad (3.101)$$

The cluster expansion of the operatorial pair distribution function can be analyzed in a similar manner to what we did for the Jastrow case, but paying attention to some additional subtleties. First of all we have to introduce other diagrammatic elements. We can split the pair correlation operator F_{12} according to

$$F_{12} = \sum_p f^p(r_{12}) O_{12}^p = f^c(r_{12}) + \sum_{p>1} f^p(r_{12}) O_{12}^p, \quad (3.102)$$

where we have defined the central correlation $f^c(r)$ as the one associated with the identity operator, conventionally chosen corresponding to the component $p = 1$. Now we can define the quantity $h(r_{12})$ as

$$f^c(r_{12})f^c(r_{12}) = 1 + h(r_{12}). \quad (3.103)$$

With this definition we can identify the following elementary contributions connecting a pair of correlated particles

$$h_{ij} = f^c(r_{ij})f^c(r_{ij}) - 1 = \begin{array}{c} \bullet \text{---} \text{---} \text{---} \bullet \\ i \qquad \qquad \qquad j \end{array} \quad (3.104)$$

$$f^c(r_{ij})f^p(r_{ij})O_{ij}^p = \begin{array}{c} \bullet \text{---} \text{---} \text{---} \bullet \\ i \qquad \qquad \qquad j \\ \qquad \qquad \qquad p \end{array} \quad p > 1 \quad (3.105)$$

$$f^q(r_{ij})f^p(r_{ij})O_{ij}^p O_{ij}^q = \begin{array}{c} \bullet \text{---} \text{---} \text{---} \bullet \\ i \qquad \qquad \qquad j \\ \qquad \qquad \qquad p \\ \qquad \qquad \qquad q \end{array} \quad p, q > 1. \quad (3.106)$$

$$F_{12}^\dagger O_{12}^p F_{12} = \begin{array}{c} \bullet \text{---} \text{---} \text{---} \bullet \\ 1 \qquad \qquad \qquad 2 \end{array} \quad (3.107)$$

In the same way as for the Jastrow approach, we can define a cluster expansion for the operator $\mathcal{F}^\dagger O_{12}^p \mathcal{F}$ as

$$\mathcal{F}^\dagger O_{12}^p \mathcal{F} = X^{(2)}(x_1, x_2) + \sum_{i \neq 1, 2} X^{(3)}(x_1, x_2; x_i) + \sum_{i < j \neq 1, 2} X^{(4)}(x_1, x_2; x_i, x_j) + \dots \quad (3.108)$$

where the general $X^{(n)}$ term accounts for an n -body cluster involving dynamical correlation. Its explicit form can be expressed through a combination of the diagrammatic elements of Eqs. (3.104)-(3.107).

$$X^{(2)}(x_1, x_2) = F_{12}^\dagger O_{12}^p F_{12} \quad (3.109)$$

$$X^{(3)}(x_1, x_2; x_i) = \mathcal{S}(F_{12} F_{1i} F_{2i})^\dagger O_{12}^p \mathcal{S}(F_{12} F_{1i} F_{2i}) - F_{12}^\dagger O_{12}^p F_{12}, \quad (3.110)$$

By defining the g_n^{FG} as

$$g_n^{FG} = \frac{A!}{(A-N)!} \frac{1}{\varrho^n} \int dx_{n+1} \cdots dx_A \Phi_0(X)^* \Phi_0(X) \quad (3.111)$$

we can finally write the expression for the numerator of the pair distribution function

as

$$\begin{aligned} \mathcal{N}^p = & \sum_{n=2}^A \frac{\varrho^{n-2}}{(n-2)!} \int d\mathbf{r}_3 \cdots d\mathbf{r}_n \text{CTr}_1 \cdots \text{CTr}_n \left\{ X^{(n)}(x_1, x_2; x_3, \dots, x_n) \right. \\ & \left. \times \left[1 - \sum_{i<j} P_{ij}^{\sigma\tau} l^2(r_{ij}) + \sum_{i<j<k} (P_{ij}^{\sigma\tau} P_{jk}^{\sigma\tau} + P_{ik}^{\sigma\tau} P_{ij}^{\sigma\tau}) l(r_{ij}) l(r_{ik}) l(r_{jk}) + \dots \right] \right\} \end{aligned} \quad (3.112)$$

The main difference between the previous equation and its counterpart in the Jastrow theory is provided by the presence of the $\text{CTr}[\cdot]$ operator. This operator returns the normalized trace over the spin and isospin matrix elements of the spin-isospin dependent operators. The trace is normalized such that $\text{CTr}[\mathcal{I}] = 1$. Moreover, because of the operatorial nature of the correlations, and therefore of the cluster contributions $X^{(n)}$, we can see the presence of the exchange operators $P_{ij}^{\sigma\tau}$ acting on the spin-isospin degrees of freedom. They are defined as

$$P_{12}^{\sigma\tau} = \frac{1}{4} (1 + \boldsymbol{\sigma}_1 \cdot \boldsymbol{\sigma}_2) (1 + \boldsymbol{\tau}_1 \cdot \boldsymbol{\tau}_2). \quad (3.113)$$

Because of the scalar nature of the dynamical clusters $X^{(n)}$ in the Jastrow approach, the CTr operators were directly applied on these exchange operators, yielding the normalization factor $1/4$ appearing in combination of the Slater functions.

As a final remark we report the expression of the pair distribution function computed at two-body cluster

$$g_2^p(\mathbf{r}_{12})|_{2b} = \text{CTr} \left\{ F_{12}^\dagger O_{12}^p F_{12} \left[1 - P_{12}^{\sigma\tau} l^2(r_{12}) \right] \right\}, \quad (3.114)$$

where we have defined $\text{CTr}[\cdot] \equiv \text{CTr}_1 \text{CTr}_2[\cdot]$.

3.4 Monte Carlo methods

An alternative approach to cluster expansion and FHNC summation scheme in order to evaluate many-body multidimensional integrals, is represented by computational techniques based on Monte Carlo methods.

Monte Carlo (MC) methods are usually addressed to all that kind of numerical techniques aiming at solving mathematical problems by means of (pseudo-) random processes. As a first example suppose we are interested in evaluating the integral of a given function $f(x)$ in the interval $[a, b]$

$$I = \int_a^b f(x) dx, \quad (3.115)$$

with only a uniform random number generator available. One way to numerical compute I is to uniformly sample a large number of random points in a rectangle that contains the full function $f(x)$, and then evaluate the area A_f under the function f by means of the approximation

$$A_f \sim \frac{N_f}{N} A_R. \quad (3.116)$$

In the above equation N_f is the number of points sampled inside the contour of the function f , and N is the number of the total sampled points. Eq. (3.116) is equivalent to assign to each sampled point the same little area $dA = A_R/N$, and then compute the area we are interested in, by summing all the contributions coming from points lying under the contour of f . Obviously as the number of samples grows-up the area dA will be smaller and the approximation works better. Usually MC methods are largely applied in problems related with probability, where one is interested in evaluate expectation values such as

$$E_p[f(x)] = \int f(x)p(x)dx \quad (3.117)$$

where $p(x)$ can be in principle any given probability distribution. Usually we don't know the actual $p(x)$, but we know its form only up to a constant. Eq. (3.117) therefore becomes

$$E_p[f(x)] = \frac{\int f(x)\tilde{p}(x)dx}{\int \tilde{p}(x)dx}. \quad (3.118)$$

This kind of integrals could be analytically very difficult, especially when the dimension of the problem increases. Suppose we can independently sample any number N of points distributed according to $p(x)$. Then we can always compute the sample mean of these points according to

$$\bar{f} = \frac{1}{N} \sum_{i=1}^N f(x_i). \quad (3.119)$$

At this point we can invoke the Law of Large Numbers stating that, for N independent, equally distributed points, as N approach to infinity, we can approximate

$$\bar{f} = \frac{1}{N} \sum_{i=1}^N f(x_i) \sim E_p[f(x)]. \quad (3.120)$$

This is essentially the basis of Monte Carlo integrations. Indeed, if we are able to independently sample a very large number of points, distributed according to a certain probability distribution $p(x)$, then the evaluation of a complicated integral reduces to the calculation of a simple sum. The Variational Monte Carlo (VMC) method in nuclear physics is based exactly on this tenet.

Let us take the expectation value of a generic operator O , over a trial wave function $|\Psi_T\rangle$. We can always express the trial wave function in terms of its discrete degrees of freedom as

$$\Psi_T(x_1, \dots, x_A) = \sum_n \psi_n(\mathbf{r}_1, \dots, \mathbf{r}_A)|n\rangle, \quad (3.121)$$

In the previous equation the index n is related to a given configuration of the discrete quantum numbers characterizing the A particles. For example given $A = 3$, we will have the following configurations

$$n = 1 \rightarrow |n \uparrow, n \uparrow, p \uparrow\rangle \quad (3.122)$$

$$n = 2 \rightarrow |n \downarrow, n \uparrow, p \uparrow\rangle \quad (3.123)$$

$$\vdots \quad (3.124)$$

At this point we can write

$$\langle \Psi_T | O | \Psi_T \rangle = \sum_{mn} \int dR \psi_m^*(R) O_{mn}(R) \psi_n(R), \quad (3.125)$$

where we have introduced the compact notation $\{\mathbf{r}_1, \dots, \mathbf{r}_A\} \equiv R$. Now we can multiply and divide the integrand by a probability density function $\mathcal{P}_{mn}(R)$, according to

$$\langle \Psi_T | O | \Psi_T \rangle = \sum_{mn} \int dR \frac{\psi_m^*(R) O_{mn}(R) \psi_n(R)}{\mathcal{P}_{mn}(R)} \mathcal{P}_{mn}(R) \equiv \sum_{mn} \int dR \tilde{O}_{mn} \mathcal{P}_{mn}(R). \quad (3.126)$$

Once the probability is chosen we can easily compute the integral through

$$\int dR \tilde{O}_{mn} \mathcal{P}_{mn}(R) \rightarrow \frac{1}{N_c} \sum_{\{R\}} \tilde{O}_{mn}(R), \quad (3.127)$$

where N_c is the number of different configurations of the R variables, randomly sampled according to the probability $\mathcal{P}_{mn}(R)$. Within the VMC approach the probability distribution is chosen to be

$$\mathcal{P}_{mn}(R) = \psi_m^*(R) \psi_n(R). \quad (3.128)$$

Besides overcoming the approximations involved in the cluster expansion and FHNC approach, this method is still plagued by the uncertainty coming from the choice of the variational wave function (other than by the uncertainty introduced by the numerical procedure). With the Diffusion Monte Carlo (DMC) method we are in principle able to get over this problem. This approach is based on the premise that the evolution of a generic state to infinite imaginary time is basically a projection onto the ground state of the system. Indeed we have that

$$\begin{aligned} U(\tau) | \Psi_T \rangle &= e^{-\tau \mathcal{H}} \sum_n C_n | \Psi_n \rangle \quad (3.129) \\ &= e^{-\tau E_0} \left[C_0 | \Psi_0 \rangle + \sum_{n \neq 0} C_n e^{-\tau(E_n - E_0)} | \Psi_n \rangle \right] \xrightarrow{\tau \rightarrow \infty} e^{-\tau E_0} C_0 | \Psi_0 \rangle. \quad (3.130) \end{aligned}$$

The evolution of the trial wave function is performed by dividing the time interval τ in short time intervals $\Delta\tau$, and then computing $\Psi(R, t + \Delta\tau)$ by means of the integral equation

$$\Psi(R, t + \Delta\tau) = \int dX' G(R, R', t, t + \Delta\tau) \Psi(R', t), \quad (3.131)$$

where $G(X, X', t, t')$ is the Green function of the Schrödinger equation at imaginary time, and the $3A$ integral involved in Eq. (3.131) is solved via Monte Carlo methods. In order to deal with the additional complexity arising from the treatment of spin-isospin degrees of freedom the formalism of DMC was extended in two different approaches, the Green's Function Monte Carlo (GFMC) and the Auxiliary Field Diffusion Monte Carlo (AFDMC) methods [116, 117]. The main difference between these two approaches lies in the treatment of the spin-isospin degrees of

freedom within the Green's Function. While in the GFMC is performed an explicit summation over the spin-isospin states, in the AFDMC spin-isospin configurations are stochastically sampled, as well as the particle coordinates allowing for a faster convergence. The extension of this formalism to uniform nuclear matter is carried out considering a finite number of nucleons in a periodic box. Numerical results for PNM have been obtained using both GFMC and AFDMC [66, 116, 118, 119]. In particular the recently performed benchmark calculations of PNM with different Hamiltonians, both with [66] and without [118] NNN forces, have shown how the main degree of uncertainty in the EOS of nuclear matter is associated with the description of nuclear dynamics rather than to the particular many-body approach.

3.5 The equation of state of Akmal Pandharipande and Revenhall

All the techniques we have discussed so far have found their application in the development of the equations of state of Akmal Pandharipande and Revenhall (APR) [62]. In this work the authors proposed four different models for the EOS of nuclear matter. The first two models do not include any three-nucleon force in the nuclear Hamiltonian, resulting in the incapability to describe neutron stars with masses as large as $\sim 2 M_{\odot}$. Moreover, the inclusion of three nucleon forces has proved to be necessary in order to account for a large set of nuclear systematics, such as the binding energies of light nuclei and the saturation properties of nuclear matter. Therefore it is clear that *ab initio* models that do not involve NNN interactions are inherently inadequate to describe nuclear matter at high density, where the contribution of many-body interactions is expected to become more and more important. For this reason, in the following we will consider only the two APR models which are based on an Hamiltonian as the one of Eq. (2.1). The difference between these two models presented by APR, that from now on will be referred to as APR1 and APR2, is the introduction in APR2 of relativistic boost corrections to the NN potential. The starting point of the APR1 model is the nuclear Hamiltonian of Eq. (2.1) comprising the Argonne v18 NN potential and the UIX NNN potential discussed in Chapter 2. Once the Hamiltonian is defined, the authors have performed variational calculation of the ground state energy for both isospin SNM, and Pure Neutron Matter (PNM) at different densities, ranging from $\rho = 0.04 \text{ fm}^{-3}$ to $\rho = 0.96 \text{ fm}^{-3}$. We recall that the nuclear saturation density corresponds to $\rho_0 = 0.16 \text{ fm}^{-3}$. The trial ground state is chosen as a correlated state

$$|\Psi_T\rangle = \frac{\mathcal{F}|\Phi_0\rangle}{\sqrt{\langle\Phi_0|\mathcal{F}^\dagger\mathcal{F}|\Phi_0\rangle}} \quad (3.132)$$

with

$$\mathcal{F} = \mathcal{S} \prod_{i<j} F_{ij} \quad (3.133)$$

and

$$F_{ij} = \sum_{p=1}^8 f^p(r_{ij}) O_{ij}^p. \quad (3.134)$$

The set of the 8 operators entering the pair correlation is the following

$$[1, \boldsymbol{\sigma}_1 \cdot \boldsymbol{\sigma}_2, S_{12}, (\mathbf{L} \cdot \mathbf{S})_{12}] \otimes [1, \boldsymbol{\tau}_1 \cdot \boldsymbol{\tau}_2]. \quad (3.135)$$

The variational energy

$$E_V = \langle \Psi_T | \mathcal{H} | \Psi_T \rangle \quad (3.136)$$

is computed by means of the cluster expansion and FHNC/SOC summation techniques. The functional form of the radial correlation functions $f^p(r)$ is found by solving the Euler-Lagrange equations associated to the functional minimization of the two-body cluster energy computed with a quenched NN potential

$$\tilde{v}_{ij} = \sum_p \alpha_p v^p(r_{ij}) O_{ij}^p. \quad (3.137)$$

In the previous equation the α_p are the so called quenching parameters, which are introduced in order to account for medium effects. The correlation functions are computed under the requirement of the following boundary conditions

$$\begin{aligned} f^p(r \geq d^p) &= \delta_{1p} \\ \left. \frac{df^p(r)}{dr} \right|_{d^p} &= 0. \end{aligned} \quad (3.138)$$

The definition of the quenching parameters α_p and the relaxation distances d^p is chosen in agreement with Ref. [96], yielding $d^1 = d^2 = d^3 = d^4 = d^7 = d^8 = d_c$, $d^4 = d^5 = d_t$, $\alpha_1 = 1$ and $\alpha_{p>1} = \alpha$. Finally the upper-bound for the ground state energy at any given density is found by the minimization of the variational energy E_V , computed within the full FHNC/SOC summation scheme, with respect to the relaxation distances d_c and d_t , and the quenching parameter α . The results for the energy per nucleon of both SNM and PNM, together with the associated variational parameters are shown in Fig. 3.4.

The second model proposed by APR, and referred to as APR2 within this Thesis, is based on a slightly modified Hamiltonian in order to account for the contribution of relativistic boost corrections. Such an Hamiltonian can be written as

$$\mathcal{H}^* = \sum_i \frac{\mathbf{P}_i^2}{2m} + \sum_{i<j} [v_{ij} + \delta v(\mathbf{P}_{ij})] + \sum_{i<j<k} V_{ijk}^*. \quad (3.139)$$

The first thing that should be noticed by looking at Eq. (3.139) is that it is slightly different from the relativistic Hamiltonian we introduced in Chapter 2. First of all there is no relativistic correction to the kinetic energy expression. Moreover, the NN potential in the center of mass frame of an interacting pair of nucleons v_{ij} is the actual AV18 potential. This choice for the Hamiltonian is justified by the authors with the following argument. The Argonne v18 phenomenological potential is based on a fit of the NN scattering phase shifts, and such fit depends also on the choice of the kinetic energy expression. Therefore introducing a modification in the kinetic energy term should be complemented with a new fit of the NN scattering data, leading to a modified version of the AV18 NN potential. Because of the large cancellation occurring between NN and kinetic energy contributions, it turns out

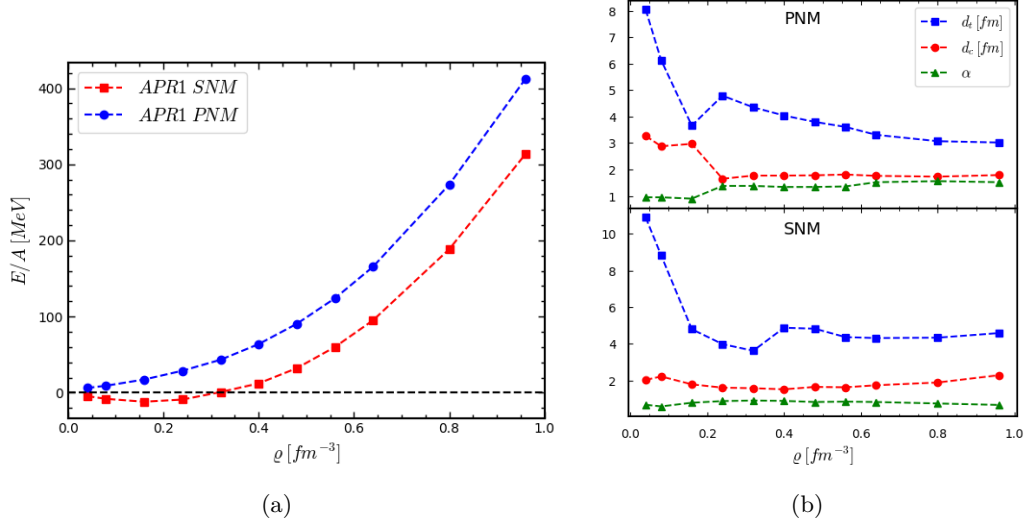


Figure 3.4. In the left panel we can see the energy per nucleon as a function of the matter density ρ of both SNM and PNM for the APR1 model. The right panel shows the variational parameters at different densities.

that in light nuclei most of the difference between a non relativistic Hamiltonian and a fully relativistic one is provided by the presence of the boost corrections δv . For this reason the authors argued that \mathcal{H}^* represents a significant improvement with respect to a non-relativistic Hamiltonian.

Last but not least, we notice the presence of a modified the NNN potential, labeled by V_{ijk}^* in the \mathcal{H}^* Hamiltonian. Indeed, as stressed by the authors, the accurate calculations of the binding energies of ${}^3\text{H}$, ${}^3\text{He}$ and ${}^4\text{He}$ with a relativistic Hamiltonian [69,70] have shown that the boost corrections account for a large part of the repulsive contribution to the nuclear binding energy. Because of this additional repulsion the strength of the repulsive V_{ijk}^R must be rescaled by a factor $\alpha_0 = 0.63$. The resulting NNN potential employed for the derivation of the APR2 EOS can be written as

$$V_{ijk}^* = V_{ijk}^{2\pi} + \alpha_0 V_{ijk}^R \quad (3.140)$$

and referred to as UIX^* . Finally in order to carry out the energy per nucleon associated to \mathcal{H}^* , the authors have not recomputed the variational parameters. The energy per nucleon of the APR2 EOS is then obtained by adding the contribution

$$\delta e = \frac{1}{A} \left[\langle \Psi_T | \sum_{i<j} \delta v(\mathbf{P}_{ij}) | \Psi_T \rangle + (\alpha_0 - 1) \langle \Psi_T | \sum_{i<j<k} V_{ijk}^R | \Psi_T \rangle \right] \quad (3.141)$$

to the energy per nucleon of the APR1 EOS. Once again we want to stress that the variational ground state $|\Psi_T\rangle$, appearing in the previous expression, is the same correlated state emerging after the minimization of the APR1 variational energy. Therefore within the above procedure the authors of Ref. [62] are treating the term $[\delta v + (\alpha_0 - 1)V^R]$ at first order in perturbation theory.

In Fig. 3.5 a comparison between the energy per nucleon of the APR1 and APR2 models is shown. By looking at Fig. 3.5 we can see that the energy associated with

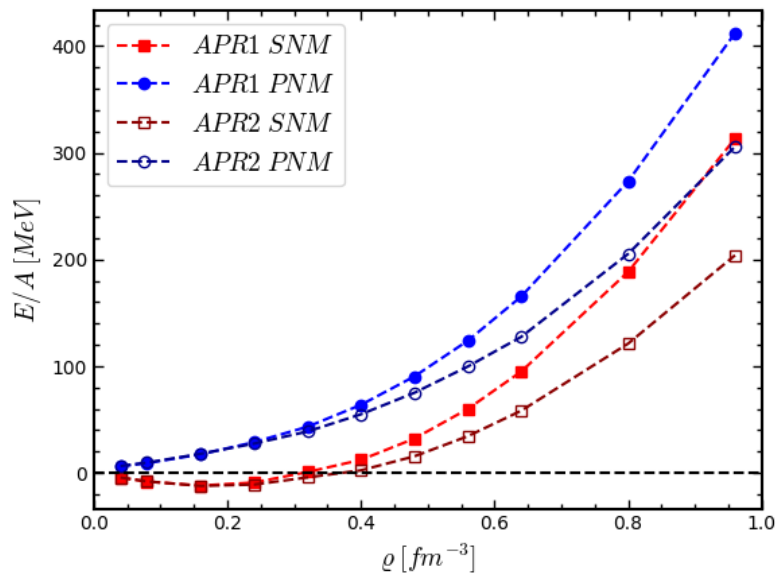


Figure 3.5. Comparison between the APR1, filled markers, and the APR2, empty markers, energy per nucleon as a function of the density ρ .

the APR2 model is lower with respect to APR1, suggesting that the overall effect of the correction (3.141) provides a lower repulsion. Since the boost correction turns out to be always repulsive, this effect has to be ascribed to the softening of the NNN repulsion that dominates over the boost corrections when the density increases.

The energy-density of nuclear matter at arbitrary baryon density ρ and proton fraction x_p has been obtained with the following parametrization, derived according to the procedure discussed in Refs. [120, 121]

$$\epsilon(\rho, x_p) = \left[\frac{\hbar^2}{2m} + f(\rho, x_p) \right] \tau_p + \left[\frac{\hbar^2}{2m} + f(\rho, 1 - x_p) \right] \tau_n + g(\rho, x_p), \quad (3.142)$$

where

$$g(\rho, x_p) = g(\rho, 1/2) + [g(\rho, 0) - g(\rho, 1/2)] (1 - 2x_p)^2. \quad (3.143)$$

The explicit expressions of the functions appearing in Eqs. (3.142) and (3.143) can be found in Appendix C. They involve a set of parameters which were determined by fitting the energy per nucleon of SNM and PNM computed within the FHNC/SOC variational approach.

The first two terms of Eq. (3.142) correspond to the proton and neutron kinetic energy respectively, whereas the function $g(\rho, x_p)$ describes the contribution arising from interactions. The assumption of quadratic dependence of the interaction energy on the neutron excess $\delta = 1 - 2x_p$ is routinely employed in the literature to obtain the EOS of β -stable matter from those of SNM and PNM, and has been shown to be remarkably accurate over a broad range of values of the proton fraction x_p ; see, e.g. Ref. [67].

Using the analytic expression of the energy density of nuclear matter at arbitrary proton fraction, composition and energy density of β -stable matter can be easily

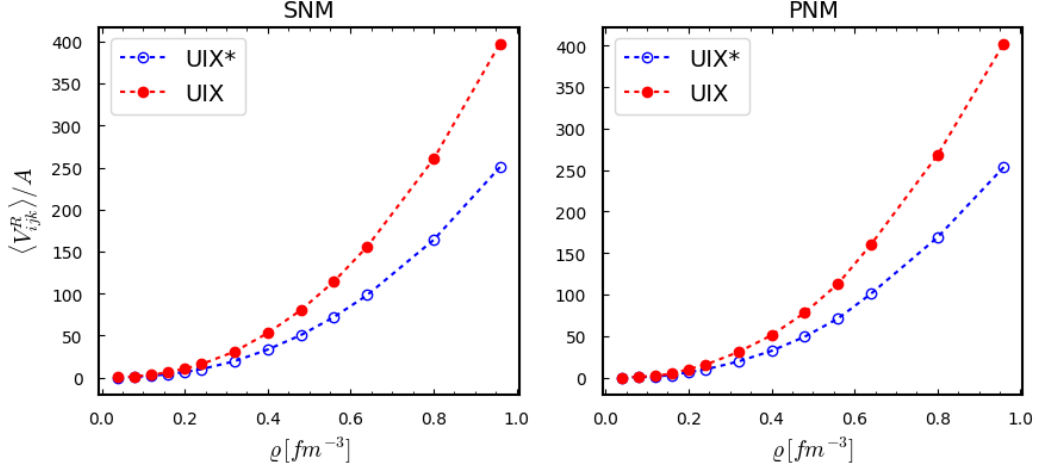
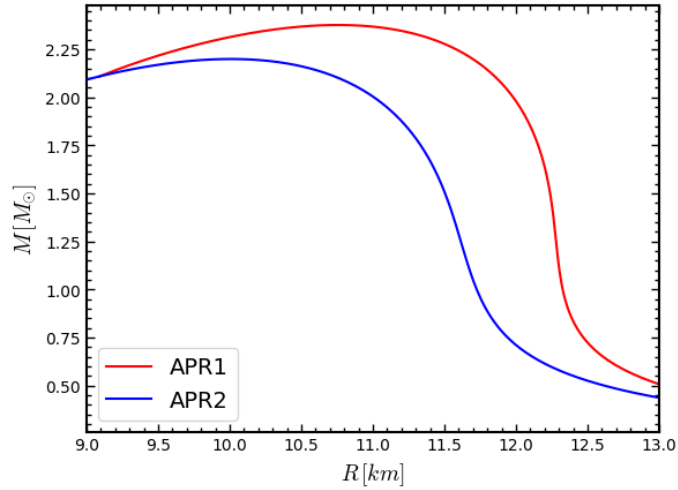


Figure 3.6. In the above figure we can see the difference between the UIX and UIX* models (in MeV) for both SNM and PNM.

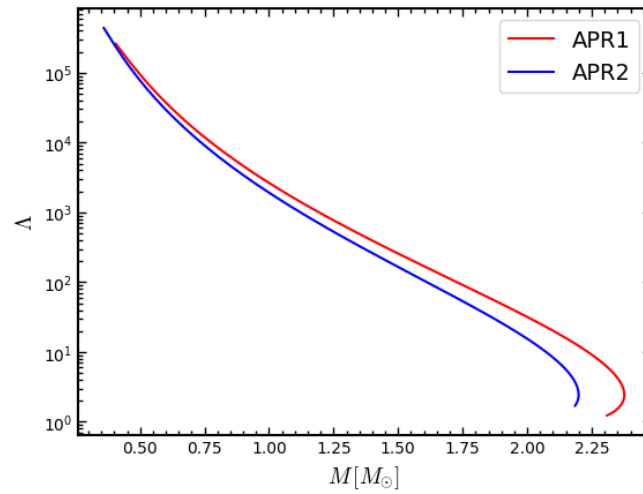
determined by minimizing with respect to x_p , with the additional constraints of conservation of baryon number and charge neutrality. Finally, the matter pressure P , derived from standard thermodynamic relations, is used to obtain the EOS $P(\epsilon)$.

3.5.1 Interplay between boost and NNN interaction

The impact of the relativistic boost corrections on the determination of the potential describing three-nucleon forces is illustrated in Fig. 3.6. It is apparent that the difference between the potential energies per particle of the UIX and UIX* interactions begins to be appreciable just above the equilibrium density of SNM $\rho_0 = 0.16 fm^{-3}$ and grows steeply with ρ . The inclusion of relativistic boost corrections to the NN potential and the associated modification of the NNN potential result in a softening of the EOS at high density, leading to a sizable change in the mass-radius relation determining the compactness, as we can see from Fig. 3.7. It is apparent that the introduction of relativistic boost corrections remarkably affect the predicted neutron star properties. We outline once again that the main effect on the EOS is not directly associated to boost corrections themselves but rather to the induced modification on the NNN repulsion, which plays a pivotal role in determining the behavior of nuclear matter at high densities. For this reason we strongly believe that a systematic study of the interplay within boost corrections and NNN potential have to be undergone. It could be a two-way road, because the development of EOS models comprising relativistic effects could lead to different interpretations of NS observed data. On the other hand, the increasing set of astrophysical observations could strongly help to constrain the high density behavior of the EOS, having the potential to shed new light on the interconnection between relativistic corrections and NNN forces.



(a)



(b)

Figure 3.7. Mass-radius diagram for the APR1 and APR2 models (a), and tidal deformability Λ as a function of the stellar mass (b).

Chapter 4

CBF Effective Interaction

In the previous chapter we have discussed some approximated techniques used to carry out a reliable estimation of the ground state properties of nuclear matter. Because of the strong repulsive core of NN interactions and the consequent impossibility of relying upon standard perturbation theory techniques, some other approaches have been developed in order to compute corrections to the variational calculations. The Correlated Basis Perturbation Theory was developed for this purpose. Under the assumption that the correlation structure of ground and excited states is the same, we can build up a complete set of correlated states by means of the correlation operator \mathcal{F} , resulting from the minimization of the variational energy E_V . Our set of correlated states will be

$$|\Psi_n\rangle = \frac{\mathcal{F}|\Phi_n\rangle}{\sqrt{\langle\Phi_n|\mathcal{F}^\dagger\mathcal{F}|\Phi_n\rangle}}, \quad (4.1)$$

where the state $|\Phi_n\rangle$ labels a generic Fermi gas state. Once the correlated basis is defined we can split the nuclear Hamiltonian \mathcal{H} in two pieces

$$\mathcal{H} = H_0 + H_1 \quad (4.2)$$

where H_0 and H_1 are defined as the diagonal and off-diagonal part of \mathcal{H} between correlated states

$$\langle\Psi_m|H_0|\Psi_n\rangle = \delta_{mn}\langle\Psi_m|\mathcal{H}|\Psi_n\rangle \quad (4.3)$$

$$\langle\Psi_m|H_1|\Psi_n\rangle = (1 - \delta_{mn})\langle\Psi_m|\mathcal{H}|\Psi_n\rangle. \quad (4.4)$$

If we have made a good choice for the correlation functions, or in other words, if the value E_V is close to the actual ground state energy of the system E_0 , then the states $|\Psi_n\rangle$ will have a great overlap with the real eigenstates of the nuclear Hamiltonian \mathcal{H} . This implies that the bracket of H_1 between these states will be very small with respect to H_0 , suggesting that a perturbative treatment of H_1 could be efficiently performed.

In the approach discussed above, one has to evaluate the matrix elements of \mathcal{H} between the new set of states, facing all the non-trivial difficulties arising when dealing with a non-orthogonal basis set. However the same results could be in principle obtained by transforming the Hamiltonian and using the Fermi gas basis.

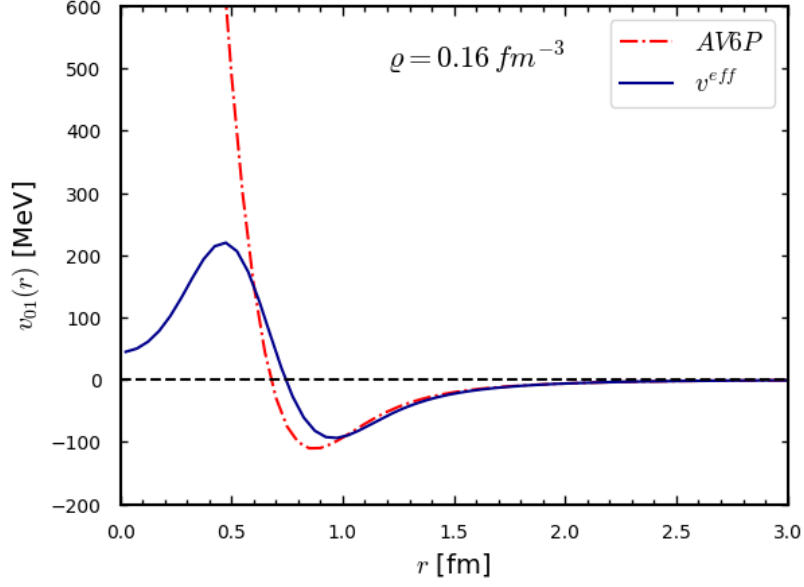


Figure 4.1. Comparison between the S=0, T=1 component of the AV6P NN potential and the corresponding effective interaction.

This procedure leads to the definition of an effective interaction embodying the effects of correlations. We will see how the inclusion of such effects turns into an appreciable softening of the strong repulsive core characterizing the NN potential, leading to an interaction which can be safely treated in perturbation theory with respect to the Fermi gas basis. This effect is clearly exposed in the example of Fig. 4.1.

The effective interaction is defined through the expectation value of the Hamiltonian over the correlated ground state

$$\langle \Psi_0 | \mathcal{H} | \Psi_0 \rangle = T_F + \langle \Phi_0 | \sum_{i < j} v_{ij}^{\text{eff}} | \Phi_0 \rangle \quad (4.5)$$

where $|\Phi_0\rangle$ labels the Fermi gas ground state and the correlated state $|\Psi_0\rangle$ is defined as

$$|\Psi_0\rangle = \frac{\mathcal{F}|\Phi_0\rangle}{\sqrt{\langle \Phi_0 | \mathcal{F}^\dagger \mathcal{F} | \Phi_0 \rangle}} \quad (4.6)$$

with

$$\mathcal{F} = \mathcal{S} \prod_{i < j} F_{ij}, \quad F_{ij} = \sum_p f^p(r_{ij}) O_{ij}^p. \quad (4.7)$$

The expectation value on the right hand side of Eq. (4.5) has the form

$$\langle \Phi_0 | \sum_{i < j} v_{ij}^{\text{eff}} | \Phi_0 \rangle = A \frac{\rho}{2} \int d\mathbf{r}_{12} \text{CTr} \left[v_{12}^{\text{eff}} \left(1 - \hat{P}_{12}^{\sigma\tau} l_{12}^2 \right) \right]. \quad (4.8)$$

A cluster expansion of the left-hand side of Eq. (4.5) leads to

$$\langle \Psi_0 | \mathcal{H} | \Psi_0 \rangle = T_F + (\Delta E)_{2b} + \dots \quad (4.9)$$

where the two-body term has the form

$$(\Delta E)|_{2b} = A \frac{\rho}{2} \int d\mathbf{r}_{12} \text{CTr} \left[\left(F_{12} v_{12} F_{12} - \frac{1}{m} \nabla F_{12} \cdot \nabla F_{12} \right) \left(1 - \hat{P}_{12}^{\sigma\tau} l_{12}^2 \right) \right] \quad (4.10)$$

By equating Eqs. (4.8) and (4.10) we can define the effective interaction at the two-body level as

$$v_{ij}^{\text{eff}} = F_{ij} v_{ij} F_{ij} - \frac{1}{m} \nabla F_{ij} \cdot \nabla F_{ij}. \quad (4.11)$$

The functional form of the correlation functions $f^p(r)$ is found by solving the Euler-Lagrange equations associated to the the minimization of the two-body cluster ground state energy with a quenched NN potential

$$\tilde{v}_{ij} = \sum_p \alpha_p v^p(r_{ij}) O_{ij}^p, \quad (4.12)$$

where α_p are the so-called quenching parameters. The correlation functions obtained have to satisfy the boundary conditions

$$\begin{aligned} f^p(r \geq d^p) &= \delta_{1p} \\ \left. \frac{df^p(r)}{dr} \right|_{d^p} &= 0. \end{aligned} \quad (4.13)$$

For the definition of the quenching parameters α_p and the relaxation distances d^p we adopt the same convention of Ref. [96] yielding

$$\begin{aligned} d^{p \neq 5,6} &= d_c, \quad d^{p=5,6} = d_t, \\ \alpha_{p=1} &= 1, \quad \alpha_{p>1} = \alpha. \end{aligned} \quad (4.14)$$

The effective interaction defined by Eq. (4.11) for any given density still depends upon the relaxation distances d_c , d_t and the quenching factor α . These are usually variational parameters which in *ab initio* calculations are fixed by minimizing the energy computed with accurate many-body techniques, such as the FHNC/SOC summation scheme or Monte Carlo methods. Within the effective interaction, which is derived at a finite order in the cluster expansion, such parameters are optimized in order to reproduce some target values. Such target values can be chosen to be both the SNM and PNM energy per nucleon, computed by means of a complete variational approach. This procedure can be seen as a sort of renormalization of the NN interaction which allows to account for screening effects induced by the presence of the nuclear medium. Basically we are fixing an observable, computed with non-perturbative and accurate methods (the energy per nucleon of SNM and PNM in this case), and then we are defining an effective Hamiltonian whose free parameters are tuned in order to reproduce such target observable at a finite order in the perturbative expansion.

First derived effective interactions included only up to two-nucleon potentials in their expression [122]. This approach, besides being extremely simple and powerful, produces an effective interaction which is unable to capture some important dynamical aspects related to the presence of three-nucleon forces. For this reason state of the art effective interactions, as the one derived by Banhar and Lovato (BL)

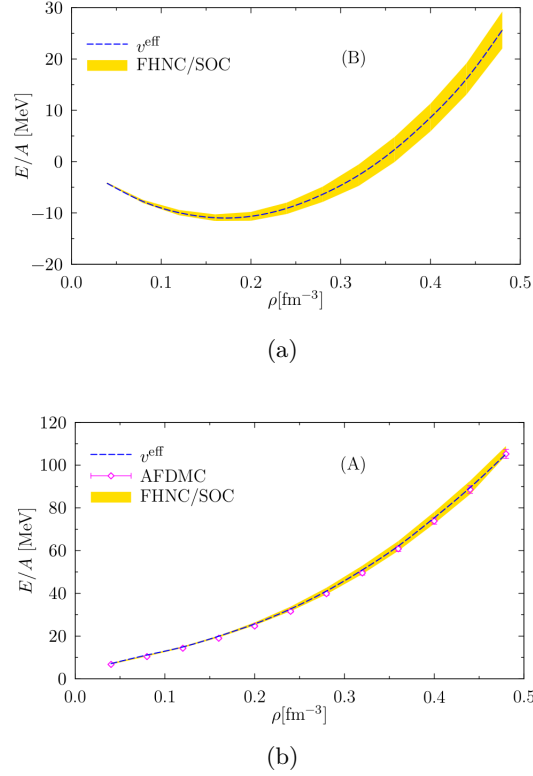


Figure 4.2. Energy per nucleon of SNM (a) and PNM (b) computed with the BL effective interaction (dashed line), taken from [67]. For comparison also the FHNC/SOC calculations for both SNM and PNM are shown as yellow shaded regions. The width of such regions is associated with the discrepancy arising from the employment of different kinetic energy prescriptions. This uncertainty can be used to gauge the precision of the FHNC/SOC procedure. For the PNM the authors reported also the values computed within the AFDMC approach.

in Refs. [67, 123] include also three-body cluster terms, coming from both NN and NNN interactions. The effective interaction derived in this way can be schematically represented as

$$\langle T - T_F \rangle|_{2b+3b} + \langle v_{NN} \rangle|_{2b+3b} + \langle V_{NNN} \rangle|_{3b} \equiv A \frac{\rho}{2} \int d\mathbf{r}_{12} \text{CTr} \left[v_{12}^{\text{eff}} \left(1 - \hat{P}_{12}^{\sigma\tau} l_{12}^2 \right) \right]. \quad (4.15)$$

We will not discuss in details the expression of the terms $\langle T \rangle|_{3b}$, $\langle v_{NN} \rangle|_{3b}$ and $\langle V_{NNN} \rangle|_{3b}$, for which a comprehensive treatment can be found in Refs. [93, 123, 124]. In Fig. 4.2 we can see the energies per nucleon of both SNM and PNM computed with this effective interaction, together with their target values. Such results have been obtained with an Hamiltonian comprising the AV6P+UIX interaction potentials. The many-body problem was solved by means of the FHNC/SOC summation scheme for SNM, and with the AFDMC for PNM. The relaxing distances and quenching parameters for the BL effective interaction are shown in Fig. 4.3.

The effective interaction formalism has proved to be remarkably powerful in computing several nuclear matter properties as for example the energy per nucleon

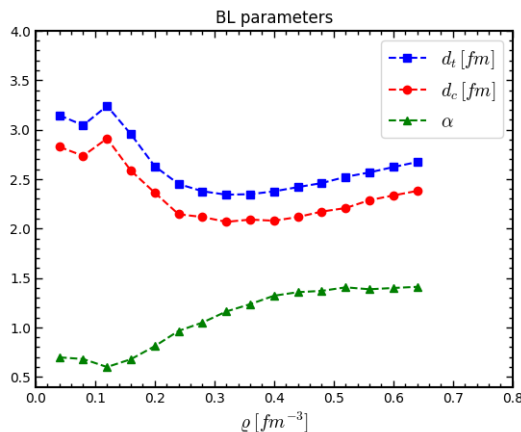


Figure 4.3. Relaxation distances and quenching parameters for the effective interaction derived by Benhar and Lovato.

of non-polarized matter at arbitrary proton fraction. Let's consider nuclear matter at baryon density

$$\varrho = \sum_{\lambda} \varrho_{\lambda} = \sum_{\lambda} \varrho x_{\lambda} \quad (4.16)$$

where $\lambda = 1, 2, 3, 4$ labels spin-up protons, spin-down protons, spin-up neutrons and spin-down neutrons respectively, with the corresponding densities being $\varrho_{\lambda} = \varrho x_{\lambda}$. In SNM $x_1 = x_2 = x_3 = x_4 = 1/4$, while in PNM $x_1 = x_2 = 0$ and $x_3 = x_4 = 1/2$. We can write the energy per nucleon as

$$\frac{E}{A} = \frac{3}{5} \sum_{\lambda} x_{\lambda} \frac{k_{F,\lambda}^2}{2m} + \frac{\varrho}{2} \sum_{\lambda\mu} x_{\lambda} x_{\mu} \int d^3r [v_{\lambda\mu}^{\text{eff},d}(\mathbf{r}) - v_{\lambda\mu}^{\text{eff},e}(\mathbf{r}) l(k_{F,\lambda}r) l(k_{F,\mu}r)] \quad (4.17)$$

with

$$v_{\lambda\mu}^{\text{eff},d}(\mathbf{r}) = \sum_p v^{\text{eff},p}(r) \langle \lambda\mu | O_{12}^p | \lambda\mu \rangle \quad (4.18)$$

$$v_{\lambda\mu}^{\text{eff},e}(\mathbf{r}) = \sum_p v^{\text{eff},p}(r) \langle \lambda\mu | O_{12}^p | \mu\lambda \rangle. \quad (4.19)$$

The derivation of the above equation can be found in Appendix D. Another remarkable property of the effective interaction formalism is the possibility to extend the treatment to finite temperature nuclear matter in a simple and elegant way. Indeed in a recent work, the BL effective interaction has been applied to study the temperature dependence of average and single-particle properties of nuclear matter relevant to astrophysical applications in Ref. [125]. A comprehensive treatment and discussion about this subject can be found in Ref. [126].

Since the BL effective interaction is carried out from a non-relativistic Hamiltonian, one of the goal of this Thesis is to study the effect of introducing boost corrections within this formalism. We are interested in studying both the impact of such relativistic effects in the functional form of the effective interaction, and in the employment of the modified UIX* NNN potential. Strictly speaking the main goal

of such a study will be the definition of an effective interaction \tilde{v}^{eff} by means of

$$\begin{aligned} & \langle T - T_F \rangle|_{2b+3b} + \langle v_{NN} \rangle|_{2b+3b} + \langle \delta v \rangle|_{2b+3b} + \langle V_{NNN}^* \rangle|_{3b} \\ & \equiv A \frac{\rho}{2} \int d\mathbf{r}_{12} \text{CTr} \left[\tilde{v}_{12}^{\text{eff}} \left(1 - \hat{P}_{12}^{\sigma\tau} l_{12}^2 \right) \right]. \end{aligned} \quad (4.20)$$

This definition will require in principle to re-optimize the free parameters of the effective interaction over *ab initio* calculations performed with the \mathcal{H}^* Hamiltonian. In order to develop a simplified procedure we investigated the possibility of defining the \tilde{v}^{eff} interaction employing the same variational parameters obtained in the BL one. In order to justify this procedure we have performed some exploratory studies defining an effective interaction optimized over the APR variational energies. We have chosen to employ the APR energies as our target values because they are the only available *ab initio* calculations performed over a broad density range and including both boosts and the modified UIX NNN interaction. In the next sections the results of this study are presented. We have seen that the employment of the same free parameters for both the \tilde{v}^{eff} and v^{eff} models appears to reproduce remarkably well the APR variational energies. Actually our model is based on a slightly simplified version of Eq. (4.20). Since the three-body cluster contribution coming from kinetic energy and NN potential appears to be smaller than their NNN counterpart, we have neglected such terms in the cluster expansion of the Hamiltonian \mathcal{H}^* . Our model for \tilde{v}^{eff} can be therefore expressed as

$$A \frac{\rho}{2} \int d\mathbf{r}_{12} \text{CTr} \left[\tilde{v}_{12}^{\text{eff}} \left(1 - \hat{P}_{12}^{\sigma\tau} l_{12}^2 \right) \right] \equiv \langle T - T_F \rangle|_{2b} + \langle v_{NN} + \delta v \rangle|_{2b} + \langle V_{NNN}^* \rangle|_{3b}. \quad (4.21)$$

4.1 Boost corrections

The boost correction implemented in our effective interaction is the same employed by APR in their work. It is a simplified version of Eq. (2.85) yielding

$$\delta v(\mathbf{P}, \mathbf{r}) = -\frac{P^2}{8m^2} v(\mathbf{r}) + \frac{(\mathbf{P} \cdot \mathbf{r})}{8m^2} \mathbf{P} \cdot \nabla v(\mathbf{r}). \quad (4.22)$$

In the above expression we are neglecting the terms arising from Thomas Precession and from the commutators with the spin-dependent parts of the NN potential. The impact of these effects on the binding energy of ${}^3\text{H}$ and ${}^4\text{He}$ was proved to be very small with respect to the contribution coming from Eq. (4.22) [102].

By choosing a NN potential with the form

$$v(\mathbf{r}) = \sum_{p=1}^6 v^p(r) O_{12}^p \quad (4.23)$$

we have

$$\delta v(\mathbf{P}, \mathbf{r}) = \sum_p \left[-\frac{P^2}{8m^2} v^p(r) + \frac{(\mathbf{P} \cdot \hat{\mathbf{r}})^2}{8m^2} r \frac{dv^p}{dr} \right] O_{12}^p + \sum_p \frac{(\mathbf{P} \cdot \mathbf{r})}{8m^2} v^p(r) \mathbf{P} \cdot \nabla O_{12}^p. \quad (4.24)$$

The last term in the previous equation involves the gradient of the tensor operator ∇S_{12} whose expectation value on non-polarized matter is zero, therefore we are considering only the expression

$$\delta v(\mathbf{P}, \mathbf{r}) = \sum_p \left[-\frac{P^2}{8m^2} v^p(r) + \frac{(\mathbf{P} \cdot \hat{\mathbf{r}})^2}{8m^2} r \frac{dv^p}{dr} \right] O_{12}^p \quad (4.25)$$

for the boost correction.

We are interested in calculating the two-body cluster contribution of the expectation value

$$\frac{\langle \Psi_0 | H | \Psi_0 \rangle}{\langle \Psi_0 | \Psi_0 \rangle} = \frac{\langle \Phi_0 | F^\dagger H F | \Phi_0 \rangle}{\langle \Phi_0 | F^\dagger F | \Phi_0 \rangle} = T_F + \langle \Phi_0 | \frac{F^\dagger [T, F]}{2} + adj + F^\dagger V F | \Phi_0 \rangle / \langle \Phi_0 | F^\dagger F | \Phi_0 \rangle \quad (4.26)$$

with

$$T = \sum_i \frac{p_i^2}{2m}, \quad V = \sum_{i < j} v_{ij} + \delta v_{ij}. \quad (4.27)$$

Evaluating the energy at two body cluster level yields

$$\langle E \rangle \approx T_F + (\Delta E)_{2b}, \quad (4.28)$$

and

$$(\Delta E)_{2b} = \frac{1}{2} \sum_{n_1, n_2} \langle n_1 n_2 | F_{12} [t_1, F_{12}] + F_{12} (v_{12} + \delta v_{12}) F_{12} | n_1 n_2 - n_2 n_1 \rangle, \quad (4.29)$$

with $t_1 = -\nabla_1^2 / 2m$.

We choose F_{12} to have the form

$$F_{12} = \sum_p f^p(r) O_{12}^p, \quad (4.30)$$

where the sum over p runs over the first 6 operators $O_{12}^p = [1, \boldsymbol{\sigma}_1 \cdot \boldsymbol{\sigma}_2, S_{12}] \otimes [1, \boldsymbol{\tau}_1 \cdot \boldsymbol{\tau}_2]$. We have already mentioned that such a set of operators forms an algebra, indeed we have

$$O_{ij}^p O_{ij}^q = \sum_l K^{pql} O_{ij}^l, \quad (4.31)$$

with K^{pql} a set of scalar coefficients. The expectation value of any operator $A_{12} = \sum_p a^p(r) O_{12}^p$ over the state $|\Psi\rangle = F_{12} |\Phi\rangle$ can always be written as

$$\langle A_{12} \rangle = \langle \Psi | A_{12} | \Psi \rangle = \langle \Phi | F_{12} A_{12} F_{12} | \Phi \rangle = \langle \Phi | B_{12} | \Phi \rangle, \quad (4.32)$$

with

$$B_{12} = \sum_p b^p(r) O_{12}^p \quad (4.33)$$

and

$$b^p(r) = \sum_{mnlq} K^{mnl} K^{qlp} f^q(r) a^m(r) f^n(r). \quad (4.34)$$

Since the part of the boost correction we are interested in can be expressed in the form

$$\delta v(\mathbf{P}, \mathbf{r}) = -\frac{P^2}{8m^2} \sum_p w^p(r) O_{12}^p + \frac{(\mathbf{P} \cdot \hat{\mathbf{r}})^2}{8m^2} \sum_p g^p(r) O_{12}^p \quad (4.35)$$

with

$$w^p(r) \equiv v^p(r), \quad g^p(r) \equiv r \frac{dv^p}{dr}, \quad (4.36)$$

we can carry out the two-body cluster expectation value $\langle \Phi_0 | F_{12} \delta v F_{12} | \Phi_0 \rangle$ by simply computing the expectation value on the uncorrelated ground state, $\langle \Phi_0 | \delta v | \Phi_0 \rangle$, and then performing the substitutions

$$\begin{aligned} w^p(r) &\rightarrow \sum_{mnlq} K^{mnl} K^{qlp} f^q(r) v^m(r) f^n(r), \\ g^p(r) &\rightarrow \sum_{mnlq} K^{mnl} K^{qlp} f^q(r) r \frac{dv^m}{dr} f^n(r). \end{aligned} \quad (4.37)$$

In order to carry out the explicit expression of $\langle \Phi_0 | \delta v | \Phi_0 \rangle$ we can define

$$\frac{\langle \delta v \rangle}{A} = \frac{1}{A} \sum_{i < j} \langle \Phi_0 | \delta v_{ij} | \Phi_0 \rangle \quad (4.38)$$

which can be written as

$$\frac{\langle \delta v \rangle}{A} = \frac{\langle \delta v \rangle_d}{A} - \frac{\langle \delta v \rangle_e}{A}. \quad (4.39)$$

The explicit expression of $\langle \delta v \rangle_d$ and $\langle \delta v \rangle_e$ turns out to be

$$\frac{\langle \delta v \rangle_d}{A} = \frac{1}{5} \frac{\rho}{16m^2} \sum_p \sum_{\lambda\mu} x_\lambda x_\mu (k_{F\lambda}^2 + k_{F\mu}^2) \langle \lambda\mu | O^p | \lambda\mu \rangle \int d^3r \left[r \frac{dv^p(r)}{dr} - 3v^p(r) \right] \quad (4.40)$$

$$\frac{\langle \delta v \rangle_e}{A} = \frac{\rho}{16m^2} \sum_p \sum_{\lambda\mu} x_\lambda x_\mu \langle \lambda\mu | O^p | \mu\lambda \rangle \int d^3r \left[r \frac{dv^p(r)}{dr} I_2 - v^p(r) I_1 \right] \quad (4.41)$$

with

$$I_1 = 2l'(k_{F\lambda}r)l'(k_{F\mu}r) - l(k_{F\lambda}r)\nabla^2 l(k_{F\mu}r) - l(k_{F\mu}r)\nabla^2 l(k_{F\lambda}r) \quad (4.42)$$

$$I_2 = 2l'(k_{F\lambda}r)l'(k_{F\mu}r) - l(k_{F\lambda}r)l''(k_{F\mu}r) - l(k_{F\mu}r)l''(k_{F\lambda}r) \quad (4.43)$$

where the prime indicates the derivative with respect to r and

$$\nabla^2 \equiv \frac{1}{r} \frac{\partial^2}{\partial r^2} r. \quad (4.44)$$

As a final comment it should be useful to stress that for both SNM and PNM the Fermi momentum $k_{F\lambda}$ is the same for all different values of the index λ . Therefore if we want to use the same notation of the previous section, explicitly figuring the CTr operator, we can define a unique k_F (which is different if we are considering SNM or PNM) and then substitute¹

$$\sum_{\lambda\mu} x_\lambda x_\mu \rightarrow \text{CTr} [\cdot]. \quad (4.45)$$

If we consider an Hamiltonian of the form

$$\mathcal{H} = \sum_i \frac{p_i^2}{2m} + \sum_{i<j} (v_{ij} + \delta v_{ij}) \quad (4.46)$$

a natural question could be: is it possible to introduce boost corrections in the functional form of the effective interaction? The answer is yes we just need to add another term to $(\Delta E)|_{2b}$ yielding

$$\langle \Phi_0 | \sum_{i<j} v_{ij}^{\text{eff}} | \Phi_0 \rangle = (\Delta E)|_{2b} + \langle \Psi_0 | \sum_{i<j} \delta v_{ij} | \Psi_0 \rangle|_{2b}. \quad (4.47)$$

In order to carry out an effective interaction of the form

$$v_{ij}^{\text{eff}} = \sum_p v_{\text{eff}}^p(\varrho, r_{ij}) O_{ij}^p \quad (4.48)$$

we need to cast the expectation value of the boost correction into the form

$$\langle \Psi_0 | \sum_{i<j} \delta v_{ij} | \Psi_0 \rangle|_{2b} = \frac{\varrho}{2} \int d\mathbf{r}_{12} \text{CTr} \left[\sum_p \delta v_{\text{eff}}^p(\varrho, r) O_{12}^p \left(1 - \hat{P}_{12}^{\sigma\tau} l_{12}^2 \right) \right]. \quad (4.49)$$

Roughly speaking this can be achieved by introducing in the explicit expression of $\langle \Psi_0 | \sum_{i<j} \delta v_{ij} | \Psi_0 \rangle|_{2b}$ the identity

$$\mathbb{1} = \left(1 - \hat{P}_{12}^{\sigma\tau} l_{12}^2 \right)^{-1} \left(1 - \hat{P}_{12}^{\sigma\tau} l_{12}^2 \right). \quad (4.50)$$

The final expression for δv_{eff}^p can be written as

$$\delta v_{\text{eff}}^p(k_F, r) \equiv \frac{1}{1 - l^4(k_F r)} \sum_m \left[\delta^{pm} + l^2(k_F r) M^{pm} \right] \xi^m(k_F, r). \quad (4.51)$$

The definition of the quantities M^{pm} and ξ^m , as well as a detailed derivation of the above expression can be found in Appendix E.

¹Actually we have also to introduce the exchange operator performing the substitution $\langle \lambda\mu | O^p | \mu\lambda \rangle \rightarrow \langle \lambda\mu | O^p \hat{P}_{12} | \lambda\mu \rangle$.

4.2 Analysis with a density dependent NN interaction

As a first exercise we included the two-body cluster boost correction in an effective interaction derived from a simplified Hamiltonian, which does not include any NNN interaction potential. The effect of NNN repulsion is taken into account by equipping the NN interaction with an additional density dependence. This Hamiltonian is written as

$$\mathcal{H} = \sum_i \frac{p_i^2}{2m} + \sum_{i<j} v_{ij} \quad (4.52)$$

where we have chosen as the NN potential the Argonne v6' model, opportunely modified in order to account for NNN repulsion. This correction is implemented by reducing the intermediate range attraction of NN potential with the addition of a density dependent term according to the procedure developed by Lagaris and Pandharipande [96]. Since the NN potential can be written as

$$v = v_\pi + v_I + v_S \quad (4.53)$$

within the approach of [96] the NNN repulsion is introduced by means of the substitution $v \rightarrow v'$ with

$$v' = v_\pi + v_I(1 - \gamma_1 \rho) + v_S. \quad (4.54)$$

An higher value of the parameter γ_1 means a greater reduction of the NN attraction and therefore accounts for a larger NNN repulsion.

The effective interaction is then computed by means of a cluster expansion of the correlated ground state energy and truncating at the two-body term. This ground state energy depends upon the correlation functions through the relaxation distances d_c , d_t and the quenching parameter α , that can be considered as free parameters. These parameters are adjusted in order to simultaneously reproduce the energy per nucleon of both PNM and SNM computed in the original work of APR [62] within a full FHNC/SOC approximation scheme. It turns out that with this approach we are able to reproduce the EOSs of APR with an effective interaction which can be easily derived without computational or technical efforts.

An interesting observation is that with this effective interaction we are able to reproduce both the APR1 and APR2 equations of state provided we use two different values of γ_1 . The EOS APR2 is reproduced with $\gamma_1 = 0.2$ whereas APR1 is reproduced with $\gamma_1 = 0.3$. This behavior is expected because in the APR2 equation of state the NNN repulsion is softened by the introduction of relativistic boost corrections. It is remarkable that the treatment of the NNN repulsion, which accounts for the main difference between the APR1 and APR2 EOSs, has the same impact on the results derived within this simplified approach.

Finally the relevance of introducing boost corrections in the effective interaction was studied. Since their contribution is repulsive we have checked if their inclusion would have altered the value of γ_1 that must be used to reproduce the APR2 EOS. It turns out that boost corrections do not affect the choice of γ_1 . This effect has to be ascribed to the fact that boost interactions yield a small correction to the energy per nucleon, if compared to the correction introduced by a modified NNN repulsion. Indeed, because of their different density dependence NNN repulsion

turns out to have a very stronger effect on the high density behavior of the EOS, with respect to boost corrections, even if they account for comparable contributions around saturation density.

In Fig. 4.4 we can see the energies per nucleon of APR1 (a) and APR2 (b), together with the results computed with the effective interaction v^{eff} discussed above. The free parameters of the effective interaction of Fig. 4.6(a), referred to as v_1^{eff} are optimized to reproduce the APR1 energies per nucleon of both PNM and SNM with a NNN repulsion parametrized by $\gamma_1 = 0.3$. Conversely the effective interaction of Fig. 4.6(b), referred to as v_2^{eff} , is obtained by optimizing the free parameters over the APR2 variational energies with $\gamma_1 = 0.2$. The free parameters resulting from this optimization procedure are shown in Fig. 4.5. The results of Fig. 4.4 show that the optimization procedure works very well even with this simplified dynamics.

Fig. 4.6 shows the results for an effective interaction obtained with the parameters optimized to reproduce APR1, i.e the ones of Fig. 4.5(a), but with the NNN repulsion parameter re-scaled from $\gamma_1 = 0.3$ to $\gamma_1 = 0.2$ (black dashed line in the figure). We can see how with this effective interaction, we obtain an energy per nucleon which lies close to the actual values of APR2 (although there seems to be a significant discrepancy at $\rho > 0.64 \text{ fm}^{-3}$) without redoing the optimization procedure. This effect underlines the pivotal role of the NNN repulsion over the optimization of the other free parameters.

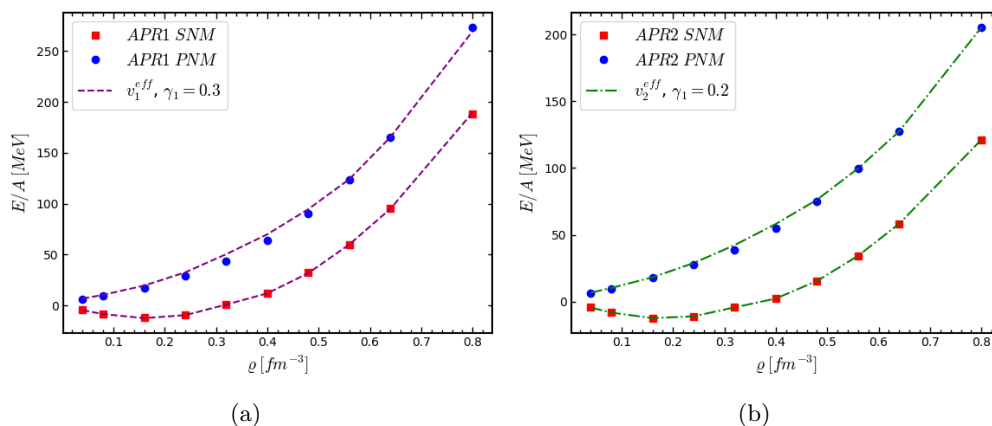


Figure 4.4. Energy per nucleon of both SNM and PNM for the effective interaction optimized to reproduce APR1 (a) and APR2 (b). Circular blue and red points represent the values of the energy per nucleon computed in [62]. The dashed purple and dot-dashed green lines refer to the results obtained with the effective interactions derived in this work.

Finally once we have an effective interaction defined as in Eq. (4.47), i.e. accounting for boost corrections, we can either add their contribution perturbatively, or redo the optimization procedure with the boost corrected effective potential. In the following we will explore both these scenarios. The interaction involving boost corrections is labeled as \tilde{v}^{eff} .

From Fig. 4.7 we can see how adding perturbatively the boost corrections to the potential v_1^{eff} with $\gamma_1 = 0.2$ of Fig 4.6, remarkably helps the results to get closer to

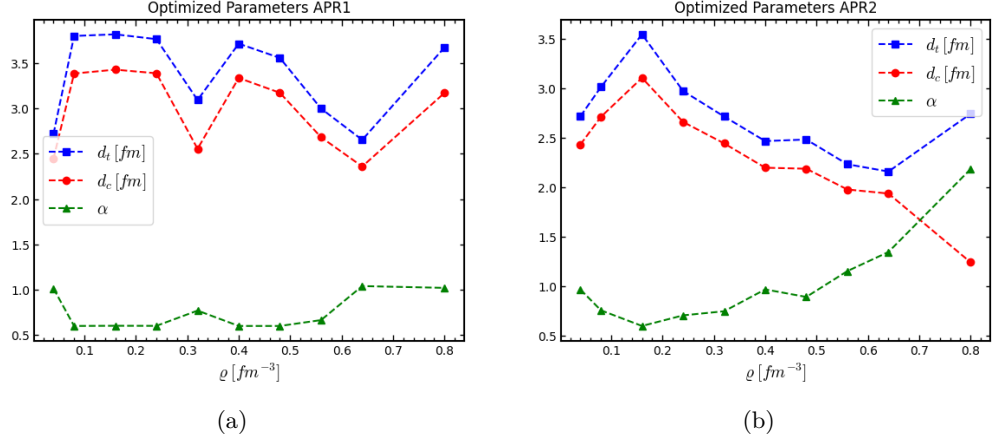


Figure 4.5. Optimized relaxation distances and quenching parameters for both APR1 (a) and APR2 (b).

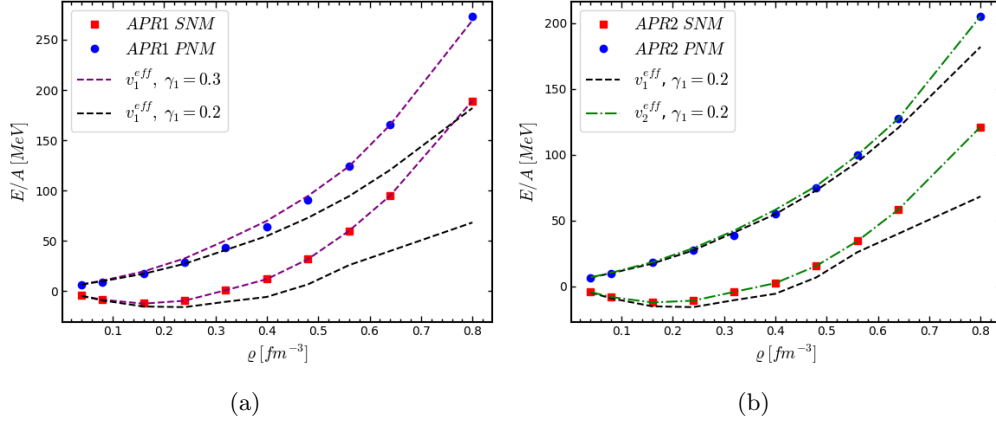


Figure 4.6. Same as Fig. 4.4 but with the addition of the effective interaction derived using the variational parameters reproducing APR1 but with $\gamma_1 = 0.2$ (black dashed line).

the APR2 target γ values (dark red dot-dashed lines), providing an improvement in the accuracy of the results.

In Fig 4.8 we can see the effects that different values of γ_1 , as well as the perturbative introduction of boost corrections, have on the radial shape of the central component of the effective interaction at different densities. In the figures we can see the central component of the three models previously described. All these models have been derived with the same set of free parameters, Fig 4.5(a). We can see how the discrepancies between these models become more important with increasing density. In particular we can see that the dominant effect is the softening of NNN repulsion, accounting for the difference between the red dashed line and the blue dot-dashed line. The inclusion of boost corrections, which account for the difference between the green solid line and the blue dot-dashed one, appears to have a very small effect.

The introduction of the boost corrections in the definition of the effective inter-

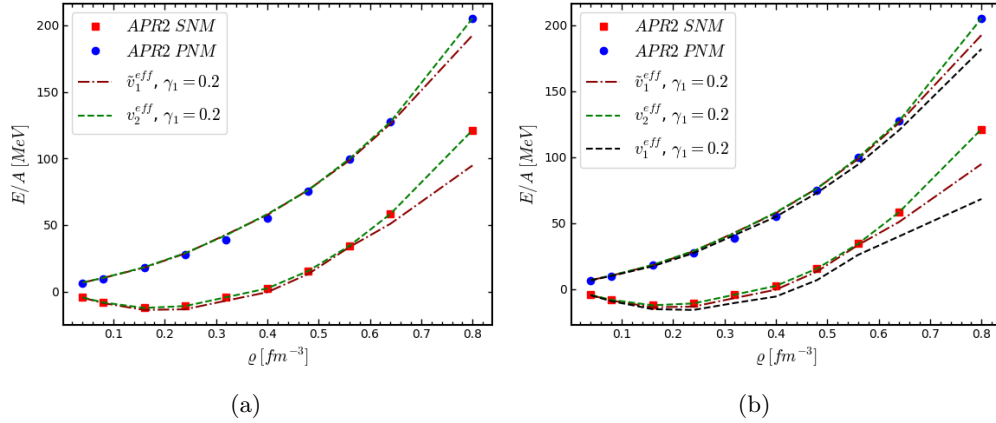


Figure 4.7. (a) Energy per nucleon obtained with an effective interaction with (dark red dashed line) perturbatively added boost corrections. (b) Comparison of the effective interaction of panel (a) with the one of Fig. 4.6. We can see how with the introduction of boost corrections the results get closer to the APR2 values.

action doesn't introduce relevant changes, as shown in panel (a) of Fig. 4.9. The optimization procedure works in the same way as without boost corrections, and there is no impact on the value of γ_1 that we have to choose in order to reproduce the APR2 EOS. The optimization parameters obtained with the boost corrected effective interaction are shown in Fig. 4.9(b). However, since the functional form of the effective interaction is different, the introduction of boost corrections could in principle affect the values of observables directly related to it. In this respect Fig. 4.10 shows the radial dependence of the central component of two effective interactions, both of them optimized to reproduce the APR2 variational energies. The four panels show the results at four different densities. Orange dashed lines represent the effective interaction obtained with the parameters of Fig. 4.5(b), $\gamma_1 = 0.2$ and without boost corrections. The purple solid line refers to the boost corrected effective interaction, obtained with the parameters of Fig. 4.9(b) and $\gamma_1 = 0.2$. We can see that at high density the difference in the radial shape of the effective potential becomes appreciable and it could in principle affect some observables such as the effective mass or the single particle energy.

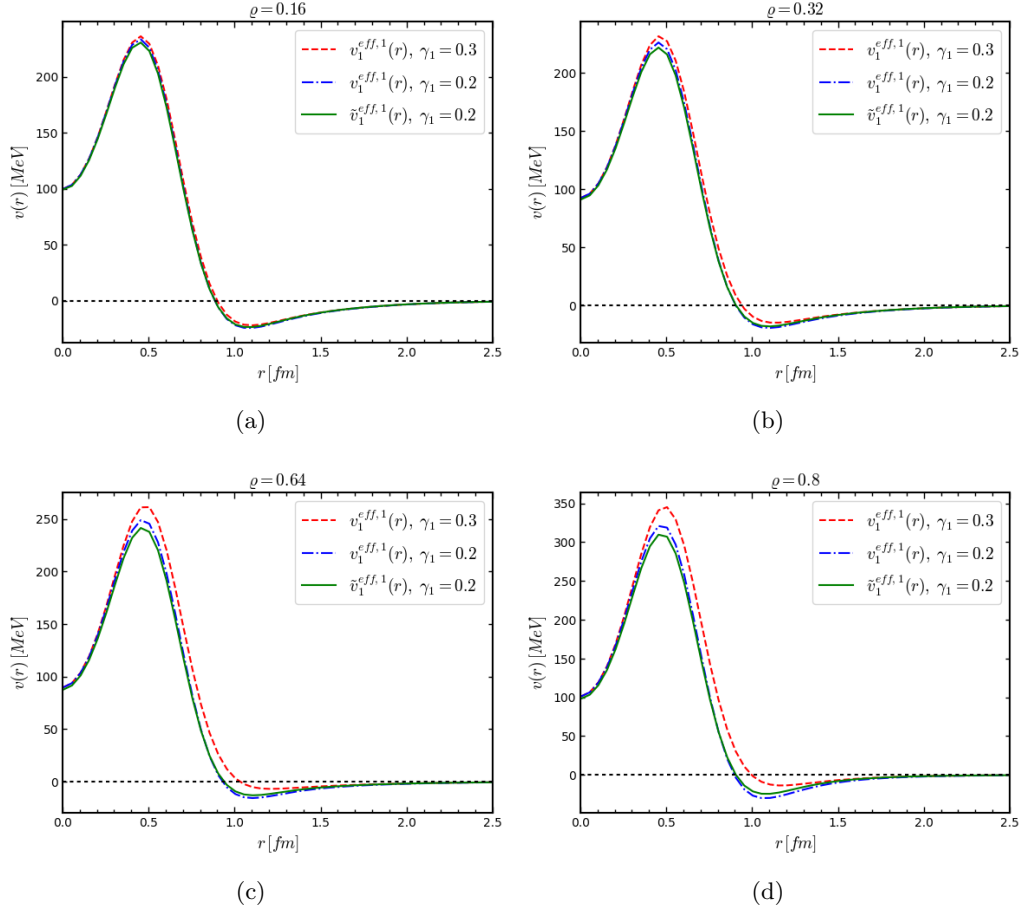


Figure 4.8. Radial dependence of the central component of three effective interactions at different densities. The density is written on top of each panel (in units of fm^{-3}). The three models are derived with the same free parameters. The red dashed line is obtained by setting $\gamma_1 = 0.3$. The blue dot-dashed line by setting with $\gamma_1 = 0.2$ and the green solid line by adding boost corrections to the blue one.

4.3 Calculation with a realistic NNN interaction

Here we are going to discuss the results of an analysis similar to the one of the previous section, but performed with an effective interaction derived from a more realistic Hamiltonian. The Hamiltonian we have considered has the form

$$\mathcal{H} = \sum_i \frac{p_i^2}{2m} + \sum_{i<j} v_{ij} + \sum_{i<j<k} V_{ijk}. \quad (4.55)$$

We can see that in this case we are explicitly considering a realistic three-nucleon interaction. The chosen interaction potentials are the AV6P NN potential and the UIX model for the NNN interaction. The effective interaction was derived by including a two-body cluster contribution for the kinetic energy and NN interaction, and a three-body cluster contribution for the NNN potential. It is defined as

$$\frac{\rho}{2} \int d\mathbf{r}_{12} \text{CTr} \left[v_1^{\text{eff}} \left(1 - \hat{P}_{12}^{\sigma\tau} l_{12}^2 \right) \right] \equiv \langle T - T_F \rangle_{2b} + \langle v_{NN} \rangle_{2b} + \langle V_{NNN} \rangle_{3b}. \quad (4.56)$$

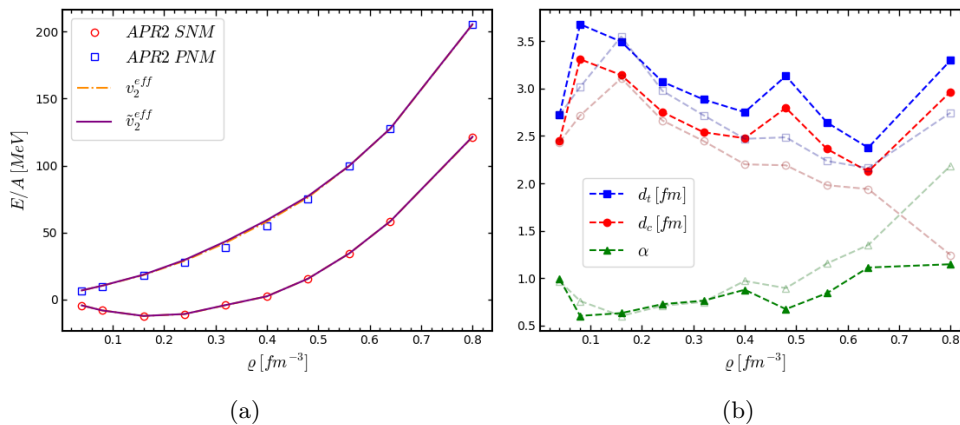


Figure 4.9. (a) Energy per nucleon of SNM and PNM obtained with an effective interaction optimized over the APR2 variational energies and including boost corrections in its definition (purple solid line). For comparison the APR2 variational energies as well as the effective interaction obtained without boost corrections (orange dashed lines) are also shown. In panel (b) we can see the parameters resulting from the optimization of the \tilde{v}_2^{eff} interaction. For comparison also the values corresponding to the model v_2^{eff} , already reported in Fig. 4.5(b), are shown with lighter colors.

As in the previous section the free parameters were determined by an optimization procedure in order to reproduce the APR1 energies per nucleon. The resulting potential is labeled as v_1^{eff} in the above equation, where the subscript "1" is referred to the APR1 optimization and the particle indices "12" have been suppressed in order to simplify the notation. In Fig. 4.11 are shown the free parameters (a) and the resulting energies (b) for this model. We can see that differently from the case discussed in the previous section, the relaxation distances show a more regular behavior, probably associated with the choice of a more realistic dynamics. The same procedure was also performed defining an interaction v_2^{eff} as

$$\frac{\rho}{2} \int d\mathbf{r}_{12} \text{CTr} \left[v_2^{\text{eff}} \left(1 - \hat{P}_{12}^{\sigma\tau} l_{12}^2 \right) \right] \equiv \langle T - T_F \rangle_{2b} + \langle v_{NN} \rangle_{2b} + \langle V_{NNN}^* \rangle_{3b}, \quad (4.57)$$

which have been optimized over the APR2 energies per nucleon. We stress once again that the only difference between the V_{NNN} and V_{NNN}^* is in the coupling constant U_0 of the repulsive term, which is chosen to be $U_0 = 0.0048$ and $U_0 = 0.00302$ respectively for the two models. The results for this effective interaction are reported in Fig. 4.12. We can see that the relaxation distances exhibit a slightly more irregular behavior. The jump around $\rho = 0.2 \text{ fm}^{-3}$ can be probably associated with the phase transition induced by the appearance of a pion condensate in PNM, as discussed in the APR original work [62]. In principle the same transition is expected to occur also in SNM but at densities around $\rho = 0.32 \text{ fm}^{-3}$.

We have repeated the same optimization procedure with the boost corrected effective interaction, referred to as \tilde{v}_2^{eff} . The tilde over the potential indicates the inclusion of boosts, whereas the subscript "2" indicates that the free parameters have

been optimized to reproduce the APR2 energies. This \tilde{v}_2^{eff} has the form

$$\frac{\rho}{2} \int d\mathbf{r}_{12} \text{CTr} \left[\tilde{v}_2^{\text{eff}} \left(1 - \hat{P}_{12}^{\sigma\tau} t_{12}^2 \right) \right] \equiv \langle T - T_F \rangle_{2b} + \langle v_{NN} + \delta v \rangle_{2b} + \langle V_{NNN}^* \rangle_{3b}. \quad (4.58)$$

The results for \tilde{v}_2^{eff} are presented in Fig. 4.13. We can see that the inclusion of boost corrections has only a marginal impact on the determination of the free parameters, and the energies per nucleon are still very accurately reproduced. In particular from Fig 4.13(a) we can see that the relaxation distances, as well as the quenching parameter α , exhibit a little kink around $\rho = 0.32 \text{ fm}^{-3}$, which should be probably ascribed to pion condensation in SNM. We indeed recall that we are optimizing the free parameters of the effective interaction in order to simultaneously reproduce both SNM and PNM energies.

Finally in Fig. 4.14 we can see the result of an effective interaction \tilde{v}_1^{eff} which is defined according to Eq. (4.58), but with the free parameters that are not re-optimized over the APR2 variational energies. We have used instead the same values arising from the optimization procedure over APR1, i.e. the ones reported in Fig. 4.11(a). The ultimate goal of such a procedure is to see if we can account for the differences between the APR1 and APR2 EOSs, by only changing the functional form of the effective interaction, i.e. by introducing a perturbative correction directly in the effective potential. The remarkable agreement that is shown in Fig. 4.14 between the APR2 variational energies and the \tilde{v}_1^{eff} model, suggests that such a treatment is possible. This could be seen as a signal that the higher cluster contributions are somehow buried inside the correlation functions obtained after the optimization procedure. Therefore the modification of the NNN repulsion, as well as the introduction of boost corrections can be implemented as a perturbative correction of the effective interaction v_1^{eff} . Because of these considerations the inclusion of the boost corrections within the BL effective interaction should not involve any particular difficulty, and the development of such a model is currently in progress.

Finally, as we have done in the previous section, we also report the radial dependence of the central component of the effective potentials derived so far. In Fig. 4.15 we can see the radial shape of the interactions optimized over the APR1 energies but figuring both different values of the coupling constant U_0 , (accounting for the difference between red dashed lines and blue dot-dashed lines), and the perturbative inclusion of boost corrections (responsible for the difference between the blue dot-dashed lines and the green dashed lines). We can see that also in this case the difference between these curves becomes more important as the density increases, even if it seems to be less remarkable than in the analysis with a density dependent NN interaction.

Figure 4.16 shows the radial dependence of the central component of the v_2^{eff} and \tilde{v}_2^{eff} potentials. We can see that the effect of boost corrections on the radial dependence of the effective interaction is even smaller than in the case of the previous section. This may suggest either that the effect of boosts is negligible when NNN forces are consistently considered, or maybe that three-body cluster contributions of the boost interaction part could be important and should be also taken into account.

As a final remark we want to stress that these results are still on a preliminary level and further investigation is necessary in order to understand every aspect of the described procedure. Anyway what emerges from this study is surely the fact

that, as expected, the contribution of the boost corrections alone on the effective interaction, even being in some sense appreciable at high density, is quite smaller than the one coming from the modification of the NNN repulsion. Slightly similar modifications of the UIX potential could turn into large discrepancies in the EOS of nuclear matter at high density. We also recall that the softening leading from the UIX to the UIX* model occurs in order to balance the repulsion introduced by boost corrections in the binding energies of three- and four- nucleon systems. This is a low density property that has a very strong impact on the high density behavior predicted by the model. Because of the phenomenological nature of the UIX potential, which is constrained only by the physics at saturation, there is no guarantee that it is suited to describe nuclear matter at very high density. In this respect the occurrence of observables that have the potential to constrain the shape of the NNN repulsion at density $\varrho > \varrho_0$ will represent a fundamental breakthrough.

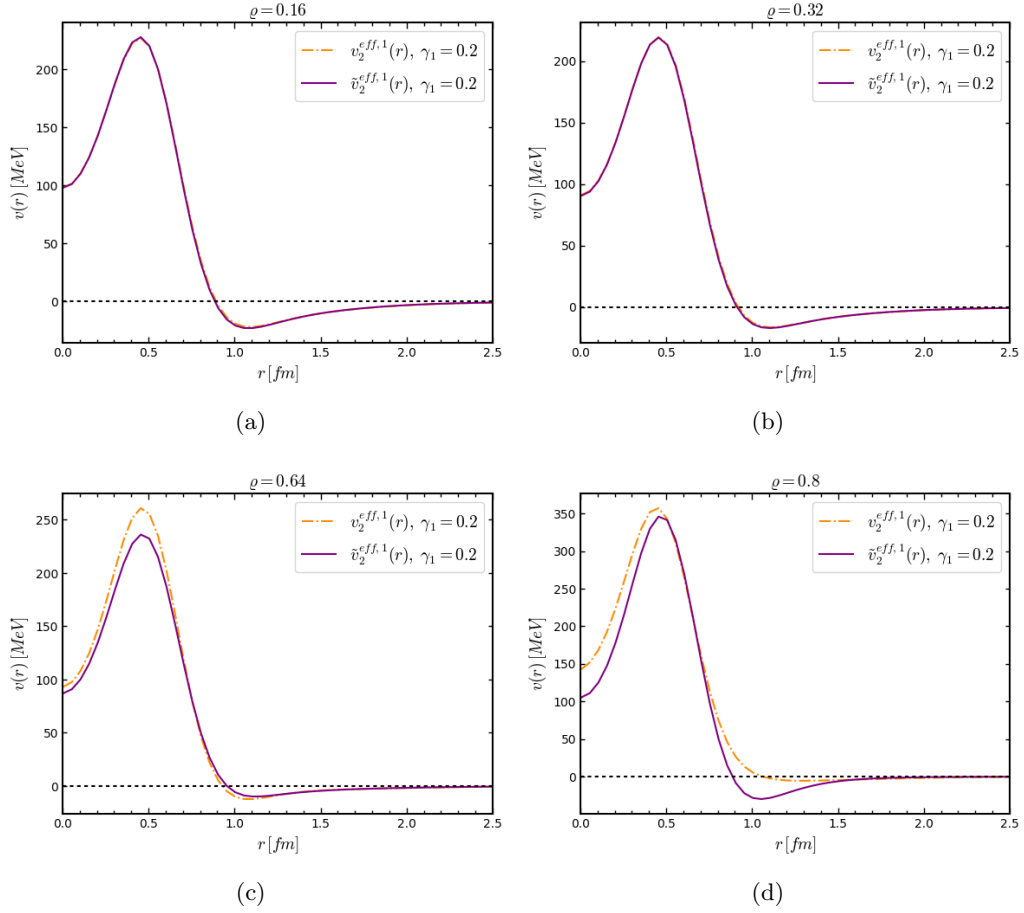


Figure 4.10. Radial dependence of the central component of two effective interactions at different densities. The density is written on top of each panel (in units of fm^{-3}). The two models are derived with (purple solid line) and without (orange dashed line) including boost corrections in the functional form of the effective Hamiltonian. Also the free parameters are different since they are obtained by optimizing different effective interactions over the same variational energies. The value of γ_1 is the same for both the models and set to $\gamma_1 = 0.2$.

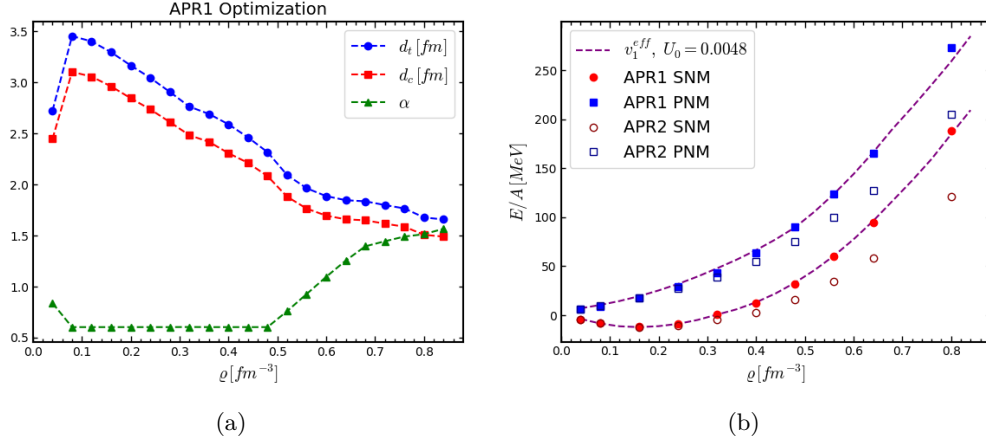


Figure 4.11. (a) Relaxation distances and quenching parameter obtained optimizing the effective interaction to reproduce APR1. (b) Energy per nucleon of both SNM and PNM for the effective interaction optimized to reproduce APR1. Square and circular points represent the values of the energy per nucleon computed in [62].

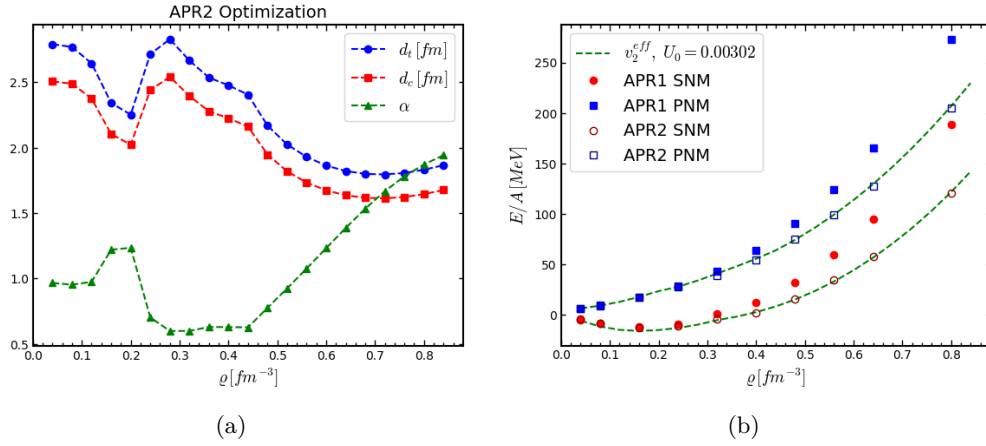


Figure 4.12. (a) Relaxation distances and quenching parameter obtained optimizing the effective interaction to reproduce APR2. (b) Energy per nucleon of both SNM and PNM for the effective interaction optimized to reproduce APR2. Square and circular points represent the values of the energy per nucleon computed in [62].

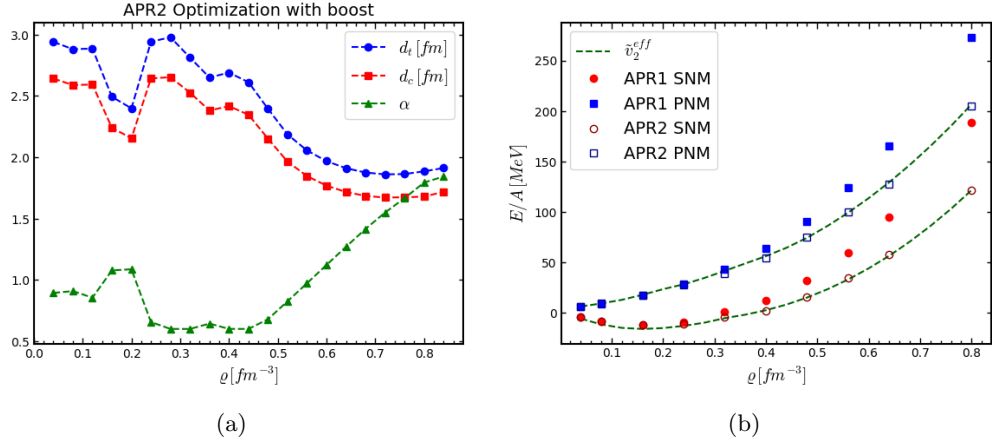


Figure 4.13. (a) Relaxation distances and quenching parameters obtained optimizing the effective interaction to reproduce APR2 including also boost corrections in its definition. (b) Energy per nucleon of both SNM and PNM for such effective interaction. Square and circular points represent the values of the energy per nucleon computed in [62].

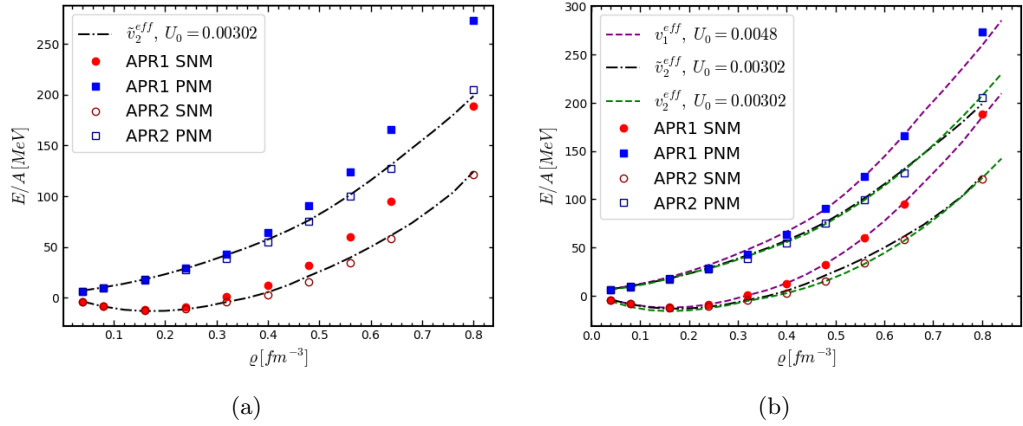


Figure 4.14. (a) Energy per nucleon with the effective interaction computed with the parameters of Fig. 4.11(a) but with an effective interaction \tilde{v} including boost corrections and a different values of the coupling of the NNN repulsion U_0 . (b) Comparison between the results obtained with different values of U_0 with and without boost corrections. Square and circular points represent the values of the energy per nucleon computed in [62].

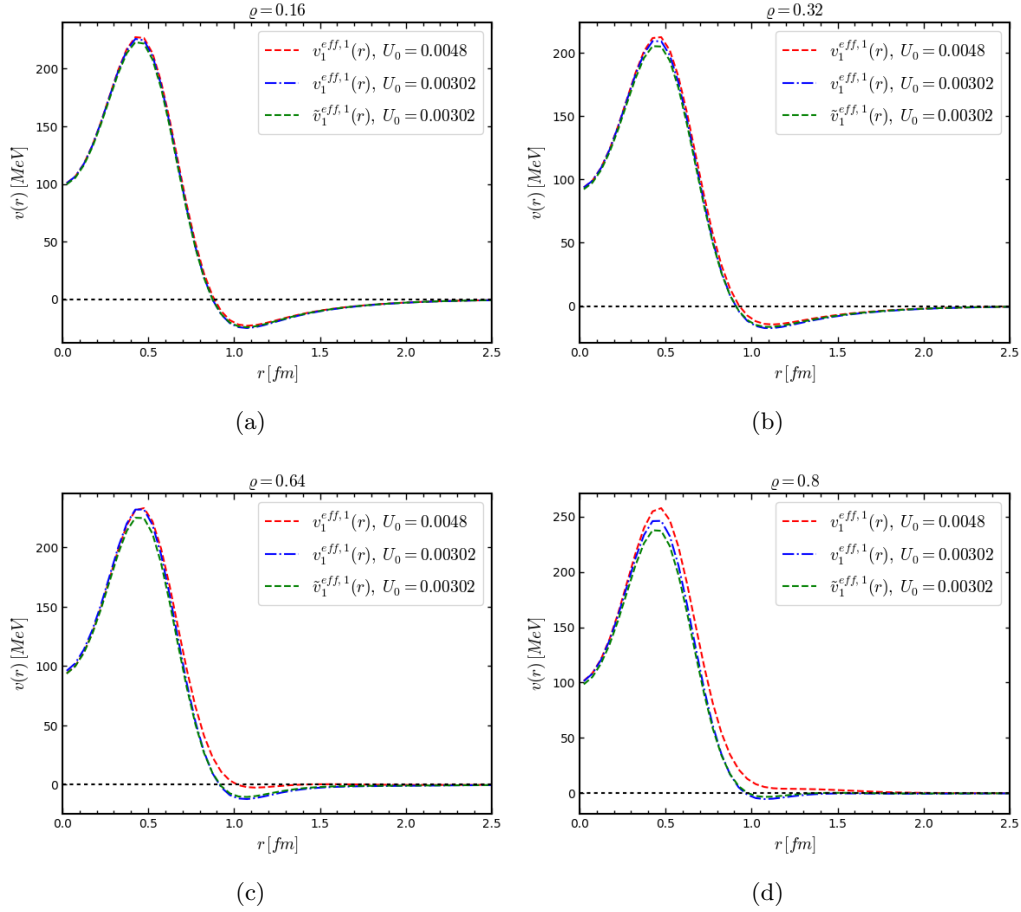


Figure 4.15. Radial dependence of the central component of three effective interactions at different densities. The density is written on top of each panel (in units of fm^{-3}). The three models are derived with the same free parameters. The red dashed line is obtained by setting $U_0 = 0.0048$. The blue dot dashed line by setting with $U_0 = 0.00302$ and the green solid line by adding boost corrections to the blue one.

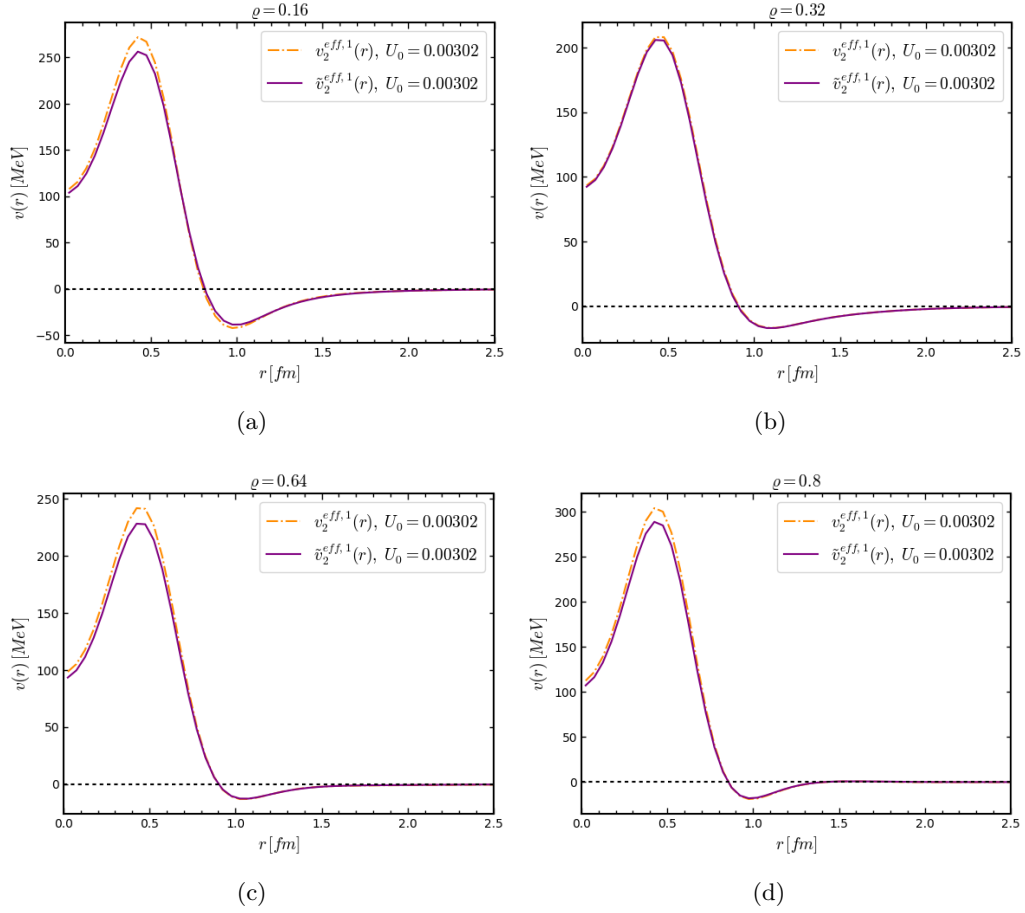


Figure 4.16. Radial dependence of the central component of two effective interactions at different densities. The density is written on top of each panel (in units of fm^{-3}). The two models are derived with (purple solid line) and without (orange dashed line) including boost corrections in the functional form of the effective Hamiltonian. Also the free parameters are different since they are obtained by optimizing different effective interactions over the same variational energies. The strength of the NNN repulsion U_0 is the same for both the models and set to $U_0 = 0.00302$.

Chapter 5

Constraining Three-nucleon Forces with Multimessenger Astronomy

In the past chapters we have underlined several times the strong effect of NNN interactions on the high density behavior of nuclear matter EOS. We have seen how the inclusion of boost corrections accounts for a large part of the repulsion provided by the NNN interaction in the full non-relativistic framework. However, the form of the NNN repulsion employed in the UIX interaction is purely phenomenological and constrained only at saturation density. We can not exclude that the UIX could be not perfectly suited to describe nuclear matter at high density. Indeed, unlike the nucleon-nucleon NN potential, the models of irreducible NNN interactions are totally unconstrained beyond nuclear density. In most models the strength of the isoscalar repulsive term—which plays a pivotal role in determining the stiffness of the nuclear matter EOS in the region relevant to neutron stars—is determined in such a way as to reproduce the empirical equilibrium density of isospin-symmetric matter [97, 127]. In this context, the availability of additional information constraining the three-nucleon potential at larger density would be a major breakthrough.

Over the past decade, the availability of astrophysical data collected by electromagnetic (EM) observatories and GW interferometers, supplemented by the information obtained from Earth-based laboratory experiments, has opened a new era for the investigation of NS structure and dynamics.

The studies aimed at constraining the EOS of NS matter have recently benefit from measurements of the tidal deformabilities [12–17]—encoding the footprint of tidal interactions on the signal emitted by a binary system—performed within the GW band. Because the tidal deformability depends on the internal composition of the stars, any information on its value is potentially a source of novel insight into the EOS. The discovery of GW170817 has triggered a large number of efforts aimed at constraining the NS structure, also exploiting multimessenger approaches based on joint GW-EM analyses [26–30, 32–41, 46–48, 128].

In this chapter we present the result of a study aimed at exploring the possibility of inferring direct information about the NNN repulsion from NS observations [72, 74]. We will see how the data set comprising the GW observation of the binary NS

event GW170817, the spectroscopic observation of the millisecond pulsars PSR J0030+0451 performed by the NICER satellite, and the high-precision measurement of the radio pulsars timing of the binary PSR J0740+6620, can, in fact, be exploited to infer quantitative insight on the strength of repulsive three-nucleon interactions in dense matter. Finally this analysis is extended to consider a near-future scenario, using current interferometers at design sensitivity and stacking multiple binary NS observations characterized by different masses and distances. In addition, we apply, for the first time, the Bayesian approach to gauge the sensitivity of the Einstein Telescope (ET), a proposed third-generation ground-based GW observatory [129–131]

5.1 Modeling nuclear dynamics beyond nuclear density

In this study, we have considered purely phenomenological Hamiltonians, which are expected to be best suited to describe the properties of nuclear matter in the density region extending up to $\sim 5\rho_0$, relevant to NS applications. The reference line of our analysis is the Hamiltonian comprising the Argonne v_{18} NN potential [95] and the Urbana IX NNN potential [97, 127], which has been employed to obtain the APR EOS [62, 65].

The AV18 potential is written as a sum of eighteen terms, needed to describe the complex operator structure of nuclear forces. It provides an accurate fit of the NN scattering phase-shifts for laboratory-frame energies up to ~ 600 MeV, a value typical of NN collisions in strongly degenerate matter at density $\rho \sim 4\rho_0$ [63]. A comparison with the central densities obtained from the solution of the Tolman-Oppenheimer-Volkoff equations [79, 80] with the APR EOS [48] suggests that this phenomenological potential is adequate to describe NSs having masses as large as $\sim 2.1 M_\odot$.

Here are the main features of the UIX model of the NNN interaction, discussed in Chapter 2. Such potential is written as the sum of an attractive potential first derived by Fujita and Miyazawa [98]—describing two-pion exchange NNN processes with excitation of a Δ -resonance in the intermediate state—and a phenomenological repulsive potential; the resulting expression is

$$V_{ijk} = V_{ijk}^{2\pi} + V_{ijk}^R . \quad (5.1)$$

The strength of the two-pion exchange contribution is adjusted to reproduce the observed ground state energies of ${}^3\text{H}$ and ${}^4\text{He}$, obtained from accurate Monte Carlo calculations [97], whereas that of the isoscalar repulsive term is fixed to obtain the empirical saturation density of SNM—inferred from nuclear data—from variational calculations carried out using advanced many-body techniques [127].

It should be kept in mind that the repulsive term V_{ijk}^R implicitly takes into account relativistic corrections to the phenomenological two-nucleon potential v_{ij} , arising from the center of mass motion of the interacting pair.

The authors of Ref. [62] have modified the free-space AV18 potential to include the boost correction δv , whose effect is an enhancement of the repulsive contribution to the potential energy. As a consequence, using the boosted AV18 potential in calculations of nuclear matter energy entails the introduction of a modified NNN potential, referred to as UIX*, which turns out to be considerably softer than the UIX.

The impact of relativistic corrections to the nuclear Hamiltonian on the description of NS properties has been recently discussed in Ref. [48].

Because of the unconstrained nature of the NNN interaction at high density we have explored the possibility of inferring the strength of the repulsive term of the UIX* potential from data collected by multimessenger astrophysical observations, which carry information on nuclear dynamics at supranuclear density. Note that to pin down the dynamics of NNN interactions it is essential that the analysis be carried out using the the boost corrected NN potential.

Our study is based on the use of a set of Hamiltonians, obtained from the AV18 + δv + UIX* model performing the replacement

$$\langle V_{ijk}^R \rangle \rightarrow \alpha \langle V_{ijk}^R \rangle . \quad (5.2)$$

The energy-density of nuclear matter at arbitrary baryon density ρ and proton fraction x_p has been obtained generalizing the parametrization employed in Ref. [62] and reported in Eqs. (3.142) and (3.143). The explicit expressions of the functions appearing in those equations involve a set of parameters which were determined by fitting the energy per nucleon of SNM and pure neutron matter computed within the FHNC/SOC variational approach [132] using the AV18+ δv + UIX* Hamiltonian.

Implementing the substitution of Eq. (5.2) is equivalent to add a term $(\alpha - 1)V^R$ at first order in perturbation theory. The corresponding change of energy density turns out to be

$$g(\rho, x_p) \rightarrow g(\rho, x_p, \alpha) = g(\rho, x_p) + \delta g(\rho, x_p, \alpha), \quad (5.3)$$

with

$$\delta g(\rho, x_p, \alpha) = \delta g(\rho, 1/2, \alpha) [1 - (1 - 2x_p)^2] + \delta g(\rho, 0, \alpha)(1 - 2x_p)^2 . \quad (5.4)$$

The functions δg can be readily expressed in terms of expectation values of V^R in the nuclear matter ground state using

$$\delta g(\rho, 1/2, \alpha) = \frac{\rho}{A} (\alpha - 1) \langle V_{ijk}^R \rangle_{\text{SNM}} \quad (5.5)$$

$$\delta g(\rho, 0, \alpha) = \frac{\rho}{A} (\alpha - 1) \langle V_{ijk}^R \rangle_{\text{PNM}} . \quad (5.6)$$

Tabulated values of $\langle V_{ijk}^R \rangle$ as a function of density can be found in Ref. [62]. In our analysis, we have employed a polynomial fit including powers up to ρ^3

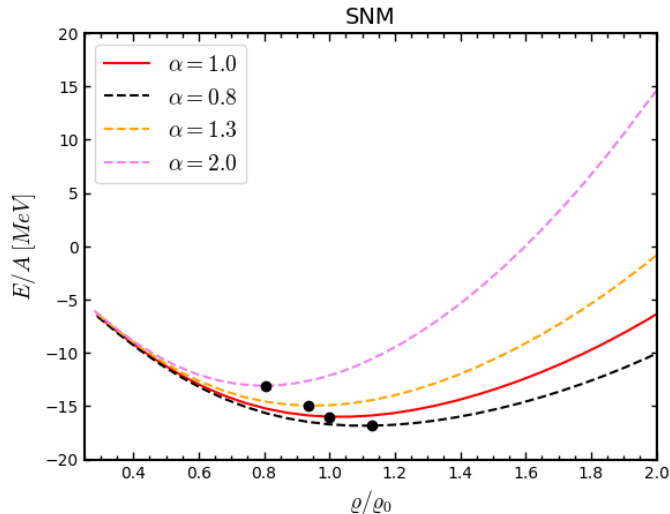
$$\langle V_{ijk}^R \rangle = a_0 + a_1 \rho + a_2 \rho^2 + a_3 \rho^3 , \quad (5.7)$$

which turned out to be very accurate. The values of the parameters a_i are reported in Table 5.1.

Using the analytic expression of the energy density of nuclear matter at arbitrary proton fraction, composition and energy density of β -stable matter can be easily determined, by minimizing with respect to x_p , with the additional constraints of conservation of baryon number and charge neutrality. Finally, the matter pressure P , derived from standard thermodynamic relations, is used to obtain the EOS $P(\epsilon)$.

Table 5.1. Values of the parameters appearing in Eq. (5.7), corresponding to $\langle V_{ijk}^R \rangle$ in MeV and ϱ in fm^{-3} .

	a_0 [MeV]	a_1 [MeV fm^3]	a_2 [MeV fm^6]	a_3 [MeV fm^9]
SNM	0.754	-16.769	214.164	77.422
PNM	0.949	-27.403	241.407	64.995

**Figure 5.1.** Density dependence of SNM for different values of the three-nucleon repulsion strength α . The minimum value of the curves, corresponding to the equilibrium density of isospin symmetric matter is marked by a filled black circle.

It has to be kept in mind that changing the strength of V_{ijk}^R affects the value of the nuclear saturation density predicted by the AV18 + δv + UIX* Hamiltonian. For this reason, we have limited the acceptable range of α to the interval $[0.7, 2.0]$. Within this range, the departure from the empirical value of ϱ_0 turns out to be $\sim 15\%$ at most, and the corresponding change of the energy per particle never exceeds 3%. The displacement of the equilibrium density of SNM for different values of α is shown in Fig. 5.1.

Moreover, because the contribution of the repulsive NNN potential becomes large at supranuclear densities, the modification of its strength α marginally affect the ground-state energy of atomic nuclei. Using the results reported in Ref. [99], obtained from accurate Quantum Monte Carlo calculations, we have found that changing α from 1 to 1.3 results in a change of 4% and 6% of the ground state energies of ${}^4\text{He}$ and ${}^{12}\text{C}$, respectively. These discrepancies appear to be fully acceptable in the context of our exploratory study. In Fig. 5.2 we can see the mass-radius diagram (a) and the Λ_1 - Λ_2 plane of a binary system for some significant values of α . These curves are plotted together with the posterior distributions of the Mass-Radius measurement of the NICER pulsar PSR J0030+0451 and of the GW170817 tidal deformabilities. Already at this stage we can see that there is strong sensitivity of NS observables with respect to small variations of α .

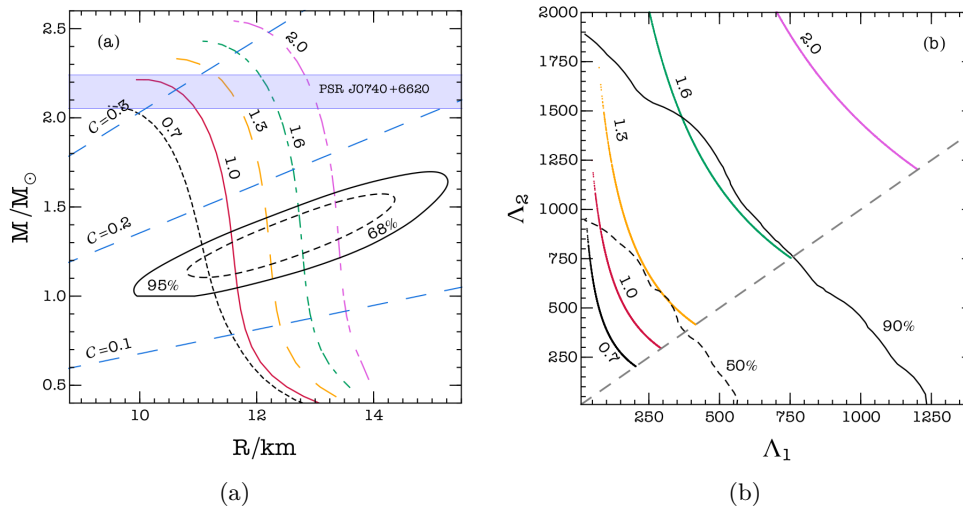


Figure 5.2. (a) Mass-radius relations of NS obtained using EOSs corresponding to the values of α specified on top of each curve. The shaded band identifies the most massive pulsar observed so far, PSR J0740+6620 [5]. The closed contours show to the 68% and 95% confidence intervals derived for the NICER pulsar [7]. The dashed straight lines correspond to constant compactness $C = M/R$. (b) NS models in the Λ_1 - Λ_2 plane for selected values of α , and corresponding to the masses measured for GW170817. The 50% and 90% confidence intervals derived using the GW170817 data [3] are also shown.

5.2 Methods and observations

We consider a family of EOSs for which the observables of a neutron star (mass, radius and tidal deformability) depend uniquely on the three-body coefficient α and on the central pressure p_c :

$$\{\alpha, p_c\} \rightarrow \{M, R, \lambda\}. \quad (5.8)$$

Figure 5.3 shows the stable stellar configurations in the mass-radius plane and the mass-tidal deformability plane. Given a set $O_{i=1,\dots,n}$ of observations, we infer $\{\alpha, p_c^{(1)} \dots p_c^{(m)}\}$ ¹ using a hierarchical Bayesian approach,

$$\mathcal{P}(\alpha, \vec{p}_c | \vec{O}) \propto \mathcal{P}_0(\alpha, \vec{p}_c) \prod_{i=1}^m \mathcal{L}(O_i | \theta_i) \quad (5.9)$$

where $\vec{p}_c = \{p_c^{(1)} \dots p_c^{(m)}\}$, $\mathcal{L}(O_i | \theta_i)$ is the likelihood of the i -th event (see Sec. 5.2.1 below) and θ_i denotes the set of relevant NS observables — mass and radius for pulsars, symmetric mass ratio and effective tidal deformability for GW observations — evaluated at $\{\alpha, p_c^{(i)}\}$ via (5.8). We assume that the priors on α and on each central pressure in Eq. (5.9) are uncorrelated.

The posteriors in Eq. (5.9) are sampled by means of Markov Chain Monte Carlo (MCMC) simulations employing the *emcee* algorithm with stretch move [133]. For

¹In general $m \neq n$: for binary coalescence events, we must sample over the pressures of both members of the binary.

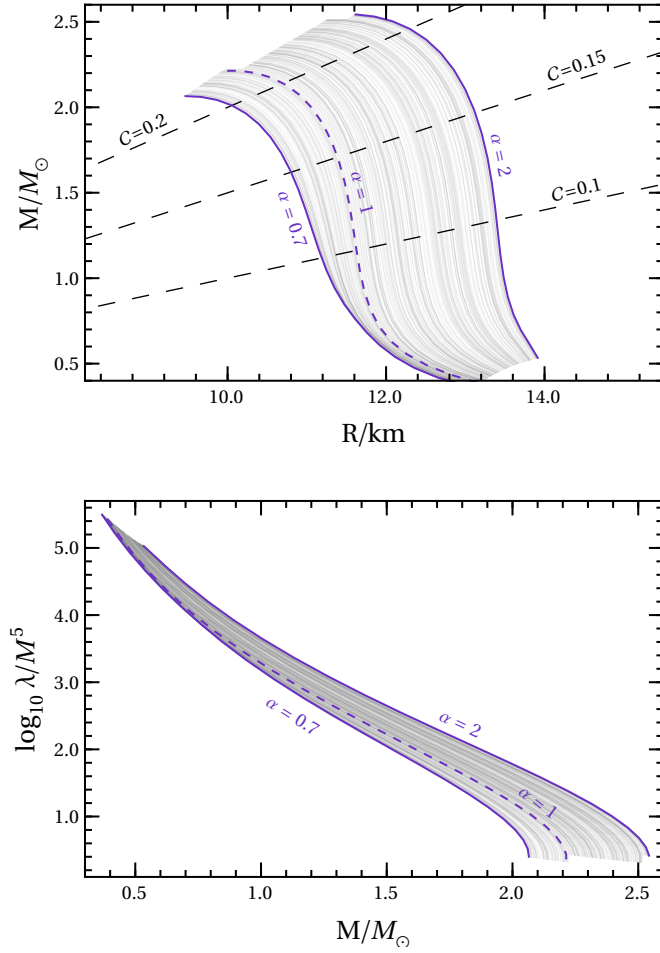


Figure 5.3. (Top) Representative ensemble of the mass-radius profiles for the family of EOS considered in this work. Each gray curve corresponds to a specific value of α drawn between the solid violet lines which refer to the lower and upper bounds of α assumed in the analysis, i.e. $\alpha = 0.7$ and $\alpha = 2$, respectively. The dashed curve identifies the baseline APR model with $\alpha = 1$. We also show lines of constant compactness $\mathcal{C} = M/R$. (Bottom) Same as top panel but for the dimensionless tidal deformability λ/M^5 as a function of the NS mass.

each observation we run 100 walkers of 10^6 samples with a thinning factor of 0.02. The final distribution for α is obtained by marginalizing over the central pressures \vec{p}_c . When presenting results, we quote the median alongside the bounds of the 90% symmetric posterior density intervals.

We sample the central pressures of each star uniformly in log-space between $\ln_{10} p_c^{\min}(\alpha) \simeq 34.58$, where p_c is expressed in dyne/cm^2 , and $\ln_{10} p_c^{\max}(\alpha)$, where p_c^{\max} corresponds to the central pressure of the heaviest stable configuration for each EOS specified by α . The lower value p_c^{\min} is chosen such that the nuclear model supports masses larger than $0.8M_\odot$. The values of α are drawn from a uniform distribution in the range $[0.7, 2]$. We also impose a causality constraint, requiring that the speed of sound $c_s = \sqrt{dp/d\epsilon}$ is subluminal at the center of each NS.

5.2.1 Astrophysical datasets

We considered three real datasets corresponding to (i) the binary coalescence GW170817, (ii) the millisecond pulsar PSR J0030+0451 and (iii) the heaviest NS observed so far PSR J0740+6620. We briefly summarize here the basic properties of each dataset and the corresponding likelihood functions that enter Eq. (5.9).

(i) — GW170817 is the first binary neutron star system observed by LIGO and Virgo. Under a low spin prior, the LVC analysis constrained the source component masses (m_1, m_2) between $\sim 1.16M_\odot$ and $\sim 1.6M_\odot$. GW170817 provided the first evidence that GW signals from coalescing systems are sensitive to matter effects induced by the NS structure, yielding a measurement for the effective tidal parameter

$$\tilde{\Lambda} = \frac{16}{13} \left[\frac{(m_1 + 12m_2)m_1^4\Lambda_1}{(m_1 + m_2)^5} + 1 \leftrightarrow 2 \right] \quad (5.10)$$

of $\tilde{\Lambda} = 300_{-230}^{+420}$ within 90% of the highest posterior density interval, with $\Lambda_{1,2} = \lambda_{1,2}/m_{1,2}^5$ being the NS individual, dimensionless, tidal deformabilities [4].

We construct the likelihood $\mathcal{L}(O_{\text{GW170817}}|\eta, \tilde{\Lambda})$ from the joint posterior $\mathcal{P}(\mathcal{M}, \eta, \tilde{\Lambda}|O_{\text{GW170817}})$ for $\tilde{\Lambda}$, the chirp mass $\mathcal{M} = (m_1 m_2)^{3/5}/(m_1 + m_2)^{1/5}$, and the symmetric mass ratio $\eta = m_1 m_2 / (m_1 + m_2)^2$. The calculation can be simplified by the fact that the chirp mass in the source frame is measured with $\sim 0.1\%$ precision, which allows to fix it to its median value $\mathcal{M}_\star = 1.186 M_\odot$ and restrict to the conditional probability $\mathcal{P}(\eta, \tilde{\Lambda}|\mathcal{M}_\star, O_{\text{GW170817}})$. Moreover, as shown in [35], the latter can be replaced by the marginalized posterior $\mathcal{P}(\eta, \tilde{\Lambda}|O_{\text{GW170817}})$ to very good accuracy. This choice reduces the number of parameters to be sampled, since the central pressure $p_c^{(2)}$ of the secondary component is uniquely determined by $\{\mathcal{M}_\star, p_c^{(1)}\}$ and α^2 , and similarly for the individual masses $m_{1,2}$ and tidal deformabilities $\Lambda_{1,2}$. The likelihood function is then obtained by re-weighting the posterior by the joint prior on η and $\tilde{\Lambda}$ as derived from [4],

$$\mathcal{L}(O_{\text{GW170817}}|\eta, \tilde{\Lambda}) = \frac{\mathcal{P}(\eta, \tilde{\Lambda}|O_{\text{GW170817}})}{\mathcal{P}_0(\eta, \tilde{\Lambda})}. \quad (5.11)$$

²More specifically, we compute m_2 from $m_1(\alpha, p_c^{(1)})$ and \mathcal{M}_\star and then we solve $m_2 \equiv m_2(\alpha, p_c^{(2)})$ for $p_c^{(2)}$.

Note that, although $p_c^{(2)}$ is not independently sampled, we still require it to lie within its prior support.

(ii) — For the millisecond pulsar PSR J0030+0451 we use the joint mass-radius posterior $\mathcal{P}(M, R|O_{J0030})$ inferred by the NICER collaboration, which has carried out two independent studies of the stellar spectroscopic observations, obtaining consistent results. The mass-radius constraints provided by the two collaborations led to $M = 1.34_{-0.16}^{+0.15}M_\odot$ and $R = 12.71_{-1.19}^{+1.14}\text{km}$ [7], and $M = 1.44_{-0.14}^{+0.15}M_\odot$ and $R = 13.02_{-1.06}^{+1.24}\text{km}$ [8] respectively (68% credibility). Here we use the data publicly available in [134], for which the likelihood can be derived straightforwardly from $\mathcal{P}(M, R|O_{J0030})$ because the joint prior on $\{M, R\}$ is flat,

$$\mathcal{L}(O_{J0030}|M, R) \propto \mathcal{P}(M, R|O_{J0030}). \quad (5.12)$$

(iii) — PSR J0740+6620 [9, 10] is the most massive pulsar discovered so far. Previous observations of this source constrained its mass to $M = 2.08_{-0.069}^{+0.072}M_\odot$ (68.3% credibility) [6]. This measurement, combined with data obtained from the XMM Newton European Photon Imaging Camera to improve the NICER background, was used in [9, 135] and [10, 136] to infer the pulsar radius, with the two teams obtaining $R = 12.39_{-0.98}^{+1.30}\text{km}$ and $R = 13.7_{-1.50}^{+2.62}\text{km}$ [10] respectively (68% credibility). Here we use the data in [137], for which the likelihood can be immediately inferred from the posterior due to uniform priors,

$$\mathcal{L}(O_{J0740}|M, R) \propto \mathcal{P}(M, R|O_{J0740}). \quad (5.13)$$

5.2.2 Simulations for 2G and 3G detectors

We simulated³ 30 binary neutron star events for two choices of the parameter α , $\alpha = 1$ and $\alpha = 1.3$, either for a network (HLV) composed by the LIGO Hanford, LIGO Livingston, and Virgo detectors at design sensitivity [139], or for the future third-generation interferometer Einstein Telescope in its ET-D configuration [130]. The distribution of the source masses, luminosity distances and effective tidal parameters are shown in Fig. 5.4. We injected 64-second long waveforms into a zero-noise configuration as described in [140], with sky location and inclination uniformly distributed over the sky. Posterior parameters are recovered using the `bilby` software [141, 142] for GW injections and parameter estimation. For both injection and recovery, we modeled binary neutron star signals with the `IMRPhenomPv2_NRTidal` waveform template [143, 144]. Injected binaries are nonspinning, while component spins are recovered imposing a low-spin prior $\chi_{1,2} \in [-0.05, 0.05]$ and assuming that spins are (anti-) aligned.

We assume that tidal parameters are recovered uniformly w.r.t. $\tilde{\Lambda}$ and the tidal parameter $\delta\Lambda$ which contributes at higher post-Newtonian order in the waveform phase expansion [145], with the additional constraint that the individual deformabilities $\Lambda_{1,2}$ of the binary components lie between 0 and 5000.

³We limit our catalog to 30 events because the recovery of the EOS is expected to be biased by a mismodeling of the BNS population distribution if the number of sources exceeds ~ 30 [138].

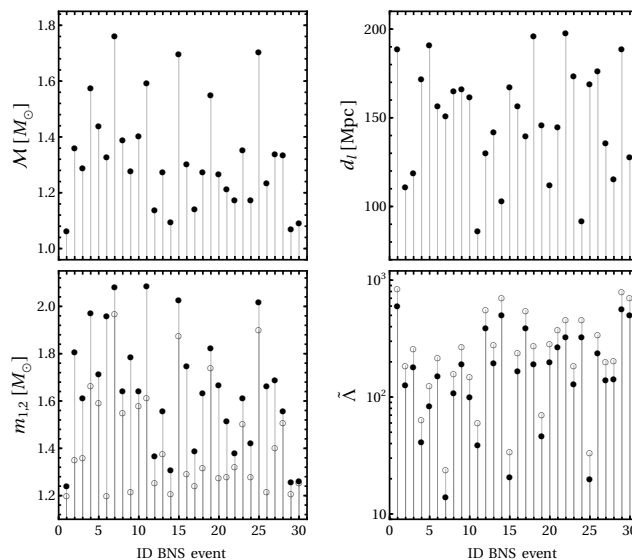


Figure 5.4. Component masses, luminosity distance, chirp mass, and tidal parameter for the catalogue of NS binaries simulated for HLV and ET observations. Full and empty dots in the left bottom panel correspond to values of m_1 and m_2 , with $m_1 \geq m_2$. Full and empty markers in the bottom right plot identify the tidal parameter for the two values of α we considered, $\alpha = 1$ and $\alpha = 1.3$, respectively.

5.3 Results

We start the discussion of our results by focusing first on the the Bayesian analysis applied to the three real observations described in the previous section.

The inferred probability distributions for α are summarized by the density plots in the left column of Fig. 5.5, together with their median values and 90% confidence intervals.

Interestingly the posterior densities of Fig. 5.5 show very similar results for the two EM observations, with a nearly identical median around $\alpha \simeq 1.4$. The probability distribution for J0740+6620 peaks around a slightly larger value compared to the lighter pulsar, J0030+0451, since larger values of α tend to support more massive configurations. Moreover, even if $\mathcal{P}(\alpha)$ shows support for the baseline model $\alpha = 1$, which lies within the 90% CL of the distributions, EM observations seem to consistently favor larger values of the three-body repulsion. Moreover we can observe that the distribution of α inferred by GW data alone is unconstrained, with the posterior rallying against the lower prior at $\alpha = 0.7$, while the multi-messenger analysis is dominated by the pulsar measurements, and in particular by J0740+6620, showing large support for $\alpha > 1$.

Constraints on α , i.e on the underlying microscopic Hamiltonian, can be translated into bounds on the stellar macroscopic observables. The right column of Fig. 5.5 shows, for example, the maximum mass density distributions predicted by the values of α inferred for each dataset. All the observations lead to median values of $M_{\max} \gtrsim 2.2M_{\odot}$, with the multi-messenger analysis yielding a probability distribution with large support for $M_{\max} \sim 2.5M_{\odot}$.

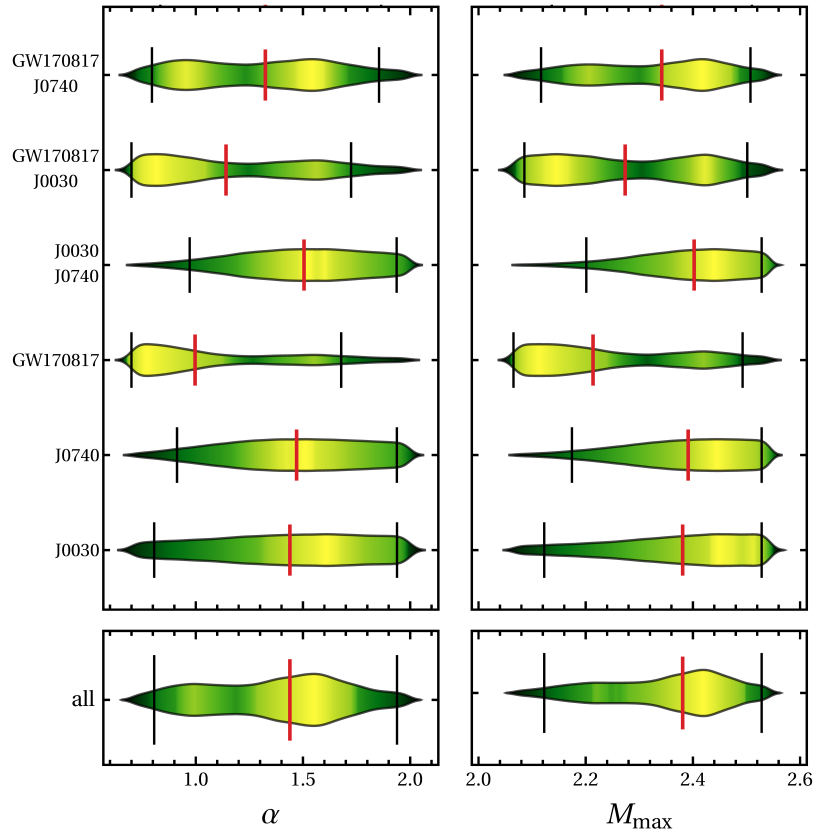


Figure 5.5. (Left Row) Posterior probability densities for α inferred from different astrophysical datasets. (Right row) Posterior densities for the maximum mass allowed by the EOS corresponding to the inferred distribution of α . Bottom panels provide results with all datasets stacked together. Vertical red and black lines identify the median and the the 90% posterior density intervals of each distribution, respectively.

In Fig. 5.6 we also show the M - R density distribution corresponding to the 90% CL of α for the multi-messenger case. Light (dark) colors identify stellar profiles with high (low) probability. Pulsar observations drive the profiles far from the $\alpha = 1$ baseline, i.e. towards stiffer NS configurations, with an expected radius $R \gtrsim 12$ km for a prototype NS with $M = 1.4M_\odot$.

So far our analysis shows that, although the constraining power of current measurements is still limited, astrophysical data are already sensitive to nucleon dynamics. We will therefore explore the insights that can be inferred on three-nucleon forces exploiting future GW observations of binary systems.

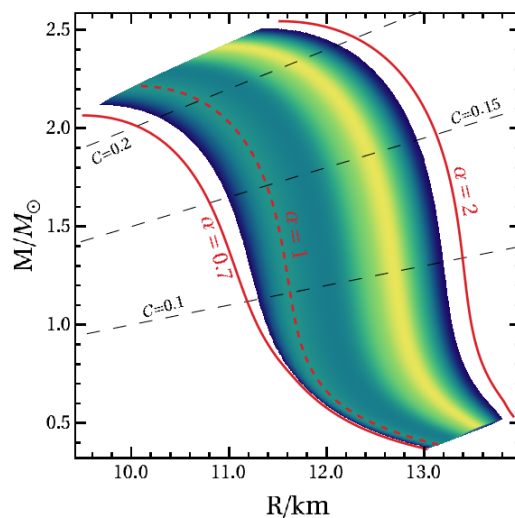


Figure 5.6. Mass-radius profile density corresponding to the 90% confidence interval of α inferred for the GW-EM multi-messenger analysis. Dark (light) regions correspond to stellar profiles with small (large) probability. As for Fig. 5.3 red curves identify configurations with specific values of the three-body strength, while dashed black lines correspond to configurations with constant compactness.

As discussed in Sec. 5.2.2 we have simulated two catalogs of 30 binary NS mergers, observed either by 2G network or by ET, assuming two different values of the three-nucleon repulsion. Source parameters, i.e. masses and tidal deformabilities, are first recovered with Bilby, and then analyzed by our Bayesian pipeline which samples the posterior distribution of α .

Figure 5.7 shows the posterior densities $\mathcal{P}(\alpha)$ of each event, for injected NSs with $\alpha = 1$, detected by the HLV network. The ability of 2G detectors to discriminate the actual value of the three-body repulsion substantially depends on both the SNR and on the component masses of the binary. We find that observations with SNR smaller than ~ 25 lead α to be almost unconstrained, with the true value always lying outside the 90% confidence interval of the distribution. However, even for strong signals, accurate measurements only occur for low-mass systems with a chirp mass $\mathcal{M} \lesssim 1.4M_\odot$. This is particular evident for the event with the largest SNR (~ 35) in our set. Such binary features two heavy NSs with a chirp mass $\mathcal{M} \simeq 1.6M_\odot$, and provides loose bounds on α . Moreover, Fig. 5.7 shows that, with the exception

of four events with $\text{SNR} > 30$ and $\mathcal{M} < 1.4M_{\odot}$, the remaining posteriors always prefer large values of α , at the edge of the upper prior boundary. This particular behavior reflects a systematic bias we find in the posteriors of $\tilde{\Lambda}$ inferred by GW observations for binaries with heavy components, which tend to favor large values of the tidal parameter. Its effect on the marginal distribution of α becomes even more pronounced in the high mass scenario where the tidal deformability becomes less sensitive to variations of α . We believe such bias may be induced by our choice of priors on the tidal parameters, which has strong support against the BBH hypothesis $\tilde{\Lambda} = 0$, and reflects the physical assumption that compact objects with $m_{1,2} \lesssim 3M_{\odot}$ are neutron stars. Moreover, the stack of multiple GW signals only partially alleviate the bias in favor of large three-body strength. We have indeed combined different observations with SNR larger than 20, finding a mild improvement of the posterior support towards the true value of α . In particular we can see in Fig. 5.8 how the combination of the six HLV best events, panel (b), slightly improves the results with respect to the single observation, panel (a). Indeed the injected value of $\alpha = 1.3$ is excluded at 90% CL from the posterior associated with the $\alpha = 1$ set of events, and vice versa.

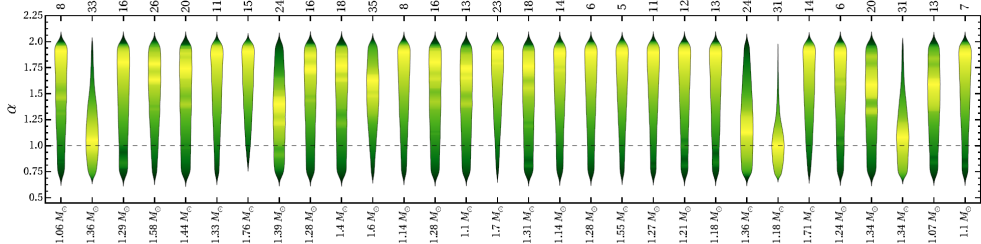


Figure 5.7. Posterior densities $\mathcal{P}(\alpha)$ inferred from simulated GW data, assuming $\alpha = 1$ (dashed horizontal line). Yellow (green) colors identify region with high (low) probability. Signals are observed by a network HLV of three advanced detectors, with a combined SNR given in the top axis of the plot. Labels in the bottom axis provide the values of the binary chirp masses.

This picture changes dramatically when signals are observed by the Einstein Telescope. Figure 5.9 shows indeed the distributions of the three-nucleon repulsion strength inferred by the 3G detector, for both families of events simulated with $\alpha = 1$ and $\alpha = 1.3$. The exquisite sensitivity of ET allows to gauge away the bias arising from the 2G network. All the posteriors peak around the injected values of α , showing no support on the prior boundaries. In the best (worse) case scenario we find that α can be constrained with $\sim 2\%$ ($\sim 30\%$) of accuracy at 68% confidence level. Such accuracy allows to disentangle the two values of α we considered. Even in the most pessimistic cases, where the inferred $\mathcal{P}(\alpha)$ are not narrow enough to identify a specific value of α , stacking of few events would render the distributions clearly distinguishable. Figure 5.10 shows the posteriors obtained by combining six events of our catalog⁴ leading to loose constraints on α . The final posteriors for $\alpha = 1$ and $\alpha = 1.3$ are clearly separated, with a negligible overlap on the tails.

⁴We choose the events number 7,15,16,18,19 and 25 of Fig. 5.9.

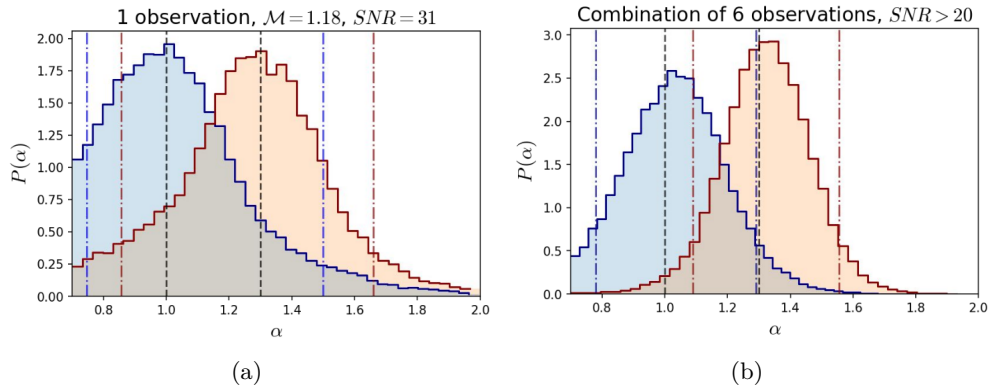


Figure 5.8. Marginal posterior distribution of α for a single HLV event (a) and for the combination of the best six events having $SNR > 20$ (b). Blue posteriors are referred to the dataset generated by injecting $\alpha = 1.0$, whereas the red ones correspond to the case $\alpha = 1.3$. The vertical dashed lines identify the injected values of α .

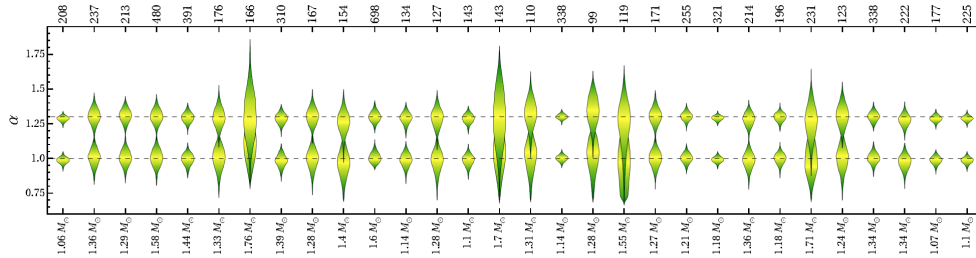


Figure 5.9. Same as Fig. 5.7 but assuming that binary NS are observed by the Einstein Telescope. We show results for signals simulated with both $\alpha = 1$ and $\alpha = 1.3$. Injected values of α are identified by the horizontal dashed lines.

Such accuracy translates into very narrow constraints on the mass-radius (or equivalently mass-tidal deformability) diagram. As an example, we show in Fig. 5.11 the $M-R$ profile density computed from the values of α inferred from event number 17 of our dataset. A direct comparison with Fig. 5.6, where a similar plot was made for data from current facilities, provides a clear hint on the possibility to use ET as a new laboratory to study the dynamics of nucleon interactions in the stellar cores.

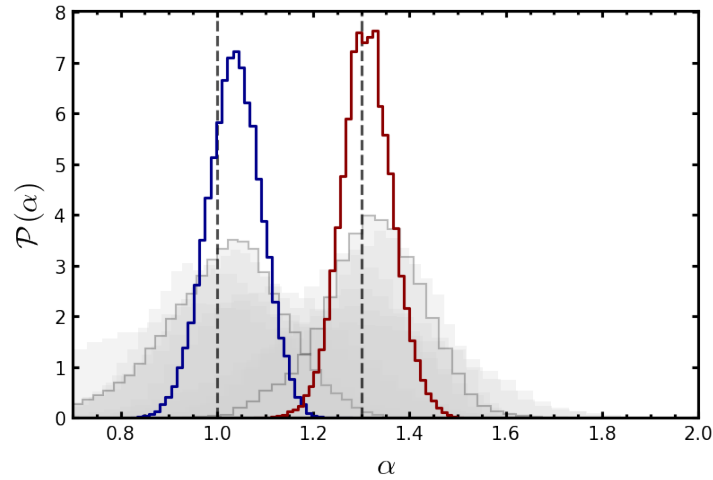


Figure 5.10. Probability distribution $\mathcal{P}(\alpha)$ obtained by stacking six events of our dataset as measured by the Einstein Telescope. Empty histograms refer to the full stacked posteriors for signals injected with $\alpha = 1$ (blue) and $\alpha = 1.3$ (red). Empty shaded histograms on the background correspond to the individual posteriors. The vertical dashed lines identify the injected values of α .

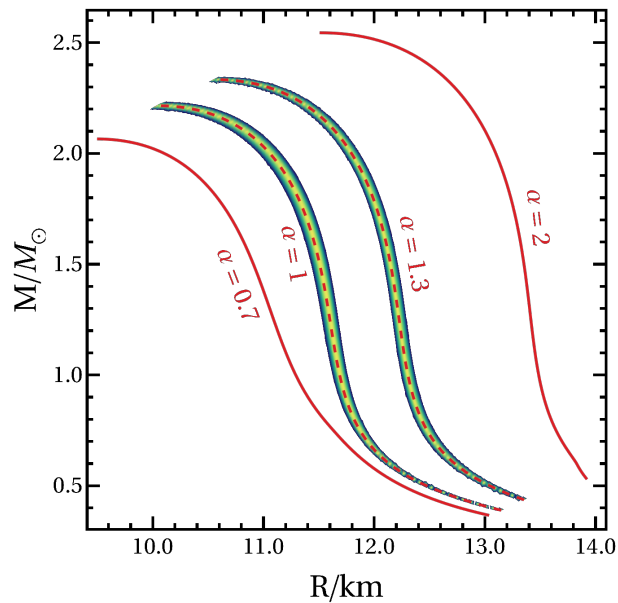


Figure 5.11. Same as Fig. 5.6 but for simulated events observed by the Einstein Telescope. The values of α used to build the mass-radius profiles correspond to event number 17 of our catalogue. We show results for both $\alpha = 1$ and $\alpha = 1.3$. Solid and dashed red curves identify the profiles corresponding to prior boundaries and to the injected values of α , respectively.

Chapter 6

Summary and Outlook

In this Thesis we have explored the effect of including relativistic boost corrections within the derivation of a nuclear effective potential—carried out from a phenomenological Hamiltonian using the formalism of CBF and cluster expansion techniques—describing the interactions between nucleons in the nuclear medium. We have explored two complementary possibilities. Boost corrections can be implemented either as a perturbation in the effective potential, without changing the nuclear correlation functions, or directly in its functional form, before carrying out the determination of the correlation parameters. In the first case boosts are mainly responsible for introducing a correction to the computed ground state energies, whereas with the second method they mainly affect the radial dependence of the effective interaction. We have analyzed two different models. The first one, obtained from a simplified Hamiltonian involving only a kinetic term and a NN interaction potential. Such a potential is suitably modified with an additional density dependent term in order to account for NNN repulsion, according to the procedure developed in Ref. [96]. The main advantage of this Hamiltonian is to provide a very simple and efficient framework allowing for fast computations. Anyway the oversimplified treatment of NNN forces result in a not fully realistic dynamics, and even if such a model is useful in order to understand some physical properties behind the formalism, it should not be trusted to perform accurate calculations of nuclear matter properties. Therefore, a more realistic interaction was studied, starting from an Hamiltonian explicitly including a microscopic NNN potential. It is relevant that the introduction of boost corrections appears to have very similar effects in both scenarios. The NN potential employed in the derivation of our effective interaction is chosen to be the AV6P in both the models analyzed. The NNN potential, when present, is chosen as the UIX model. The correlation functions appearing in the effective interaction are optimized in such a way as to reproduce the variational energies computed by Akmal Pandharipande and Revenhal in Ref. [62]. The use of the AV6P NN potential instead of the AV18 employed in the APR work is justified by the recent results of Ref. [66], showing that the AV6P+UIX and AV18+UIX Hamiltonians yield very similar results in calculations of nuclear matter energies.

Our results show that the perturbative correction introduced by boost interactions alone is quite small, and likely to be negligible in the context of neutron star physics, where the uncertainty on astrophysical observables is still significant. However it

should be kept in mind that the introduction of such relativistic corrections must be complemented with a softening of the isoscalar NNN repulsion. Because of the different density dependence, even if responsible for comparable effects at typical nuclear densities, a modification of the NNN force turns out to strongly affect the high density behavior of the nuclear matter equation of state. In this sense, within the phenomenological approach, the availability of empirical information able to constrain nuclear dynamics in high density matter will be of fundamental importance. This subject is discussed in Chapter 5 where we have presented the results of a pioneering study aimed at inferring information on the NNN repulsion from multimessenger NS observations.

We have investigated the sensitivity of NS observations to the strength of repulsive NNN forces, which are known to be critical in determining the stiffness of the nuclear matter EOS at supranuclear densities. Our analysis is based on the AV18 + δv + UIX* nuclear Hamiltonian and involves a single free parameter, to be constrained by data, determining the coupling constant appearing in the repulsive contribution to the UIX* potential.

We have performed bayesian inference employing the currently available multimessenger datasets in order to constrain this parameter. We have then repeated the analysis with a set of simulated GW observations that could be performed by both current (LIGO/Virgo) and future (Einstein Telescope) interferometers at design sensitivity. This analysis has the main purpose to explore the potential of next generation facilities into inferring crucial information about the microscopic dynamics of nuclear matter.

Our results suggest that even if current facilities show a clear sensitivity to small variations of the NNN repulsive potential, they are not accurate enough to capture significant insights. This picture is cross-validated by the population analysis performed with mocked LIGO/Virgo data, with binaries generated with two different values of the NNN repulsion strength, $\alpha = 1$ and $\alpha = 1.3$. Only few, low-mass and high signal-to-noise ratio events provide a meaningful constraint on α , with posterior distributions correctly peaked around the injected values. Moreover, even for the most constraining event, the inferred posteriors do not allow a clear disentanglement between the two values of α we considered. The picture improves only slightly with the stacking of multiple observations.

These results exhibit a striking upgrade when we assume that the the population of binaries is observed by the Einstein Telescope. In most of the cases, the large SNRs obtained by such events in combination with the 3G detector allow the posteriors for the injected values of α to be clearly separated, and only a single observation is needed to resolve them.

Moreover, in the few cases where posteriors overlap, stacking of $\sim 2 - 3$ observations would allow to unambiguously distinguish between $\alpha = 1$ and $\alpha = 1.3$.

This analysis has confirmed once again that the upcoming future of multimessenger astronomy will bring fundamental insights on the behavior of nuclear matter, having the potential to shed a completely new light on our knowledge of nuclear dynamics.

It is important to remark that all the results derived within this Thesis are obtained in the framework of non-relativistic NMBT. Such a framework, besides being extremely consistent and with a remarkable predictive power has obviously

some limitations. The most important one is linked to the non-relativistic nature of the formalism. Indeed, having its roots in non-relativistic quantum mechanics, issues related with causality violations are expected to occur when the density increases too much. In particular the APR models predict a superluminal value of the speed of sound in the innermost region of NSs with masses larger than $\sim 2.1 M_{\odot}$. Moreover at very high density also the appearance of degrees of freedom other than nucleons, which are not present in the nuclear Hamiltonian, should be considered. Finally the role of four- and many-body forces at high density is still unclear. In fact, even if it is true that their contribution is negligible at typical nuclear densities, indeed they turn out to be unnecessary in order to correctly describe the properties of nuclei with a large number of constituents, their relevance can increase with density in a similar way to what happens with the three-body forces. However, this formalism appears to be perfectly suited to describe NSs in the mass range observed so far.

Regarding the effective interaction, in spite of being only an exploratory analysis, our work highlighted the importance of developing a consistent treatment of boost corrections and NNN forces.

Future perspectives of our study spans several possibilities. First of all it could be useful to perform new calculations of the properties of ${}^3\text{H}$, ${}^3\text{He}$ and ${}^4\text{He}$ including boost corrections with a set of different Hamiltonians. Indeed, the approach presented within this Thesis is completely general and can be extended to any nuclear Hamiltonian. In particular calculations performed within the χEFT framework would be of great importance in order to further understand the relation between boosts and NNN interactions. Once that the interplay between boosts and NNN interaction is understood at nuclear density, accurate state-of-the-art *ab initio* many-body calculations, involving both boost corrections and the corresponding NNN potential, will be necessary. We recall that relativistic corrections are accounted in the APR calculations only at first order in perturbation theory, but to which extent their outcome at high density is actually a perturbation may be questionable. Such many-body calculations will also serve as new target values in order to carry out a fully consistent effective interaction accounting also for relativistic effects. Indeed our results were derived by optimizing the effective interaction over the only existing variational calculations including both the effects of boosts, and the consequent modification of NNN repulsion. Since the effective interaction formalism provides a very powerful and consistent framework to study properties of nuclear matter well beyond the ground state ones, the development of a further refined model, with respect to the one derived in this work, will be a prominent breakthrough. However the effective interaction discussed within this Thesis can already be used to perform some exploratory calculations and a work where it is used to compute finite temperature properties is currently in progress.

Last but not least, formal improvements in our procedure are also possible. Our effective interaction is developed by including boost corrections only at the two-body level. Although higher order contributions have been estimated to be small, fully quantitative assessment of their role—which does not involve any additional conceptual difficulty—will certainly be needed.

Appendix

Appendix A

Derivation of One-Pion Exchange Potential

Let us consider the invariant amplitude written in Chapter 2 regarding the OPE contribution to NN scattering reported in Fig. 2.2

$$i\mathcal{M} = -g^2 \bar{u}(p_{2'}, s_{2'}) \gamma^5 u(p_2, s_2) \frac{1}{k^2 - m_\pi^2} \bar{u}(p_{1'}, s_{1'}) \gamma^5 u(p_1, s_1) \langle \tau_1^a \rangle \langle \tau_2^a \rangle. \quad (\text{A.1})$$

We remind that we are considering the states $|i\rangle = |p_1, s_1; p_2, s_2\rangle$ and $|f\rangle = |p_{1'}, s_{1'}; p_{2'}, s_{2'}\rangle$ to be respectively the initial and final states. The S-matrix element $\langle f|S|i\rangle = S_{fi}$ is given by

$$S_{fi} = \sqrt{\frac{m}{E_1}} \sqrt{\frac{m}{E_2}} \sqrt{\frac{m}{E_{1'}}} \sqrt{\frac{m}{E_{2'}}} (2\pi)^4 \delta^{(4)}(p_{2'} + p_{1'} - p_2 - p_1) [\mathcal{M} - \mathcal{M}'], \quad (\text{A.2})$$

where \mathcal{M}' is the invariant amplitude associated with the diagram in which the index 1' is replaced by 2' and vice versa. It has the same shape as \mathcal{M} , with the substitution of the indices mentioned above and with $k = p_{1'} - p_2$ instead of $k = p_{2'} - p_2$. The minus sign between the two invariant amplitudes comes from the Fermi exclusion principle. In this section we will consider only the contribution coming from \mathcal{M} to the S-matrix element, because it is sufficient to derive the expression of the one-pion-exchange potential. Therefore when we talk about the S-matrix element, we will consider (A.2) without the contribution arising from \mathcal{M}' . From now on we label the generic spinor $u(p_i, s_i)$ with u_i .

The matrix γ^5 is defined as $\gamma^5 = i\gamma^0\gamma^1\gamma^2\gamma^3$, where the gammas are 4×4 matrices defined as

$$\gamma^0 = \begin{pmatrix} 1 & 0 \\ 0 & -1 \end{pmatrix}, \quad \gamma^i = \begin{pmatrix} 0 & \sigma^i \\ -\sigma^i & 0 \end{pmatrix}, \quad (\text{A.3})$$

with σ^i being the Pauli matrices. The spinors are normalized such that $\bar{u}u = 1$, i.e. we have

$$u_i = \sqrt{\frac{E_i + m}{2m}} \begin{pmatrix} \chi_i \\ \frac{\boldsymbol{\sigma} \cdot \mathbf{p}_i}{E_i + m} \chi_i \end{pmatrix}. \quad (\text{A.4})$$

Therefore, in the non-relativistic limit where we can take $E_i \approx E_{i'} \approx m$, we have

$$\begin{aligned} \bar{u}_{2'} \gamma^5 u_2 &= \frac{(E_2 + m)^{1/2} (E_2' + m)^{1/2}}{2m} \left(\chi_{2'}^\dagger \frac{\boldsymbol{\sigma} \cdot \mathbf{p}_2}{E_2 + m} \chi_2 - \chi_{2'}^\dagger \frac{\boldsymbol{\sigma} \cdot \mathbf{p}_2'}{E_2' + m} \chi_2 \right) \\ &\approx \chi_{2'}^\dagger \frac{\boldsymbol{\sigma} \cdot (\mathbf{p}_2 - \mathbf{p}_2')}{2m} \chi_2 = -\chi_{2'}^\dagger \frac{\boldsymbol{\sigma} \cdot \mathbf{k}}{2m} \chi_2 \end{aligned} \quad (\text{A.5})$$

and similarly for $\bar{u}_1 \gamma^5 u_1$. Therefore in the non-relativistic limit we can approximate $k^2 = (E_{i'} - E_i)^2 - |\mathbf{k}|^2 \approx -|\mathbf{k}|^2$. The meson propagator in this case becomes

$$\frac{i}{k^2 - m_\pi^2} \approx -\frac{i}{|\mathbf{k}|^2 + m_\pi^2}. \quad (\text{A.6})$$

Substituting all these results into the expression of the S-matrix element (A.2) we find

$$\begin{aligned} S_{fi} &\approx -i \frac{g^2}{4m^2} (2\pi)^4 \delta^{(4)}(p_{1'} + p_{2'} - p_1 - p_2) \cdot \\ &\quad \cdot \langle \tau_1^a \tau_2^a \rangle \chi_{1'}^\dagger \chi_{2'}^\dagger \frac{-(\boldsymbol{\sigma}_1 \cdot \mathbf{k})(\boldsymbol{\sigma}_2 \cdot \mathbf{k})}{|\mathbf{k}|^2 + m_\pi^2} \chi_2 \chi_1. \end{aligned} \quad (\text{A.7})$$

We are interested into finding a non-relativistic nucleon-nucleon potential that depends on the relative distance between the two nucleons $v^\pi(\mathbf{r})$ with $\mathbf{r} = \mathbf{r}_2 - \mathbf{r}_1$. This potential is translationally invariant, thus its Fourier transform depends only on the relative momentum \mathbf{k} .

We can define the interaction potential through the relation

$$S_{fi} = -i(2\pi)^4 \delta^{(4)}(p_{1'} + p_{2'} - p_1 - p_2) \langle v^\pi(\mathbf{k}) \rangle, \quad (\text{A.8})$$

where the bracket indicates that the potential $v^\pi(\mathbf{k})$ is evaluated between the spinors and the isospin spinors of the initial and final states. Putting together Eqs. (A.7) and (A.8) we have

$$\begin{aligned} v^\pi(\mathbf{k}) &= -\frac{g^2}{4m^2} \frac{(\boldsymbol{\sigma}_1 \cdot \mathbf{k})(\boldsymbol{\sigma}_2 \cdot \mathbf{k})}{\mathbf{k}^2 + m_\pi^2} \tau_1^a \tau_2^a \\ &= -\left(\frac{f_\pi}{m_\pi}\right)^2 \frac{(\boldsymbol{\sigma}_1 \cdot \mathbf{k})(\boldsymbol{\sigma}_2 \cdot \mathbf{k})}{\mathbf{k}^2 + m_\pi^2} \tau_1^a \tau_2^a \end{aligned} \quad (\text{A.9})$$

with $g^2/4\pi = 14$ and

$$f_\pi^2 = g^2 \frac{m_\pi^2}{4m^2} \approx 4\pi \cdot 14 \frac{(140)^2}{4 \cdot (939)^2} \approx 4\pi \cdot 0.08 \approx 1. \quad (\text{A.10})$$

The expression of the potential in the configuration space can be found through

$$\begin{aligned} v^\pi(\mathbf{r}) &= -\frac{f_\pi^2}{m_\pi^2} \int \frac{d^3k}{(2\pi)^3} \tau_1^a \tau_2^a (\boldsymbol{\sigma}_1 \cdot \mathbf{k})(\boldsymbol{\sigma}_2 \cdot \mathbf{k}) \frac{1}{\mathbf{k}^2 + m_\pi^2} e^{-i\mathbf{k} \cdot \mathbf{x}} \\ &= \frac{f_\pi^2}{m_\pi^2} \tau_1^a \tau_2^a (\boldsymbol{\sigma}_1 \cdot \nabla)(\boldsymbol{\sigma}_2 \cdot \nabla) \int \frac{d^3k}{(2\pi)^3} \frac{1}{\mathbf{k}^2 + m_\pi^2} e^{-i\mathbf{k} \cdot \mathbf{x}} \\ &= \frac{f_\pi^2}{m_\pi^2} (\tau_1^a \tau_2^a) (\boldsymbol{\sigma}_1 \cdot \nabla) (\boldsymbol{\sigma}_2 \cdot \nabla) \frac{e^{-m_\pi r}}{r}. \end{aligned} \quad (\text{A.11})$$

We remark the fact that the Yukawa function

$$y_\pi(r) = \frac{e^{-m_\pi r}}{r} = \int \frac{d^3k}{(2\pi)^3} \frac{1}{\mathbf{k}^2 + m_\pi^2} e^{-i\mathbf{k}\cdot\mathbf{x}}, \quad (\text{A.12})$$

satisfies the equation

$$(-\nabla^2 + m_\pi^2) y_\pi(r) = 4\pi\delta(\mathbf{r}), \quad (\text{A.13})$$

that tells us that the laplacian of the Yukawa function involves a δ -function singularity at the origin. The gradients in Eq. (A.11) must be evaluated taking this singularity into account. We are dealing with an object of the form

$$(\sigma_1^i \partial_i) (\sigma_2^j \partial_j) y_\pi(r) = \sigma_1^i \sigma_2^j [\partial_i \partial_j y_\pi(r)]. \quad (\text{A.14})$$

We said that the laplacian of the Yukawa function involves a δ -function singularity, therefore we will have troubles with the trace of the operator $\partial_i \partial_j$. We can therefore split this operator in two pieces, isolating the contribution of the trace, through

$$\partial_i \partial_j = \left(\partial_i \partial_j - \frac{1}{3} \delta_{ij} \partial_k \partial_k \right) + \frac{1}{3} \delta_{ij} \partial_k \partial_k, \quad (\text{A.15})$$

where the first term is clearly traceless. When we apply the first term on the right hand side of the above equation to the Yukawa function, the δ -function will not appear. We can therefore make usual derivatives, together with the substitution $\nabla^2 y_\pi = m_\pi^2 y_\pi$. We obtain

$$\begin{aligned} (\boldsymbol{\sigma}_1 \cdot \nabla) (\boldsymbol{\sigma}_2 \cdot \nabla) y_\pi(r) &= \\ &= \left(\boldsymbol{\sigma}_1 \cdot \nabla \boldsymbol{\sigma}_2 \cdot \nabla - \frac{1}{3} \boldsymbol{\sigma}_1 \cdot \boldsymbol{\sigma}_2 \nabla^2 \right) y_\pi(r) + \frac{1}{3} \boldsymbol{\sigma}_1 \cdot \boldsymbol{\sigma}_2 \nabla^2 y_\pi(r). \end{aligned} \quad (\text{A.16})$$

The first term on the right and side of the above equation gives rise to

$$\begin{aligned} \left(\boldsymbol{\sigma}_1 \cdot \nabla \boldsymbol{\sigma}_2 \cdot \nabla - \frac{1}{3} \boldsymbol{\sigma}_1 \cdot \boldsymbol{\sigma}_2 \nabla^2 \right) y_\pi(r) &= \\ &= \left(\boldsymbol{\sigma}_1 \cdot \hat{r} \boldsymbol{\sigma}_2 \cdot \hat{r} - \frac{1}{3} \boldsymbol{\sigma}_1 \cdot \boldsymbol{\sigma}_2 \right) \left(m_\pi^2 + \frac{3m_\pi}{r} + \frac{3}{r^2} \right) y_\pi(r), \end{aligned} \quad (\text{A.17})$$

where $\hat{r} = \mathbf{r}/r$. The second term on the right hand side of (A.16) satisfies

$$\frac{1}{3} \boldsymbol{\sigma}_1 \cdot \boldsymbol{\sigma}_2 \nabla^2 y_\pi(r) = \frac{1}{3} \boldsymbol{\sigma}_1 \cdot \boldsymbol{\sigma}_2 \left[m_\pi^2 y_\pi(r) - 4\pi\delta(\mathbf{r}) \right]. \quad (\text{A.18})$$

Putting all these results together, and defining

$$S_{12} = \frac{3}{r^2} (\boldsymbol{\sigma}_1 \cdot \mathbf{r}) (\boldsymbol{\sigma}_2 \cdot \mathbf{r}) - (\boldsymbol{\sigma}_1 \cdot \boldsymbol{\sigma}_2) \quad (\text{A.19})$$

we finally find the expression of the one-pion-exchange potential

$$v^\pi(\mathbf{r}) = \frac{1}{3} \frac{1}{4\pi} f_\pi^2 m_\pi \tau_1^a \tau_2^a \left[T_\pi(r) S_{12} + \left(Y_\pi(r) - \frac{4\pi}{m_\pi^3} \delta(\mathbf{r}) \right) \boldsymbol{\sigma}_1 \cdot \boldsymbol{\sigma}_2 \right], \quad (\text{A.20})$$

with

$$Y_\pi(r) = \frac{e^{-m_\pi r}}{m_\pi r}, \quad (\text{A.21})$$

and

$$T_\pi(r) = \left(1 + \frac{3}{m_\pi r} + \frac{3}{m_\pi^2 r^2} \right) Y_\pi(r). \quad (\text{A.22})$$

Appendix B

AV6 Algebra

Within this section we report some useful properties of the AV6 operators, i.e. the set

$$O_{12}^p = (1, \boldsymbol{\sigma}_1 \cdot \boldsymbol{\sigma}_2, S_{12}) \otimes (1, \boldsymbol{\tau}_1 \cdot \boldsymbol{\tau}_2). \quad (\text{B.1})$$

Within this whole section we understood summation over repeated indices. The standard notation usually employed in literature addresses with $p = 1, 3, 5$ the isospin independent operators, i.e. $(1, \boldsymbol{\sigma}_1 \cdot \boldsymbol{\sigma}_2, S_{12}) \otimes 1$, whereas $p = 2, 4, 6$ refer to $(1, \boldsymbol{\sigma}_1 \cdot \boldsymbol{\sigma}_2, S_{12}) \otimes (\boldsymbol{\tau}_1 \cdot \boldsymbol{\tau}_2)$. The tensor operator S_{12} has the form

$$S_{12} = \frac{3}{r^2} (\boldsymbol{\sigma}_1 \cdot \mathbf{r})(\boldsymbol{\sigma}_2 \cdot \mathbf{r}) - (\boldsymbol{\sigma}_1 \cdot \boldsymbol{\sigma}_2). \quad (\text{B.2})$$

We recall also the basic properties of the Pauli matrices

$$\{\sigma^i, \sigma^j\} = 2\delta^{ij} \quad (\text{B.3})$$

$$[\sigma^i, \sigma^j] = 2i\epsilon^{ijk}\sigma^k, \quad (\text{B.4})$$

where the indices i, j, k run from 1 to 3. Their explicit expression is the following

$$\sigma^1 = \begin{pmatrix} 0 & 1 \\ 1 & 0 \end{pmatrix}, \quad \sigma^2 = \begin{pmatrix} 0 & -i \\ i & 0 \end{pmatrix}, \quad \sigma^3 = \begin{pmatrix} 1 & 0 \\ 0 & -1 \end{pmatrix}. \quad (\text{B.5})$$

The τ matrices are defined in the same way as the σ but acting on the isospin space.

We have already mentioned that the O^p operators form an algebra, i.e. they exhibit closed composition relations (we suppress the subscript "12" from the operators O_{12}^p from now on)

$$O^p O^q = K^{pql} O^l. \quad (\text{B.6})$$

The coefficients K^{pql} can be easily computed with some algebraic manipulations. By simply applying the commutation relations (B.3) and (B.4) it is straightforward to see that

$$(\boldsymbol{\sigma}_1 \cdot \boldsymbol{\sigma}_2)(\boldsymbol{\sigma}_1 \cdot \boldsymbol{\sigma}_2) = 3 - 2(\boldsymbol{\sigma}_1 \cdot \boldsymbol{\sigma}_2) \quad (\text{B.7})$$

$$S_{12}(\boldsymbol{\sigma}_1 \cdot \boldsymbol{\sigma}_2) = (\boldsymbol{\sigma}_1 \cdot \boldsymbol{\sigma}_2)S_{12} = S_{12} \quad (\text{B.8})$$

$$S_{12}S_{12} = 6 - 2S_{12} + 2(\boldsymbol{\sigma}_1 \cdot \boldsymbol{\sigma}_2). \quad (\text{B.9})$$

Another useful property regards the gradient of the tensor operator

$$\nabla S_{12} = \frac{3}{r^2} \left[\boldsymbol{\sigma}_1(\boldsymbol{\sigma}_2 \cdot \mathbf{r}) + \boldsymbol{\sigma}_2(\boldsymbol{\sigma}_1 \cdot \mathbf{r}) - 2\frac{\mathbf{r}}{r^2}(\boldsymbol{\sigma}_1 \cdot \mathbf{r})(\boldsymbol{\sigma}_2 \cdot \mathbf{r}) \right]. \quad (\text{B.10})$$

Therefore we have that

$$\mathbf{r} \cdot \nabla S_{12} = 0 \quad (\text{B.11})$$

and consequently for any given function $g(r)$

$$\nabla g \cdot \nabla S_{12} = \frac{1}{r} \frac{dg}{dr} \mathbf{r} \cdot \nabla S_{12} = 0. \quad (\text{B.12})$$

Finally we also have

$$\nabla S_{12} \cdot \nabla S_{12} = \frac{6}{r^2} (6 + 2\boldsymbol{\sigma}_1 \cdot \boldsymbol{\sigma}_2 - S_{12}). \quad (\text{B.13})$$

B.1 Projection operators

In this section we will briefly discuss the projectors P_S onto the two invariant subspaces with total spin $S = 1$ and $S = 0$, characterizing the composition of two particles with spin $1/2$. In a two dimensional vector space we can define the representation of the spin operator \mathbf{s}_1 acting on particle 1 as

$$\mathbf{s}_1 \equiv \frac{1}{2} \boldsymbol{\sigma}_1. \quad (\text{B.14})$$

Being $\mathbf{S} = \mathbf{s}_1 + \mathbf{s}_2$ and therefore

$$\mathbf{s}_1 \cdot \mathbf{s}_2 = \frac{1}{2} (S^2 - s_1^2 - s_2^2), \quad (\text{B.15})$$

it's easy to prove that

$$4(\mathbf{s}_1 \cdot \mathbf{s}_2) |S = 1, S_3\rangle = 1 \quad (\text{B.16})$$

$$4(\mathbf{s}_1 \cdot \mathbf{s}_2) |S = 0, 0\rangle = -3. \quad (\text{B.17})$$

Because of the above properties we can define the projectors

$$P_1 = \frac{1}{4} (3 + \boldsymbol{\sigma}_1 \cdot \boldsymbol{\sigma}_2), \quad P_0 = \frac{1}{4} (1 - \boldsymbol{\sigma}_1 \cdot \boldsymbol{\sigma}_2). \quad (\text{B.18})$$

In the same way we can define the projector Π_T with $T = 1, 0$ for the total isospin states by replacing the σ matrices with the τ ones.

B.2 Pair exchange operator

The projection operators derived in the previous section can be used to build up the pair exchange operator in the spin space, defined as P^σ . This operator has to fulfil the following requirements

$$P^\sigma |\uparrow\downarrow\rangle = |\downarrow\uparrow\rangle \quad (\text{B.19})$$

$$P^\sigma P^\sigma = 1. \quad (\text{B.20})$$

Since we have that

$$|\uparrow\downarrow\rangle = \frac{1}{\sqrt{2}}(|1,0\rangle + |0,0\rangle) \quad (\text{B.21})$$

$$|\downarrow\uparrow\rangle = \frac{1}{\sqrt{2}}(|1,0\rangle - |0,0\rangle), \quad (\text{B.22})$$

we will have

$$\begin{aligned} P_1|\uparrow\downarrow\rangle &= \frac{1}{\sqrt{2}}|1,0\rangle \\ P_0|\uparrow\downarrow\rangle &= \frac{1}{\sqrt{2}}|0,0\rangle \\ \Rightarrow (P_1 - P_0)|\uparrow\downarrow\rangle &= |\downarrow\uparrow\rangle. \end{aligned} \quad (\text{B.23})$$

Since $P_1 + P_0 = 1$ it's easy to prove that the definition $P^\sigma \equiv P_1 - P_0$ is a good choice for the exchange operator. In the same way we can define the exchange operator on the isospin space as $P^\tau = \Pi_1 - \Pi_0$. Finally the pair exchange operator on the full spin-isospin space can be written as

$$P^{\sigma\tau} \equiv P^\sigma \otimes P^\tau = \frac{1}{4}(1 + \boldsymbol{\sigma}_1 \cdot \boldsymbol{\sigma}_2)(1 + \boldsymbol{\tau}_1 \cdot \boldsymbol{\tau}_2) = \frac{1}{4} \sum_{p=1}^4 O^p. \quad (\text{B.24})$$

As a final remark we also notice how the exchange operator works on the $|S, S_3\rangle$ basis

$$P^\sigma |S, S_3\rangle = (-1)^{S+1} |S, S_3\rangle. \quad (\text{B.25})$$

Appendix C

Parametrization of the APR Energy Density

In this Appendix, we report the explicit expression of the energy density of nuclear matter employed to carry out our analysis. This expression was originally derived from a fit to the EOSs of SNM and PNM obtained by Akmal *et al.* [62] using the AV18 + δv + UIX* nuclear Hamiltonian and the variational FHNC/SOC formalism.

The energy density of nuclear matter at baryon density ϱ and proton fraction x_p is written according to Eqs. (3.142) and (3.143)

$$\begin{aligned} \epsilon(\varrho, x_p) = & \left[\frac{\hbar^2}{2m} + f(\varrho, x_p) \right] \tau_p + \left[\frac{\hbar^2}{2m} + f(\varrho, 1 - x_p) \right] \tau_n \\ & + g(\varrho, 1/2) \left[1 - (1 - 2x_p)^2 \right] + g(\varrho, 0) (1 - 2x_p)^2, \end{aligned} \quad (\text{C.1})$$

with

$$\tau_p = \varrho x_p \frac{3}{5} (3\pi^2 \varrho x_p)^{2/3}, \quad (\text{C.2})$$

$$\tau_n = \varrho (1 - x_p) \frac{3}{5} [(3\pi^2 \varrho (1 - x_p))]^{2/3}. \quad (\text{C.3})$$

The explicit form of the functions $f(\varrho, x_p)$ and $g(\varrho, x_p)$ appearing in Eq. (C.1) are

$$f(\varrho, x_p) = (a_1 + x_p a_2) \varrho e^{-a_3 \varrho} \quad (\text{C.4})$$

and

$$g(\varrho, x_p) = \begin{cases} g_L(\varrho, x_p) & \varrho \leq \bar{\varrho} \\ g_H(\varrho, x_p) & \varrho \geq \bar{\varrho} \end{cases}, \quad (\text{C.5})$$

where

$$\begin{aligned} g_L(\varrho, 1/2) &= -\varrho^2 \left[a_4 + a_5 \varrho + a_6 \varrho^2 + (a_7 + a_8 \varrho) e^{-a_3^2 \varrho^2} \right], \\ g_L(\varrho, 0) &= -\varrho^2 \left(a_{10} \varrho^{-1} + a_{11} + a_{12} \varrho \right), \\ g_H(\varrho, 1/2) &= g_L(\varrho, 1/2) - \varrho^2 a_{13} (\varrho - a_{14}) e^{a_{15} (\varrho - a_{14})}, \\ g_H(\varrho, 0) &= g_L(\varrho, 0) - \varrho^2 a_{16} (\varrho - a_{17}) e^{a_{18} (\varrho - a_{17})}. \end{aligned} \quad (\text{C.6})$$

The density $\bar{\rho} \lesssim 2\rho_0$ corresponds to the onset of the high-density phase—featuring spin-isospin density waves associated with neutral pion condensation—predicted by the study of Ref. [62].

The values of the parameters appearing in the above equations are given in Table C.1

Table C.1. Values of the parameters appearing in the definition of the energy density of nuclear matter of Eqs. (C.1)- (C.6), expressed in MeV fm^{-3} .

a_1	a_2	a_3	a_4	a_5	a_6
[MeV fm ⁵]	[MeV fm ⁵]	[fm ³]	[MeV fm ³]	[MeV fm ⁶]	[MeV fm ⁹]
89.8	-59.0	0.457	337.2	-382.	-19.1
a_7	a_8	a_9	a_{10}	a_{11}	a_{12}
[MeV fm ³]	[MeV fm ⁶]	[fm ³]	[MeV]	[MeV fm ³]	[MeV fm ⁶]
69.0	-33.0	6.4	0.35	214.6	-384.0
a_{13}	a_{14}	a_{15}	a_{16}	a_{17}	a_{18}
[MeV fm ⁶]	[fm ⁻³]	[MeV fm ⁶]	[MeV fm ⁶]	[MeV]	[fm ³]
175.0	0.32	-1.45	287.0	0.195	-1.54

Appendix D

Energy Per Nucleon

The contribution of the interaction to the energy per nucleon is given by

$$e_I = \frac{1}{A} \sum_{i < j} \langle \Phi_0 | v_{ij} | \Phi_0 \rangle. \quad (\text{D.1})$$

Because of the symmetry property of the ground state we have

$$\sum_{i < j} \langle \phi_0 | v_{ij} | \phi_0 \rangle = \frac{A(A-1)}{2} \langle \phi_0 | v_{12} | \phi_0 \rangle \quad (\text{D.2})$$

yielding

$$\begin{aligned} \langle \phi_0 | v_{12} | \phi_0 \rangle &= \frac{(A-2)!}{A!} \times \\ &\sum_{x_1, x_2} \int d^3 r_1 d^3 r_2 \phi_{x_1}^*(\mathbf{r}_1) \phi_{x_2}^*(\mathbf{r}_2) v_{12} [\phi_{x_1}(\mathbf{r}_1) \phi_{x_2}(\mathbf{r}_2) - \phi_{x_2}(\mathbf{r}_1) \phi_{x_1}(\mathbf{r}_2)]. \end{aligned} \quad (\text{D.3})$$

The indices x_1 and x_2 label the set of all quantum numbers of the single particle wave functions that we can identify with the momentum \mathbf{k} and another discrete quantum number λ . Since the potential can be written as $v_{12} = \sum_p v^p(r_{12}) O_{12}^p$ we find

$$\begin{aligned} \sum_{i < j} \langle \phi_0 | v_{ij} | \phi_0 \rangle &= \frac{1}{2V^2} \sum_{\lambda, \mu} \sum_{\mathbf{k}_1, \mathbf{k}_2} \int d^3 r_1 d^3 r_2 \\ &\times \sum_p v^p(r_{12}) [\langle \lambda \mu | O^p | \lambda \mu \rangle - \langle \lambda \mu | O^p | \mu \lambda \rangle e^{i\mathbf{k}_1 \cdot (\mathbf{r}_1 - \mathbf{r}_2)} e^{-i\mathbf{k}_2 \cdot (\mathbf{r}_1 - \mathbf{r}_2)}] \\ &= \frac{V}{2} \frac{1}{(2\pi)^6} \sum_{\lambda \mu} \sum_p \int d^3 r v^p(r) \\ &\times \int d^3 k_1 d^3 k_2 [\langle \lambda \mu | O^p | \lambda \mu \rangle - \langle \lambda \mu | O^p | \mu \lambda \rangle e^{i\mathbf{k}_1 \cdot \mathbf{r}} e^{-i\mathbf{k}_2 \cdot \mathbf{r}}] \\ &= \frac{V}{2} \varrho^2 \sum_{\lambda \mu} x_\lambda x_\mu \int d^3 r \sum_p v^p(r) [\langle \lambda \mu | O^p | \lambda \mu \rangle - \langle \lambda \mu | O^p | \mu \lambda \rangle l(k_{F, \lambda} r) l(k_{F, \mu} r)]. \end{aligned} \quad (\text{D.4})$$

Finally we have

$$\begin{aligned} \frac{1}{A} \sum_{i<j} \langle \phi_0 | v_{ij} | \phi_0 \rangle &= \frac{\rho}{2} \sum_{\lambda\mu} x_\lambda x_\mu \int d^3r \sum_p v^p(r) [\langle \lambda\mu | O^p | \lambda\mu \rangle - \langle \lambda\mu | O^p | \mu\lambda \rangle l(k_{F,\lambda}r) l(k_{F,\mu}r)] \\ &= \frac{\rho}{2} \sum_{\lambda\mu} x_\lambda x_\mu \int d^3r [\langle v \rangle_d - \langle v \rangle_e l(k_{F,\lambda}r) l(k_{F,\mu}r)], \end{aligned} \quad (\text{D.5})$$

with

$$l(x) = 3 \frac{\sin(x) - x \cos(x)}{x^3}. \quad (\text{D.6})$$

D.1 Matrix elements

In this section we provide the explicit expression of the matrix elements for the operators O^p , appearing in the definition of the energy per nucleon. We define the quantities

$$A^p(\cos \theta) = \langle \lambda\mu | O^p | \lambda\mu \rangle \quad (\text{D.7})$$

$$B^p(\cos \theta) = \langle \lambda\mu | O^p | \mu\lambda \rangle, \quad (\text{D.8})$$

with $\cos \theta = \mathbf{r}/r$. We have

$$\begin{aligned} A^1 &= \begin{pmatrix} 1 & 1 & 1 & 1 \\ 1 & 1 & 1 & 1 \\ 1 & 1 & 1 & 1 \\ 1 & 1 & 1 & 1 \end{pmatrix}, & A^2 &= \begin{pmatrix} 1 & 1 & -1 & -1 \\ 1 & 1 & -1 & -1 \\ -1 & -1 & 1 & 1 \\ -1 & -1 & 1 & 1 \end{pmatrix}, \\ A^3 &= \begin{pmatrix} 1 & -1 & 1 & -1 \\ -1 & 1 & -1 & 1 \\ 1 & -1 & 1 & -1 \\ -1 & 1 & -1 & 1 \end{pmatrix}, & A^4 &= \begin{pmatrix} 1 & -1 & -1 & 1 \\ -1 & 1 & 1 & -1 \\ -1 & 1 & 1 & -1 \\ 1 & -1 & -1 & 1 \end{pmatrix}, \end{aligned}$$

$$\begin{aligned} A^5 &= A^3(\cos^2 \theta - 1), \\ A^6 &= A^4(\cos^2 \theta - 1). \end{aligned} \quad (\text{D.9})$$

Then

$$\begin{aligned}
 B^1 &= \begin{pmatrix} 1 & 0 & 0 & 0 \\ 0 & 1 & 0 & 0 \\ 0 & 0 & 1 & 0 \\ 0 & 0 & 0 & 1 \end{pmatrix}, & B^2 &= \begin{pmatrix} 1 & 0 & 2 & 0 \\ 0 & 1 & 0 & 2 \\ 2 & 0 & 1 & 0 \\ 0 & 2 & 0 & 1 \end{pmatrix}, \\
 B^3 &= \begin{pmatrix} 1 & 2 & 0 & 0 \\ 2 & 1 & 0 & 0 \\ 0 & 0 & 1 & 2 \\ 0 & 0 & 2 & 1 \end{pmatrix}, & B^4 &= \begin{pmatrix} 1 & 2 & 2 & 4 \\ 2 & 1 & 4 & 2 \\ 2 & 4 & 1 & 2 \\ 4 & 2 & 2 & 1 \end{pmatrix}, \\
 B^5 &= \begin{pmatrix} 1 & -1 & 0 & 0 \\ -1 & 1 & 0 & 0 \\ 0 & 0 & 1 & -1 \\ 0 & 0 & -1 & 1 \end{pmatrix} (\cos^2 \theta - 1), \\
 B^6 &= \begin{pmatrix} 1 & -1 & 2 & -2 \\ -1 & 1 & -2 & 2 \\ 2 & -2 & 1 & -1 \\ -2 & 2 & -1 & 1 \end{pmatrix} (\cos^2 \theta - 1).
 \end{aligned} \tag{D.10}$$

Appendix E

Boost Calculation Details

In this section we are going to see how we can carry out the expression of Eq. (4.49) starting from

$$\begin{aligned} \frac{1}{A} \langle \Phi_0 | \sum_{i < j} \delta v_{ij} | \Phi_0 \rangle &= \frac{\varrho}{16m^2} \left\{ \frac{2}{5} k_F^2 \int d^3 r \left(r \frac{dv^p}{dr} - 3v^p \right) \text{CTr}[O^p] \right. \\ &\quad \left. - \int d^3 r \left(r \frac{dv^p}{dr} I_2 - v^p I_1 \right) \text{CTr}[O^p \hat{P}_{12}] \right\}. \end{aligned} \quad (\text{E.1})$$

In the previous equation and in the following of this section we understood summation over repeated indices of the AV6 algebra. By defining

$$\begin{aligned} A^p(k_F, r) &\equiv \frac{1}{8m^2} \frac{2}{5} k_F^2 \left[\frac{dv^p(r)}{dr} - 3v^p(r) \right] \\ B^p(k_F, r) &\equiv \frac{1}{8m^2} \left[\frac{dv^p(r)}{dr} I_2(k_F, r) - v^p(r) I_1(k_F, r) \right] \end{aligned} \quad (\text{E.2})$$

we have

$$\frac{1}{A} \langle \Phi_0 | \sum_{i < j} \delta v_{ij} | \Phi_0 \rangle = \frac{\varrho}{2} \left\{ \int d^3 r A^p(k_F, r) \text{CTr}[O^p] - \int d^3 r B^p(k_F, r) \text{CTr}[O^p \hat{P}_{12}] \right\}. \quad (\text{E.3})$$

Since the exchange operator can be written as

$$\hat{P}_{12} = \frac{1}{4} \sum_{q=1}^4 O^q \quad (\text{E.4})$$

employing the property of Eq. (4.31) we have

$$\frac{1}{A} \langle \Phi_0 | \sum_{i < j} \delta v_{ij} | \Phi_0 \rangle = \frac{\varrho}{2} \int d^3 r \text{CTr}[O^m] \left\{ A^p(k_F, r) \delta_{pm} - \frac{1}{4} \sum_{q=1}^4 K^{pqm} B^p(k_F, r) \right\}. \quad (\text{E.5})$$

At this point we define the following quantities

$$\begin{aligned} \xi^m(k_F, r) &= \left\{ A^m(k_F, r) - \frac{1}{4} \sum_{q=1}^4 K^{pqm} B^p(k_F, r) \right\} \\ M_{pm} &= \frac{1}{4} \sum_{q=1}^4 K^{pqm}. \end{aligned} \quad (\text{E.6})$$

$$\frac{1}{A} \langle \Phi_0 | \sum_{i < j} \delta v_{ij} | \Phi_0 \rangle = \frac{\varrho}{2} \int d^3 r \text{CTr}[O^m] \xi^m(k_F, r) \quad (\text{E.7})$$

$$= \frac{\varrho}{2} \int d^3 r \text{CTr}[O^m] \left[\delta_{mn} - l^2(k_F r) M_{mn} \right] \\ \times \left[\delta_{np} - l^2(k_F r) M_{np} \right]^{-1} \xi^p(k_F, r). \quad (\text{E.8})$$

Since

$$\left[\delta_{mp} - l^2(k_F r) M_{mp} \right]^{-1} = \frac{1}{1 - l^4(k_F r)} \left[\delta_{mp} + l^2(k_F r) M_{mp} \right], \quad (\text{E.9})$$

we can finally write

$$\frac{1}{A} \langle \Phi_0 | \sum_{i < j} \delta v_{ij} | \Phi_0 \rangle = \frac{\varrho}{2} \int d^3 r \text{CTr}[O^m] \left[\delta_{mp} - l^2(k_F r) M_{mp} \right] \delta v^p(k_F, r) \quad (\text{E.10})$$

where we have defined

$$\delta v^p(k_F, r) \equiv \frac{1}{1 - l^4(k_F r)} \left[\delta_{pm} + l^2(k_F r) M_{pm} \right] \xi^m(k_F, r). \quad (\text{E.11})$$

By recalling that the operator M is linked to the exchange operator, Eq. (E.10) can be written as

$$\frac{1}{A} \langle \Phi_0 | \sum_{i < j} \delta v_{ij} | \Phi_0 \rangle = \frac{\varrho}{2} \int d^3 r \text{CTr} \left[O^p \left(1 - l^2 \hat{P}_{12} \right) \right] \delta v^p(k_F, r) \quad (\text{E.12})$$

which is the expression we were looking for.

Finally I'm going to show how we can derive the expression of Eq. (E.9). Since the operator we want to invert has the form

$$\mathbb{1} - l^2 M \quad (\text{E.13})$$

we have that

$$\left(\mathbb{1} - l^2 M \right) \left(\mathbb{1} + l^2 M^{-1} \right) = \left(1 - l^4 \right) \mathbb{1} - l^2 M + l^2 M^{-1}. \quad (\text{E.14})$$

Therefore if we show that

$$M = M^{-1} \quad (\text{E.15})$$

we have done. We start from the identity

$$O^m O^p O^q = K^{mpl} K^{lqs} O^s \quad (\text{E.16})$$

and summing over $p, q = 1, 4$ we have

$$\sum_{p, q=1}^4 O^m O^p O^q = O^m \sum_{p=1}^4 O^p \sum_{q=1}^4 O^q = O^m (4 \hat{P}_{12}) (4 \hat{P}_{12}) = 16 O^m \hat{P}_{12}^2 = 16 O^m. \quad (\text{E.17})$$

Therefore we can write

$$O^m = \frac{1}{16} \sum_{p, q=1}^4 O^m O^p O^q = \left(\frac{1}{4} \sum_{p=1}^4 K^{mpl} \right) \left(\frac{1}{4} \sum_{q=1}^4 K^{lqs} \right) O^s = M_{ml} M_{ls} O^s \quad (\text{E.18})$$

which implies

$$M_{ml} M_{ls} = \delta_{ms} \Rightarrow M = M^{-1}. \quad (\text{E.19})$$

Bibliography

- [1] Mikhail Stephanov. QCD phase diagram: an overview. *PoS*, LAT2006:024, 2006.
- [2] M. Järvinen. Holographic modeling of nuclear matter and neutron stars. *The European Physical Journal C*, 82(282), Apr 2022.
- [3] B. P. Abbott et al. GW170817: Observation of Gravitational Waves from a Binary Neutron Star Inspiral. *Phys. Rev. Lett.*, 119(16):161101, 2017.
- [4] B. P. Abbott et al. Properties of the binary neutron star merger GW170817. *Phys. Rev. X*, 9(1):011001, 2019.
- [5] H. Thankful Cromartie et al. Relativistic Shapiro delay measurements of an extremely massive millisecond pulsar. *Nature Astron.*, 4(1):72–76, 2019.
- [6] E. Fonseca et al. Refined Mass and Geometric Measurements of the High-mass PSR J0740+6620. *Astrophys. J. Lett.*, 915(1):L12, 2021.
- [7] Thomas E. Riley et al. A *NICER* View of PSR J0030+0451: Millisecond Pulsar Parameter Estimation. *Astrophys. J. Lett.*, 887(1):L21, 2019.
- [8] M. C. Miller et al. PSR J0030+0451 Mass and Radius from *NICER* Data and Implications for the Properties of Neutron Star Matter. *Astrophys. J. Lett.*, 887(1):L24, 2019.
- [9] Thomas E. Riley et al. A *NICER* View of the Massive Pulsar PSR J0740+6620 Informed by Radio Timing and XMM-Newton Spectroscopy. *Astrophys. J. Lett.*, 918(2):L27, 2021.
- [10] M. C. Miller et al. The Radius of PSR J0740+6620 from *NICER* and XMM-Newton Data. *Astrophys. J. Lett.*, 918(2):L28, 2021.
- [11] B. P. Abbott et al. GW190425: Observation of a Compact Binary Coalescence with Total Mass $\sim 3.4M_{\odot}$. *Astrophys. J. Lett.*, 892(1):L3, 2020.
- [12] Tanja Hinderer. Tidal Love numbers of neutron stars. *Astrophys. J.*, 677:1216–1220, 2008.
- [13] Thibault Damour and Alessandro Nagar. Relativistic tidal properties of neutron stars. *Phys. Rev. D*, 80:084035, 2009.

- [14] Taylor Binnington and Eric Poisson. Relativistic theory of tidal Love numbers. *Phys. Rev. D*, 80:084018, 2009.
- [15] Eanna E. Flanagan and Tanja Hinderer. Constraining neutron star tidal Love numbers with gravitational wave detectors. *Phys. Rev. D*, 77:021502, 2008.
- [16] Justin E. Vines and Eanna E. Flanagan. Post-1-Newtonian quadrupole tidal interactions in binary systems. *Phys. Rev. D*, 88:024046, 2013.
- [17] Justin Vines, Eanna E. Flanagan, and Tanja Hinderer. Post-1-Newtonian tidal effects in the gravitational waveform from binary inspirals. *Phys. Rev. D*, 83:084051, 2011.
- [18] G. Colò. The compression modes in atomic nuclei and their relevance for the nuclear equation of state. *Physics of Particles and Nuclei*, 39(2):286–305, March 2008.
- [19] Bao-An Li and Xiao Han. Constraining the neutron-proton effective mass splitting using empirical constraints on the density dependence of nuclear symmetry energy around normal density. *Phys. Lett. B*, 727:276–281, 2013.
- [20] P. Russotto et al. Results of the ASY-EOS experiment at GSI: The symmetry energy at suprasaturation density. *Phys. Rev. C*, 94(3):034608, 2016.
- [21] M. B. Tsang, Yingxun Zhang, P. Danielewicz, M. Famiano, Zhuxia Li, W. G. Lynch, and A. W. Steiner. Constraints on the density dependence of the symmetry energy. *Phys. Rev. Lett.*, 102:122701, 2009.
- [22] Pawel Danielewicz, Roy Lacey, and William G. Lynch. Determination of the equation of state of dense matter. *Science*, 298:1592–1596, 2002.
- [23] B. Alex Brown. Constraints on the Skyrme Equations of State from Properties of Doubly Magic Nuclei. *Phys. Rev. Lett.*, 111(23):232502, 2013.
- [24] Zhen Zhang and Lie-Wen Chen. Constraining the symmetry energy at sub-saturation densities using isotope binding energy difference and neutron skin thickness. *Phys. Lett. B*, 726:234–238, 2013.
- [25] D. Adhikari et al. Accurate Determination of the Neutron Skin Thickness of ^{208}Pb through Parity-Violation in Electron Scattering. *Phys. Rev. Lett.*, 126(17):172502, 2021.
- [26] Eemeli Annala, Tyler Gorda, Alekski Kurkela, and Alekski Vuorinen. Gravitational-wave constraints on the neutron-star-matter Equation of State. *Phys. Rev. Lett.*, 120(17):172703, 2018.
- [27] Ben Margalit and Brian D. Metzger. Constraining the Maximum Mass of Neutron Stars From Multi-Messenger Observations of GW170817. *Astrophys. J. Lett.*, 850(2):L19, 2017.
- [28] David Radice, Albino Perego, Francesco Zappa, and Sebastiano Bernuzzi. GW170817: Joint Constraint on the Neutron Star Equation of State from Multimessenger Observations. *Astrophys. J. Lett.*, 852(2):L29, 2018.

- [29] Andreas Bauswein, Oliver Just, Hans-Thomas Janka, and Nikolaos Stergioulas. Neutron-star radius constraints from GW170817 and future detections. *Astrophys. J. Lett.*, 850(2):L34, 2017.
- [30] Yeunhwan Lim and Jeremy W. Holt. Neutron star tidal deformabilities constrained by nuclear theory and experiment. *Phys. Rev. Lett.*, 121(6):062701, 2018.
- [31] Yeunhwan Lim, Anirban Bhattacharya, Jeremy W. Holt, and Debdeep Pati. Radius and equation of state constraints from massive neutron stars and GW190814. *Phys. Rev. C*, 104(3):L032802, 2021.
- [32] Elias R. Most, Lukas R. Weih, Luciano Rezzolla, and Jürgen Schaffner-Bielich. New constraints on radii and tidal deformabilities of neutron stars from GW170817. *Phys. Rev. Lett.*, 120(26):261103, 2018.
- [33] Soumi De, Daniel Finstad, James M. Lattimer, Duncan A. Brown, Edo Berger, and Christopher M. Biwer. Tidal Deformabilities and Radii of Neutron Stars from the Observation of GW170817. *Phys. Rev. Lett.*, 121(9):091102, 2018. [Erratum: *Phys.Rev.Lett.* 121, 259902 (2018)].
- [34] Eemeli Annala, Tyler Gorda, Alekski Kurkela, Joonas Nättilä, and Alekski Vuorinen. Evidence for quark-matter cores in massive neutron stars. *Nature Phys.*, 16(9):907–910, 2020.
- [35] G. Raaijmakers et al. Constraining the dense matter equation of state with joint analysis of NICER and LIGO/Virgo measurements. *Astrophys. J. Lett.*, 893(1):L21, 2020.
- [36] M. Coleman Miller, Cecilia Chirenti, and Frederick K. Lamb. Constraining the equation of state of high-density cold matter using nuclear and astronomical measurements. 4 2019.
- [37] Bharat Kumar and Philippe Landry. Inferring neutron star properties from GW170817 with universal relations. *Phys. Rev. D*, 99(12):123026, 2019.
- [38] Margherita Fasano, Tiziano Abdelsalhin, Andrea Maselli, and Valeria Ferrari. Constraining the Neutron Star Equation of State Using Multiband Independent Measurements of Radii and Tidal Deformabilities. *Phys. Rev. Lett.*, 123(14):141101, 2019.
- [39] Philippe Landry, Reed Essick, and Katerina Chatziioannou. Nonparametric constraints on neutron star matter with existing and upcoming gravitational wave and pulsar observations. *Phys. Rev. D*, 101(12):123007, 2020.
- [40] H. Güven, K. Bozkurt, E. Khan, and J. Margueron. Multimessenger and multiphysics Bayesian inference for the GW170817 binary neutron star merger. *Phys. Rev. C*, 102(1):015805, 2020.
- [41] Silvia Traversi, Prasanta Char, and Giuseppe Pagliara. Bayesian Inference of Dense Matter Equation of State within Relativistic Mean Field Models using Astrophysical Measurements. *Astrophys. J.*, 897:165, 2020.

- [42] G. Raaijmakers, S. K. Greif, K. Hebeler, T. Hinderer, S. Nissanke, A. Schwenk, T. E. Riley, A. L. Watts, J. M. Lattimer, and W. C. G. Ho. Constraints on the Dense Matter Equation of State and Neutron Star Properties from NICER’s Mass–Radius Estimate of PSR J0740+6620 and Multimessenger Observations. *Astrophys. J. Lett.*, 918(2):L29, 2021.
- [43] I. Tews, J. Margueron, and S. Reddy. Critical examination of constraints on the equation of state of dense matter obtained from gw170817. *Phys. Rev. C*, 98:045804, Oct 2018.
- [44] I. Tews, J. Carlson, S. Gandolfi, and S. Reddy. Constraining the speed of sound inside neutron stars with chiral effective field theory interactions and observations. *The Astrophysical Journal*, 860(2):149, jun 2018.
- [45] Collin Capano, Ingo Tews, Stephanie Brown, Ben Margalit, Soumi De, Sumit Kumar, Duncan Brown, Badri Krishnan, and Sanjay Reddy. Stringent constraints on neutron-star radii from multimessenger observations and nuclear theory. *Nature Astronomy*, 4:1–8, 06 2020.
- [46] Josef Zimmerman, Zack Carson, Kristen Schumacher, Andrew W. Steiner, and Kent Yagi. Measuring Nuclear Matter Parameters with NICER and LIGO/Virgo. 2 2020.
- [47] Hector O. Silva, A. Miguel Holgado, Alejandro Cárdenas-Avendaño, and Nicolás Yunes. Astrophysical and theoretical physics implications from multimessenger neutron star observations. *Phys. Rev. Lett.*, 126(18):181101, 2021.
- [48] Andrea Sabatucci and Omar Benhar. Tidal Deformation of Neutron Stars from Microscopic Models of Nuclear Dynamics. *Phys. Rev. C*, 101(4):045807, 2020.
- [49] David Blaschke, Alexander Ayriyan, David Edwin Alvarez-Castillo, and Hovik Grigorian. Was GW170817 a Canonical Neutron Star Merger? Bayesian Analysis with a Third Family of Compact Stars. *Universe*, 6(6):81, 2020.
- [50] Shao-Peng Tang, Jin-Liang Jiang, Wei-Hong Gao, Yi-Zhong Fan, and Da-Ming Wei. Constraint on phase transition with the multimessenger data of neutron stars. *Phys. Rev. D*, 103(6):063026, 2021.
- [51] Bhaskar Biswas, Prasanta Char, Rana Nandi, and Sukanta Bose. Towards mitigation of apparent tension between nuclear physics and astrophysical observations by improved modeling of neutron star matter. *Phys. Rev. D*, 103(10):103015, 2021.
- [52] Costantino Pacilio, Andrea Maselli, Margherita Fasano, and Paolo Pani. Ranking Love Numbers for the Neutron Star Equation of State: The Need for Third-Generation Detectors. *Phys. Rev. Lett.*, 128(10):101101, 2022.
- [53] Tuhin Malik and Constança Providência. Bayesian inference of signatures of hyperons inside neutron stars. 5 2022.

- [54] Sinan Altıparmak, Christian Ecker, and Luciano Rezzolla. On the Sound Speed in Neutron Stars. 3 2022.
- [55] Pawan Kumar Gupta, Anna Puecher, Peter T. H. Pang, Justin Janquart, Gideon Koekoek, and Chris Broeck Van Den. Determining the equation of state of neutron stars with Einstein Telescope using tidal effects and r-mode excitations from a population of binary inspirals. 5 2022.
- [56] G.F. Burgio, H.-J. Schulze, I. Vidaña, and J.-B. Wei. Neutron stars and the nuclear equation of state. *Progress in Particle and Nuclear Physics*, 120:103879, 2021.
- [57] Luca Baiotti. Gravitational waves from neutron star mergers and their relation to the nuclear equation of state. *Prog. Part. Nucl. Phys.*, 109:103714, 2019.
- [58] Katerina Chatziioannou. Neutron star tidal deformability and equation of state constraints. *Gen. Rel. Grav.*, 52(11):109, 2020.
- [59] H A Bethe. Theory of nuclear matter. *Annual Review of Nuclear Science*, 21(1):93–244, 1971.
- [60] R. B. Wiringa. From deuterons to neutron stars: variations in nuclear many-body theory. *Rev. Mod. Phys.*, 65:231–242, Jan 1993.
- [61] J. Carlson, S. Gandolfi, F. Pederiva, Steven C. Pieper, R. Schiavilla, K. E. Schmidt, and R. B. Wiringa. *Rev. Mod. Phys.*, 87:1067, 2015.
- [62] A. Akmal, V.R. Pandharipande, and D.G. Ravenhall. Equation of state of nucleon matter and neutron star structure. *Phys. Rev. C*, 58:1804, 1998.
- [63] O. Benhar. *Int. J. Mod. Phys. E*, 9:2130009, 2021.
- [64] Reed Essick, Ingo Tews, Philippe Landry, Sanjay Reddy, and Daniel E. Holz. Direct astrophysical tests of chiral effective field theory at supranuclear densities. *Phys. Rev. C*, 102:055803, Nov 2020.
- [65] A. Akmal and V. R. Pandharipande. Spin-isospin structure and pion condensation in nucleon matter. *Phys. Rev. C*, 56:2261–2279, Oct 1997.
- [66] A. Lovato, I. Bombaci, D. Logoteta, M. Piarulli, and R. B. Wiringa. Benchmark calculations of infinite neutron matter with realistic two- and three-nucleon potentials. *Phys. Rev. C*, 105:055808, May 2022.
- [67] O. Benhar and A. Lovato. Perturbation theory of nuclear matter with a microscopic effective interaction. *Phys. Rev. C*, 96:054301, 2017.
- [68] R. A. Krajeck and L. L. Foldy. Relativistic center-of-mass variables for composite systems with arbitrary internal interactions. *Phys. Rev. D*, 10:1777–1795, Sep 1974.
- [69] J. Forest, Vijay R. Pandharipande, and James L. Friar. *Phys. Rev. C*, 52:568, 1995.

- [70] J. Carlson, V. R. Pandharipande, and R. Schiavilla. Variational monte carlo calculations of ${}^3\text{H}$ and ${}^4\text{He}$ with a relativistic hamiltonian. *Phys. Rev. C*, 47:484–497, Feb 1993.
- [71] J. L. Forest, V. R. Pandharipande, and A. Arriaga. Quantum monte carlo studies of relativistic effects in light nuclei. *Phys. Rev. C*, 60:014002, Jun 1999.
- [72] Andrea Maselli, Andrea Sabatucci, and Omar Benhar. Constraining three-nucleon forces with multimessenger data. *Phys. Rev. C*, 103(6):065804, 2021.
- [73] Andrea Sabatucci. Constraining three-nucleon forces with multimessenger data. *Proceedings of the International Astronomical Union*, 16(S363):195–198, 2020.
- [74] Andrea Sabatucci, Omar Benhar, Andrea Maselli, and Costantino Pacilio. Sensitivity of neutron star observations to three-nucleon forces. *Phys. Rev. D*, 106:083010, Oct 2022.
- [75] G. Baym and S.A. Chin. Can a neutron star be a giant mit bag? *Physics Letters B*, 62(2):241–244, 1976.
- [76] Norman K. Glendenning. *Compact Stars: Nuclear Physics, Particle Physics and General Relativity*. Astronomy and Astrophysics Library. Springer New York, 1997.
- [77] D. G. Ravenhall, C. J. Pethick, and J. R. Wilson. Structure of matter below nuclear saturation density. *Phys. Rev. Lett.*, 50:2066–2069, Jun 1983.
- [78] Minoru Okamoto, Toshiki Maruyama, Kazuhiro Yabana, and Toshitaka Tatsumi. Nuclear “pasta” structures in low-density nuclear matter and properties of the neutron-star crust. *Phys. Rev. C*, 88:025801, Aug 2013.
- [79] Tolman, R. C. Static solutions of Einstein’s field equations for spheres of fluid. *Phys. Rev.*, 55:364, 1939.
- [80] Oppenheimer, J. R. and Volkoff, G. M. On massive neutron cores. *Phys. Rev.*, 55:374, 1939.
- [81] Valeria Ferrari. Lecture notes for the master’s degree courses: "Relatività Generale" and "Onde gravitazionali, stelle e buchi neri".
- [82] Ian Harry and Tanja Hinderer. Observing and measuring the neutron-star equation-of-state in spinning binary neutron star systems. *Classical and Quantum Gravity*, 35(14):145010, jun 2018.
- [83] Tanja Hinderer, Benjamin D. Lackey, Ryan N. Lang, and Jocelyn S. Read. Tidal deformability of neutron stars with realistic equations of state and their gravitational wave signatures in binary inspiral. *Phys. Rev. D*, 81:123016, Jun 2010.
- [84] Kip S. Thorne and Alfonso Campolattaro. Non-Radial Pulsation of General-Relativistic Stellar Models. I. Analytic Analysis for $L \geq 2$. *Astrophysical Journal*, vol. 149, p.591, September 1967.

- [85] N. K. Glendenning and S. A. Moszkowski. Reconciliation of neutron-star masses and binding of the Λ in hypernuclei. *Phys. Rev. Lett.*, 67:2414–2417, Oct 1991.
- [86] James M. Lattimer and F. Douglas Swesty. A generalized equation of state for hot, dense matter. *Nuclear Physics A*, 535(2):331–376, 1991.
- [87] Glòria Montaña, Laura Tolós, Matthias Hanauske, and Luciano Rezzolla. Constraining twin stars with gw170817. *Phys. Rev. D*, 99:103009, May 2019.
- [88] Jonas P. Pereira, Michał Bejger, Lucas Tonetto, Germán Lugones, Paweł Haensel, Julian Leszek Zdunik, and Magdalena Sieniawska. Probing elastic quark phases in hybrid stars with radius measurements. *The Astrophysical Journal*, 910(2):145, apr 2021.
- [89] L. Tonetto and G. Lugones. Discontinuity gravity modes in hybrid stars: Assessing the role of rapid and slow phase conversions. *Phys. Rev. D*, 101:123029, Jun 2020.
- [90] Alekski Kurkela, Eduardo S. Fraga, Jürgen Schaffner-Bielich, and Alekski Vuorinen. Constraining neutron star matter with quantum chromodynamics. *The Astrophysical Journal*, 789(2):127, jun 2014.
- [91] Oleg Komoltsev and Alekski Kurkela. How perturbative qcd constrains the equation of state at neutron-star densities. *Phys. Rev. Lett.*, 128:202701, May 2022.
- [92] Ingo Sick. Proton charge radius from electron scattering. *Atoms*, 6(1), 2018.
- [93] Omar Benhar and Stefano Fantoni. *Nuclear Matter Theory (1st ed.)*. CRC Press, 2020.
- [94] Hideki Yukawa. On the Interaction of Elementary Particles. I. *Progress of Theoretical Physics Supplement*, 1:1–10, 01 1955.
- [95] Robert B. Wiringa, V. G. J. Stoks, and R. Schiavilla. An Accurate nucleon-nucleon potential with charge independence breaking. *Phys. Rev. C*, 51:38–51, 1995.
- [96] I.E. Lagaris and V.R. Pandharipande. Phenomenological two-nucleon interaction operator. *Nuclear Physics A*, 359(2):331–348, 1981.
- [97] B. S. Pudliner, Vijay R. Pandharipande, J. Carlson, and Robert B. Wiringa. Quantum Monte Carlo calculations of $A \leq 6$ nuclei. *Phys. Rev. Lett.*, 74:4396–4399, 1995.
- [98] J. Fujita and H. Miyazawa. Pion Theory of Three-Body Forces. *Prog. Theor. Phys.*, 17:360–365, 1957.
- [99] J. Carlson, S. Gandolfi, F. Pederiva, Steven C. Pieper, R. Schiavilla, K. E. Schmidt, and R. B. Wiringa. Quantum monte carlo methods for nuclear physics. *Rev. Mod. Phys.*, 87:1067–1118, Sep 2015.

- [100] J.D Walecka. A theory of highly condensed matter. *Annals of Physics*, 83(2):491–529, 1974.
- [101] Leslie L. Foldy. Relativistic particle systems with interaction. *Phys. Rev.*, 122:275–288, Apr 1961.
- [102] J. L. Forest, V. R. Pandharipande, J. Carlson, and R. Schiavilla. Variational monte carlo calculations of ^3H and ^4He with a relativistic hamiltonian. *Phys. Rev. C*, 52:576–577, Aug 1995.
- [103] Steven Weinberg. Nuclear forces from chiral lagrangians. *Physics Letters B*, 251(2):288–292, 1990.
- [104] Maria Piarulli and Ingo Tews. Local nucleon-nucleon and three-nucleon interactions within chiral effective field theory. *Frontiers in Physics*, 7, 2020.
- [105] D. Lonardonì, I. Tews, S. Gandolfi, and J. Carlson. Nuclear and neutron-star matter from local chiral interactions. *Phys. Rev. Res.*, 2:022033, May 2020.
- [106] Bombaci, Ignazio and Logoteta, Domenico. Equation of state of dense nuclear matter and neutron star structure from nuclear chiral interactions. *A&A*, 609:A128, 2018.
- [107] B. D. DAY. Elements of the brueckner-goldstone theory of nuclear matter. *Rev. Mod. Phys.*, 39:719–744, Oct 1967.
- [108] John W. Clark. Variational theory of nuclear matter. *Progress in Particle and Nuclear Physics*, 2:89–199, 1979.
- [109] V. R. Pandharipande and H. A. Bethe. Variational method for dense systems. *Phys. Rev. C*, 7:1312–1328, Apr 1973.
- [110] John W. Clark and Paul Westhaus. Method of correlated basis functions. *Phys. Rev.*, 141:833–857, Jan 1966.
- [111] V.R. Pandharipande, R.B. Wiringa, and B.D. Day. Do lowest-order approximations adequately describe nuclear matter? *Physics Letters B*, 57(3):205–209, 1975.
- [112] O. Benhar, C. Ciofi degli Atti, S. Fantoni, S. Rosati, A. Kallio, L. Lantto, and P. Toropainen. Lowest-order and hyper-netted-chain calculations of nuclear matter. *Physics Letters B*, 64(4):395–398, 1976.
- [113] J.M.J. van Leeuwen, J. Groeneveld, and J. de Boer. New method for the calculation of the pair correlation function. i. *Physica*, 25(7):792–808, 1959.
- [114] Rosati S. Fantoni S. The hypernetted-chain approximation for a fermion system. *Nuovo Cimento A*, 25:593–615, 1975.
- [115] V. R. Pandharipande and R. B. Wiringa. Variations on a theme of nuclear matter. *Rev. Mod. Phys.*, 51:821–861, Oct 1979.

- [116] K.E. Schmidt and S. Fantoni. A quantum monte carlo method for nucleon systems. *Physics Letters B*, 446(2):99–103, 1999.
- [117] Ingo Tews. *Quantum Monte Carlo calculations with chiral effective field theory interactions*. PhD thesis, Technische Universität, Darmstadt, 2015.
- [118] M. Piarulli, I. Bombaci, D. Logoteta, A. Lovato, and R. B. Wiringa. Benchmark calculations of pure neutron matter with realistic nucleon-nucleon interactions. *Phys. Rev. C*, 101:045801, Apr 2020.
- [119] A. Gezerlis, I. Tews, E. Epelbaum, S. Gandolfi, K. Hebeler, A. Nogga, and A. Schwenk. Quantum monte carlo calculations with chiral effective field theory interactions. *Phys. Rev. Lett.*, 111:032501, Jul 2013.
- [120] D. Vautherin and D. M. Brink. Hartree-fock calculations with skyrme’s interaction. i. spherical nuclei. *Phys. Rev. C*, 5:626–647, Mar 1972.
- [121] V. R. Pandharipande and D. G. Revenhall. *Proceedings of a NATO Advanced Research Workshop on Nuclear Matter and Heavy Ion Collisions, Les Houches*, page 103, 1989.
- [122] S. Cowell and V. R. Pandharipande. Neutrino mean free paths in cold symmetric nuclear matter. *Phys. Rev. C*, 70:035801, Sep 2004.
- [123] Alessandro Lovato, Cristina Losa, and Omar Benhar. Weak response of cold symmetric nuclear matter at three-body cluster level. *Nuclear Physics A*, 901:22–50, 2013.
- [124] Alessandro Lovato, Omar Benhar, Stefano Fantoni, Alexey Yu. Illarionov, and Kevin E. Schmidt. Density-dependent nucleon-nucleon interaction from three-nucleon forces. *Phys. Rev. C*, 83:054003, May 2011.
- [125] Lucas Tonetto and Omar Benhar. Thermal effects on nuclear matter properties. *Phys. Rev. D*, 106:103020, Nov 2022.
- [126] Omar Benhar, Alessandro Lovato, and Giovanni Cameli. Modeling neutron star matter in the age of multimessenger astrophysics. *The Astrophysical Journal*, 939(1):52, nov 2022.
- [127] J. Carlson, Vijay R. Pandharipande, and Robert B. Wiringa. *Nucl. Phys. A*, 401:59, 1983.
- [128] Zack Carson, Andrew W. Steiner, and Kent Yagi. Constraining nuclear matter parameters with GW170817. *Phys. Rev. D*, 99(4):043010, 2019.
- [129] M. Punturo et al. The Einstein Telescope: A third-generation gravitational wave observatory. *Class. Quant. Grav.*, 27:194002, 2010.
- [130] S. Hild et al. Sensitivity Studies for Third-Generation Gravitational Wave Observatories. *Class. Quant. Grav.*, 28:094013, 2011.
- [131] Michele Maggiore et al. Science Case for the Einstein Telescope. *JCAP*, 03:050, 2020.

- [132] Vijay R. Pandharipande and Robert B. Wiringa. *Rev. Mod. Phys.*, 51:821, 1979.
- [133] Daniel Foreman-Mackey, David W. Hogg, Dustin Lang, and Jonathan Goodman. emcee: The MCMC Hammer. *PASP*, 125(925):306, March 2013.
- [134] Thomas E. Riley, Anna L. Watts, Slavko Bogdanov, Paul S. Ray, Renee M. Ludlam, Sebastien Guillot, Zaven Arzoumanian, Charles L. Baker, Anna V. Bilous, Deepto Chakrabarty, Keith C. Gendreau, Alice K. Harding, Wynn C. G. Ho, James M. Lattimer, Sharon M. Morsink, and Tod E. Strohmayer. A NICER View of PSR J0030+0451: Nested Samples for Millisecond Pulsar Parameter Estimation, March 2020.
- [135] Thomas E. Riley, Anna L. Watts, Paul S. Ray, Slavko Bogdanov, Sebastien Guillot, Sharon M. Morsink, Anna V. Bilous, Zaven Arzoumanian, Devarshi Choudhury, Julia S. Deneva, Keith C. Gendreau, Alice K. Harding, Wynn C.G. Ho, James M. Lattimer, Michael Loewenstein, Renee M. Ludlam, Craig B. Markwardt, Takashi Okajima, Chanda Prescod-Weinstein, Ronald A. Remillard, Michael T. Wolff, Emanuel Fonseca, H. Thankful Cromartie, Matthew Kerr, Timothy T. Pennucci, Aditya Parthasarathy, Scott Ransom, Ingrid Stairs, Lucas Guillemot, and Ismael Cognard. A NICER View of the Massive Pulsar PSR J0740+6620 Informed by Radio Timing and XMM-Newton Spectroscopy: Nested Samples for Millisecond Pulsar Parameter Estimation, April 2021.
- [136] M.C. Miller, F. K. Lamb, A. J. Dittmann, S. Bogdanov, Z. Arzoumanian, K. C. Gendreau, S. Guillot, W. C. G. Ho, J. M. Lattimer, S. M. Morsink, P. S. Ray, M. T. Wolff, C. L. Baker, T. Cazeau, S. Manthripragada, C. B. Markwardt, T. Okajima, S. Pollard, I. Cognard, H. T. Cromartie, E. Fonseca, L. Guillemot, M. Kerr, A. Parthasarathy, T. T. Pennucci, S. Ransom, I. Stairs, and M. Loewenstein. NICER PSR J0740+6620 Illinois-Maryland MCMC Samples, April 2021.
- [137] G. Raaijmakers, S.K. Greif, K. Hebeler, T. Hinderer, S. Nissanke, A. Schwenk, T.E. Riley, J.M. Lattimer, and W.C.G. Ho. Constraints on the dense matter equation of state and neutron star properties from NICER’s mass- radius estimate of PSR J0740+6620 and multimessenger observations: posterior samples and scripts for generating plots, April 2021.
- [138] Daniel Wysocki, Richard O’Shaughnessy, Leslie Wade, and Jacob Lange. Inferring the neutron star equation of state simultaneously with the population of merging neutron stars. 1 2020.
- [139] Matthew Pitkin, Stuart Reid, Sheila Rowan, and Jim Hough. Gravitational Wave Detection by Interferometry (Ground and Space). *Living Rev. Rel.*, 14:5, 2011.
- [140] Leslie Wade, Jolien D. E. Creighton, Evan Ochsner, Benjamin D. Lackey, Benjamin F. Farr, Tyson B. Littenberg, and Vivien Raymond. Systematic and statistical errors in a bayesian approach to the estimation of the neutron-star

- equation of state using advanced gravitational wave detectors. *Phys. Rev.*, D89(10):103012, 2014.
- [141] Gregory Ashton et al. BILBY: A user-friendly Bayesian inference library for gravitational-wave astronomy. *Astrophys. J. Suppl.*, 241(2):27, 2019.
- [142] I. M. Romero-Shaw et al. Bayesian inference for compact binary coalescences with bilby: validation and application to the first LIGO–Virgo gravitational-wave transient catalogue. *Mon. Not. Roy. Astron. Soc.*, 499(3):3295–3319, 2020.
- [143] Tim Dietrich, Sebastiano Bernuzzi, and Wolfgang Tichy. Closed-form tidal approximants for binary neutron star gravitational waveforms constructed from high-resolution numerical relativity simulations. *Phys. Rev. D*, 96(12):121501, 2017.
- [144] Tim Dietrich et al. Matter imprints in waveform models for neutron star binaries: Tidal and self-spin effects. *Phys. Rev. D*, 99(2):024029, 2019.
- [145] Gonçalo Castro, Leonardo Gualtieri, Andrea Maselli, and Paolo Pani. Impact and detectability of spin-tidal couplings in neutron star inspirals. 4 2022.